THE ROLE OF ELETROMAGNETIC FIELDS IN NEURONAL HEALTH

JAMES HARRY SKOYLES

Doctor of Philosophy

ASTON UNIVERSITY

September 2025

Thesis summary

Modern wireless technology saturates our airways in electromagnetic radiation. There is ongoing debate about the safety of the signals used in these industries. Despite some evidence of biological effects, regulatory bodies are satisfied that these technologies are safe. This project aimed to explore the ability of radiofrequency electromagnetic radiation to influence cellular biology in a neuronal context. The antennae used to generate this radiation operated with low emission power, to minimise or eliminate the likelihood of heating effects being involved. Initial work involved establishing a Faraday chamber adapted to suit cell culture work. This was done to create a kind of electromagnetic radiation dead space inside the chamber, which could then be used to analyse biological effects associated with specific signals introduced using a signal generator. Alongside this a simple 5G phone setup was used to run experiments in parallel for comparative purposes. Next, a series of biological assays were carried out in both setups in the presence and absence of electromagnetic radiation. These assays were designed to probe various aspects of cellular biology, such as metabolic viability, redox homeostasis and energy metabolism. The final section includes genetic expression profile analysis of whole-cell lysates from irradiated and non-irradiated cells. Collectively our results present compelling evidence of biological effects occurring as a result of radiofrequency electromagnetic radiation exposure – despite their perceived safety.

Dedication

The older I get, the more I learn to appreciate friends and family. Mom, Dad, Usmaan – thank you for everything.

Acknowledgments

Firstly, I'd like to thank Iru, Andrew and Lisette. Your guidance was essential. Without your support, I simply wouldn't have been able to complete this project. This undertaking felt overwhelming at times, but all three of you were always there to nudge me along. Not all people who take on the mantle of "supervisor" are suited to it, but you three have provided excellent support. So, thank you for everything.

A special mention to Theo for your assistance with data analysis. You are an excellent academic and have been tremendously helpful.

A special thanks also to Lorena. You taught me a great deal and provided a huge amount of assistance along the way, as you've done for many others in the lab. Thank you for taking me under your wing at times.

A long list of other people also aided me and contributed significantly to this project, each in their own way. It would take too many words to describe each supportive act individually, so, I will do the thanking equivalent of a group hug. A big thank you to the following people, in no particular order; Mohammed, Dan, Nona, Tom, Brad, Rowan, Boris, Swaroopa, Kam, Mandeep, Diarmuid and the L40 workshop team.

I would also like to thank and acknowledge Aston University itself, for providing me this opportunity and facilitating this project.

This work was supported by the Biotechnology and Biological Sciences Research Council (BBSRC) and University of Aston funded Midlands Integrative Biosciences Training Partnership (MIBTP) [grant number 66468].

List of contents

List of abbreviations

5G NR – Fifth Generation New Radio

AP – Access Point

ATCC – American Biological Culture Collection

CAPEX – Capital Expenditure

CIM – CO_2 Independent Media

CNS – Central Nervous System

CTB – Cell-Titer Blue

DEGs – Differentially Expressed Genes

EM – Electromagnetic

EMR – Electromagnetic Radiation

EMF – Electromagnetic Field

ETC – Electron Transport Chain

FCC – Federal Communications Commission

FCCP – Carbonyl cyanide-4 (trifluoromethoxy) phenylhydrazone

FDM – Frequency-Density Multiplexing

FBS – Fetal Bovine Serum

GSH – Glutathione

IARC – International Association for Research on Cancer

ICNIRP – International Commission on Non-Ionizing Radiation Protection

IEEE – Institute of Electrical and Electronics Engineers

IMT – International Mobile Telecommunications

IP – Internet Protocol

IPSC – Induced Pluripotent Stem Cell

IRPA – International Radiation Protection Association

ISI – Intersymbol Interference

ISM – Industrial, Scientific and Medical

LTE – Long-Term Evolution

MAC – Medium Access Control

MIMO – Multiple-Inout Multiple-Output

MU-MIMO – Multi-User Multiple-Input Multiple-Output

NAS – U.S. National Academy of Sciences Committee

OCR – Oxygen Consumption Rate

OFDM – Orthogonal Frequency-Division Multiplexing

OFDMA – Orthogonal Frequency-Division Multiple Access

OPEX – Operating Expenditure

PBS – Phosphate Buffered Saline

QAM – Quadrature Amplitude Modulation

RCF – Relative Centrifugal Force

RF – Radiofrequency

RNS – Reactive Nitrogen Species

ROS – Reactive Oxygen Species

SAR – Specific Absorption Rate

SOD1 – Superoxide Dismutase 1

TMEM – Transmembrane Protein

WHO – World Health Organisation

WLAN – Wireless Local Area Network

List of tables and figures

Tables

Figures

Chapter 1 – Introduction

1.1 Electromagnetic radiation

Electromagnetic radiation (EMR) is classically defined as a form of radiated energy that exists in waveform through interaction of the electric and magnetic fields (Purcell and Morin 2013). Each component of an electromagnetic wave is perpendicular to each other and the direction of travel of the waveform, often depicted diagrammatically as seen below (figure 1).

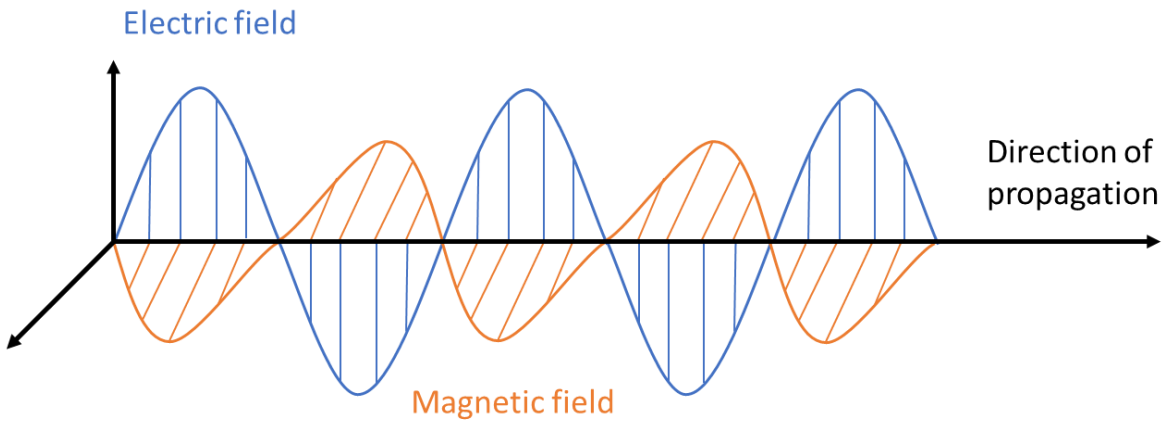

Figure 1 – classical interpretation of electromagnetic waves. They are composed of oscillations in the electric field (blue) and magnetic field (orange).

The parameters of these waveforms greatly influence the way in which they interact with matter, leading to the stratification of electromagnetic radiation into different types of waves in an electromagnetic spectrum (Serway, Jewett et al. 2000). The main properties of electromagnetic waves are; amplitude (height of peak), frequency (number of cycles per second) and wavelength (distance of 1 complete cycle). Frequency and wavelength are inversely proportional to one another, with high frequency waves having very short wavelengths (e.g. gamma radiation has wavelengths below 10^{-11} m and frequencies above 10^{18} Hertz). But EMR may also exhibit particle-like properties, giving rise to the "wave-particle duality" concept and may be considered in terms of particle and quantum physics (Ekspong 1999). The frequency of an electromagnetic wave also determines its "photon energy" i.e. the amount of energy conveyed in each individual energy packet, or photon, when considering EMR from a quantum perspective (Ekspong 1999). This is mathematically defined by the following equation, showing how the energy of a single photon is calculated

(where h = Planck's constant, v = frequency, c = speed of light constant and λ = wavelength).

Energy (photon) = h x v = h x c ÷ λ

One consequence of this property of EMR means that high frequency, high photon energy waves (e.g. gamma rays) can be considerably more dangerous to biology than low frequency waves (e.g. radio waves). In terms of safety considerations, this has led to the distinction of two categories of EMR within the EM spectrum; ionizing and non-ionizing radiation (Sowa, Rutkowska-Talipska et al. 2012).

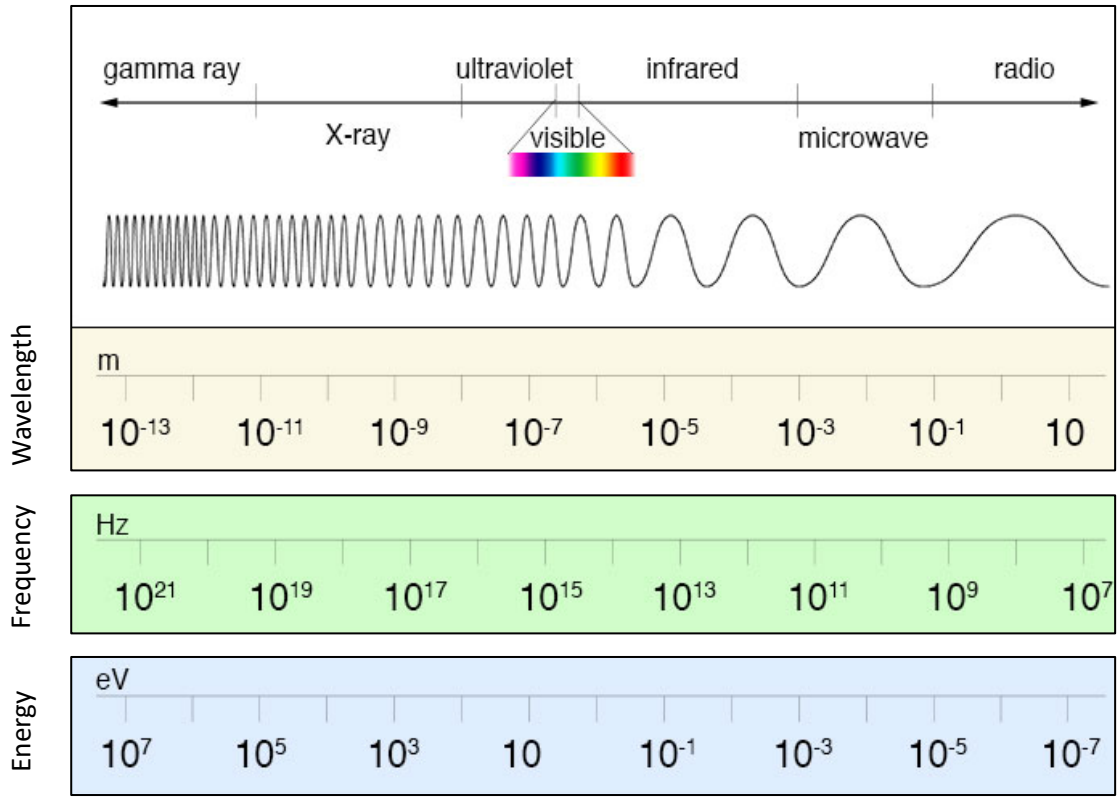

Figure 2 – the electromagnetic spectrum. The photon energy threshold at which EMR becomes ionizing is **~10 electron volts (eV)**, which occurs in the higher frequency portion of the ultraviolet region (wavelength 100-400nm). EMR with wavelengths shorter or frequencies higher than this range is sufficiently energetic to displace electrons, creating ions and causing molecular damage to living tissue. Telecommunications generally utilizes radio waves (typically classified as frequencies below 300 GHz by safety regulatory bodies, although frequencies above 1 GHz may instead be considered as microwaves in certain contexts). Note; image adapted from the NASA website https://imagine.gsfc.nasa.gov/science/toolbox/emspectrum2.html.

Ionizing radiation is radiation that possesses sufficient energy to displace electrons from atomic orbit in exposed material, creating ions (Sowa, Rutkowska-Talipska et al. 2012). This process has been well-established as being harmful to tissue over many years, leading to stringent safety regulations around the use of ionizing radiation in medicine, research and other fields (McBride and Schaue 2020).

But below this energy threshold, photons can still interact with matter and energy deposition may still occur (Braeuer 2015). There are several mechanisms through which this can occur (electronically, rotationally, translationally and vibrationally) and, importantly, the intensity of energy deposition is determined by the relationship between photon energy and available energy states of atomic components of exposed matter, i.e. the closer the energy of a photon is to a potential energy state of a subatomic particle, the more likely it is to deposit energy (Braeuer 2015). These “excitations” and “relaxations” of particles occur at specific energy levels as a result of quantum phenomena, which have shown energy to be absorbed and emitted in specific, discrete patterns (Artaud 1905). A natural consequence of this is that wavelength becomes critically important in determining how transparent a substance is to different types of EMR. Very low energy photons, e.g. those found in low frequency radio waves, will generally have a low chance of depositing energy because of a lack of proximity to available energy states found in matter. This is why radio waves are able to effectively penetrate the walls of buildings to a significant extent and deliver radio communications where many other wavelengths of EMR, with higher photon energies, would be completely scattered or absorbed (e.g. visible light). However, this does not mean solid material is completely transparent to low-energy photons, as even with a low probability of energy deposition it may still occur (Braeuer 2015).

This relationship between EM wavelength and penetration through a material is defined as penetration depth – the depth at which EMR intensity has dropped to approximately 37% its value at the surface, or 1/e, where e = Euler’s number or 2.718… (Feynman, Leighton et al. 1965). Wavelength is the main factor that determines how far EMR will penetrate through a material, with higher frequencies (shorter wavelengths) typically penetrating far less than lower frequences. For example, the penetration depth of industrial 915 MHz microwaves is about three times larger than the penetration depth of standard consumer 2.45 GHz microwaves (Afolabi and Sohail 2017).

Another important consideration of EMR is wave propagation - the way in which EMR propagates through space and scatters through interactions with matter when considered as a waveform (Ishimaru 2017). Various propagation mechanisms of EM waves have been

established, such as direct or “line-of-sight” paths, ground waves or ionospheric bouncing (Ishimaru 2017).

Wave propagation is especially relevant when designing radar and telecommunications systems, where various factors must be considered, including; distance between transmitter and receiver, proposed frequency range and local terrain (for example, ground waves which propagate along the Earth’s surface may be significantly diffracted by mountains) (Ulaby, Dobson et al. 2019). Ideally, line-of-sight paths between transmitter and receiver allow for minimal loss of signal through matter interactions, but this is often not a feasible solution, particularly in urbanised areas, where the majority of people live (Sizun and de Fornel 2005). A common result of wave propagation phenomena is that multipath propagation is often the more practical outcome, particularly in environments which contain many potential signal reflectors and scatterers (Turin, Clapp et al. 1972). Multipath propagation of EMR occurs when a waveform is transmitted and arrives at a receiver in separate parts, with each component taking a distinct path (Siller Jr 1984). Because of this, each component of a transmitted EM wave (or signal) may be exposed to distinct interference patterns dependent upon the path taken and the nature of reflectors and scatterers encountered (Siller Jr 1984).

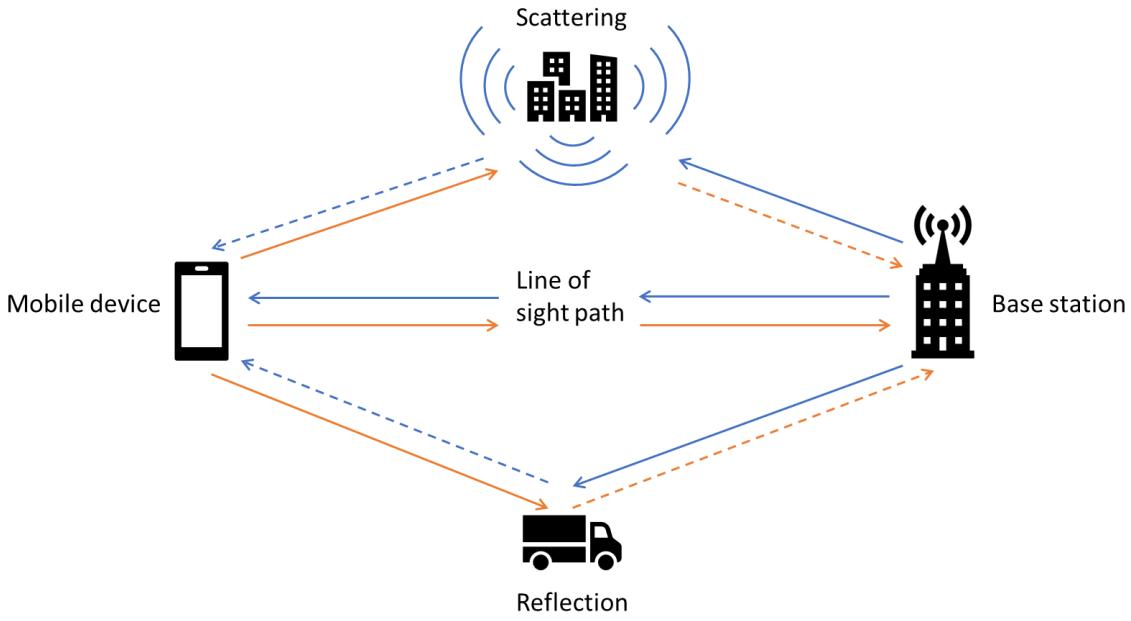

Figure 3 – A diagrammatic representation of direct Line-of-Sight and multipath propagation. Various objects may act as signal reflectors and scatterers, common examples being buildings and vehicles in urbanised areas. These waveform-matter interactions can cause a transmitted signal to arrive in several distinct components, each with their own parameters (e.g. time delay). With clever use of compensatory technologies and methods, these issues can be overcome and the original signal reconstituted at receiving antennas.

Examples of causes of signal interference in rural environments may include hills, mountains, trees, water bodies and other natural terrain features. Within urban areas, buildings contribute significantly to signal disruption, making cities one of the least optimal environments for wave propagation and telecommunications systems (Turin, Clapp et al. 1972). This is equally true for wave propagation within indoor environments, where walls, ceilings and doors can degrade signal quality (Saleh and Valenzuela 1987). Despite these issues, multipath propagation of EMR is effectively utilised in telecommunications systems, where attempts are made to compensate for signal distortion or "multipath fading", which can cause a transmitted wave to arrive at a receiving antenna in multiple copies, each with differing properties such as attenuation, phase shift and time delay (Siller Jr 1984). A key concept in mitigating multipath fading is making use of signal diversity. Splitting signals into multiple channels which differ in some parameter (e.g. frequency or time) effectively spreads the risk posed by fading and allows for signals to be coherently reconstituted at the receiver, reducing the overall impact of fading and improving signal-to-noise ratios (Watteyne, Lanzisera et al. 2010). Various technologies and approaches have been developed to achieve this fading compensation, which include rake receivers, multi-input and multi-output (MIMO) methodology and orthogonal frequency-division multiplexing (OFDM), which will be explored later (Armstrong 2009, Sen and Nehorai 2010, Larsson, Edfors et al. 2014).

Finally, in terms of sources of EMR, they can be both natural in origin or a result of man-made technologies and people are consistently exposed to EMR throughout their lifespan (Zamanian and Hardiman 2005). But despite this exposure, human tissues can generally tolerate low intensity doses fairly well (Zamanian and Hardiman 2005). Examples of natural sources of EMR include; sunlight (visible light, UV & infrared), radioactive materials in the Earth's crust, cosmic rays from outer space or even rocks undergoing nanocrack nucleation (Zamanian and Hardiman 2005, Greiling and Obermeyer 2010). Modern technology has produced a wide array of artificial sources of EMR, these include medical devices (e.g. X-ray computed tomography, MRI or radiotherapy), radios, radar, satellites, microwave ovens, personal computers, routers, mobile phones and cell towers. Unlike most naturally occurring radiation, many of these technologies utilize frequencies in the radio wave range (sub 300 GHz), particularly in the case of telecommunications technology (Kottou, Nikolopoulos et al. 2014). One of the main drivers behind this project is concern around airways that are increasingly saturated with telecommunications-associated EMR, leading to ever higher radio wave exposures for most people (Obile 2016).

1.2 Telecommunications

Use of EMR in telecommunications began as early as the end of 19th century, with inventor Guglielmo Marconi's work on "wireless telegraphy" or radio communication, which drew inspiration from James Clerk Maxwell's earlier research on electromagnetism (Garratt 1994). But widespread use of EMR-based telecommunication in homes of ordinary people occurred later, in the 20th century – with two of the first major consumer technologies coming in the form of radio broadcasting, then later in broadcast television (Huurdeman 2003). This allowed large numbers of people to remotely receive audio and visual information into their homes from a single, centralised source and marked the beginning of a trend towards increasing use of wireless forms of technology that continues today (Huurdeman 2003, Ericsson 2021).

In modern times, it is common for households in developed nations to make use of many wireless devices, which can include; tablet computers, routers, smart TVs, AM/FM radios, Bluetooth speakers, cameras, personal computers and mobile phones (Pahlavan and Krishnamurthy 2021). Much of the data transmission these devices generate occurs over WiFi, which is one of the most popular ways of delivering Internet Protocol (IP) traffic and providing internet connectivity to laptops and mobile phones (Pahlavan and Krishnamurthy 2021). WiFi is a type of Wireless Local Area Network (WLAN) that makes use of the Institute of Electrical and Electronics Engineers (IEEE) 802.11 protocols – a set of standards maintained by IEEE that specifies medium access control (MAC) and physical layer (PHY) configuration for a WLAN (Kaushik 2012). Several iterations of these WiFi standards exist, offering different data transfer rates and utilising different frequency bands. Two of the most common frequency bands utilised by WiFi are 2.4 GHz and 5 GHz, with data transfer rates ranging from 1-100,000 Mbits/sec, with newer standards (such as WiFi 8's IEEE 802.11bn) typically providing higher data transfer rates than previous generations (Reshef and Cordeiro 2022). Table 1 below shows the progression of WiFi from 1st to the upcoming 8th generation, with the latest set of standards expected to be finalised by 2028 (Reshef and Cordeiro 2022). As table 1 shows, most of the developmental focus of WiFi (and wireless technology in general) is directed towards increasing the data transfer rate. The 2.4 and 5 GHz frequency bands have been heavily utilised over many years, with the only recent change coming in the use of a 6 GHz band, implemented in 2021 with WiFi 6E (Sankaran and Gulasekaran 2021). Over the same time period, data transfer rates have increased exponentially from single digit megabits per second rates to an upper limit of 23,000 in 2024 with WiFi 7 (Deng, Fang et al. 2020).

Generation	IEEE standard	Year	Frequency (GHz)	Bit rate (Mbit/sec)
WiFi	802.11	1997	2.4	1-2
WiFi 1	803.11b	1999	2.4	1-11
WiFi 2	804.11a	1999	5	6-54
WiFi 3	805.11g	2003	2.4	6-54
WiFi 4	806.11n	2009	2.4, 5	6.5-600
WiFi 5	807.11ac	2013	5	6.5-6933
WiFi 6	808.11ax	2021	2.4, 5	0.4-9608
WiFi 6E	809.11ax	2021	6	0.4-9608
WiFi 7	810.11be	2024	2.4, 5, 6	0.4-23059
WiFi 8	811.11bn	2028	2.4, 5, 6	up to 100000

Table 1 – the progress of WiFi standards over the years.

Frequencies used in WiFi belong to the unlicenced regions of the radio spectrum, commonly called ISM bands (Industrial, Scientific and Medical). These are frequencies which anyone can freely broadcast in and does not require ownership of a licence for the right to broadcast (Kumbhar 2017). These licence-free bands are interspersed throughout the radio wave spectrum, with ISM bands having frequencies ranging from 6 KHz to 245 GHz (Kumbhar 2017). Although the original intent of ISM was to protect medical and industrial devices from interference, they are increasingly being utilised by consumer telecoms devices, including WiFi (Kumbhar 2017). A natural consequence of this is that some environments may become saturated in telecoms and WiFi devices operating in similar frequencies, which can lead to particularly “dense” networks and potential interference problems (Zhong, Kulkarni et al. 2015). This issue has led to more recent WiFi standards, such as 808.11ax, to place more emphasis on spectrum efficiency and improve performance in highly signal dense scenarios, as seen in public spaces with many devices in a relatively small area (e.g. a filled stadium environment) (Zhong, Kulkarni et al. 2015).

Although the frequency bands used in WiFi are commonly designated as a single number (e.g. 2.4, 5 or 6 GHz), in practice these bands occupy a small but significant range in the radio spectrum, broken up into several channels (Naik, Park et al. 2020). For example, the 2.4 GHz band is 80 MHz wide, ranging from 2402-2482 MHz and is capable of operating over 3 non-overlapping 20 MHz channels (Committee 2009). The newer 5 GHz band is up to 700 MHz wide, occupying 5150-5850 MHz, and capable of utilising up to 25 non-overlapping 20 MHz channels (Dolińska, Jakubowski et al. 2017). The newest 6 GHz band is wider still,

with a width of 1200 MHz in the US and similar width being proposed in the UK (Naik, Park et al. 2020). The width of these bands and channel number is important because overlapping use of channels by multiple devices is a common source of interference, which can lead to a drop in device performance (Dolińska, Jakubowski et al. 2017). It is particularly relevant to the 2,4 GHz band, which has the fewest number of channels and the highest number of legacy devices operating at similar frequencies (Dolińska, Jakubowski et al. 2017). Examples of these legacy technologies include Bluetooth devices and most household microwave ovens, which both typically operate at 2.4 GHz (Dolińska, Jakubowski et al. 2017). This is one of the reasons there has been a push to use higher frequencies for wireless technology in recent years (Dolińska, Jakubowski et al. 2017). But the major driver of development in WiFi and other wireless technology is user demand for higher performance (Michaloliakos, Rogalin et al. 2016, Obile 2016). This user expectation for higher data transfer rates and better network reliability is coupled with ever increasing numbers of user devices, meaning more devices each wanting more data (Obile 2016). One key technique employed by WiFi to deal with this issue is signal modulation (Hwang, Yang et al. 2008).

Modulation involves using fluctuations in some parameter of a carrier wave to convey bits of information, where a carrier wave is a simple periodic waveform (e.g. sinusoidal). The patterns of irregularity introduced to the carrier wave become code for bits of information, similar in principle to the dots and dashes of Morse code. This process is carried out by a modulator at the signal source, which is then reversed at the receiver by a demodulator (Sturley 1945, Faruque 2017). Figure 4 below illustrates a simple example of how this process works in the case of classic frequency modulation, still used today for FM radio. Modulation techniques exploit the fact that electromagnetic waves may interact with each other, where the modulation signal is said to be “impressed” upon the carrier signal (Faruque 2017). This phenomena of EM waves interacting with each other is also observed in interference – where two or more waveforms may “constructively” or “destructively” interact, both of which can result in unwanted distortions of information-carrying signals (Gummadi, Wetherall et al. 2007, Dolińska, Jakubowski et al. 2017). Many forms of analogue and digital modulation are still used in telecoms, including amplitude modulation (e.g. AM radio), frequency modulation (e.g. FM radio), phase modulation (e.g. satellite TV), Direct-Sequence Spread Spectrum (DSSS), Frequency-Shift Keying (FSK), Phase-Shift Keying (PSK), Amplitude-Shift Keying (ASK) and various others (Sharma, Mishra et al. 2010, Barnela and Kumar 2014).

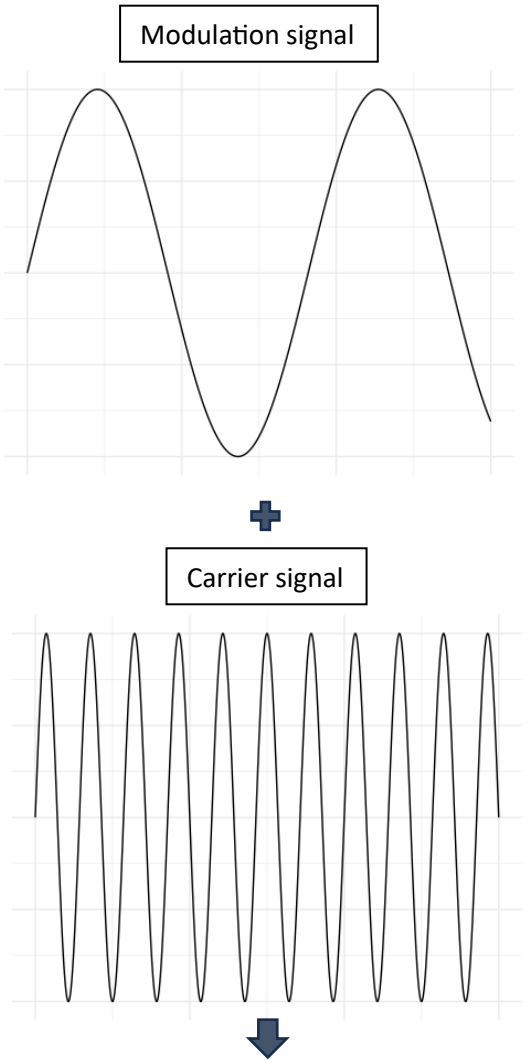

Figure 4 – classic analogue frequency modulation. A modulation signal is imposed on a carrier wave, altering its frequency.

In terms of modern digital modulation techniques, they are far more complex and allow for greater information density when contrasted with classic analogue techniques, but are not always ideal due to requiring sophisticated equipment to manage modulation and demodulation (Litwin and Pugel 2001, Hwang, Yang et al. 2008). WiFi and other wireless technologies (e.g. 4G and 5G cellular networks) have made extensive use of one particular modulation technique called Orthogonal Frequency-Density Multiplexing (OFDM) for several years, with the earliest appearance of OFDM in the history of WiFi being 1999's 802.11a standards (IEEE 1999). OFDM is developed from the earlier Frequency-Density Multiplexing (FDM), in which the bandwidth of an information-containing signal to be transmitted is broken up into several smaller components or "subcarriers" (Bolcskei 2006). Each subcarrier conveys bits of coded information using symbols and have non-overlapping frequencies to prevent subcarriers from interfering with each other (Litwin and Pugel 2001, Hwang, Yang et al. 2008). This is achieved by leaving small gaps or "guards" between subcarriers, a process called subcarrier spacing, which lowers Inter Carrier Interference (ICI) and makes transmissions resistant to degradation by multipath fading, as previously described (Litwin and Pugel 2001, Bolcskei 2006, Hwang, Yang et al. 2008, Sen and Nehorai 2010). OFDM further extends this principle of breaking down a signal into multiple subcarriers by exploiting orthogonality. Because waveform components that are orthogonal to each other do not interact, OFDM allows for more subcarriers to be packed into this additional domain – allowing even greater subcarrier per unit bandwidth, or more simply,

better spectral efficiency (Bolcskei 2006). The end result is a transmission that contains many narrowly spaced subcarriers, where use of orthogonality means at each component's peak, the contribution of other subcarriers is null (Bolcskei 2006). Each subcarrier may be modulated using a wide variety of modulation schemes, some previously mentioned, but in the case of WiFi standards, Quadrature Amplitude Modulation (QAM) is the dominant technique employed in combination with OFDM (IEEE 1999, IEEE 2013, Deng, Fang et al. 2020).

QAM in its simplest terms is a modulation technique that combines both amplitude and phase modulation techniques together, using either digital (ASK and PSK) or analogue (AM and PM) approaches (Hanzo, Ng et al. 2004). Quadrature describes a state two components, or signals, that are out of phase with each other by 90 degrees - this is the phase modulation or quadrature aspect of QAM. Each component may also have its own pattern of amplitude modulation, hence Quadrature Amplitude Modulation. Even if the two components have the same frequency, because they are phase-shifted 90 degrees, they will not interfere with each other significantly and may be coherently demodulated at the receiver (Hanzo, Ng et al. 2004). As such QAM generates 2-dimensional signals, with one of the two components commonly designated as I(t) or just I, for being In-phase relative to the carrier wave, while the other is designated Q(t) or Q, due to its orthogonality or quadrature relative to the carrier. In digital QAM, values provided by I and Q components can be used to build what is called a constellation map (Ma, Gao et al. 2019). An example of 16-QAM is shown in figure 5 below. These diagrams are commonly grid-like arrangements of points, with each point representing the output of the I and Q values, which typically encode information in binary form. This results in a grid of points with different combinations of 1's and 0's, which represents the encoded data being transmitted. Different forms of these QAM constellation maps exist, some being "higher order" – having more points on the grid – than others. The most common forms of QAM use square-like grids, such as 4-QAM, 256-QAM, 64-QAM and 256-QAM etc, although non-square grids are sometimes used. As the constellation maps move through higher orders, they offer higher bits per symbol transmitted, therefore needing lower bandwidth to send the same volume of information and being more spectrally efficient (Winzer 2012). But the drawback to this is that the constellation maps become more densely packed, with less space between points. This means that the chances of the receiver making errors and mistaking one point for another is increased – i.e. they are more error-prone (Kumar, Gour et al. 2025). Despite this drawback, higher order QAM is often employed in wireless communication systems (e.g. 256-QAM being included in WiFi 5 onwards) and the highest order of QAM included in WiFi standards has increased with time. For example, the newest iterations of WiFi standards include up to 4096-QAM, which is included in WiFi 7's

modulation scheme (Choi, Ahn et al. 2023). This is because there are methods to compensate for the error-prone nature of higher order QAM, such as improving signal-to-noise ratio by using more signal power or by utilising more sophisticated equalization techniques to compensate for signal noise (Yuan and Tsai 2005).

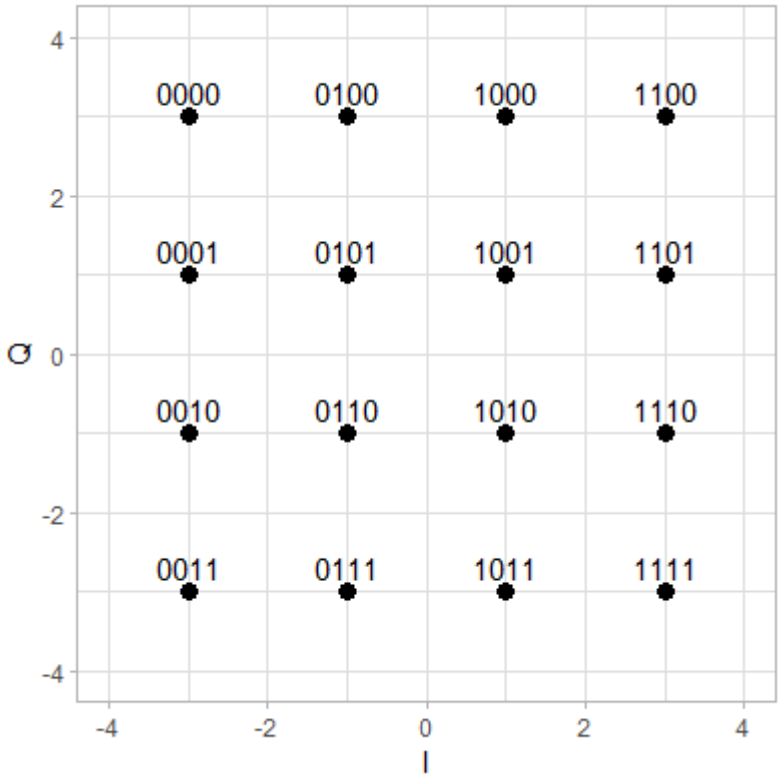

Figure 5 – a 16QAM modulation constellation map. It has 16 symbols, binary combinations corresponding to the relevant phase and amplitude of each I and Q component. Each individual symbol encodes 4 bits of data. Because of quadrature, both components may be transmitted together.

In more recent WiFi standards (802.11ax, 802.11be and 802.11bn) the OFDM modulation scheme has been updated to include simultaneous transmissions from multiple users in a scheme called Orthogonal Frequency-Division Multiple Access (OFDMA) (Yin and Alamouti 2006). OFDMA achieves this by allocating OFDM components to individual users in sub-channels. Additionally, this scheme may be combined with Multiple-Input Multiple-Output (MIMO) and Multi-User Multiple-Input Multiple-Output (MU-MIMO) antenna techniques to further improve performance in dense networks. This is seen with the inclusion of MU-MIMO in the 802.11ac WiFi standards from WiFi 5 onwards (IEEE 2013).

MU-MIMO is a variant of MIMO approaches where antenna arrays or Access Points (APs) exchange data with multiple user devices simultaneously (Liao, Bellalta et al. 2014). This is contrasted with Single-User-MIMO (SU-MIMO), where data streams are directed towards a single user device, hence SU-MIMO. The main advantages of MU-MIMO when compared to SU-MIMO are higher throughput and diversity and the potential for lower-cost production (Liao, Bellalta et al. 2014). The overall result of these successive improvements to WiFi has

led to remarkably sophisticated, signal-dense networks that can handle high numbers of simultaneous users while maintaining both high data rates and reliable performance (Chen, Chen et al. 2022, Reshef and Cordeiro 2022). The high performance of WiFi networks is also leveraged by other areas of telecoms technology, for example, with ISPs and cellular networks both offloading significant proportions of internet traffic to WiFi networks, resulting in WiFi being one of the dominant players in the Internet-of-Things and telecoms today (Lee, Lee et al. 2012).

Mobile phone technology, another major player in wireless technology, has also undergone significant expansion and innovation over the last few decades, with some advancements overlapping with those seen in WiFi technology (e.g. use of OFDM). Although there has been a lot of change to cellular networks through generations, they are all based on the same core idea of breaking up larger service areas into smaller sections, called “cells”, with each cell having its own base station and range of operating frequencies (Poole 2006). The signal intensity of a base station decreases with distance and is affected by terrain features, leading to a roughly circular, but highly irregular, area of coverage for each station. In practice, cell networks are most often designed using hexagonal cell shapes, for convenience and to avoid issues of overlapping coverage which would occur from trying to use groups of circles or irregular shapes. Each cell is designed and optimised in such a way to provide good signal coverage for the geographical area it is designated, but not interfere with signals of neighbouring cells i.e. as the signal intensity from one base station begins to drop below a satisfactory level, a neighbouring station takes over. Because of this design system, each base station does not meaningfully interfere with the signals of nearby cells (Poole 2006). But it is not perfect. In reality there may be gaps in coverage or the signals from two or more base stations may possess significant intensity in a particular spot or area, potentially leading to interference (Poole 2006). A common method for dealing with this issue is to allocate specific frequency bands to each cell, where for any given cell all neighbouring cells utilise different frequency bands, reducing or eliminating signal interference between nearby cells (Poole 2006). Cells that are distant from each other may reuse the same frequency bands without issue.

There are several types of cells which depends on the physical size of the coverage area in question, these are shown below in table 2 and range from femtocells (few meters) to mega cells (hundreds of kilometres).

Cell type	Size (M)
Femtocell	<10
Picocell	>10
Microcell	>100
Macrocell	>1000
Mega cell	>100k

Table 2 – the approximate service area sizes and names of network cells.

Cells are grouped together into “clusters” and the number of cells per cluster (or per unit of geographical area) is important. Denser clusters, with more cells per cluster, tend to be more resistant to inter-cell interference, due to having more cells to allocate specific frequency bands to, reducing the likelihood of neighbouring cells having overlapping frequencies (Poole 2006). But this has the drawback of increasing the monetary cost of a cluster – i.e. more dense clusters require more base stations.

Most modern cell networks (4G and onwards) adopt a design approach termed Heterogenous Network, or HetNet. In this design scheme, low-power small cells (e.g. femtocells, picocells) are deployed within a larger, higher power macrocell. Such layering of cells has the potential to increase network performance and user quality of service, but has two major drawbacks that must be addressed to realise this potential. Firstly, layered cells operating in the same area at different power levels presents interference problems both within and between cells that are absent from older, simpler designs (Wang and Ran 2016). This problem of inter and intra cell interference can be resolved with advanced signal processing techniques, such as coordinated multipoint transmission/reception and inter-cell interference coordination (Wang and Ran 2016). Secondly, because of the required advanced signal processing and layering of cells, these HetNet are more expensive and require more investment. This includes the initial build cost, or Capital Expenditure (CAPEX), and operating cost, or Operating Expenditure (OPEX) (Wang and Ran 2016). Despite these issues, HetNet deployments are set to feature prominently in the future of WLANs, especially in urban areas where the highest user to unit area ratios are anticipated (Wang and Ran 2016, Xu, Gui et al. 2021). But there are concerns around the limits of performance gains due to signal processing techniques and increased cluster density, particularly in light of increasing consumer demands and expectations (Wang and Ran 2016).

The earliest iterations of fully mobile consumer telephony units began appearing around 1980. These devices ultimately followed on from a long series of technological advancements in the telephony field spanning decades of work that began in the 1940s (Farley 2005). These early mobile phones adhered to a set of standards that have been retroactively labelled “1G”, as in first generation cellular network, but were not named such

at the time. 1G networks were analogue in nature and allowed for transmission of voice data only, similar in essence to traditional AM/FM radio broadcasting (Gawas 2015). Successive generations of cell networks switched over to using digital transmission and expanded the capability of cellular networks, first adding text messaging features (2G), then email access, multimedia functionality (early 3G) and ultimately arriving at the mobile broadband access seen today (later 3G iterations and onwards) (Gawas 2015). This feature and functionality development has gone hand-in-hand with generally improved network performance (higher data exchange rates, better connectivity and reliability etc), which is needed to cope with more demanding, data-intensive tasks such as video streaming (Gawas 2015). Within each generation are several sets of standards that determine what performance criteria a network must meet in order to satisfy the relevant label, e.g. a “3G” network must satisfy the International Mobile Telecommunications-2000 (IMT-2000) standards, which require a minimum consistent Internet speed of 144 Kbps and a peak rate of 384 Kbps or greater (Chaudhury, Mohr et al. 1999). Generally speaking, the data transfer rates of generations and their associated standards have increased substantially over time. For example, the Advanced Mobile Phone System (AMPS) deployed in USA during the 1G era had a frequency band of 824-894MHz and supported data transfer speeds of up to 2.4 Kbps. This was succeeded in most regions by 2G’s Global System for Mobile Communication (GSM) standards, which had a bandwidth of 30-200KHz and boasted speeds of up to 64 Kbps, representing a 26 fold increase in maximal data transfer rate in one generational step (Gawas 2015). The latest 5G standards (IMT-2020) minimum requirements specify a peak data transfer rate of 20 Gbps downstream and 10 Gbps upstream, with a “user experienced” download rate of 100 Mbps – all exponentially higher than previous generations capabilities (Shafi, Molisch et al. 2017). Some of the requirements a cellular network must satisfy to meet the IMT-2020 (5G) standards are shown below in table 3.

Performance Indicator	**Value**
Peak data rate	DL 30 Gbps, UL 10 Gbps
Peak spectral efficiency	DL 30 bps/Hz, UL 15 bps/Hz
User experienced data rate	DL 100 Mbps, UL 50 Mbps (dense urban)
Average spectral efficiency	DL 9 Mbps/Hz/TRxP, UL 6.7 Mbps/Hz/TRxP (indoor hotspot)
Area Traffic Capacity	DL 10 Mbps/m² (indoor hotspot)
Connection density	1,000,000 devices/km²

Table 3 – 5G’s IMT-2020 standards.

Improvements to cellular network performance (speed, spectral efficiency, reliability etc) are being driven by ever-increasing consumer demands. Video streaming in particular has been singled out as a major source of increased data consumption (Shafi, Molisch et al. 2017). Because displays of mobile phones have been improving and screen resolutions have increased with time, the amount of data needed per device has also risen. Many modern phones are capable of 4K screen resolution, which will require a data rate of ~15 Mbps per device (Shafi, Molisch et al. 2017). By the end of 2024, video streaming is expected to account for 74% of global mobile data traffic (Ericsson 2024). But the full picture of consumer trends is far broader than this.

Global cellular data traffic has been increasing significantly since the inception of consumer mobile phones, with traffic estimated to have increased approximately 300 fold in the span of 10 years from 2011 to 2021 (Ericsson 2021). In terms of estimated amounts of global data traffic per month (both uplink and downlink), in Q1 of 2018 traffic totalled ~18 exobytes (or EB, which is ~10^8 bytes of data), which rose to ~29 EB in Q1 of 2019, ~45 EB in Q1 of 2020, ~67 EB in Q1 of 2021 and continued rising each year to reach an estimated monthly consumption of ~145 EB per month by Q1 of 2024 (Ericsson 2024). Although the rate of increase has begun to slowly and steadily decline over time, having peaked in Q4 of 2018, overall global cellular data consumption continues steadily increasing, a trend which is expected to continue into the near future with no foreseeable saturation point (Ericsson 2024).

Perhaps unsurprisingly, increases in data traffic have been concordant with increases in mobile subscription numbers. Global mobile subscriptions totalled 8.7 billion by the end of 2024, with an expectation of reaching ~9.5 billion by 2030 (Ericsson 2024). The nature of these subscriptions is also changing with time, as people increasingly make use of newer generations of cellular network technology. As of 2024, 4G was the dominant technology, accounting for ~5.1 billion mobile subscriptions, followed by 5G at ~2.9 billion subscriptions. Combined older generations (up to 3G), accounted for just ~1.5 billion subscriptions (Ericsson 2024). 4G and older subscription numbers are steadily falling, with 5G numbers rising and accounting for an increasingly large share of the global market. It is forecast that 5G subscriptions will overtake those of 4G by 2027, and continue rising to reach ~6.3 billion by 2030, at which point 6G will begin to enter the consumer market (Ericsson 2024).

Previous generations of cell networks (4G and older) all operate in the sub 6 GHz frequency range, with the highest frequency band in common use for consumer mobile phones being the 4G ~3.5 GHz band and higher frequencies being reserved for niche uses such as 4G's

V2X vehicle communication system, which operates at ~5.9 GHz (Tan, Li et al. 2015, Garcia-Roger, González et al. 2020). However, unique to 5G will be utilisation of frequency bands above 6 GHz, so-called “mmWave” frequencies bands – because their wavelength will dip into the millimetre range.

5G NR (New Radio) is the global standard for 5G cellular networks. It is currently comprised of two main frequency ranges (FRs), FR1 and FR2. FR1 includes 0.4 to 7.1 GHz and FR2 ranges from 24 to 52 GHz (Parkvall, Dahlman et al. 2018, Rochman, Sathya et al. 2023). An additional band to cover the gap between FR1 and FR2 (7.1 to 24 GHz) is being considered and is likely to come into use in the future as FR3 (Tang, Zhang et al. 2025). FR1 overlaps heavily with previous generations and is subject to many of the same considerations and bandwidth congestion issues, but is a necessary inclusion in 5G because of the trade-off between coverage and speed. Lower frequencies (FR1) tend to have better propagation and penetration than higher frequencies and require fewer base stations per unit area, but offer lower data transfer speeds and network performance (Rochman, Sathya et al. 2023). These frequencies are ideally suited to environments where coverage is a primary concern, such as rural areas which are not likely to receive dense base station clusters. Higher frequencies (FR2) rely on investing in many low-cost base stations per unit area and offer consumers much higher data throughput, while sacrificing coverage per individual station (Rochman, Sathya et al. 2023).

Because of this need for higher numbers of base stations and the use of higher frequencies (20 GHz+), the introduction of 5G technology has provoked significant public concern (Jolley and Paterson 2020, Sofri, Rahim et al. 2021). This concern has resulted in the rise of conspiracy theories related to COVID-19 and even caused violence directed towards 5G infrastructure (Jolley and Paterson 2020). This is despite exposure testing being a routine part of any cellular network development, where exposure levels are consistently reported being well below those suggested by EMR regulatory bodies (Chiaraviglio, Lodovisi et al. 2021, Sofri, Rahim et al. 2021). In the United States, the Federal Communications Commission (FCC) provides regulatory framework for tolerably safe Electromagnetic Field (EMF) exposure levels for the human body. Internationally, it is the International Commission on Non-Ionizing Radiation Protection (ICNIRP) that fulfils this role for most of the developed world (ICNIRP 2020, Hardell, Nilsson et al. 2021).

According to the ICNIRP 2020 guidelines for EMF exposure, adherence to their suggested exposure levels is “...intended to protect people from all substantiated harmful effects of radiofrequency (RF) EMF exposure.” (ICNIRP 2020). The guidelines go on to clarify how the

ICNIRP arrives at their suggested exposure levels and places clear emphasis on their criteria for judging the validity and relevance of scientific articles for consideration, stating that articles providing evidence of harmful effects must be independently verified (ICNIRP 2020). But it also states that the stringency of their selection process may be "relaxed" in the event of greater expansion of our understanding of a biological, non-thermal mechanism of action for EMF exposure (ICNIRP 2020). This is especially relevant because one of the main criticisms levelled at the ICNIRP's guidelines by some scientific researchers is that they are ignoring potentially significant evidence of biological effects in favour of focusing only on potential harm associated with heating effects, a point which will be expanded upon later (Starkey 2016, ICBE-EMF 2022). To date there has been no strong evidence put forth for a proposed mechanism of action for biological effects of RF-EMF, although an unknown temperature-independent mechanism has been suggested and considered for some time, for example in the context of electrophysiology (Sluijter and Racz 2002).

In terms of the history and background of the ICNIRP, it is a Non-Governmental Organisation that was established in 1992 by the International Radiation Protection Association (IRPA) in a move designed to create a truly independent commission following a rise in the influence of IRPA through the 1970s and 1980s (Repacholi 2017). As such, its members are prohibited from commercial employment and there are strict guidelines related to ICNIRP funding sources to reduce or eliminate potential bias from the telecoms industry (Repacholi 2017). The initial set of EMR exposure limits proposed by the ICNIRP were published in 1998, following a review of current and relevant literature carried out by ICNIRP in 1996 (Protection 1998). The 1998 guidelines cite and consider many different articles, including work from epidemiology, electrophysiology, audiology, oncology, cellular models, animal behavioural studies and more. These include articles that produced both positive and negative results, although the majority of articles cited reported no significant effect following RF radiation in various contexts (Barron and Baraff 1958, Daels 1973, Cohen, Lilienfeld et al. 1977, Robinette, SILVERMAN et al. 1980, Selvin, Schulman et al. 1992, Rothman, Loughlin et al. 1996). Examples of some of the articles reporting positive results include two articles reporting a link between RF exposure and birth defects and two articles reporting association between exposure and cancer (Larsen 1991, Ouellet-Hellstrom and Stewart 1993, Hocking, Gordon et al. 1996, Szmigielski 1996). In these cases, the ICNIRP guidelines cite conflicts of outcome with similar studies and/or criticise the methodology used (e.g. that the "assessment of EMF exposure was not well defined") (Protection 1998). Ultimately, the overall conclusion of the ICNIRP based on reviewed literature was that RF (10 MHz to 10 GHz) exposure resulting in a dose equivalent to a whole-body Specific Absorbance Rate (SAR) of 4 W/kg causes a body temperature rise of less than 1 ºC, where SAR is a unit

measuring the rate of RF energy absorption per unit mass. This is judged to be an important temperature change threshold, where rises above this are expected to be potentially harmful based on previous work reviewed by the World Health Organisation (WHO) (Bulman 1994). Findings from several animal studies contributed significantly to the basis of this safety temperature threshold, including a trio of studies carried out by American Navy scientists in the 1980s. These studies involved both rats and monkeys and measured changes in response times or body temperature following RF exposure (de Lorge and Ezell 1980, de Lorge 1984, Lotz 1985). Various frequencies, power densities and other parameters were used for each study. For example, in one study monkeys were irradiated for 60 minutes using frequencies of 0.2 GHz, 1.3 GHz and 5.8 GHz before lever response times were measured (de Lorge 1984). It was reported that a dose equivalent to a SAR ranging from 3.2 to 8.4 W/kg was required to lower response times relative to sham exposure (de Lorge 1984). In a similar study using rats irradiated for 40 minutes at 1.2 and 5.6 GHz frequencies, it was reported that a whole-body SAR between 3.8 to 4.9 W/kg was required to lower response times (de Lorge and Ezell 1980). Finally, and perhaps most significantly in the eyes of the ICNIRP, another study looked at mean body temperatures of monkeys irradiated for 4 hours at 1.29 GHz using a range of power densities (Lotz 1985). It was reported that a whole-body SAR of 4 W/kg was associated with a 0.7 ºC increase in average body temperature (Lotz 1985). These animal papers and others like them form the foundation of the exposure limits established by the WHO and ICNIRP, with a mind to keeping whole-body SAR below 4 W/kg and, consequently, expected body temperature rises below 1 ºC – which is below the threshold where behavioural and physiological changes are observed in multiple studies (de Lorge and Ezell 1980, Lotz 1985, Postow and Swicord 1986, Bulman 1994, Protection 1998).

On top of this 4 W/kg SAR threshold, the ICNIRP applied a 10-fold safety factor for exposure of occupational workers, giving a safe exposure limit of 0.4 W/kg SAR. For the general population, an additional 5-fold safety factor was applied (Protection 1998). But these limits and the way they were decided upon have caused some concern among some researchers (ICBE-EMF 2022). Several issues arise when considering some of the articles cited by the ICNIRP as a basis for their guidelines. Firstly, many of the animal studies cited use relatively short exposure times (such as 40 minutes, 60 minutes or 4 hours). This is in stark contrast with human EMR exposure - which is likely to be highly frequent, be of long duration (hours) and occurring over a very long period of time for large groups of people in developed nations (Obile 2016, Ericsson 2021). In fact, most people in developed nations spend the majority of their lives at work or at home or in an urbanized environment, meaning they are likely to spend a large portion of their life being exposed to telecoms signals. Therefore, any

consequences resulting from chronic exposure lie utterly beyond the scope of acute effect studies and exposure limits that are protective against acute health effects do not necessarily guard against chronic or cumulative effects. Indeed, evidence already exists to suggest that chronic exposure below the 4 W/kg threshold may produce biologically significant changes in living organisms (D'Andrea, Gandhi et al. 1979, D'Andrea, Dewitt et al. 1986, Belyaev, Alipov et al. 1994, Belyaev 2017). For example, D'Andrea at al found that rats irradiated over the course of up to 16 weeks at 2.4 GHz at average SARs of 0.7 to 1.23 W/kg demonstrated significantly different behaviour relative to sham exposure (D'Andrea, Gandhi et al. 1979). Interestingly, this exact frequency is employed as one of the major WiFi bands and is utilised in other wireless technologies (e.g. Bluetooth) in addition to being in close proximity to several cellular network bands (e.g. 2.3 and 2.6 GHz bands). Another paper looking at genome conformational state in *E. coli* exposed to low-power density EMR, found that duration of exposure was an important factor in determining genomic responses (Belyaev, Alipov et al. 1994). A resonance effect was observed at power densities of just 10^{-19} W/cm^2. It is also worth noting that the frequencies used were in the mmWave range (41 or 51 GHz), these are higher frequencies in the mm wavelength range are a defining characteristic of 5G and future cellular network designs (Belyaev, Alipov et al. 1994, Parkvall, Dahlman et al. 2018).

Additionally, the ICNIRP guidelines make no mention of signal modulation patterns, instead focusing on frequency and power parameters (Protection 1998, ICNIRP 2020). As described earlier, modulation schemes employed in the telecoms industry can significantly influence the behaviour and nature of waveforms, raising the possibility that they be a relevant factor when considering EMR safety. This issue is something that has already been considered within the scientific community, although more work is required before any firm conclusions can be drawn about the influence of modulation on biological effects of EMR and which modulation schemes might be more biologically relevant (Foster and Repacholi 2004). But some evidence for modulation effects does already exist, particularly in the context of frequency modulation and pulsing (Pakhomov and Murphy 2000, Blackman 2009). For example, increased reactive oxygen species (ROS) and DNA damage has been linked to frequency modulation of carrier waves (Panagopoulos, Karabarbounis et al. 2021). Given the increasing variety and constant development of new, typically more complex modulation schemes, it is an area of study that is likely to continue to raise questions in the future and should be included in safety testing (Winzer 2012, Banelli, Buzzi et al. 2014, Abid, al-Azzawi et al. 2023).

The latest ICNIRP exposure limits for frequencies up to 300 GHz are shown below in table 4.

	Frequency range	Whole-body SAR (W/Kg)	Local head/torso SAR (W/Kg)	Local limb SAR (W/Kg)	Local absorbed PD (W/m²)
Occupational	100 kHz to 6 GHz	0.4	10	20	NA
	>6 GHz to 300 GHz	0.4	NA	NA	100
General Public	100 kHz to 6 GHz	0.08	2	4	NA
	>6 GHz to 300 GHz	0.08	NA	NA	20

Table 4 – current 2020 ICNIRP exposure limits for radiofrequencies above 100 kHz.

There are several things to note about these guidelines. Firstly, they are still based on the same 4 W/kg threshold with a safety factor of 10x/15x applied, originally established in 1998 (Protection 1998). That is to say, all research carried out between 1998 and 2020 and wireless technological advancement over the same period has not had any impact on the foundational harm threshold values upon which the ICNIRP bases its recommendations. It is also significant to note that the units for SAR are averaged values over specific time periods. Whole-body average SAR is to be averaged over 30 minutes and local SAR is averaged over 6-minute intervals (ICNIRP 2020). This is especially relevant to any concerns relating to modulation techniques, such as pulsing mentioned above. An assumption is being made that a continuous waveform (e.g. sinusoid) exposure for 30 minutes is functionally identical to exposure of a similar averaged power modulated waveform. The reasoning behind the ICNIRP's choice to take this view is attributed to findings from two articles which specifically investigated modulation effects (Kowalczuk, Yarwood et al. 2010, Juutilainen, Höytö et al. 2011). The 2020 ICNIRP guidelines state that "…there is no evidence that continuous (e.g., sinusoidal) and discontinuous (e.g., pulsed) EMFs result in different biological effects" based on these publications. It is certainly true that there is conflicting evidence around modulation effects (Pakhomov and Murphy 2000, Blackman 2009, Kowalczuk, Yarwood et al. 2010, Juutilainen, Höytö et al. 2011, Panagopoulos, Karabarbounis et al. 2021). But is not necessarily clearly understood why the ICNIRP has decided to favour the conclusion that EMF modulation is biologically irrelevant when only a small proportion of all modulation schemes have been studied (several types of modulation receiving no focus in literature at all). Indeed, one of the articles cited by the ICNIRP itself seems to contradict the notion that modulation effects should be ignored (Juutilainen, Höytö et al. 2011). While it does state

“...previous review in 1998 indicated that experimental evidence for modulation-specific effects of RF energy is weak” and “…the majority of recent studies have reported no modulation-specific effects”, it goes on to say “…there are a few interesting exceptions indicating that there may be specific effects from amplitude-modulated RF fields on the human central nervous system” and suggests that follow-up studies are needed (Juutilainen, Höytö et al. 2011).

It can been seen that the ICNIRP have attempted to take account of distinct absorption properties of different radiofrequencies (ICNIRP 2020). This is based largely on earlier work by Durney et al on RF dosimetry (Durney, Massoudi et al. 1986, Protection 1998). The ICNIRP used this work as a knowledge base to group radiofrequencies into 4 main absorption phenotypes based on frequency range; 100 kHz to 20 MHz, 20 MHz to 300 MHz, 300 MHz to several GHz and finally 10 GHz up to 300 GHz (Protection 1998). Generally speaking, lower frequencies are noted to penetrate tissues more deeply than higher frequencies, particularly when climbing above 10 GHz (so-called mmWave territory), where energy absorption occurs majorly at the surface of tissue, with minimal penetration (Protection 1998). This explains why the exposure limits shown in table 4 are separated into two distinct categories, up to 6 GHz and above 6 GHz (because penetration becomes less important as frequency climbs above 6 GHz towards 10 GHz, hence surface area becomes the preferred unit). This is a useful and necessary inclusion given the future plans for 5G and beyond, where frequencies in the range of tens of GHz are set to come into common use over the next few decades and surface level absorption and potential effects on skin is likely to become a major consideration (Rappaport, Xing et al. 2017, Shafi, Molisch et al. 2017, Parkvall, Dahlman et al. 2018, Naik, Park et al. 2020, Xu, Gui et al. 2021).

Epidemiology studies have a well-established history of providing good quality, meaningful evidence for disease risk factors, even in the absence of detail regarding underlying mechanisms (Greenland, Gago-Dominguez et al. 2004). Consequently, the ICNIRP guidelines make reference to many epidemiology papers, presenting evidence both for and against possible health effects of RF-EMF exposure, some of which have already been mentioned (Barron and Baraff 1958, Robinette, SILVERMAN et al. 1980, Selvin, Schulman et al. 1992, Szmigielski 1996, Council, Earth et al. 1997, Linet, Hatch et al. 1997, Protection 1998, ICNIRP 2020). Many of the epidemiology articles cited are cancer-focused and the body of work referenced for exposures up 100 kHz frequency is almost exclusively concerned with childhood cancer (Protection 1998). The effect of living in close proximity to power lines and possible association with childhood cancers is considered in detail with more than 13 articles being referenced, of which the ICNIRP concludes that findings related

to leukemia are the “most consistent”, stating; “Out of 13 studies, all but five reported relative risk estimates of between 1.5 and 3.0” (Protection 1998). This observation was mirrored by the U.S. National Academy of Sciences Committee (NAS), which the ICNIRP guidelines note led the NAS to “…conclude that children living near power lines appear to be at increased risk of leukemia” in 1996 (Council, Earth et al. 1997, Protection 1998). Other articles are mentioned, including a sizeable study with over 500 childhood cancer cases carried out in Norway, which found no association between magnetic field exposure and cancer risk (Tynes and Haldorsen 1997). But this is contrasted by two other studies the ICNIRP notes found a link between magnetic field exposure and childhood cancer (Linet, Hatch et al. 1997, Michaelis, Schüz et al. 1997). Particular praise was given to one large US study with >600 cancer patients and >600 control group members, with the ICNIRP stating “…the measurement results are suggestive of a positive association between magnetic fields and leukemia risk” (Linet, Hatch et al. 1997, Protection 1998). Despite this evidence, the ICNIRP was not convinced that the association between power line proximity and childhood cancer was due to magnetic fields resulting from power lines operation, arguing that magnetic field meter readings taken from homes of children with and without leukemia pointed to some unknown confounding factor associated with power lines (Protection 1998). This resulted in an overall conclusion that the body of epidemiology evidence investigating low frequency EMF exposure and cancer risk was “…not strong enough in the absence of support from experimental research” to form the basis of exposure guidelines (Protection 1998).

In terms of higher frequencies (100 kHz to 300 GHz), the original ICNIRP guidelines contained far less epidemiology work overall, most of which has already been discussed (Barron and Baraff 1958, Daels 1973, Cohen, Lilienfeld et al. 1977, Selvin, Schulman et al. 1992, Grayson 1996, Hocking, Gordon et al. 1996, Rothman, Loughlin et al. 1996, Szmigielski 1996, Protection 1998). Again, the majority of studies considered by the ICNIRP were focused on cancer risk, although reproductive risks were also considered (Protection 1998). Most were carried out in a military or industrial context, with the majority reporting no association between occupational EMR exposure and cancer risk or increased mortality, although Szmigielski’s paper is an exception that reported increased cancer risk (Barron and Baraff 1958, Cohen, Lilienfeld et al. 1977, Beall, Delzell et al. 1996, Grayson 1996, Szmigielski 1996). Outside of this industrial context, one of the more significant articles cited looked at mobile phone use in the general population and total mortality, finding no significant effect of mobile phone use (Rothman, Loughlin et al. 1996).

By the time the ICNIRP 2020 guidelines were published a substantial body of work had been conducted further exploring mobile phone use and disease risk, including animal and human

subjects and with a particular focus on various types of brain tumours, a fact acknowledged by ICNIRP itself (Group 2010, Aydin, Feychting et al. 2011, Group 2011, Pettersson, Mathiesen et al. 2014, Falcioni, Bua et al. 2018, TR 2018, ICNIRP 2020). This is largely due to the increased exposure of the head due to how mobile phones are commonly held pressed against one side of the head. Of those articles considered using animal models, two using rat models reported carcinogenesis effects associated with chronic exposure to telecoms signals (Falcioni, Bua et al. 2018, TR 2018). But the ICNIRP points out that relatively high power fields were used in both studies, where the most significant effects were only seen in the high dosage groups, for example a 50 V/m field promoting heart tumours (Falcioni, Bua et al. 2018, TR 2018). This is a valid criticism to make, given that in the UK a person would likely need to spend long periods of time closer than ~8m to a base station or mere centimetres distant from microcell stations in order to chronically receive exposures above the limits set by the ICNIRP (Mann, Cooper et al. 2000). But it is worth noting that some carcinogenicity was reported with a dose equivalent to a SAR of 1.5 W/Kg, with no working theory to attribute this to heating effects, leaving the possibility of DNA damage through alternative means open (TR 2018).

In terms of new epidemiology contributions in the context of cancer risk, the ICNIRP notes that "...A large number of epidemiological studies of mobile phone use and cancer risk have also been performed", but goes on to criticise the approach taken by most of these articles (ICNIRP 2020). The case-control design and retroactive, self-reported mobile phone use history is suggested as a central issue, with concerns around implicit recall bias and how it may impact the investigative weight of any potential outcomes (ICNIRP 2020). There are many examples of such work, with many, but not all, reporting an increase in brain cancer risk correlating with mobile phone use (Hardell, Hallquist et al. 2002, Hardell, Mild et al. 2006, Hepworth, Schoemaker et al. 2006, Lahkola, Auvinen et al. 2007, Lahkola, Salminen et al. 2008). Interestingly, the ICNIRP guidelines do not cite specific articles when referring to this large body of epidemiology work, choosing instead to focus on a few cohort studies regarded as being exceptions to this problematic study design (Group 2010, Group 2011, Pettersson, Mathiesen et al. 2014, ICNIRP 2020). The two cohort studies highlighted are the Interphone study, conducted by the International Association for Research on Cancer (IARC), and a Swedish case-control study of acoustic neuroma, with particular attention paid to the Interphone study (ICNIRP 2020). There is good reason for this, as, to date, the Interphone study does represent one of the most robust and complete epidemiology investigations into mobile phone use and disease risk, receiving a large number of citations by many researchers and being widely regarded as a high value contribution to the field (Group 2010, Group 2011, Swerdlow, Feychting et al. 2011). The ICNIRP says of the

Interphone study that it "…did not provide evidence of a raised risk of brain tumours, acoustic neuroma, or parotid gland tumours among regular mobile phone users, and the risk estimates did not increase with longer time since first mobile phone use". But the study did report an increased risk of cancer for the heaviest users of mobile phones with the highest cumulative call times (Group 2010, Group 2011). The ICNIRP is sceptical of this highest exposure group finding, arguing that all other exposure levels showed no such association and that the second highest cumulative exposure group produced some of the lowest odds ratios (ICNIRP 2020). It is not clear why patterns observed in one exposure group should be taken as directly informative about what is reported within a separate group, given that they are different exposures, it is reasonable to expect they might produce different outcomes which are valid in their own right. It is also interesting to note that findings derived from some exposure conditions appear readily accepted as presented by the ICNIRP, with no such comparisons or arguments deemed necessary (ICNIRP 2020). It could also be said that the conclusion of the ICNIRP is in conflict with the view taken by the IARC itself, the WHO research body that conducted the Interphone study. Shortly after the publication of the Interphone study, the IARC chose to classify RF-EMFs as possibly carcinogenic to humans (Cancer 2011). This stance has since been fortified by several reviews which indicate a possible association between RF exposure and cancer risk (Prasad, Kathuria et al. 2017, Yang, Guo et al. 2017, Bortkiewicz 2019).

This arguably dismissive stance towards cancer risk is one example of decision making and reasoning given by the ICNIRP that has led some scientists to raise concerns about possible bias and lack of adequate basic researcher representation within EMF regulatory bodies (Hardell, Nilsson et al. 2021, ICBE-EMF 2022, Nordhagen and Flydal 2023). A central and consistent argument behind this concern is that a significant and growing body of evidence pointing to several biological effects of sub-thermal RF-EMFs appears to be largely ignored or dismissed (ICBE-EMF 2022). For example, the accepted baseline harm threshold of 1 W/kg SAR (onto which safety factors are applied) appears to be contradicted by numerous behavioural studies that have reported disturbances to Central Nervous System (CNS) function with EMF doses below 1 W/kg SAR, troublingly, with one paper discovering effects with a dose as low as 0.016 W/kg (Schneider and Stangassinger 2014, Tang, Zhang et al. 2015, Razavinasab, Moazzami et al. 2016). Reporting of radio EMF health effects are by no means restricted to nerves or electrophysiology, or indeed animal models. Human examples of health effects include a lot of work done investigating sperm cells, which are known to be highly sensitive to DNA damage and radiation exposure – both ionizing and RF in origin (Mandl 1964, Agarwal, Desai et al. 2009, Kesari, Agarwal et al. 2018). Several meta-analyses of existing literature have drawn a possible link between mobile phone signal

exposure and a reduction in male fertility (Adams, Galloway et al. 2014, Kim, Han et al. 2021, Yu, Bai et al. 2021). Regardless of the cellular context, cancer or neurological or gametes, a clearly stated reservation of the ICNIRP is due to a lack of mechanistic offerings from basic research (Protection 1998, ICNIRP 2020). Essentially, it is the view of the ICNIRP that, in their consideration, because no mechanism of action for low-power (sub-thermal) RF-EMF exists to explain reported health effects, it cannot be accepted that RF-EMF exposure is the causative agent in these instances – because it is not firmly established how it could do this (ICNIRP 2020). This viewpoint was affirmed by the ICNIRP in 2009 in the context of DNA damage, stating "…low energy photons of RF radiation are too weak to affect ionization or cause significant damage to biological molecules such as DNA" (Vecchia, Matthes et al. 2009). Strictly speaking, this is a truthful statement that accurately describes how low frequency radiation behaves. But it is a conclusion directly contradicted by many studies specifically investigating this issue, a body of work effectively summarised by Lai and colleagues in 2021 (Lai 2021). They assessed the work of over 150 publications and indicated the potential of sub-thermal RF-EMF to harm genetic material, saying that cellular responses "...are consistent with the findings that EMF causes genetic damages" (Lai 2021).

Although it is true that a specific, detailed mechanism of action for harm causation of sub-thermal RF-EMR does not currently exist, there are certainly clues to how it might work and educated guesses can be made based on the likely interaction partners of electromagnetic waves. For example, voltage-gated ion channels have long been suspected as possible players in the action mechanism of RF-EMF biological effects (Bauréus Koch, Sommarin et al. 2003). If these fields can influence ion channel behaviour, the next logical step is that intracellular and extracellular ion concentrations might be affected, which is known to influence various cellular responses (Yu-Hong, Yong et al. 2007, Zhao, Yang et al. 2008). From a first principles point-of-view, it stands to reason that electric and magnetic field oscillations that comprise an electromagnetic wave might be able to exert influence over proteins that are sensitive to nearby electric potential changes. Similarly, small charged particles, such as electrons, can themselves be directly influenced by EM waves. This is the underlying principle behind how Faraday cages work – the free electrons of electrically conductive material orient themselves so as to counteract fluctuations in the electric and magnetic fields of an incoming EM wave, as a form of electrostatic induction (Chapman, Hewett et al. 2015). But seemingly little or no research exists into this topic, perhaps due to difficulty of experimental design or because the low-power nature of telecoms signals makes measurable effect detection unlikely. Although, somewhat similar ideas regarding ion manipulation have been previously proposed in the context of membrane potentials (Panagopoulos, Karabarbounis et al. 2002). It is worth noting that other evidence further

implicates membranes and membrane permeability as being a good area to explore for mechanistic understanding of RF-EMFs, such as the apparent disruption of the blood brain barrier integrity by EMFs, which manifests as altered permeability across the barrier (Oscar and Hawkins 1977, Salford, Brun et al. 1994, Tang, Zhang et al. 2015).

But perhaps one of the most well-researched and characterised candidates for possible biological action mechanisms of these signals comes in the form of ROS dysregulation and redox homeostasis disruption (Repacholi and Greenebaum 1999, Jajte, Grzegorczyk et al. 2002, Oktem, Ozguner et al. 2005, Akdag, Bilgin et al. 2007, Simkó 2007, Kovacic and Somanathan 2010, Consales, Merla et al. 2012). Which, when combined with the likely high exposure of the head to mobile phone signals, suggested EMF electrophysiological effects, blood brain barrier disturbance, possible alterations to neurotransmitter levels and inherently high metabolic activity and sensitivity of neurons, taken as a whole, points to neurons as being of particular concern in the context of health risks associated with EMR (Hardell, Hallquist et al. 2002, Hossmann and Hermann 2003, Ferreri, Curcio et al. 2006, Khadrawy, Ahmed et al. 2009, Noor, Mohammed et al. 2011). However, it is important to point out that neuronal EMF exposure evidence is by no means completely uniform and clear. This is best demonstrated by reports that point to possible neuroprotective effects of some types of exposure, in specific contexts (Consales, Merla et al. 2012). For example, Arendash et al shockingly reported in 2010 that long term exposure to mobile phone signals (up to 9 months, ~900 MHz frequency at 0.25 W/kg SAR) appeared to confer cognitive benefits and protect against neurodegeneration using a mouse model of Alzheimer's disease (Arendash, Sanchez-Ramos et al. 2010). This was followed-up with another study, in which elderly mice with particularly heavy Amyloid beta pathology were exposed to long term RF-EMFs and a remarkable reduction of Amyloid beta deposition was observed, coupled with some cognitive benefits and an apparent lack of oxidative stress burden (Arendash, Mori et al. 2012). But these findings have yet to be replicated in normal, healthy mice and may be an experimental artefact somehow associated with the transgenic model being used.

It is worth pointing out that, if time and evidence proves oxidative stress to be a real consequence of telecom signal exposure, it would provide an obvious link between exposure and various health consequences, some of which are described above, because oxidative stress is a well-known driver of many different diseases and ailments in humans (Spector 2000, Forman and Zhang 2021). Notably, this includes cancer, so demonstration of oxidative stress promotion would provide a causal link to DNA damage and subsequent cancer risk increases previously outlined within ICNIRP reports, as it is firmly established that excess ROS generation and oxidative stress can lead to significant DNA damage and promote

cancer (Kang 2002, Barzilai and Yamamoto 2004, Kryston, Georgiev et al. 2011). But it is fair to say the overall picture of safety research relating to the telecoms industry and the signals used within it is one with filled with conflicting evidence, multiple viewpoints, agendas and is lacking a clear, decisive consensus (Protection 1998, ICNIRP 2020, ICBE-EMF 2022). The aim of basic research must be to try to identify the energy threshold at which biological effects begin to occur and prove beyond any reasonable doubt that they do occur at that threshold. This is very difficult to do in a way that effectively marries basic research findings to real world conditions, in large part because the specific detail of the types of exposure people receive in real world scenarios can be so diverse and is constantly changing as telecoms technology advances (e.g. 5G NR). The underlying assumptions made by the ICNIRP and other regulatory bodies about signal parameters not meaningfully influencing health risk must also be investigated, particularly in light of the new, higher frequencies being implemented in much of the developed world (e.g. 5G NR 20-70 GHz frequency bands). These new mm wavelengths will have higher photon energy, require much denser cell networks and will exhibit vastly different absorption and penetration properties when compared to older generations, such as the 800 MHz band of 4G (Rappaport, Xing et al. 2017, Shafi, Molisch et al. 2017, Parkvall, Dahlman et al. 2018, Naik, Park et al. 2020). These safety research objectives need to be achieved in a timely manner, because industry will continually innovate and refine, focusing on improving data performance metrics and almost certainly continuing the trend of increasing signal density and exposure for most people – all while operating on the premise that this technology is safe, provided exposure stays within the ICNIRP limits (White 2010, Obile 2016, Ericsson 2024).

As a final note, it is worth considering that the monetary value of the global smartphone industry alone is approximately $500 billion and rising, with the total value of all wireless internet technology (WiFi, modems, routers, Bluetooth devices, wireless network cards etc) likely far exceeding this number (Statista 2024). If overwhelming evidence of biological effects of telecoms signals emerges, the adjustment of exposure guidelines in favour of more strict regulations is likely to be met with resistance from industry. This behaviour has been demonstrated by large corporations numerous times in other industries with a similarly high market value, such as the tobacco or pharmaceutical industries, where lobbying and campaigning can significantly interfere with the function of governments and regulatory bodies (Saloojee and Dagli 2000, Markussen and Svendsen 2005, Wouters 2020). This external pressure can result in disruption or delays to; identification and acceptance of public health risks by relevant authorities, formulation of regulations or laws to safeguard against potential health risks and proper implementation and enforcement of such regulations or laws (Saloojee and Dagli 2000). As the body of work dedicated to exploring possible

biological effects of EMFs develops, the scientific community and policy makers will need to be robust against any potential external pressures seeking to uphold the view that telecoms signals are safe for continued financial gain.

1.3 Neurons

As briefly outlined in the previous section, brain cells are of particular interest when considering exposure to telecoms signals, in large part due to mobile phone positioning against the side of the head leading to high exposure (Hardell, Hallquist et al. 2002, Hossmann and Hermann 2003, Salford, Brun et al. 2003, Zhao, Zou et al. 2007, Iqbal-Faruque, Aisyah-Husni et al. 2014, Razavinasab, Moazzami et al. 2016). The brain is an organ that serves as the centre of the nervous system in most animals, receiving and processing sensory information, manifesting emotions and cognition and controlling motion through muscle contractions, among many other critical functions (Eccles 1973, Squire, Berg et al. 2012). In humans, it has long been identified as the seat of consciousness, the physical basis for all emotion, memory and thought – more than any other thing, it is what makes us who we are and is responsible for a sense of self (Squire, Berg et al. 2012). As with all organs, it is comprised of several cell types, working in concert to achieve this outcome of function. These brain cells are split into two categories, glial cells and neurons. Glial cell types include; ependymal cells, astrocytes, oligodendrocytes and microglia (Squire, Berg et al. 2012). Their role is only partially understood, but in broad and simple terms they are traditionally thought to play a largely supportive role towards neurons – aiding their survival and facilitating function (Squire, Berg et al. 2012). But their role is not entirely restricted to supporting neurons. For example, astrocytes are known to be capable of communicating with neurons via chemical signalling, modulating their function (Bezzi and Volterra 2001). More work is required to fully and completely characterise their biological role.

But it is neurons that are the electrically active, excitable cells that have evolved to use the firing of action potentials to send and receive signals, communicating with various other cells, tissues and organs to regulate function, control the body and store information (Levitan and Kaczmarek 2002). There are many different types of neurons, with hundreds of named types already existing and work towards identification of all types continuing as its own specialised field (Masland 2004, Zeng and Sanes 2017). Classification of neurons is not simple and very subtle variations in cellular structure and physiology exist, which is additionally confounded with complicated naming systems that are not universal among all areas of research (Stevens 1998, Masland 2004, Bota and Swanson 2007, Zeng and Sanes 2017). As is the case in most areas of biology, one of the most common ways of attempting to distinguish one neuronal cell type from another is to look at morphology and structure – because molecular or cellular structure is typically a powerful predictor of function, as observed in protein folding (Hegyi and Gerstein 1999, Orengo, Todd et al. 1999, Masland

2004). When adopting this structural view, the clearest and most important distinction is between what are known as “intrinsic” and “projection” neurons (Masland 2004). Intrinsic neurons are those which only form connections, or synapses, where their main cell body, or soma, is located. Projection neurons are those which form long protrusions, called axons, that grow outwards and away from their soma – allowing them to form synapses at distance from the main cell body (Masland 2004). But neurons may also be classified by several other means, such as physiological role or by the number and nature of synapses. Examples of such classifications include; motor neurons, sensory neurons, relay or interneurons, unipolar neurons, bipolar neurons or multipolar neurons (Zeng and Sanes 2017). Figure 6 below gives a diagrammatic representation of some of these commonly used neuron classifications.

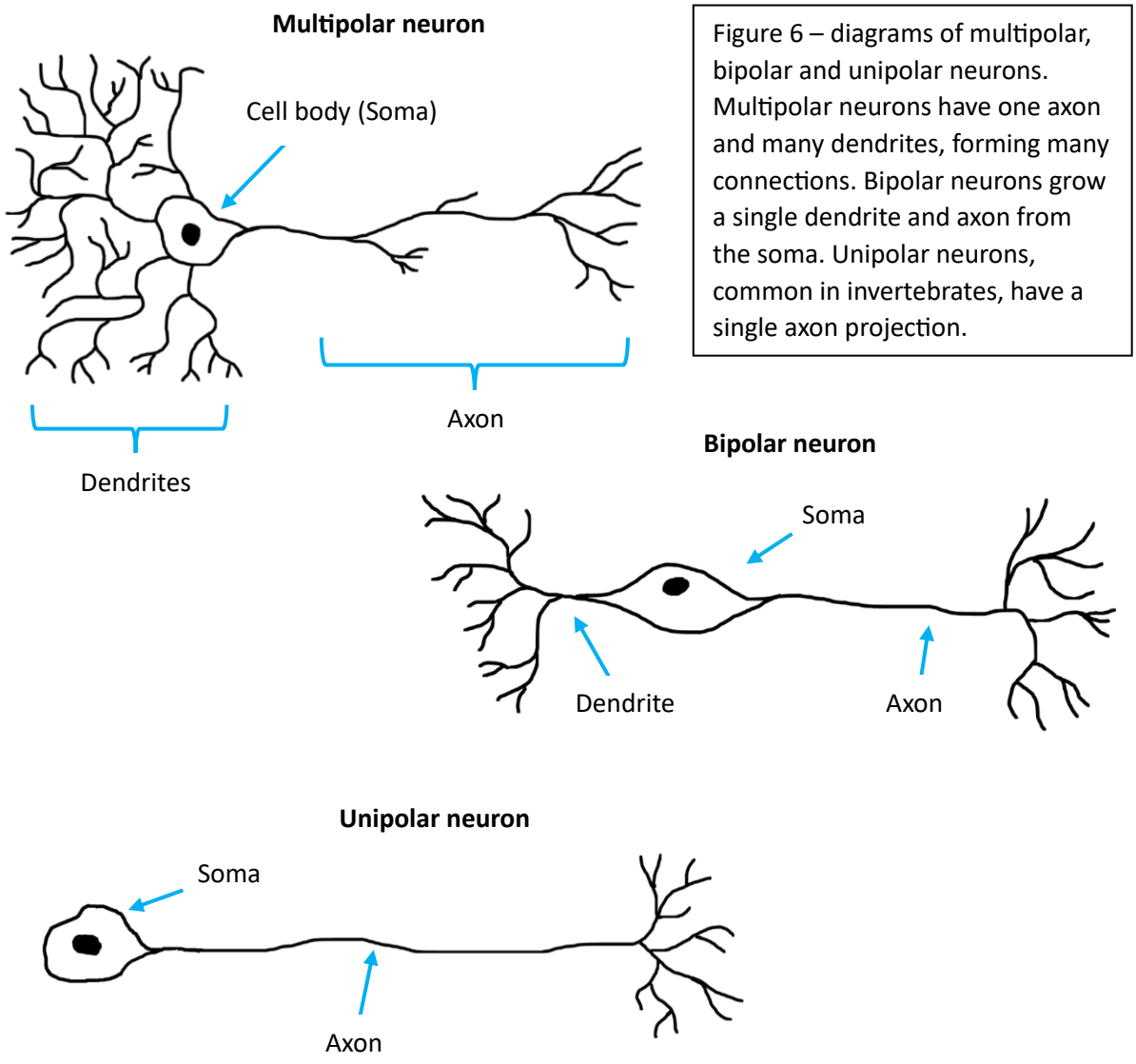

Figure 6 – diagrams of multipolar, bipolar and unipolar neurons. Multipolar neurons have one axon and many dendrites, forming many connections. Bipolar neurons grow a single dendrite and axon from the soma. Unipolar neurons, common in invertebrates, have a single axon projection.

But the true picture of neuron diversity is very broad, with three main approaches of classification being utilised; morphological, electrophysiological and molecular expression profiling (Zeng and Sanes 2017). Morphological classification approaches are the oldest and, arguably, most intuitive way to tell neurons apart. Early work carried out by famous neuroscientist Santiago Ramon y Cajal and colleagues made heavy use of Golgi stain to visualise neurons in dramatic detail towards the end of the 19th century (y Cajal 1902, DeFelipe and Jones 1992, Masland 2004). Even at this early stage, Santiago Ramon y Cajal was keen to explore the relationship between structure and function, showing how the morphology of neurons greatly informs their physiological role (y Cajal 1902). A clearly articulated example of this is shown in the crossing of the retinal nerves in humans, in order to correct visual distortions that would otherwise result from evolving eyes that have poor overlap of their fields of vision (y Cajal 1902, DeFelipe and Jones 1992). He was also one of the first researchers to investigate the compartmentalisation of the brain, illustrating how different regions may develop unique, tightly organised clusters of neurons arranged into specialised biological circuits (y Cajal 1902, DeFelipe and Jones 1992). One of the most striking and morphologically distinct neuronal cell types is the Purkinje cell, named after Czech anatomist Jan Evangelista Purkyně, who first identified them in 1837 (Purkinje 1837). They are abundant in the cerebellum of the human brain and exhibit tremendous and extensive networks of dendrites, making them some of the largest neurons in the brain (McKay and Turner 2005). These vast, complex and interwoven networks of dendrite projections are responsible for co-ordination of movement using sophisticated interlinked firing patterns and subsequent excitability modulation (Gilbert and Thach 1977, Ojakangas and Ebner 1992, Barash, Melikyan et al. 1999, Xu-Wilson, Chen-Harris et al. 2009, Herzfeld, Kojima et al. 2015). This mechanism of action has recently begun to be elucidated in some detail, for example, in the context of eye movement (Herzfeld, Kojima et al. 2015). Although, there is a long way to go before the full method of movement control by Purkinje cells is characterised, Herzfeld and colleagues are some of the first researchers to detail how movement is encoded in the brain and thereby tie together the elaborate forms of Purkinje cells and their biological role (Herzfeld, Kojima et al. 2015).

Another important factor to consider for neuron classification is electrophysiology, which is, potentially, particularly important in the context of exposure to EMFs (Yu-Hong, Yong et al. 2007, Bertagna, Lewis et al. 2021, Panagopoulos, Karabarbounis et al. 2021). More specifically, the resting potential and firing rate of neurons can vary greatly between different types of neurons (Zeng and Sanes 2017). But to explore these characteristics, we must first introduce the idea of neuron action potentials. Action potentials are, essentially, biology's way of sending electro-chemical signals, or impulses, through neuronal projections to axon

terminals, where a chemical signal may then be released to communicate with nearby neurons, modulating their activity in some way (Barnett and Larkman 2007, Grider, Jessu et al. 2019). This process begins with the resting potential, a physiological phenomenon first described by Hodgkin and Huxley in 1939 using the nerve of a giant squid (Hodgkin and Huxley 1939). They famously reported a transmembrane electric potential of -60 mV inside the nerve axon relative to outside, under resting conditions. Later research has since identified the molecular basis of how this is maintained – transmembrane ion channels that restrict and control the passage of ions (K+, Na+ and Ca2+, for example) across the plasma membrane (Barnett and Larkman 2007, Grider, Jessu et al. 2019). Because it is differences in the concentrations of ions inside and outside the cell that cause this resting potential to arise, i.e. it is an electrochemical gradient across the membrane (Barnett and Larkman 2007, Grider, Jessu et al. 2019). This resting membrane potential exists in all cells, due to this electrochemical gradient, and typically remains fairly constant, with the main exceptions being electrically active or “excitable” cells that may undergo rapid changes in membrane potential during a process called depolarisation or hyperpolarisation, which takes place during the initial phase of an action potential (Barnett and Larkman 2007, Grider, Jessu et al. 2019). This electrical excitability and capacity to fire action potentials is the main defining characteristic of all neurons, regardless of specific type, a trait shared with few other cell types (e.g. muscle cells). The four main phases of a typical action potential are as follows;

- Depolarisation
- Repolarisation
- Hyperpolarisation
- Refractory period

Depolarisation occurs in response to various stimuli that may cause a deviation from the resting membrane potential. In neurons, a classic example would be synaptic input from nearby neurons, such as the release of excitatory signalling molecules called neurotransmitters from axon terminals of adjacent neurons at a synaptic interface (Barnett and Larkman 2007, Grider, Jessu et al. 2019). There are many types of neurotransmitters, with some exhibiting excitatory effects (such as Glutamate) and others exhibiting inhibitory effects (such as Gamma-aminobutyric acid or GABA), but they may also act as either excitatory or inhibitory in a context dependent manner (Hyman 2005). Excitatory signals are those which make an action potential more likely to occur in affected neurons, i.e. they modulate ion channel behaviour in affected neurons in a way that moves the membrane potential towards the firing threshold – the membrane potential at which an action potential will be initiated and rapid depolarisation will occur (Hyman 2005, Barnett and Larkman

2007). Inhibitory signals have the opposite effect, reducing the likelihood of action potential firing. If sufficient excitatory signals are received by a neuron such that the firing threshold is reached, rapid depolarisation occurs as a result of the activity of voltage-gated ion channels (Barnett and Larkman 2007, Grider, Jessu et al. 2019). These channels are sensitive to electrochemical activity and may adopt either open or closed conformations depending on the electrochemical gradient that exists across the plasma membrane. Depolarisation is, in effect, the opening of these channels in response to reaching the firing threshold such that they allow the rapid flow of positive ions (e.g. Na+) into the cell down their electrochemical gradient – creating a positive feedback loop that leads to more channels opening and manifesting the large and rapid depolarisation observed during the start of an action potential (Barnett and Larkman 2007, Grider, Jessu et al. 2019). A common value of the resting potential of neurons in the human brain is -70 mV, with a firing threshold of -55 mV, but this may vary significantly between different neurons (Barnett and Larkman 2007). Depolarisation can result in a very large upwards swing in membrane potential, before reaching a peak of approximately +40 mV in a typical neuron, although, again, the exact value may vary significantly dependent upon context.

Reaching this peak value signals the entry into the next phase of an action potential; repolarisation. This is essentially a reversal of the depolarisation phase – where previously opened voltage-gated channels close in response to the changed membrane potential, cutting off the flow of ions into the cell. It also leads to the opening of other voltage-gated ion channels, such as voltage-gated K+ channels, which allows potassium ions to begin to rapidly flow out of the cell into the extracellular space down their own electrochemical gradient, causing a rapid decline in the membrane potential that often overshoots the resting potential, resulting in a state called hyperpolarisation (Barnett and Larkman 2007, Grider, Jessu et al. 2019). This state essentially overlaps with the refractory period – the final phase of an action potential where neurons become extremely resistant to generation of a new action potential and where most voltage-gated ion channels become inactivated or closed (Barnett and Larkman 2007, Grider, Jessu et al. 2019). It is also the phase where neurons begin to restore the resting membrane potential, an active process that requires significant ATP energy input to pump ions against their electrochemical gradient via the constant activity of ion transport proteins, such as the sodium-potassium pump, or Na+/K+-ATPase (Barnett and Larkman 2007, Grider, Jessu et al. 2019). As neurons return to the resting state, they exit the refractory period and become sensitive to stimuli once more, ready to repeat the cycle of events and fire another impulse. The entire process of an action potential occurs over short timescales measured in fractions of a second, with some rapidly firing neurons being capable of generating bursts of activity, firing many times in less than a

second (Grace and Bunney 1984, Krahe and Gabbiani 2004). In addition to being a useful tool for distinguishing neuron subpopulations from each other, these impulse firing patterns have also been revealed to be an important feature of encoding information in the brain – i.e. the "neural code" of the human brain has a significant temporal element (Engel, König et al. 1992, Gerstner, Kempter et al. 1996, Gerstner, Kreiter et al. 1997, Ainsworth, Lee et al. 2012).

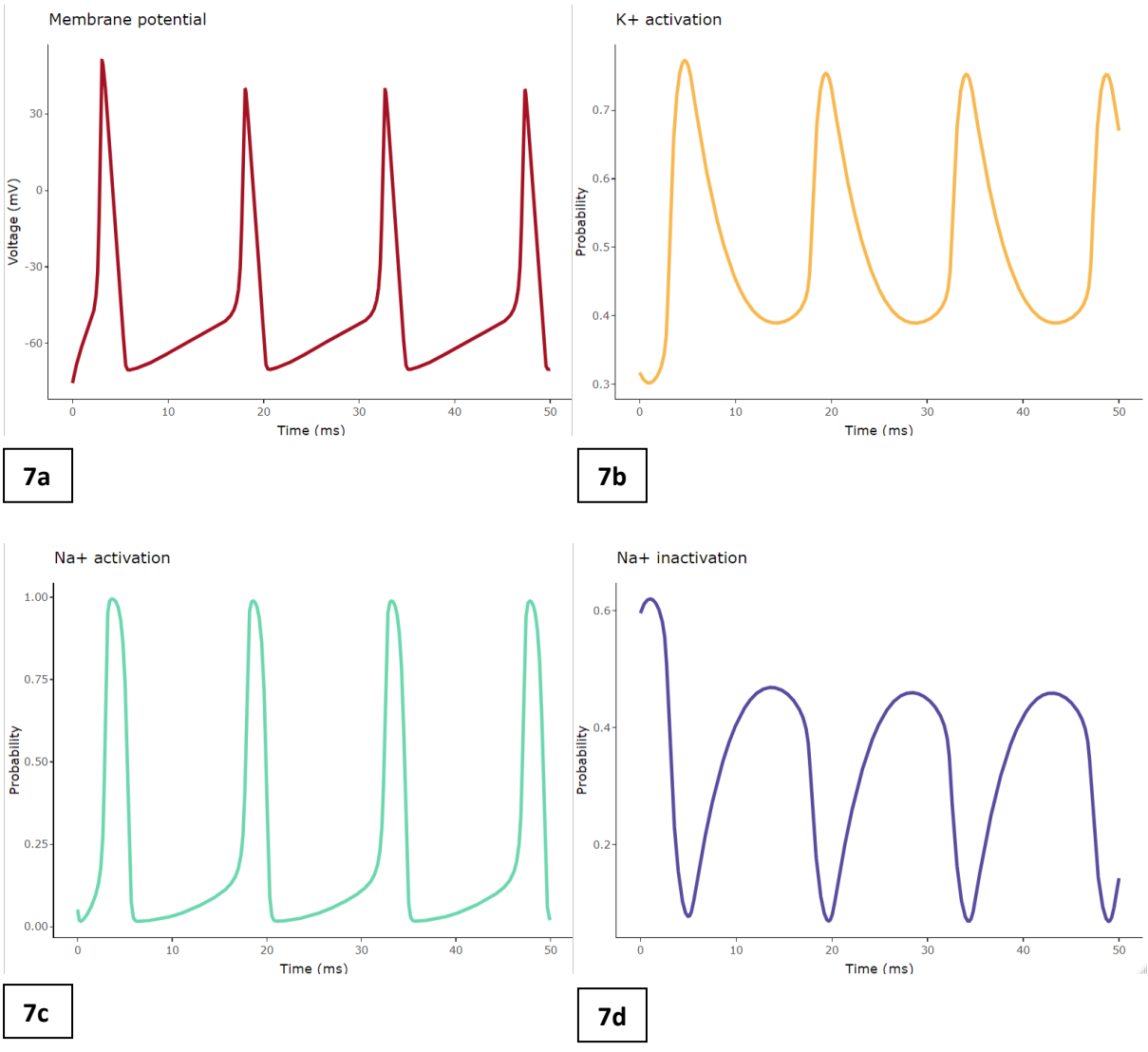

Figure 7 – a typical action potential firing pattern following external stimulus, generated using the Hodgkin and Huxley model. **7a** shows the membrane potential change, **7b**, **7c** and **7d** show ion channel behaviours. Credit to https://www.r-bloggers.com/2021/05/propagating-nerve-impulse-in-hodgkin-huxley-model-modeling-with-r-part-1/ for providing adapted base code.

The last major method for neuron classification is to look at molecular and expression profiles (Zeng and Sanes 2017). Due to advances in experimental approaches, particularly in the realm of transcriptomics, it has become possible to probe the genetic expression profile of individual neurons with relative ease (Zeng and Sanes 2017). A good example of this is high throughput single-cell RNA-sequencing (scRNA-seq), which can produce a vast array of expression profiles representative of thousands of individual neurons (Zeng and Sanes 2017). Using these approaches, distinct subpopulations of neurons have emerged, each possessing their own clusters of genetic expression – helping to differentiate neuron types that may exhibit similar electrophysiological or morphological phenotypes. Of course, these various factors can also inform each other. For example, the expression profile of ion channels can and will greatly influence the electrophysiology of a given neuron (Chen, England et al. 1998, Schulz, Temporal et al. 2008, Zeng and Sanes 2017).

Regardless of the specific type of neuron, they all share the trait of being electrically active and have the capacity to fire impulses, as described above. To restore and maintain the resting membrane potential and fire impulses requires significant energy investment in the form of ATP, which is why all neurons have some of the highest energy demands of all cells and why the brain itself is one of the most energy-consuming organs in the human body (Rolfe and Brown 1997, Magistretti, Pellerin et al. 1999, Attwell and Laughlin 2001, Niven 2016). This is best expressed by the observation that the brain accounts for just 2% of the total mass of a typical human body, but approximately 20% of the entire body's energy consumption at rest may be attributed to the brain (Attwell and Laughlin 2001). But it is worth noting that despite these high energy demands, the pervading view of neuroscience literature is that the brain operates and processes information in an overall efficient manner, where trade-offs between information processing performance and energy consumption have evolved (Levy and Baxter 1996, Sengupta and Stemmler 2014, Niven 2016, Yu and Yu 2017). This high demand for chemical energy also explains why neurons are sensitive to disturbances in energy metabolism, or more precisely, disorders relating to the mitochondria organelle (Schon and Manfredi 2003, Schapira 2006, Chaturvedi and Beal 2013). This is because the mitochondria is the primary site of ATP generation through the process of oxidative phosphorylation via the electron transport chain (ETC) (Guo, Gu et al. 2018, Zhao, Jiang et al. 2019). So, mitochondrial dysfunction can lead to failure to meet the energy demands of neurons, resulting in neuronal dysfunction and, ultimately, loss of neurons, degeneration of the brain and manifestation of medical conditions such as Parkinson's disease, Alzheimer's disease or motor neuron disease (Chaturvedi and Beal 2013).

Interestingly, the mitochondria is also commonly regarded as one of the major sites of physiological ROS generation – i.e. the ETC generates a relatively low-level of ROS due to rare reactions involving electrons as they progress through the chain of protein complexes that comprise the ETC (Lambert and Brand 2009). Under physiological conditions, cells have evolved to utilise these reactive species, and others from alternative sources such as peroxisomes, in various processes such as intracellular signalling pathways and activation of adaptive genetic responses (Camoes, Bonekamp et al. 2009, Brieger, Schiavone et al. 2012, Di Meo, Reed et al. 2016). But if the balance between reactive species generation and clearance or metabolism is perturbed in favour of increasing levels of reactive species, it proves harmful to cells and they may enter a state of oxidative stress, an outcome heavily associated with neurodegenerative disorders mentioned above (Chaturvedi and Beal 2013, Di Meo, Reed et al. 2016). The observation that nonthermal EMF exposure may promote generation of ROS implicates the mitochondria as a high value investigative target when exploring EMF safety and possible biological effects – and by extension also elevates neurons to high value status as a cellular model and investigative tool, due their uniquely high bioenergetic sensitivity and strict reliance on effective mitochondrial function (Repacholi 1998, Jajte, Grzegorczyk et al. 2002, Schon and Manfredi 2003, Oktem, Ozguner et al. 2005, Akdag, Bilgin et al. 2007, Simkó 2007, Consales, Merla et al. 2012, Sengupta and Stemmler 2014, Niven 2016).

In basic research various models are utilised to investigate neuronal health, each with their own set of benefits and drawbacks. Three of the most popular and widely used types of cellular investigative tools are; primary human cells, animal cells or human cancer cell lines. In the context of neurons, these include very rare primary human neurons, sourced directly from medical operations or donors and containing a variety of cell types (neurons and glial cells), cells harvested from animal brains, which are also heterogenous, or human cancer cell lines (Banker and Cowan 1977, Gordon and Amini 2021, Goshi, Morgan et al. 2022). Primary human cells are prized for their likeness or close proximity to how our cells exist in their natural state in our brains, i.e. there is only a relatively small degree of abstraction between cultured primary neurons and somatic cells. This makes them the most “translatable” of all available cellular tools, giving the highest likelihood of accurately reflecting what occurs in our bodies and producing the most relevant findings (Gordon and Amini 2021). But there are several significant disadvantages to using primary neurons. Firstly, they are very difficult to source (Gordon and Amini 2021). Because they may only be obtained from rare medical events or donation, very few are available to the scientific community at any given time. This is coupled with the fact that there is a high demand from various groups to use them if and when they are made available – meaning obtaining them

is not a practical possibility for many scientists. Additionally, depending on the location of researchers, they are also likely to meet stringent ethics approval processes, which further complicates procurement. A second major consideration is the purity of primary cultures. It is not always desirable to have co-cultures of brain cells, which may mean an additional step of specific cell type isolation is necessary – which is not always easy to do and may result in less robust cells, i.e. neurons rely on glial cells for support and can be difficult to maintain in isolation (Brewer 1997, Katzenell, Cabrera et al. 2017, Park, Schweder et al. 2020, Gordon and Amini 2021). Finally, primary cells are generally far less robust and have far slower growth cycles than the majority of cell lines (Gordon and Amini 2021). This can manifest in higher sensitivity to additives designed to suppress microbial contamination, increasing risk of contamination, reduced cellular viability or even loss of entire sample cultures due to their relatively delicate constitution. This is especially true when hoping to culture primary cells over a longer period of time, which is far more challenging than most other cellular models (Mains and Patterson 1973, Ray, Peterson et al. 1993, Gordon and Amini 2021).

Brain cells harvested from animal models have some similarity with human primary brain cultures. They too may require additional purification or isolation steps and may also exhibit high sensitivity and reduced proliferation when compared to cell lines, meaning long-term cell culture may prove especially challenging (Mains and Patterson 1973, Ray, Peterson et al. 1993, Brewer 1997, Brewer and Torricelli 2007, Gordon and Amini 2021). But there are several key differences when compared to human primary cells. Firstly, there is an additional level of abstraction when attempting to make inferences based on observations made in non-human cells, i.e. what occurs in rat or mouse neurons may not be reflective of human cell biology because of interspecies differences. This, arguably, makes work performed with animal models less translatable than work done with human cells (Gordon and Amini 2021). This is a view reinforced by the observation that many neuroprotective therapies that are reportedly effective in animal models do not prove successful in human trials, e.g. in the context of strokes, roughly 1 in 500 drug candidates suggested by rodent models may progress through human clinical trials to market (O'Collins, Macleod et al. 2006). But it is hard to gauge how much of this candidate attrition may be attributed specifically to animal models, as other approaches also demonstrate high attrition rates in the pharmaceutical development pipeline, regardless of candidate origin (Kola and Landis 2004, Waring, Arrowsmith et al. 2015). It is difficult or impossible to fully account for these many and varied interspecies differences, but non-human animal cells are nonetheless functional somatic cells and have a good likelihood of proving informative about human conditions, even if they do not have a high yield of human drug candidates (Chesselet and Carmichael 2012, Gordon and Amini 2021). One advantage animal models have compared to human primary

cells is their improved availability. Although, there are still strict ethical approval processes involved with their use, procurement of animal brain tissues, such as rat or mouse, is typically easier when compared to human primary cells, as they have a well-established history of use in neurological research and are widely utilised (Chesselet and Carmichael 2012, Gordon and Amini 2021).

Another popular option is to use human cancer cell lines as an investigative tool, such as the neuroblastoma patient, bone-marrow cancer derived SH-SY5Y cell line (Kovalevich and Langford 2013). This option is significantly different from primary cells and animal models, in large part due to the genomic volatility and aberrant cellular biology that is characteristic of cancer cells (Negrini, Gorgoulis et al. 2010, Yao and Dai 2014). Despite being human cells, this adds a significant level of abstraction from healthy, functional somatic cells, with frequent debate arising regarding their clinical relevance outside of cancer contexts, which they are more directly related to (Gillet, Varma et al. 2013, Kovalevich and Langford 2013, Wilding and Bodmer 2014, Mirabelli, Coppola et al. 2019). But regardless of this debate, they are the most widely used cell model and have proven useful in many areas of basic research (Jämsä, Hasslund et al. 2004, Xicoy, Wieringa et al. 2017, de Medeiros, De Bastiani et al. 2019, Mirabelli, Coppola et al. 2019, Gordon and Amini 2021). One of the major advantages cell lines have is their tendency to be highly robust and that they often demonstrate favourably rapid and long-term proliferation potential relative to other cell models (Kovalevich and Langford 2013, Mirabelli, Coppola et al. 2019, Gordon and Amini 2021). This can make them far easier to culture and significantly increase the pace of investigative progress. They are also relatively easy to procure and their use is subject to far less stringent control processes when compared to primary cells or animal models, effectively lowering the barrier to their usage (Andersen and Winter 2017).

Overall, different cellular approaches to neurological research questions are typically a trade-off between how directly translatable they are to somatic cells and ease of use and availability (Gordon and Amini 2021). Human cancer cell lines offer basic researchers an easy route of entry to a research topic and make for an excellent starting point to any new investigation – before graduating to animal models or primary human cells for validation of any potentially meaningful research output (Mirabelli, Coppola et al. 2019).

Chapter 2 – Methods

2.1 – Undifferentiated SH-SY5Y growth conditions

SH-SY5Y cells (American Biological Culture Collection, or ATCC, designation CRL-2266) are a cell line subcloned from the SK-N-SH cell line (ATCC HTB-11) that were first reported in 1978 (Biedler, Roffler-Tarlov et al. 1978). The SK-N-SH cell line was itself established in 1973, using metastatic bone marrow tumour samples taken from a 4-year-old neuroblastoma patient (Biedler, Helson et al. 1973). SH-SY5Y cells have since been widely used as a cellular model to investigate various neurological conditions, with examples including Parkinson's disease, Alzheimer's disease and motor neuron disease (Carrì, Ferri et al. 1997, Jämsä, Hasslund et al. 2004, Nonaka, Arai et al. 2009, Lopes, Schröder et al. 2010, Xicoy, Wieringa et al. 2017, de Medeiros, De Bastiani et al. 2019).

In the initial phase of this project, some aliquots from early passage (P10) undifferentiated SH-SY5Y cells were donated from a colleague. These initial samples were then used to grow a significant stock of cells, which could then be drawn from to perform all later experiments. Growth cycles using undifferentiated SH-SY5Y cells typically began with seeding a T75 cell culture flask with ~200-300K cells (Thermo Scientific™ Nunc™ Cell Culture Treated EasYFlasks™, catalogue number 156499). To do this, RPMI 1640 media was used (Gibco™ RPMI 1640 Medium, catalogue number 11875093), further enriched with the following additives;

- 10% Fetal Bovine Serum or FBS (Gibco™ Fetal Bovine Serum, catalogue number A5256801)
- 1% Penicillin-Streptomycin (Gibco™ Penicillin-Streptomycin (10,000 U/mL, catalogue number 15140122)

Seeded cell flasks were then placed in an incubator with a fixed internal temperature of 37ºC and 5% CO_2 enrichment to facilitate adequate pH buffering capacity of cell media. Fresh media was added every other day and cells were grown until ~90% confluency before being detached to seed new flasks and/or produce aliquots of cells for freezing at -80ºC. Prior to detachment, flasks were washed with ~5 ml warm Phosphate Buffered Saline (PBS) to remove traces of RPMI media (Gibco™ PBS, pH 7.4, catalogue number 10010023). Detachment was performed using 1x Trypsin at room temperature for ~5 minutes (Gibco™ Trypsin-EDTA, no phenol red, product code 10779413), which was diluted from x10 stock using PBS. After detachment was confirmed using a light microscope, trypsin action was quenched by adding a saturating volume of enriched RPMI media (+FBS, +Pen/Strep) to

flasks. This cellular suspension mixture was then transferred to a 15 ml falcon tube for centrifugation at 200 Relative Centrifugal Force (RCF) for ~5 minutes in a desktop centrifuge (Thermo Scientific™ Nunc™ Conical Sterile Polypropylene Centrifuge Tubes, catalogue number 339650). The cell pellet was then ready for further use in seeding new flasks and/or generating cell aliquots for cryopreservation.

2.2 – Cryopreservation and thawing of SH-SY5Y cells

To ready cells for cryopreservation at -80ºC, freezing media was prepared by adding 10% Dimethyl sulfoxide (DMSO) to enriched RPMI media shortly before cell aliquot preparation (Thermo Scientific Chemicals Dimethyl sulfoxide, catalogue number J66650.AE). Pelleted cells were resuspended in freezing media to give approximately 500k cells per ml of freezing media, which was then quickly portioned out into several 1ml cryopreservation vials, before being placed into a cell freezing container which was then immediately transferred into a -80ºC freezer (Thermo Scientific™ Nalgene™ General Long-Term Storage Cryogenic Tubes, catalogue 5000-1012).

Thawing was carried out using a benchtop metal bead heat bath, set to 37ºC. Vials for thawing were placed into it to be brought promptly up to temperature over ~5 minutes. Once fully thawed, the cellular suspension was transferred to a 15 ml falcon tube and pre-warmed enriched RPMI was added up to ~10 ml, and tubes were centrifuged for 5 minutes at 200 RCF to form a cell pellet. Following centrifugation, the DMSO-containing supernatant was removed and the cell pellet was resuspended with warm, enriched RPMI as appropriate for seeding a new flask or for use in experimentation.

2.3 – Neuron-like differentiation of SH-SY5Y cells

In almost all cases, SH-SY5Y cells were differentiated into a more neuronal-like phenotype prior to experimentation. This was achieved by use of all-trans retinoic acid (Thermo Scientific Chemicals Retinoic Acid 97%, catalogue number 044540.02), in a process adapted from a well-established differentiation protocol (Encinas, Iglesias et al. 2000). 1 day after seeding cells were treated with 10 µM all-trans Retinoic Acid. For subsequent daily media changes, RPMI media additionally enriched with 10 µM Retinoic Acid was used up to and including day 5 post-seeding. From day 6 onwards, media was switched to Neurobasal media (Gibco™ Neurobasal™ Medium, catalogue number 21103049) supplemented with the following;

- 20mM KCl (Invitrogen™ KCl (2 M), RNase-free, catalogue number AM9640G)

- 20ng/ml BDNF (Gibco™ Human/Mouse/Rat BDNF Recombinant Protein, PeproTech®, catalogue number 450-02-10UG)
- 2% B-27 (Gibco™ B-27™ Supplement (50X), serum free, catalogue number 17504044)
- 1% Penicillin-Streptomycin (Gibco™ Penicillin-Streptomycin (10,000 U/mL, catalogue number 15140122)

Daily media changes with this supplemented Neurobasal media continued from day 6 post-seeding until day 10 post-seeding. After 10 days, cells were then detached/processed as necessary and used in experiments.

2.4 – Cell-Titer blue metabolic viability assay

This assay uses a fluorometric method to estimate the number of viable cells present in a sample. The dye Resazurin is introduced, which healthy cells will metabolise into Resorufin – a molecule which has a different spectra profile. The extent of this reduction may be quantified using an appropriate plate reader and used to infer viability percentages of the analysed sample. A diagram of this reaction is shown below in figure 8.

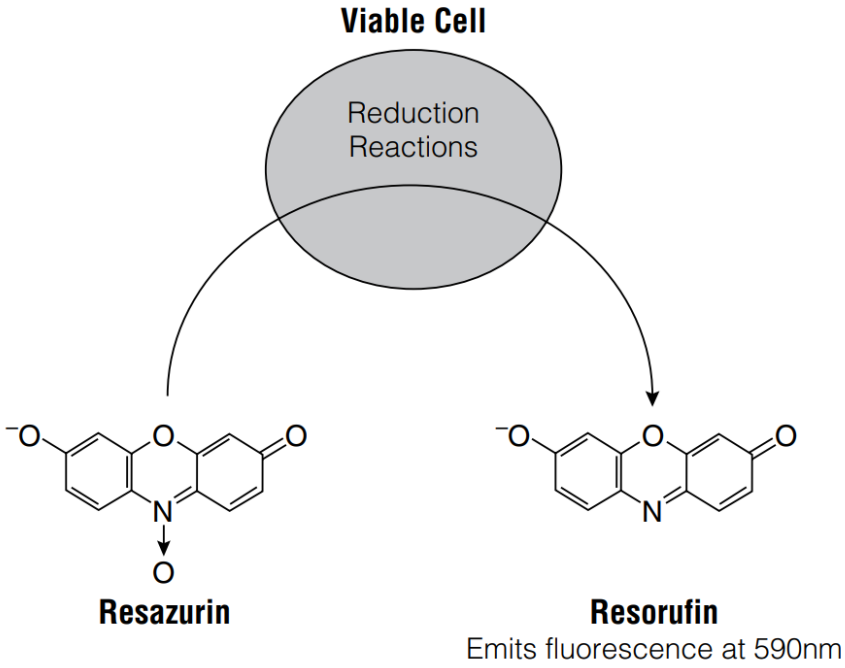

Figure 8 – the essential reaction of the Cell-Titer blue assay. Figure taken from the Promega CTB protocol guide.

Resazurin possesses no fluorescence properties, but if reduced to Resorufin it becomes highly fluorescent with a spectra profile of 579 nm Excitation / 584 nm Emission. The fluorescence produced by this reaction is taken to be proportional to the number of viable cells. A relatively straightforward protocol is involved where an appropriate volume of Cell-Titer Blue (CTB) reagent is added to 96 or 384-well plates (e.g. 20µl is added per well to 96-well plates), plates are then incubated for 1-4 hours before being read on a plate reader that is capable of 560_{EX} / 590_{EM} functionality. Both forms of the dye used in this assay are sensitive to degradation by light energy and are therefore carried out under low-light or dark conditions to the fullest extent practically possible. CTB reagent demonstrates low cytotoxicity and the assay offers sensitivity that is at least comparable to and possibly slightly more sensitive than other viability assays, such as the popular MTT or ATP-based assays (Squatrito, Connor et al. 1995, O'brien, Wilson et al. 2000, Hamid, Rotshteyn et al. 2004).

2.5 – Agilent Seahorse XF Cell Mito Stress Test

Agilent's Cell Mito Stress Test is a live cell assay designed to assess mitochondrial function by measuring Oxygen Consumption Rate (OCR) on a Seahorse XF Extracellular Flux Analyzer. It allows real time quantification of OCR and offers the user the ability to introduce up to four compounds into the reaction chamber. These are typically compounds that modulate mitochondrial function in some manner, but users can also introduce experimental compounds to assess their capacity to modulate mitochondrial function. The most commonly used compounds are Oligomycin, Carbonyl cyanide-4 (trifluoromethoxy) phenylhydrazone (FCCP), Antimycin A and Rotenone. Each of these compounds inhibits a specific protein complex within the ETC.

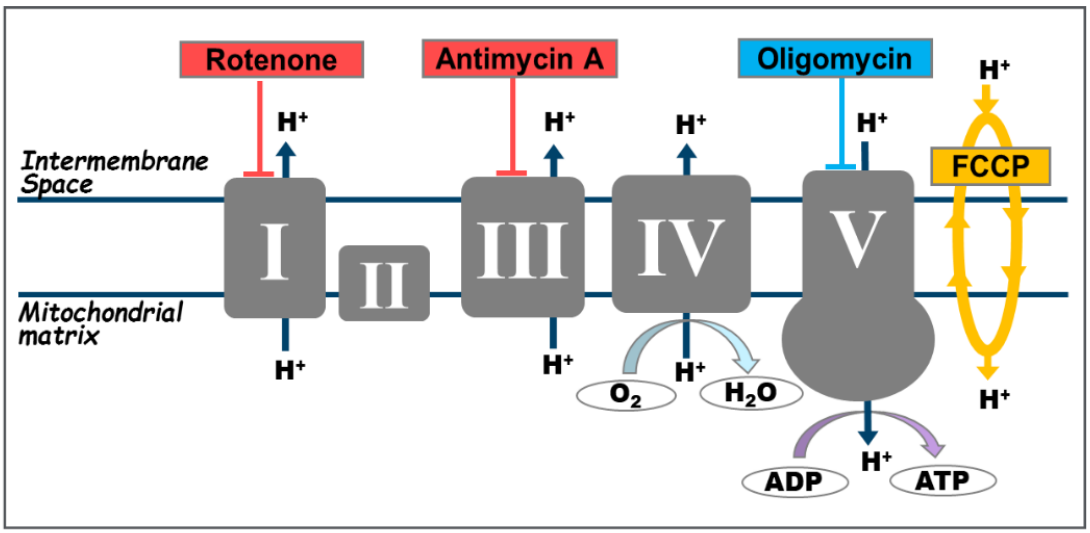

Figure 9 – The ETC and selective protein complex inhibition of Mito Stress Test compounds. Figure taken from the Agilent Cell Mito Stress Test protocol.

In a typical Mito Stress Test reaction scheme, basal OCR is measured first before introducing any compounds. After these readings are taken, Oligomycin is injected – which inhibits protein complex 5 and reduces OCR. Reduction in OCR observed here may be attributed to ATP production (which requires ATP synthase or complex 5 activity). Next, FCCP is added, which acts as an uncoupling agent – disrupting the proton gradient across mitochondrial membranes and allowing free flow of protons into and out of the mitochondrial matrix. This effectively maximises the OCR output of complex 4, revealing the so-called "spare capacity", i.e. the difference between basal and theoretical maximal respiration. The third and final injection contains both Antimycin A and Rotenone, which inhibit protein complexes 3 and 1 respectively. These combined compounds effectively halt all mitochondrial associated respiration, with any remaining activity therefore being attributed to non-mitochondrial sources, if there is any.

2.6 – Statistical analysis

In this study the comparison of interest is between irradiated and non-irradiated samples from each experimental setup, in an effort to estimate the likelihood of differences in results obtained being attributable to RF irradiation or naturally occurring variation. Before selecting which statistical test to use for this purpose, the Shapiro-Wilk test for normality was applied to raw data. The Shapiro-Wilk test is specifically designed to test the null hypothesis that the sample data comes from a normally distributed population and a low p-value (in our use case below 0.05) is used as a basis to reject the null hypothesis, i.e. p-values below the 0.05 threshold mean that the data likely deviates from a normal distribution. P-values above 0.05 were taken as a satisfactory indicator of normality. This was done as an initial step to discern whether parametric or non-parametric tests were appropriate tools for analysis. Where data were found to be normally distributed, an unpaired, two-tailed Student's t-test was selected for statistical analysis. This test was chosen for three reasons;

- A Student's t-test is specifically designed to probe differences between two groups to see if they belong to the same population, i.e. it produces a p-value estimating the probability of obtaining results as extreme or more extreme than those observed if the null hypothesis is true (that the two group means belong to the same population). This type of two group comparison is precisely what is required here
- When making a comparison between two groups of data that are normally distributed, the t-test of often the preferred and recommended statistical test to use (Chicco, Sichenze et al. 2025)

- Even with very small sample size (as is the case here in this study), evidence exists suggesting the t-test can be a worthwhile and useful test to perform statistical analysis (De Winter 2013)

However, the Student's t-test makes several assumptions about the data, such as being normally distributed and having equal variance among both groups and violations of these assumptions can influence its applicability. It is worth mentioning that several alternative statistical tests exist, prominent examples being the Mann-Whitney U-test or the unequal variance t-test (Ruxton 2006, Chicco, Sichenze et al. 2025). The Mann-Whitney U-test is a non-parametric method that involves sorting the data into ranked order to derive the test statistic, rather than using the mean values as seen in a Student's t-test. This gives it the advantage of being more robust to the influence of outlier values, which the t-test can be sensitive to (Chicco, Sichenze et al. 2025). But the t-test has been consistently shown to perform well in some contexts when compared to the U-test, particularly when dealing with larger sample variance (Zimmerman 1987). Ultimately, the Student's t-test was chosen because it is widely deemed an appropriate test to use under the condition its underlying assumptions are met by the data and it is known to be able to provide good insight into data (Zimmerman 1987, De Winter 2013, Chicco, Sichenze et al. 2025). Unless otherwise stated, an alpha threshold of p=0.05 was used as a boundary for statistical significance when performing statistical analysis.

2.7 – Specific Absorbance Rate (SAR)

SAR (W/kg) is the amount of power deposited by a RF field in a mass of tissue and is widely regarded as an appropriate unit when considering RF-EMR exposures for frequency ranges used in this project (up to ~5 GHz). This is because RF radiation is effectively able to penetrate tissue at these frequencies, meaning the entire mass of an organism or part of an organism may be considered when trying to quantify exposures (ICNIRP 2020). To calculate SAR, the following formula was used;

$$SAR = \sigma \times E^2 / m_d$$

Where σ = electrical conductivity (S/m), E = root mean square electric field (V/m) and m_d = mass density (kg/m^3). A reference value of 4 S/m was used for σ, which was obtained from existing literature, in particular a paper which quantified grey matter electrical conductivity over a range of frequencies up to 10 GHz (Gabriel, Gabriel et al. 1996). For mass density, a reference value of 1.05 g/ml (or 1050 kg/m^3) was used based on existing literature, which has reported a range of values between 1.01 and 1.1 for a range of cell types, with a value

of ~1.05 being common (Howard and Clark 2002, Grover, Bryan et al. 2011, Liu, Oh et al. 2022). E was calculated separately using the following formula;

$E = \sqrt{30} \times Pt \times Gt / d$

Where Pt = transmitter power (Watts), Gt = antenna gain (linear numeric value) and d = distance from transmitter (meters). This calculation is based on established antenna theory methods for calculating field strength based on antenna power, antenna gain and distance from transmitter (Balanis 2016). For the sinusoidal waveform, the transmitter power is 16.5 dBm in accordance with the signal generator maximum specifications, but the QAM modulated waveform has a maximum baseline amplitude of 3 dBm – to allow for both increases and decreases in power as the amplitude fluctuates as part of the modulation scheme. In this case, an average power of 3 dBm was used to calculate SAR. The antenna gain was taken directly from the technical specification datasheet, with a value of 2 dBi or 1.58 in linear numeric value. The distance between the transmitter and exposed cells was measured at 0.3 m.

Inserting values into the relevant equations results in the following SAR;

- For the 16.5 dBm sinusoid, SAR = 8.9898E-04 W/kg
- For the 3 dBm QAM modulated waveform, SAR = 4.016E-05 W/kg

In the absence of continuous monitoring, it is practically impossible to accurately estimate the SAR actually received within the 5G phone setup. This is because the device dynamically switches between multiple different frequency bands and power parameters during operation while data streaming. This will result in continuously fluctuating values for various parameters within the SAR calculation formulae. However, it is worth noting that mobile phone manufacturers produce SAR data for each handset using maximum power settings. For our phone (product code SM-A136B), Samsung reports the following values; head SAR = 0.845 W/Kg, body SAR = 1.332 W/Kg (Samsung 2025). But it is important to recognise that these values reflect the theoretical maximum exposure possible with this phone, which is unlikely to be representative of what is occurring here in our setup. But it does provide evidence that phones can achieve significant levels of RF emission that is orders of magnitude above what is being used here in the Faraday shield setup.

Chapter 3 – Results

Establishing a Faraday shielded chamber and neuronal cell model for Radiofrequency Electromagnetic Field (RF-EMF) exposure experiments

Preface

Radiofrequency Electromagnetic Fields (RF-EMFs) are widely regarded as being a relatively safe means of providing telecommunication services. But some evidence for biological effects exists. In this chapter, the objective was to create a scientifically valid means of investigating any potential biological effects resulting from low-power RF-EMF exposure while minimizing the influence of background sources of Electromagnetic (EM) radiation. A Faraday shield was constructed to create an EMF insulted space, complete with ports to connect external machines (e.g. signal generator and spectrum analyser) to antennas inside the shield. This should provide a level of precision and detail regarding RF-EMF exposure parameters previously unseen in most papers published on EMF safety, giving a high degree of confidence about possible causal links between RF irradiation and biological effects.

3.1 – Introduction

Despite the existence of a significant amount of basic research suggesting that low-power RF-EMFs may provoke biological effects, such as promoting ROS generation, regulatory bodies have maintained the same foundational exposure limits for a number of years (Protection 1998, Consales, Merla et al. 2012, Schneider and Stangassinger 2014, Tang, Zhang et al. 2015, Bortkiewicz 2019, ICNIRP 2020, Panagopoulos, Karabarbounis et al. 2021, Sofri, Rahim et al. 2021). It is the function of regulatory bodies such as the ICNIRP to make judgements about the value and relevance of this research output and arrive at a specific dosage value for what is to be considered safe for people and telecommunications workers. This is not an easy or simple task to do and has resulted in the ICNIRP being dismissive or critical of some findings whilst being accepting of others, based on their own judgement criteria (Protection 1998, ICNIRP 2020). Many different articles have been considered in this process, but a common criticism raised by the ICNIRP for papers they take a negative view towards is related to researcher methodologies (Protection 1998, ICNIRP 2020). More specifically, about the nature of signals used by researchers and a lack of strict and robust signal exposure qualification and quantification, i.e. that the exact nature of EMF exposure is not clearly defined (Protection 1998, ICNIRP 2020). This is sometimes used by the ICNIRP as justification to dismiss or attach low value to findings resulting from several studies. It is a valid concern, because many things may correlate with each other because of some unknown confounding variable. But the conclusions of the ICNIRP are not well-received by all researchers operating in the field of RF-EMF research – with some being highly critical of their decision-making processes (ICBE-EMF 2022).

It is also true that telecommunication signal diversity and abundance is increasing significantly with time (Obile 2016, Ericsson 2021, Ericsson 2024). This means people are being exposed to a wider array of signal types, in increasingly dense networks involving more antenna arrays that are emitting more complex signals in communication with more user devices. This type of environment makes causal links incredibly difficult to prove, where any number of unknown interactions or synergies exist and may exert meaningful influence over the overall output and any potential biological effect. The advent of 5G NR is particularly significant because it will lead to the widespread introduction of frequency bands that are far higher than previous generations of cellular network technology, e.g. 20 GHz, 40 GHz and even 60 GHz bands (Rappaport, Xing et al. 2017, Parkvall, Dahlman et al. 2018, Rochman, Sathya et al. 2023). Given that a commonly used 4G band is approximately 3.4 GHz, this may represent up to a 20X fold increase in frequency in some cases. This will dramatically change the way these waveforms behave and properties they possess,

potentially introducing new effects that cannot be predicted based on research done using older technologies or signal parameters – which is the category the vast majority of considered RF-EMF safety research falls into (Protection 1998, ICNIRP 2020). A good example of this signal behavioural shift is in energy deposition into tissues and penetration depth. According to the ICNIRP's own conclusions, frequencies beyond 10 GHz tend to have very low penetration depth and energy deposition will occur majorly at or near the skin's surface (Protection 1998). The effect these new frequencies may have on human skin is unclear and this is just one of the changes that will occur with the introduction of 5G – there are many others including advances in other technologies such as antenna arrays, modulation schemes and cell network design (Banelli, Buzzi et al. 2014, Rappaport, Xing et al. 2017, Shafi, Molisch et al. 2017, Parkvall, Dahlman et al. 2018, Chiaraviglio, Lodovisi et al. 2021, Abid, al-Azzawi et al. 2023, Rochman, Sathya et al. 2023).

This backdrop of complex signal diversity, increasingly EMF saturated environments and conflicting evidence and viewpoints on biological effects creates a need for a workspace in which we can be confident that the only meaningful RF signal present is one deliberately and specifically introduced by the researcher. This would allow a clear and direct investigation into the capacity of specific waveforms to induce biological effects in cells. Alongside this a simple 5G phone inside a desktop mini-incubator setup will also be established to provide independent verification of results obtained using the Faraday shield and deliver a platform that is directly comparable to real world scenarios. So, the objectives for this chapter were as follows;

1. Construct a Faraday shield that is able to significantly block incoming RF-EMF signals from the surrounding environment
2. Test and quantify the shielding capability of the Faraday shield, for signals leaking into the inner chamber from outside and those leaking outwards from within
3. Make the chamber interior more cell culture friendly by providing heating to approximately the same temperature as a standard cell incubator (36 – 38ºC)
4. Find and test an alternative means of buffering against media pH changes, due to standard cell media relying on a CO_2 enriched environment to perform this function
5. Establish a simple 5G phone experimental setup using a mini-desktop incubator
6. Confirm neuron-like cell model differentiation using retinoic acid and test resulting change in metabolic sensitivity

3.2 – Methods

3.2.1 – CellTiter-Blue metabolic viability assay

Either differentiated or undifferentiated cells were seeded onto 96-well plates (Corning® 96-well Clear Flat Bottom TC-treated Microplate, 20 per Bag, with Lid, Sterile, product number 3628) in 100µl supplemented RPMI media at a seeding density of 20,000 cells per well. Plates were left to settle overnight before progressing with the CellTiter-Blue (CTB) protocol the following day.

For negative control and background signal removal purposes, each plate contained cell-free wells which were otherwise treated the same.

To analyse metabolic viability and how differentiation may affect this, wells were exposed to various concentrations of hydrogen peroxide (Sigma-Aldrich, product code H1009-100ML), or none at all, then incubated at 37ºC for 2 hours. H_2O_2 concentrations used were; 0 µM, 50 µM, 100 µM and 200 µM.

After H_2O_2 incubation, 20µl CTB reagent was added to each well (20µl per 100µl volume) and plates were incubated for an additional 2 hours. Care was taken to cover plates to protect against fluorescent signal from degradation due to ambient light.

After 2 hours incubation with CTB reagent, plates were read on a fluorescent plate reader (TECAN SPARK 10M, software SPARKCONTROL V2.2) with the following settings; 10 second plate shake and 560nm excitation / 590nm emission wavelengths.

3.2.2 – RPMI and CO_2 independent media pH time course

To investigate the capacity of RPMI and CO_2 independent media (CIM, Gibco™ CO_2 Independent Medium, product code 11580536) to buffer against pH changes outside of the CO_2 rich microenvironment, cells were seeded onto 6 well plates at ~200,000 cells per well then left to settle overnight. The following day plates were removed from the main CO_2 enriched incubator and transferred to a small desktop incubator (set to 37 ºC) without CO_2 supply. pH readings were taken at the start of the process (T0) and after having been left in the desktop incubator for various lengths of time. In the case of RPMI, plates were left for 0, 2 or 4 hours, then a pH reading was taken, before being returned to the main CO_2 enriched incubator for 2 hours to recover – after which a final pH reading was taken. For CIM, plates were left in the desktop incubator for 0, 24, 48 or 72 hours before a pH reading was taken.

3.2.3 – Immunofluorescence Microscopy

Cells were seeded onto 10mm glass coverslips placed inside 35mm dishes using a seeding density of 10,000 cells per coverslip and left overnight to settle in 1ml supplemented RPMI media. For cells undergoing differentiation, seeding density was 2,500 cells per coverslip to account for continued growth over the 10-day differentiation cycle.

The day after seeding (undifferentiated cells), or after differentiation, dishes were washed in PBS before fixing cells using 4% paraformaldehyde/PBS (Thermo-Fisher Scientific, product code 15670799) for 20 minutes at room temperature. Dishes were then washed with PBS to remove fixative before adding 0.15% Triton-X-100/PBS (Thermo-Fisher Scientific, product code A16046.AP) solution for 10 minutes at room temperature to permeabilize cells. This was followed with another PBS wash before adding blocking buffer for 1 hour at room temperature to suppress non-specific antibody binding. Blocking buffer used was 10% goat serum in PBS with 0.1% TWEEN 20 (Goat serum from Sigma-Aldrich, product code G9023-5ML, TWEEN 20 from Sigma-Aldrich, product code P1379-500ML).

After blocking, dishes were washed in PBS before incubating overnight at 4ºC with primary antibody in blocking buffer solution. Two different primary antibodies were used to confirm neuronal-like differentiation; Rabbit Polyclonal Anti-NeuroFilament-Heavy chain IgG (1:1000 dilution, purchased from Sigma-Aldrich, product code ABN76) and Mouse Monoclonal Anti-Tau IgG (1:250 dilution, purchased from Thermo-Fisher Scientific, product code 13-6400).

The next day, dishes were washed three times with PBS to remove any unbound primary antibody. Following this, dishes were incubated with secondary antibody in blocking buffer solution for 2 hours at room temperature on a rocker, while being protected from light to preserve fluorescent signal. Secondary antibodies used were; Goat Polyclonal Anti-Rabbit IgG (1:500 dilution, from Thermo-Fisher Scientific, product code 35552) and Donkey Polyclonal Anti-Mouse IgG (1:500 dilution, from Thermo-Fisher Scientific, product code R37115).

After secondary antibody application, triplicate PBS washes were performed to remove any unbound antibody. Finally, one drop of DAPI mounting media was applied to each coverslip (Thermo-Fisher Scientific, SlowFade Diamond Antifade Mountant with DAPI, product code S36968), before being carefully picked up using tweezers, inverted and placed cells facing downwards onto a glass slide. Nail polish was lightly applied around the outer edges of coverslips to attach them to their glass slide.

Slides were left to incubate in DAPI mounting media for 20 minutes at room temperature under dark conditions prior to visualization. Images were acquired using a Nikon Eclipse Ti microscope (software; NIS Elements AR, version 5.10.00) at X20 magnification.

3.2.4 – Faraday shield RF-EMF blocking ability

To investigate the capacity of the Faraday shield/box to block external RF-EMFs penetrating into the internal chamber, a transmitting antenna (5G Cellular Antenna from Low Power Radio Solutions, product code LPRS-ANTB-5G-SMA) was connected to an RF signal generator (TSG4106A RF Signal Generator from Tektronix) and placed at varying distances from the Faraday shield. Inside the box was a receiving antenna (Omnidirectional Broadband Antenna from AARONIA AG, product code OmniLOG 30800) connected to a spectrum analyser (RSA306 Spectrum Analyzer from Tektronix), to detect and quantify any signals leaking through into the internal space.

Using pencil markings on a benchtop, the transmitting antenna (Tx) was kept up to 1 meter away, before being moved progressively closer to the Faraday shield until it was immediately adjacent to it (1m, 0.8m, 0.6m...0m). Then, the Faraday box was rotated anti-clockwise 45º and the process was repeated until every side panel and corner of the box had been tested (8 sets of 6 readings, representing 8 different axis). At each distance point, the receiving antenna (Rx) and spectrum analyser were used to take a reading and record detected signal strength in dBm. This approach is illustrated below in figure 10.

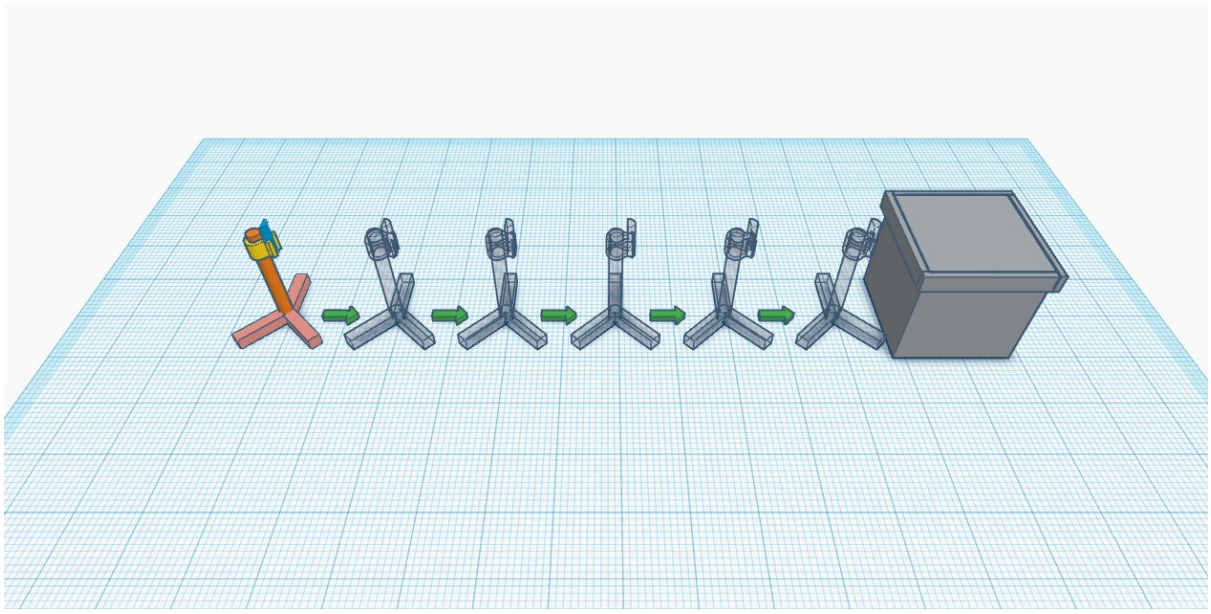

10a

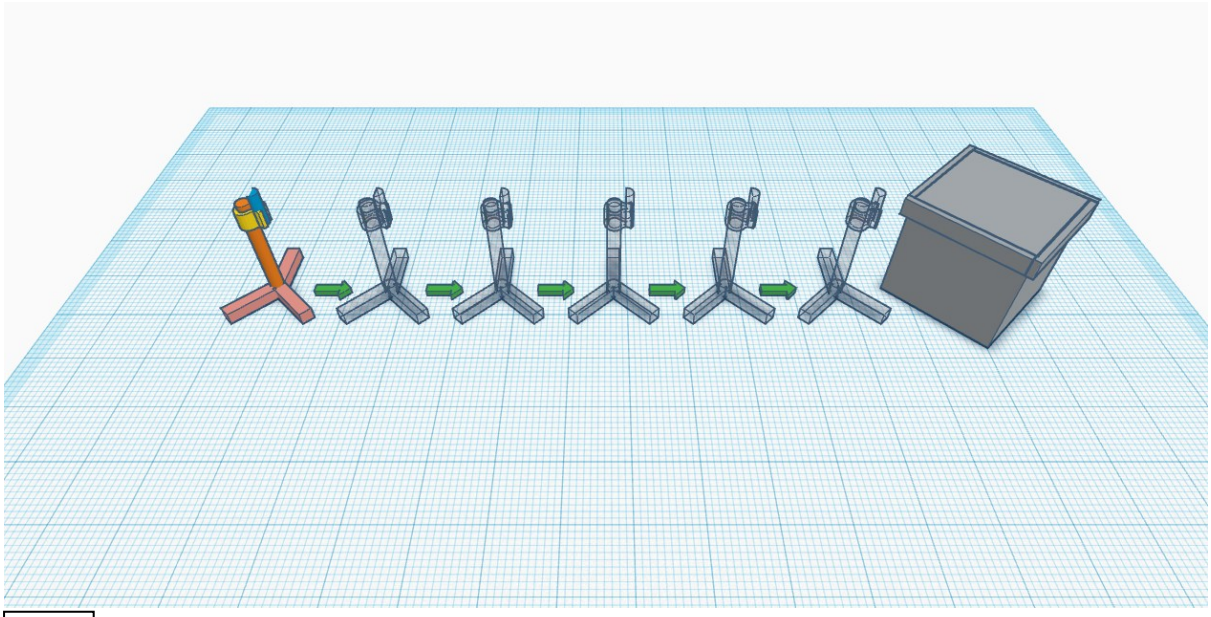

10b

Figure 10 – **10a** is a CAD image depicting a representation of the clamp stand holding the transmitter (Tx), in orange, starting at 1m distance from the box and being moved progressively closer in 20cm increments. **10b** shows the same process after the box has been rotated by 45º. This was repeated until all 4 side panels and all 4 corners had been tested for all Tx distances (1m, 0.8m, ... 0m).

Settings used for signal generation were determined by device upper limits according to their specifications. The signal generator was set to 4.9 GHz frequency with an amplitude of 16.5 dBm. The spectrum analyser was centred on the same frequency (4.9GHz) with a span of 40MHz and resolution bandwidth of 300 kHz.

This testing process was then done in reverse, with the Rx outside and the Tx inside the box, to test the capacity of the box to shield RF-EMF leakage to the external environment from signals generated inside.

Finally, both Tx and Rx were placed inside the box and a reading was taken to determine the maximal signal amplitude, A_{max} (without Faraday shield blocking action).

3.2.5 – Alternate experimental setup using 5G phone and mini-desktop incubator

A new 5G phone was purchased in hopes of being the most representative of consumer devices and typical signal exposures going forward as 5G infrastructure is deployed nationwide (Samsung Galaxy A13 5G, product code SM-A136B). A SIM card loaded with 120 GB data was installed in it to provide cellular network connectivity and allow data exchange over cellular networks (EE 120GB Pay As You Go Data Only Sim Card, EAN: 5025744872008). But the actual signal type and quality received was likely determined in large part by the physical location of our laboratory and the structure of the university building, i.e. there was significant building material (bricks, plasterboard, wood etc) between the phone and the nearest cell tower. Initial testing with the spectrum analyser showed that most cellular network activity occurred over the ~840 MHz band (LTE band 20), a frequency band used primarily as a coverage backstop in areas of poor coverage and signal quality (supplementary data). It also proved to be a somewhat intermittent connection and afforded fairly slow internet speeds. In terms of peak amplitudes of this intermittent signal, they were coincidentally very similar to the amplitude value recorded for A_{max}, with a narrow peak that fluctuated around approximately -10 dBm magnitude. Partly because of the intermittent nature of the cellular data signal, but also to remain as representative of consumer devices in real-world use scenarios, WiFi was also enabled to firm up the internet connection and allow for more consistent data packet transfer. WiFi testing revealed an amplitude peak in the common 5 GHz WiFi band that was broader than the cellular data peak, with recorded frequencies ranging from 5.1 to 5.5 GHz and a significantly lower peak amplitude with values ranging between -32 to -40 dBm (supplementary data). With both cellular data and WiFi switched on, the internet connection was robust, stable and capable of supporting continuous video streaming for prolonged exposure experiments.

When it came to working with cells in this setup, the phone was placed inside a mini-desktop incubator that was capable of controlling internal temperature at 37ºC (Thermo Scientific™ Heratherm™ Compact Microbiological Incubators, catalogue number 50125882). Flasks or plates containing cells were placed on top of the phone. For non-irradiated control experiments, the phone was switched off entirely for the duration of the experiment. When exposing cells, it was switched on, with WiFi and cellular data both enabled with a continuous data stream maintained for the duration of the experiment (audio and visual information, but with the phone speakers switched off).

3.3 – Results

3.3.1 – Confirmation of neuron-like cell model

To generate a neuron-like cell model, SH-SY5Y cells were treated with all-trans retinoic acid and neurotrophic growth factors over 10 days, an established method of encouraging neuron-like differentiation of cells previously described. Success of this approach was demonstrated by immunofluorescence visualization of neuronal protein markers, Tau and neurofilament, shown below in figure 10. There is significant expression of both markers in both untreated and differentiated cells, which is not surprising given the neuroblastoma origins of SH-SY5Y cells. But there were some very clear differences in phenotype and morphology based on RF exposure conditions. Differentiated cells show a clear shift towards a more neuron-like phenotype with long, interconnected protrusions extending from main cell bodies, a feature which is absent in untreated cells. This was particularly evident in the case of Tau primary antibody, which reveals some striking and significantly long extensions (figure 11e).

11a

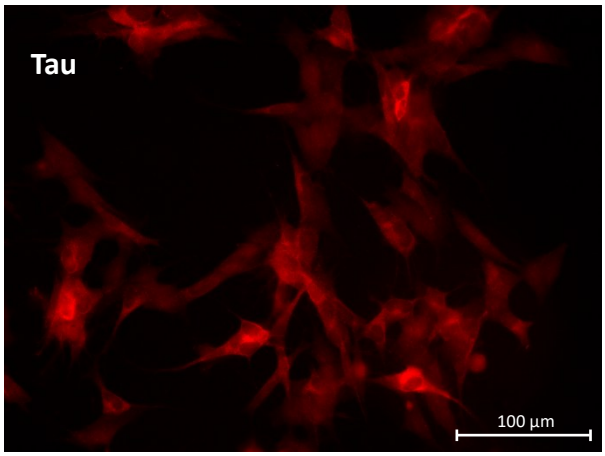

11b

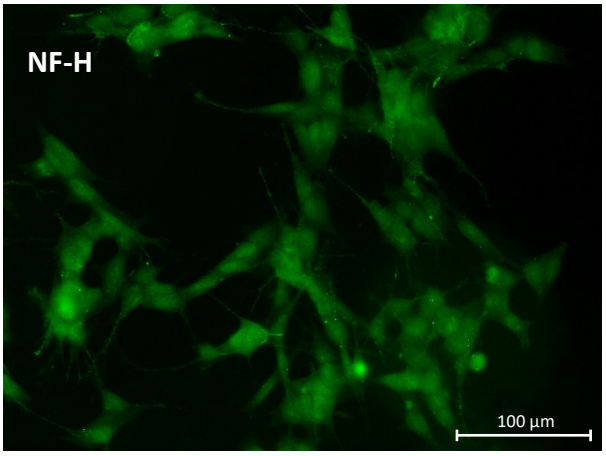

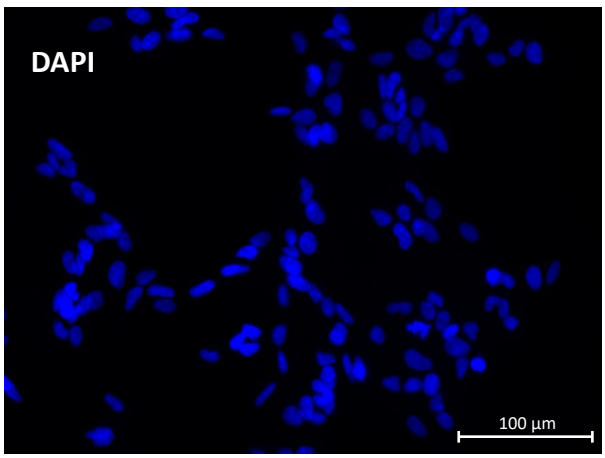

11c

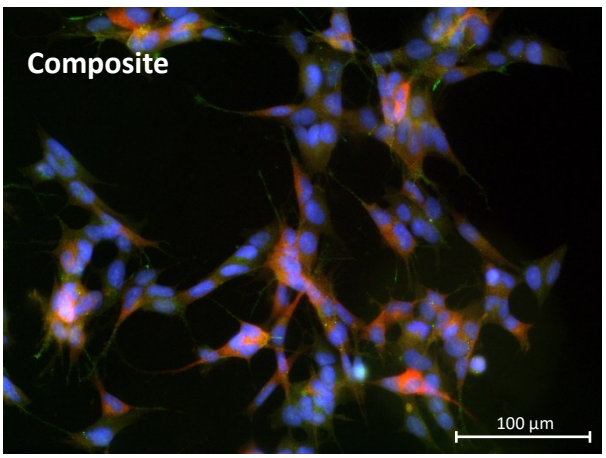

11d

11e **11f**

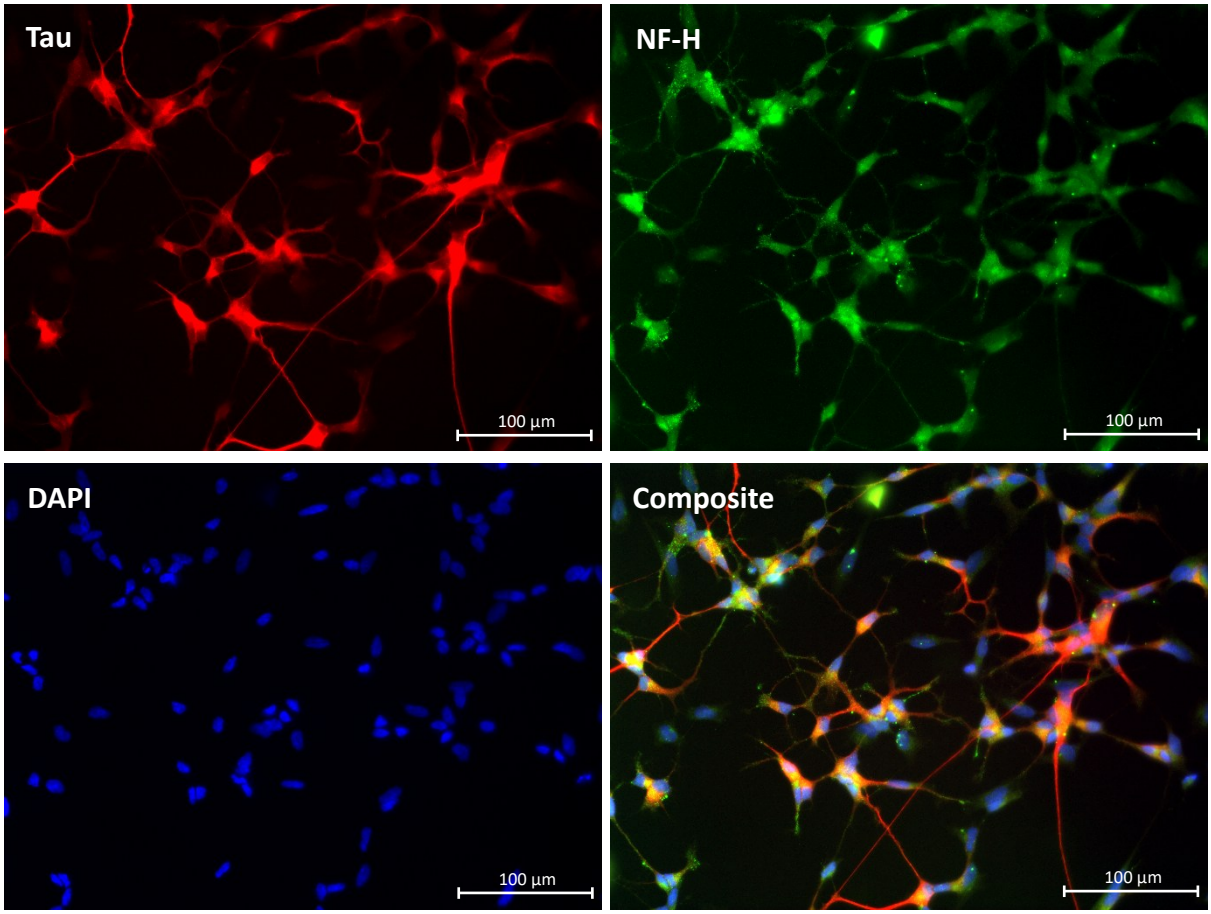

11g **11h**

Figure 11 - immunofluorescence images captured from undifferentiated SH-SY5Ycells treated with anti-Tau primary Ab (**11a**), anti-neurofilament heavy-chain primary Ab (**11b**), DAPI staining of nuclei (**11c**) and a composite image of all 3 RGB channels (**11d**). **11e-11h** show retinoic acid differentiated SH-SY5Y cells with similar primary Ab treatments and image ordering. Exposure settings were consistent between both differentiated and undifferentiated, with 20X magnification used for all images.

To attempt to quantify any effect differentiation might have on metabolic sensitivity, differentiated and undifferentiated cells were given various concentrations of H_2O_2 and their metabolic viability tested with a CellTiter-Blue assay, the results of which are shown below in figure 12.

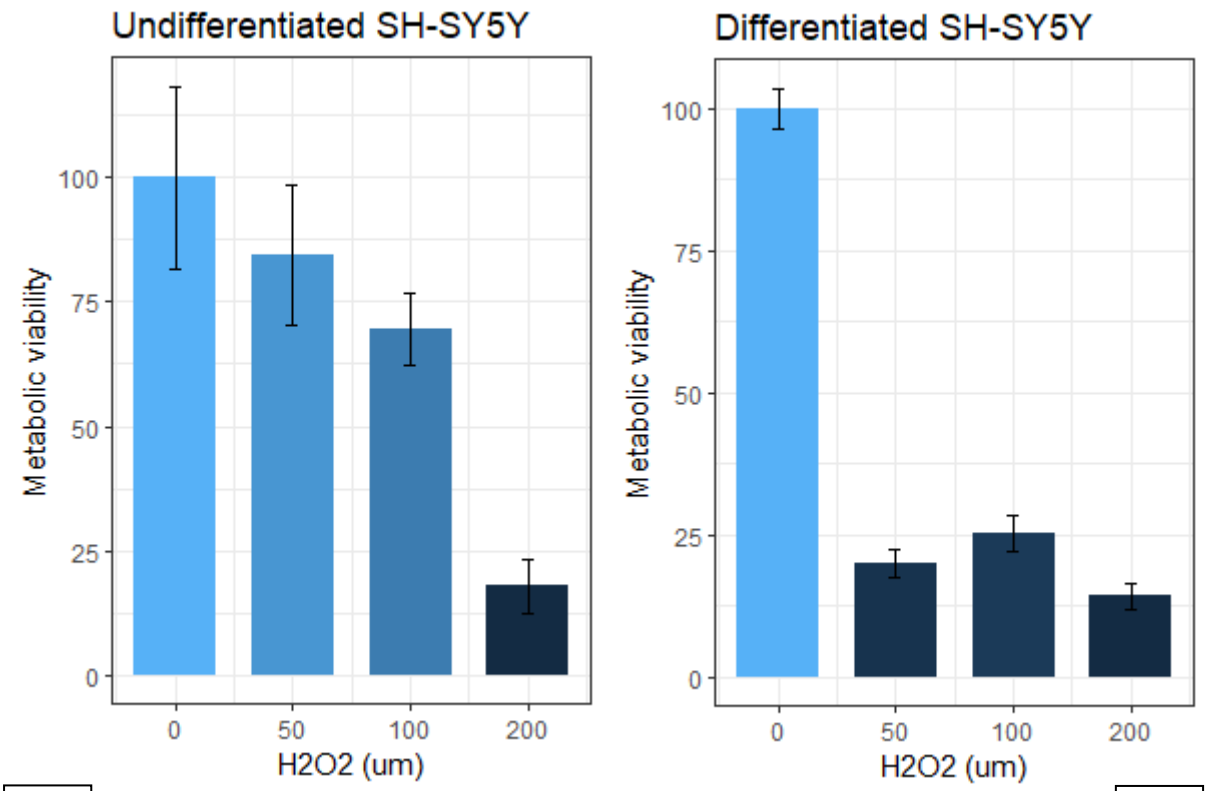

12a **12b**

Figure 12 – **12a** shows results from a CellTiter-Blue metabolic viability assay following H_2O_2 treatment of undifferentiated SH-SY5Y cells. **12b** shows results from the same experiment using differentiated SH-SY5Y cells. In both cases, data were normalized to untreated cells. Bars show mean metabolic viability, with error bars showing sample standard deviation. Data is representative of 3 independent experiments for both groups.

Although sample variance was much higher for undifferentiated cells, there was a clear pattern of undifferentiated SH-SY5Y cells being substantially more resistant to metabolic insult (figure 12). At 50 µm H_2O_2, undifferentiated cells maintained an average ~85% metabolic viability, which dropped to ~70% at 100 µm, then down to ~18% at 200 µm H_2O_2. This is contrasted with differentiated cells, which fell to an average metabolic viability of ~20% with just 50 µm H_2O_2 exposure and remained low for higher concentrations.

3.3.2 – Media pH stability outside incubator microenvironment

To address concerns about the pH stability of RPMI cell culture media outside of the CO_2 enriched incubator microenvironment, SH-SY5Y cells were plated out and placed inside a non-CO_2 regulated mini-incubator for up to 4 hours. There was clear evidence of significant pH drift towards basic pH (figure 13a, below), rising from an average pH of ~7.8 to ~8.4 within just 2 hours and climbing further to ~8.6 after 4 hours. This pH drift was remedied by

returning plates to a standard CO_2 incubator for 2 hours, causing pH to drop back down to near starting pH (~7.8 and ~7.7 after being in the mini-incubator for 2 and 4 hours respectively).

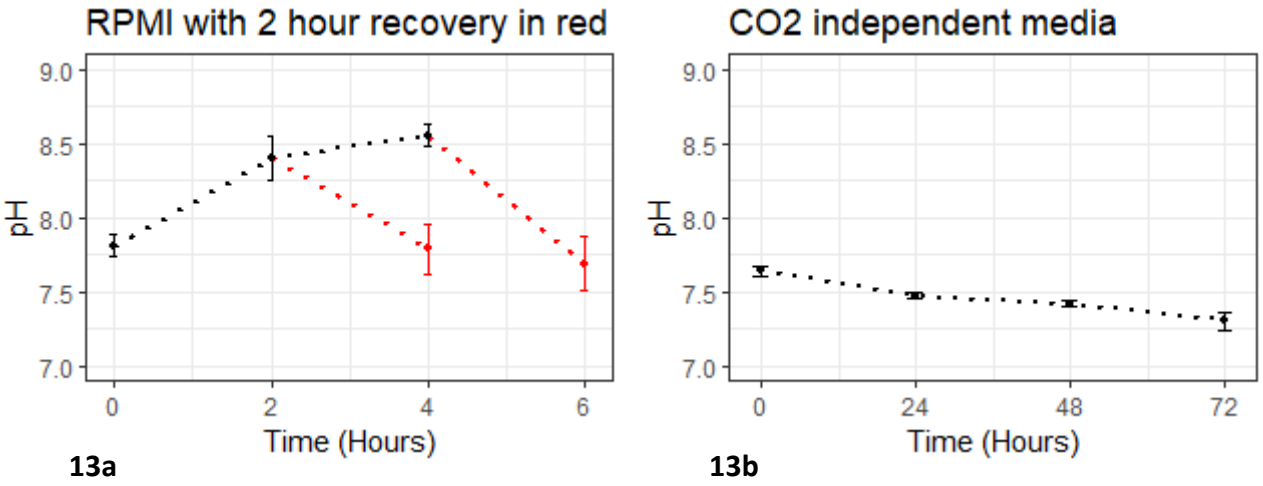

Figure 13 – **13a** shows pH readings of RPMI media samples taken from dishes growing SH-SY5Y cells that had been left out of a CO_2 enriched environment for 2 or 4 hours (black lines), followed by 2 hours recovery after being placed back inside a CO_2 enriched environment (red lines), n=3. **13b** shows pH readings taken from dishes growing SH-SY5Y cells in CO_2 independent media kept in a non-CO_2 enriched mini-incubator for up to 72 hours. Error bars show sample standard deviation. Data is representative of 3 independent experiments.

Because cells inside the Faraday shield will not be supplied CO_2, an alternative media was sought to provide good pH buffering capacity for prolonged, multi-day EMF exposure experiments. To test the ability of Gibco's CO_2 Independent Media (CIM) to perform in this capacity, cells were plated out and left in a non-CO_2 enriched mini-incubator for up to 72 hours before obtaining pH readings (figure 13b). CIM demonstrated a very robust ability to buffer against pH drift in the absence of CO_2 enrichment. From a starting average pH of ~7.6, it remained stable at ~7.5 and ~7.4 after 24 and 48 hours respectively. Even after 72 hours the pH had only dropped to ~7.3, just ~0.3 difference from the starting pH.

3.3.3 – Temperature control inside the Faraday shield

The other major variable lacking control inside the Faraday shield was temperature. Most cells, including SH-SY5Y cells, prefer temperatures close to physiological conditions (~37ºC). But the Faraday shield is essentially a metal box and has no means of regulating internal temperatures, meaning the interior space would be at or around room temperature

(~21ºC). To provide more favourable conditions for cellular growth, a large hot plate was obtained and the Faraday shield placed on top of it (Cole-Parmer HP-200D-XL-S Digital Hot Plate). However, the minimum temperature setting for the hot plate is 50ºC, far above the ideal cell culture temperature of ~37ºC. A temperature probe was placed inside the box to record the internal temperature with the hot plate switched on at its lowest setting (50ºC), which showed that the temperature inside the box plateaued at ~41.5ºC (figure 14a, below).

14a

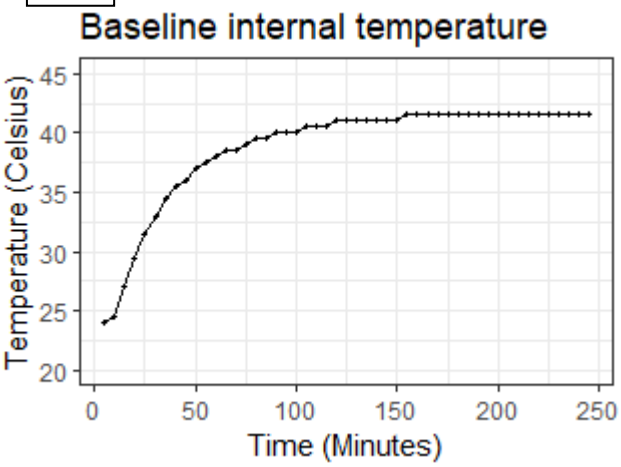

14b

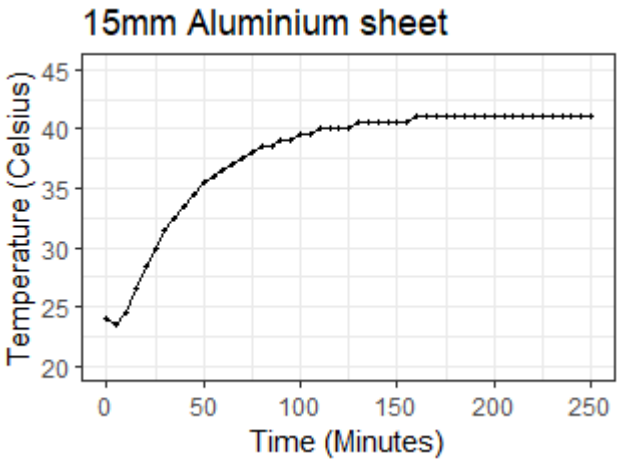

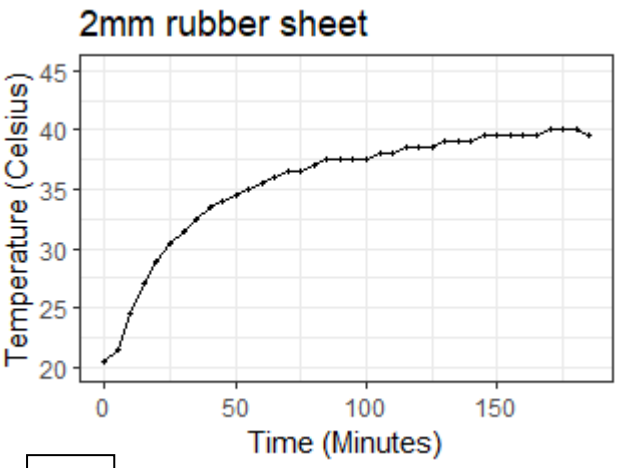

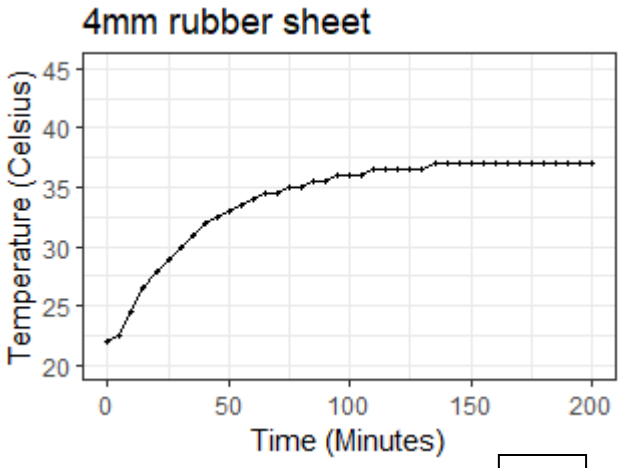

14c

14d

Figure 14 – shows the internal temperature of the Faraday shield when placed atop a hot plate set at 50 ºC, reaching a plateau of ~41.5 ºC with no insulating layers (**14a**). **14b-14d** all show data from the same experiment, but with various materials placed between the Faraday shield and the surface of the hot plate. Materials tested were a 15mm thick aluminium metal sheet, a 2mm rubber sheet and 4mm of rubber (figure 14b, 14c & 14d respectively). 4mm rubber insulation produced the desired 37ºC plateau.

In order to bring this temperature down to a more desirable level, various materials were placed between the box and the hot plate surface (figure 14b – 14d). The first material tested was a 15mm thick sheet Aluminium, which resulted in a plateau of 41ºC after ~160 minutes (figure 14b). Next, a 2mm sheet of rubber was tested, which resulted in a plateau at ~39.5ºC after ~150 minutes (figure 14c).

Finally, a 4mm thick rubber barrier was tested, by placing two 2mm rubber sheets on top of each other. This setup provided more robust heat insulation, resulting in an internal temperature plateau of ~37ºC, which remained stable even after 200 minutes of 50ºC heating (figure 14d).

3.3.4 – Faraday EMF shielding

The ability of the Faraday shield to block RF-EMFs, creating a kind of EMF dead space inside, forms an important part of the project. To test and quantify the effectiveness of the Aluminium box to perform this role, a receiving antenna (Rx) was placed inside, trying to pick up signals coming from a transmitter (Tx) placed outside the box at various distances. The signal generator and transmitter were configured to operate at the maximum power allowable for the equipment available (16.5 dBm) and 4.9 GHz was used as frequency settings. After each series of readings, the box was rotated 45 degrees until all 4 side panels and all 4 corners had been tested. Each of these 8 box orientations was considered its own axis and assigned a distinct colour in the figures below. This process was repeated with the Tx and Rx orientation reversed to analyse leakage of signal from inside to outside (i.e. the Tx was placed inside the box and the Rx placed at various distances outside the box). The results obtained from both experiments are illustrated below in figure 15.

In terms of EM radiation leaking into the box from the outside, a Tx distance of 1m from the box was sufficient to push the detected signal inside the box low relative to general background noise (figure 15a). The average background reading at this Tx distance was approximately -72 dBm amplitude and the highest peak detected was approximately -50 dBm, which was recorded during one of the corner-facing orientations. This means a difference of ~20 dBm above background noise exists with the Tx 1m away for the least insulating box orientation. In general, the box corners tended to be a bit more “leaky” than side panels, with slightly higher peaks being detected when compared to side panel orientations.

There was a general tendency for the peak amplitude to decrease as the transmitter was moved further away from the box (figure 15b), with the average peak amplitude at 0m Tx

distance being -48.8 dBm, which falls to an average of -60.35 dBm at 1m Tx distance. But even with the transmitter close to the box, the strongest signal detected at 4.9 GHz was -39.52 dBm, significantly below the maximal signal intensity (-12.94 dBm, Amax).

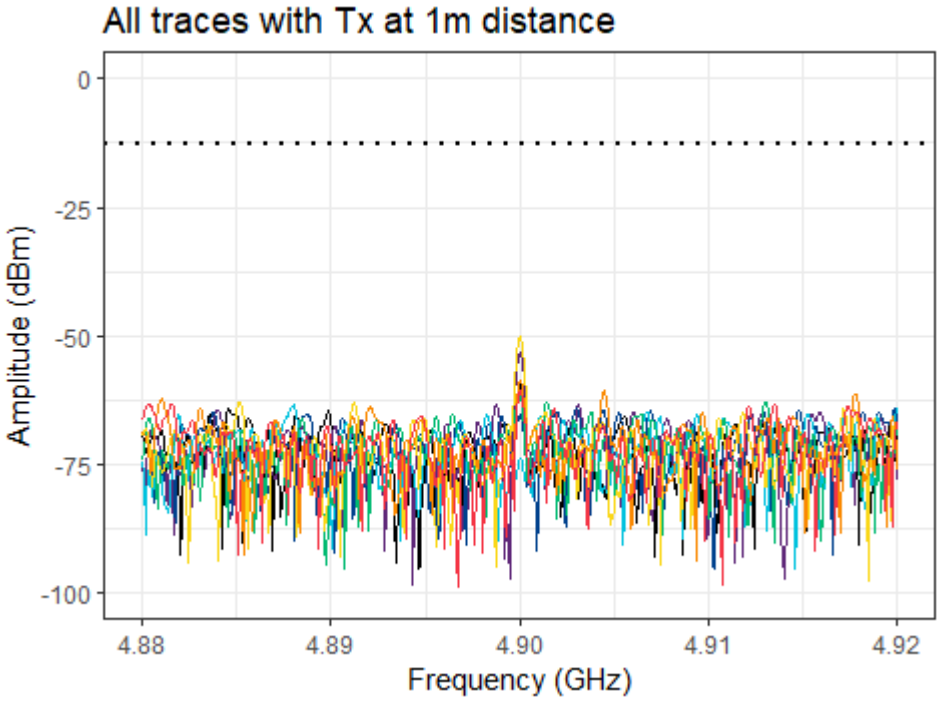

15a

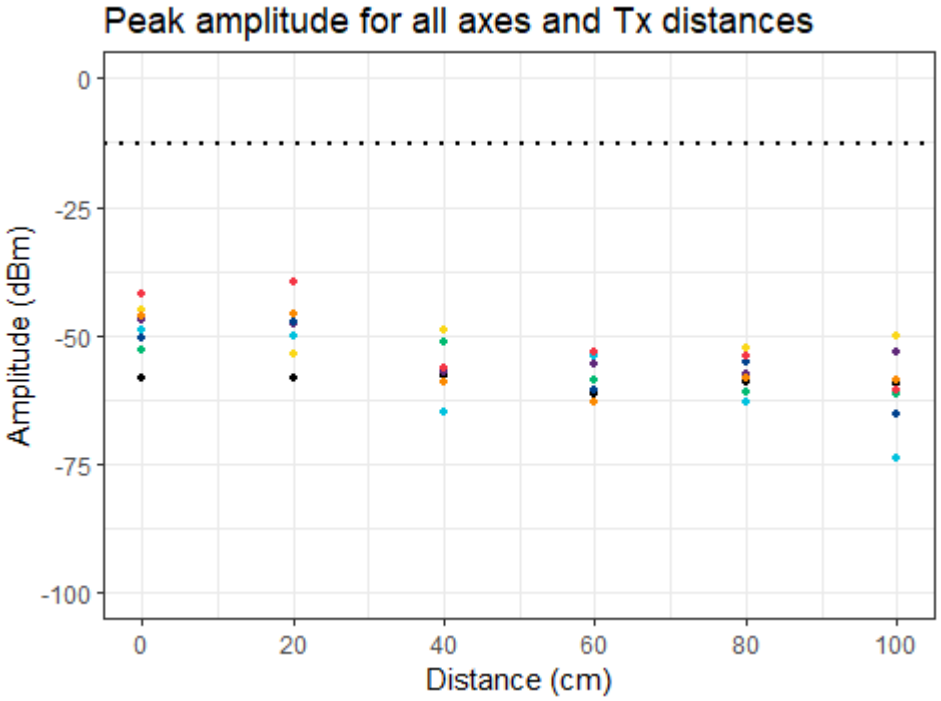

15b

Figure 15 – **15a** shows full traces obtained with the Tx 1m away from the box and the Rx inside the box, for all box orientations (8 axes in total). Each coloured line represents a different axis/box orientation. The dashed horizontal line across the top of the graph shows the maximal signal amplitude (A_{max}), recorded with both Tx and Rx inside the box (-12.94 dBm). **15b** shows peak amplitude, centred on 4.9 GHz, with the Tx at various distances from the box (0m to 1m) and the Rx inside. The dashed line again shows A_{max}.

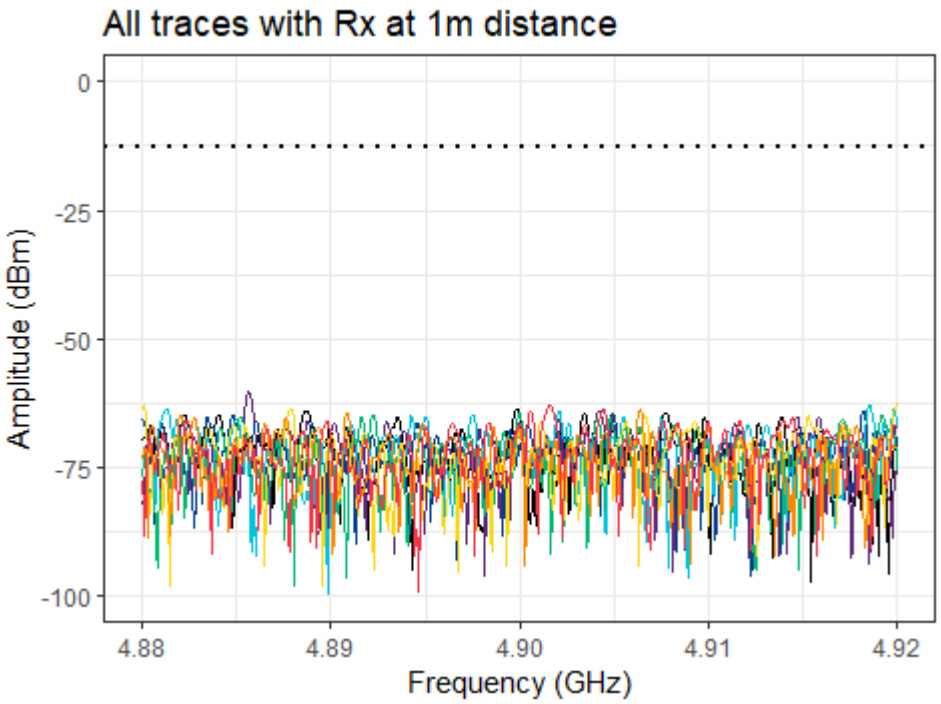

15c

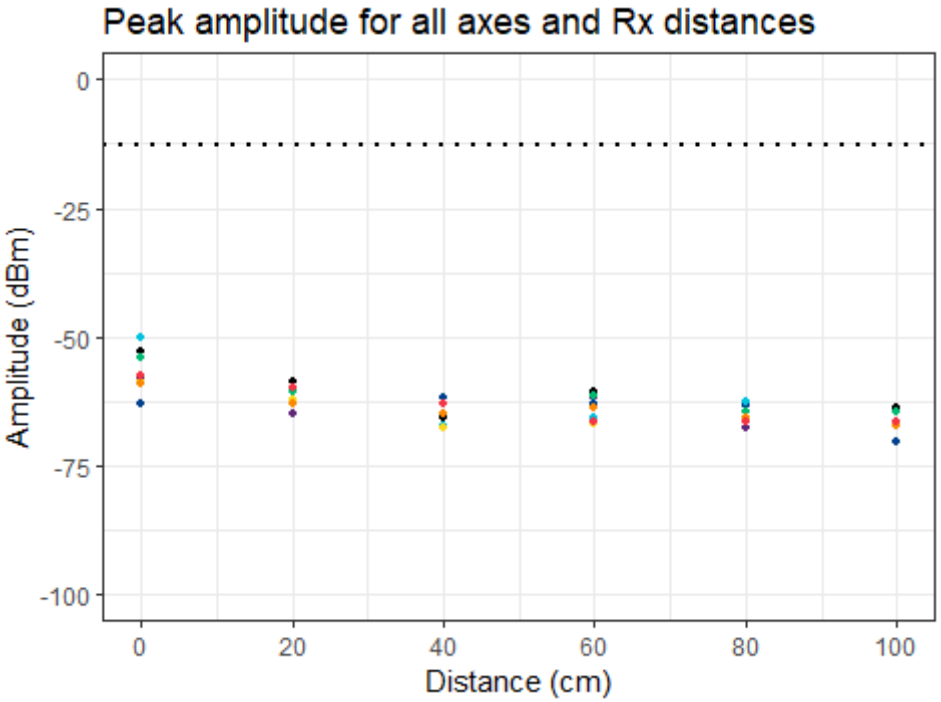

15d

Figure 15 (cont.) – **15c** shows full traces obtained with the Rx 1m away from the box and the Tx inside, for all orientations (8 axes in total). Each coloured line represents a different axis/box orientation. The dashed horizontal line across the top of the graph shows the maximal signal amplitude (A_{max}, -12.94 dBm). **15d** shows peak amplitude, centred on 4.9 GHz, with the Rx at various distances from the box (0m to 1m) and the transmitter inside, where each dot colour represents a different axis. The dashed horizontal line shows A_{max}.

The shield demonstrated even better EM radiation blocking capability for signals originating inside and travelling outwards through it. When placed outside, the receiver could detect no appreciable signal above background noise at 4.9 GHz when 1m distant from the box, with the transmitter inside operating at full power (figure 15c). This observation was corroborated by peak amplitude at 4.9 GHz vs receiver distance data (figure 15d). The average peak amplitude remained comparable or close to average background noise for all but the shortest Rx distances, with average peak amplitude ranging from approximately -66 dBm to -64 dBm for 1m to 0.4m distance respectively. This rose to an average of approximately -62 dBm at 0.2m distance and climbing slightly to -56 dBm at 0m. For this dataset, the highest peak amplitude recorded was -52.86 dBm at 0m distance, significantly below the highest reading with the Tx outside the box and Rx inside (-39.52 dBm).

3.4 – Discussion

Retinoic acid differentiation of SH-SY5Y cells is known to induce a significant shift towards a more neuron-like phenotype, including various changes to morphology, metabolism and neurotransmitter sensitivity (Encinas, Iglesias et al. 2000, Korecka, van Kesteren et al. 2013). This differentiation process was clearly visible in the morphology of SH-SY5Y cells treated with retinoic acid, which grew long protrusions that are typical of neurons (figure 11). This was best seen in the immunofluorescent microscopy image where Tau primary antibody had been used (figure 11e). Further evidence of this phenotypic shift was seen in experiments with CellTiter-Blue assay kit – which revealed a clear increase in sensitivity to hydrogen peroxide insult following differentiation (figure 12). This data supports the choice to utilise differentiated SH-SY5Y cells as a cellular model for this project. They are robust and easy to work with, grow quickly and can be made to exhibit high sensitivity to metabolic insult through differentiation – which is ideal given the investigative focus of this project shall be directed towards detection of, potentially quite subtle, biological effects. Disturbances to cellular metabolism can be reasonably expected if it is true that RF-EMF exposure may induce oxidative stressor effects. Although, sensitivity to hydrogen peroxide insult does not necessarily mean these cells will be sensitive to other, functionally distinct insults.

The faraday shield used for this project is a 50cm wide, 50cm long and 40cm high lidded box constructed with 10mm thick Aluminium (Al). Al was chosen due to its good electrical conductance properties, which is one of the main parameters that influences the ability of a material to act as a Faraday shield through interactions with the electrical field component of electromagnetic waves (Weibler and Enclosures 1993). For this reason, Al is widely used in RF shielding applications and was deemed an appropriate choice here (Weibler and Enclosures 1993). Thickness of the shielding material is another major parameter that contributes to shielding ability, hence sheets of 10mm Al were chosen over cheaper, thinner alternatives. Practicality, financial constraints and availability made even thicker metal sheets less desirable as it was estimated that 10mm may be sufficient to provide robust EMF shielding properties for the signals used in this project.

Thankfully, the shield demonstrated good RF shielding ability for the maximal output settings of the equipment sourced for the project (figure 15). The maximal signal amplitude recorded, with both transmitter and receiver inside the box and no shielding interference, was -12.94 dBm, which is equivalent to 5.0816e-2 mW. Whereas the highest power detected for waves penetrating through to the interior of the shield from the outside environment was -39.52 dBm, equivalent to 1.11169e-4 mW, which is approximately a 450-fold decrease in power

due to shielding. Additionally, this value was only achieved with the transmitter placed very close to the box (20cm distant) and facing a box corner, instead of a side panel. It is known that seams and joins in faraday shield constructs can lead to “leakage” of waveforms through the material used, much like soundwaves through small air gaps (Weibler and Enclosures 1993).

The average amplitude of outside-to-inside penetrating waves dropped to -60.35 dBm (equivalent to 9.2257e-7 mW, a roughly 50,000-fold decrease in power relative to Amax) with just 1m distance between the transmitter and the box. These figures, combined with the observation that any external source of RF radiation, not introduced as part of experimental design, is certain to be significantly more distant from the box, provide a good level of confidence in the reliability of the box to act as a Faraday shield for future experiments. Additionally, the ability of waves to penetrate outwards from a transmitter placed inside the box appears even lower than outside-to-inside waveform penetration (figure 15c and 15d). For all but the shortest receiver to box distances, the signal recorded was indistinguishable from background noise (figure 15d). Even with the receiver immediately adjacent to the box (0m), the average peak amplitude at 4.9 GHz was just -56 dBm, which is equivalent to 2.5119e-6 mW. Although, it is possible this apparent superior RF-EMF blocking ability for inside-to-outside waveforms may be partially attributed to slight flaws and variances in receiver orientation relative to the transmitter inside the box. But efforts were made to keep antennae orientation as consistent as possible for all axes tested using benchtop markings. Still, this dataset provides a reasonable degree of confidence of the safety of the experimental setup. Subsequent RF-EMF exposure experiments will be conducted with both antennae inside the box and these data indicate that leakage of signals to the surrounding environment should be minimal and orders of magnitude below recommended safe power levels.

Despite the apparent success of the EMF shielding ability of the box, numerous obstacles presented themselves when planning early experiments with cells. Namely, pH, temperature and humidity control within the box microenvironment. Although the box shields waveforms relatively effectively, it is far less ideal for cell culture. Initially, it was anticipated that pH stability over the course of long, multi-day exposure experiments in the shield could be problematic with standard cell culture media due to reliance on carbonic acid formation within standard cell incubators. When tested, cell-containing RPMI media showed rapid pH drift, climbing from 7.8 to 8.4 average pH in just 2 hours and rising to 8.6 after 4 hours outside a CO_2 enriched environment (figure 13a). The observation that pH returned to baseline after being returned to an incubator for 2 additional hours confirmed RPMI reliance

on CO_2 enrichment and carbonic acid formation for pH buffering activity, rendering it unsuitable for experiments within the box – which has no capacity to regulate CO_2 and might leak signals if modified to do so. Thankfully, Gibco also offer a specialist media designed for use in cell work outside the incubator microenvironment; CO_2 Independent Media (CIM). When tested, it showed an impressive ability to buffer against pH changes over a prolonged period, even in the presence of living, metabolically active cells (figure 13b). With an average starting pH of 7.6, it dropped ~0.1 pH units after each 24-hour period, falling to 7.5, 7.4 and 7.3 average pH after 24, 48 and 72 hours respectively. This means that even after being left for 72 hours, the pH had lowered only ~0.3 from the starting pH, which is significantly lower magnitude than the average pH change of RPMI media after just 2 hours outside an incubator (RPMI pH rose 0.6 in 2 hours). These results confirmed the suitability of CIM for this experimental setup, which will be used for all cell work performed outside the incubator going forward.

However, despite confidence in the pH buffering activity of CIM, preliminary flow cytometry data using this media indicated a significant degree of cellular debris by the 48-hour time point for cells kept inside the box at room temperature (21ºC), regardless of RF exposure applied. This was attributed to be largely the result of a lack of proper temperature control within the box microenvironment. To remedy this, a hot plate was used to provide heating and attempt to bring the internal box temperature close to that of standard cell incubators, ~37ºC. But the minimum setting of the hot plate was 50ºC, necessitating some kind of heat insulation between the surface of the hot plate and the base of the box. Initial tests with freely available scrap metal sheets indicated that a 13mm thick sheet of unknown metal alloy may be suitable, as temperature began to plateau at ~38ºC inside the box after 160 minutes heating time. But the dimensions of the scrap sheet were not appropriate for the surface of the hot plate and box, creating stability issues (i.e. the sheet was markedly narrower than the base of the box). To solve this, a 15mm sheet of Al alloy was purchased with more appropriate dimensions in the hope that it would provide similar box internal heat reduction, whilst offering a more physically stable setup. However, internal temperature testing revealed that the heating reduction effect was lost, with the internal temperature almost reaching the same ~41.5ºC plateau as observed with no material between the box and hot plate surface (figure 14a and 14b). In retrospect, it is thought that the scrap metal sheet was able to generate a cooling effect partly because of its narrower dimensions – effectively reducing surface contact between the base of the box and the hot plate surface, thereby reducing heat transfer from the hot plate to the base of the box. But it was also of an unknown alloy and may well have contained metals that are less effective heat conductors when compared to the 15mm Al sheet tested. Although metal would have been a good

material to use from a fire safety perspective (it cannot be melted or burned by achievable hot plate temperatures in the event of a malfunction), other materials were then considered alongside cutting channels into the 15mm Al sheet to reduce surface contact.

Rubber is widely used for heat insulation purposes and was considered for use here. A 2mm thick sheet of rubber was cut to match the dimensions of the hot plate surface and its effect on the internal temperature plateau was tested (figure 14c). Disappointingly, it had limited effect on internal temperature, reaching a plateau of ~39.5ºC, which is ~2ºC below the baseline internal temperature with no heat insulation. However, when another 2mm thick rubber sheet was cut to the same dimensions and placed on top of the original rubber sheet, creating a 4mm thick rubber barrier in total, the desired insulation effect was achieved (figure 14d). The internal box temperature reached a plateau of ~37ºC, remaining stable after 200 minutes heating, an ideal temperature for future cell culture work.

Finally, to address the lack of humidity control within the box, a water bath filled with distilled water was placed inside the box. Additionally, wherever possible the outermost wells of cell culture plates were filled with PBS during testing to provide additional protection against evaporation during testing procedures. A side-view schematic of the final layout of the Faraday shield setup is detailed below, showing the placement of all major components (antennae, cell flasks or plates, water bath etc).

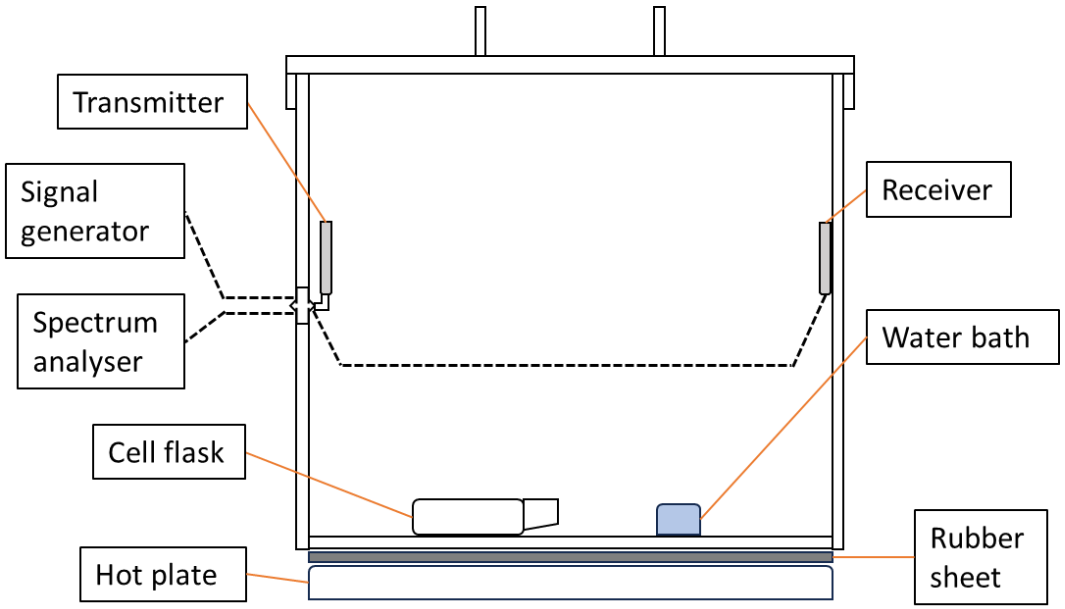

Figure 16 – a schematic showing a side view of the internal arrangement of the Faraday shield setup and its various components during RF-EMF exposure experiments. Dashed black lines represent coaxial SMA cables connecting external machines to internal antennae; a spectrum analyser and signal generator connected to the receiver and transmitter respectively. Depending on experimental procedure, cell culture plates may be used in place of cell culture flasks.

In terms of antenna and cell flask/plate placement within the box, the received signal was tested with various antennae positioning – to ensure the dose received by cells did not meaningfully change due to position. To achieve this, the internal space within the box was divided up into sections and the received signal analysed with the transmitter switched on. Additional readings were taken in the Z axis, or height domain, to confirm that height did not also meaningfully change signal intensity. Receiver position within the internal space was observed to have negligible effect on signal intensity – which is unsurprising given the omni-directional nature of the transmitter and the relatively small dimensions involved.

With control measures in place to regulate cell culture conditions within the box, including temperature, pH and humidity, it is hoped that multi-day RF-EMF exposure experiments may be conducted without inducing high levels of cellular or oxidative stress. Resolution of biological effects resulting from RF-EMF exposure becomes increasingly difficult as background cellular stress levels rise. There is already evidence indicating that biological effects and consequences of RF-EMF exposure may accumulate or become more apparent over time, as demonstrated by a group in 2020 that found significantly reduced cellular proliferation of several cell lines in the presence of RF-EM radiation over a 72-hour period (Choi, Min et al. 2020). Interestingly, one of the cell lines used in this study included

undifferentiated SH-SY5Y cells, which were found to be particularly sensitive to higher doses of RF-EM radiation, giving further weight to the choice to use this cell line here.

Unfortunately, it will not be possible to accurately detect, record and control temperature within cell media itself in our experimental setup. This is a slight cause for concern as regulatory bodies currently place heavy emphasis on heating effects being a primary source of potential harm to cells and tissues within the context of RF-EM radiation (ICNIRP 2020). However, the maximum power output of the signal generator used here (16.5 dBm) is low relative to international safety standards and below the power output of mobile phones, which can regularly achieve a power output of 30 dBm when moving between cellular network cells (Lönn, Forssen et al. 2004). Therefore, it is not anticipated that heating effects are likely to be a major causative factor in any detected biological effects – because the emission power is lower than that of commercially available devices, which are themselves deemed to be biologically safe and below the energy threshold for significant heating effects (ICNIRP 2020). When tested, average temperatures recorded in cell media did not change following signal emission using a thermometer sensitive to 0.5 ºC changes. But this does not eliminate the possibility of small intensity fluctuations (<0.5 ºC), transient heating effects or localised heating effects occurring, which is a concern because different types of biological material and cellular compartments may possess distinct energy absorption properties (Banu, Vanaja et al. 2013, Subramanian, Sundarambal et al. 2018). Localised heating effects have previously been speculated as a potential confounding factor in this context, meaning more precise temperature control would have been desirable here in this study and is an area for potential improvement in the future (Koivisto, Revonsuo et al. 2000).

Modulation of carrier waves with complex patterns of modulation is an important part of modern cellular networks, enabling the transmission of data to and from many different users simultaneously for any given cell. For example, Orthogonal Frequency Division Multiplexing (OFDM) has been heavily utilised in both 4G and 5G networks, which is just one of the various modulation methods being considered for 5G networks (Cai, Qin et al. 2017). Unfortunately, limitations with the signal generator used in this project means exact emulation of modulation patterns most commonly used in 5G and WiFi networks will not be possible, particularly full OFDM. This is a significant consideration as demodulation effects in tissue may be relevant in explaining and understanding how RF-EMFs might cause biological effects (Foster and Repacholi 2004, Challis 2005, Silny 2007, Juutilainen, Höytö et al. 2011). Thankfully, some modulation techniques are available, such as FSK, PSK and QAM – meaning there will be some ability to probe potential biological effects specifically associated with demodulation. Among the modulation schemes available to us, QAM was

chosen because of the use of orthogonality to improve spectral efficiency – a trait that is a key characteristic of OFDM modulation schemes. It is also true that QAM itself is utilised to some extent in wireless networks, some examples being CDMA, WiMAX-16d, WiMAX-16e and WLAN-11a OFDM (Alex and Jalloul 2008, Hong, Sagong et al. 2014, Wu, Wang et al. 2016).

But the overall focus of this chapter is on establishing a platform that provides an experimental space where external signals are not able to effectively penetrate, thereby creating a clear and definite link between artificially introduced signals and possible biological effects. The influence of full OFDM modulation will be explored using a different setup with a 5G phone placed inside a mini-incubator, to capture any potential demodulation effects that may be otherwise missed. This alternative experimental approach also serves as a means of comparing and verifying results obtained using the Faraday shield that might otherwise be dismissed as an artefact resulting from the design of the shield itself. The 5G phone setup also has the added advantage of being extremely representative of real-world exposure scenarios, with almost no abstraction whatsoever from typical use cases – i.e. the signals transmitted and received from the phone are identical to those of other consumer phones.

Chapter 4 – Results

Cellular redox homeostasis changes in response to RF-EMF exposure

Preface

Much of the evidence for biological effects of nonthermal RF-EMFs points towards increased ROS generation in exposed cells. But despite this, strong epidemiology evidence for disease burden associated with telecoms signals has not yet materialised – at least from the perspective of regulatory bodies, such as the ICNIRP. Therefore, the objective of this chapter was two-fold; to look for direct evidence of the promotion of oxidative stress in RF-EMF exposed cells to corroborate existing literature that suggests it might occur and also to investigate cellular redox homeostasis mechanisms that may mask detection of redox homeostasis disruption, particularly over short timeframes (days). This investigation will include enzymatic assays in an attempt to elucidate new information on the signalling responses to RF-EMF exposure underlying the observed and documented increase in ROS production.

4.1 – Introduction

A good amount of evidence has been accumulated over the years indicating that RF-EMF exposure may lead to increased ROS generation in cells (Oktem, Ozguner et al. 2005, Zeni, Di Pietro et al. 2007, Yao, Wu et al. 2008, Luukkonen, Hakulinen et al. 2009, Consales, Merla et al. 2012, Kang, Lee et al. 2014, Usselman, Hill et al. 2014, Yakymenko, Tsybulin et al. 2016, Choi, Min et al. 2020, Panagopoulos, Karabarbounis et al. 2021). But cells have a natural ability to regulate concentrations of potentially damaging reactive species, such as superoxide and nitric oxide, through the use of various homeostatic mechanisms (Willems, Rossignol et al. 2015, Ursini, Maiorino et al. 2016, Le Gal, Schmidt et al. 2021). Under normal, physiological conditions cells will generate a certain level of these species, but signalling feedback loops, often involving the reactive species themselves, typically prevent concentrations within a cell from rising too high (He, He et al. 2017). This balance between generation and clearance of reactive species is critical to the health of cells – with robust evidence conclusively demonstrating that if reactive species generation becomes overwhelming, cells experience molecular damage and enter a state of oxidative stress, leading to dysfunction, cell death and the probability of various disease outcomes rising (Newsholme, Haber et al. 2007, de Vries, Witte et al. 2008, Ziech, Franco et al. 2011, He, He et al. 2017). The mitochondria is an organelle closely involved with this redox homeostasis process and provides one of the best-studied examples of how ROS levels are able to influence cellular function, with ROS themselves being used as a modulating signal.

Mitochondria are widely known for their ability to generate chemical energy in the form of ATP during the process of oxidative phosphorylation, which occurs at the mitochondrial membrane (Mitchell 1961). Essentially, this is the process of using NADH and FADH (which are themselves derived from nutrient metabolism) as electron donors in combination with molecular oxygen to produce ATP and involves a series of protein complexes and reactions collectively termed the Electron Transport Chain, or ETC (Guo, Gu et al. 2018). Although, it has become clear the mitochondria has other cellular functions, including “energy sensing” and homeostatic roles (Duchen 1999). But this process of ATP generation is imperfect and oxidative phosphorylation will naturally lead to the production of ROS within a normal, physiological range of concentrations (Willems, Rossignol et al. 2015). Complexes 1 and 3 of the ETC are likely the most common sites of ROS formation, but they may arise at other sites via different reactions (Murphy 2009, Koopman, Nijtmans et al. 2010, Mailloux, McBride et al. 2013). Superoxide is the most common ROS formed at the mitochondria, which can be converted into hydrogen peroxide by a family of enzymes called SuperOxide Dismutases, or SOD enzymes (Auchère and Rusnak 2002). Superoxide may also react with hydrogen

peroxide to form an extremely reactive hydroxyl radical, which will almost immediately react with any molecules that happen to be nearby, forming various rare products, such as lipid radicals (Auchère and Rusnak 2002, Winterbourn 2020). But hydrogen peroxide may also be enzymatically converted into water via the activity of catalase (CAT) enzymes, highlighting the potentially diverse outcomes for reactive species (Mailloux, McBride et al. 2013, Ighodaro and Akinloye 2018). In addition to being a site of ROS generation, mitochondria may also be exposed to other reactive species, such as nitric oxide, which is important when considering redox signalling and how it can influence mitochondrial function (Valerio and Nisoli 2015, Willems, Rossignol et al. 2015).

One of the ways these reactive species contribute to redox signalling is manifested in the morphology of mitochondria. Mitochondria are organelles that undergo continuous change to their shape and structure over time, cycling between a more fused and more fragmented morphology (Chan 2012). Fission events are thought to be mediated by recruitment of a cytosolic protein called Dynamin-related protein 1 (Drp1) to the outer mitochondrial membrane, which involves a number of chaperone proteins that includes; human fission protein 1 (hFis1), mitochondrial fission factor (Mff), and mitochondrial elongation factors (MIEF1/MiD51 and MIEF2/MiD49) (Lackner and Nunnari 2010, Chan 2012, Losón, Song et al. 2013). Whereas fusion events, an ATP-requiring activity, are mediated by mitofusins (Mfn1/Mfn2; MOM-fusion) and the optic atrophy 1 protein (OPA1) (Meeusen, McCaffery et al. 2004, Frezza, Cipolat et al. 2006, Chan 2012). These remodelling events and the proteins associated with them are important when considering how reactive species modulate mitochondria morphology and function.

There is good evidence showing a clear connection between cellular concentrations of Reactive Nitrogen Species (RNS) / ROS and the morphological state of mitochondria (Blanchet, MC Buydens et al. 2011). Elevated levels of RNS/ROS are associated with a generally more fragmented mitochondrial morphology and may be indicative of a state of cellular stress and lead to increased mitophagy (Willems, Rossignol et al. 2015). Lower RNS/ROS levels are associated with a more fused phenotype and is commonly seen in healthy cells, although, it is worth remembering that mitochondrial morphology is a dynamic process and oversimplification must be avoided (Picard, Shirihai et al. 2013, Willems, Rossignol et al. 2015). Specific examples of these processes and molecules critical to them can be seen in several studies. Such as a 2011 paper by Rakovic et al, in which they used mutations to highlight the importance of mitofusin ubiquitination and mitochondrial fission and mitophagy events (Rakovic, Grünewald et al. 2011). But as part of this work, they also introduced exogenous H_2O_2 to control cells and reported a clear response of mitofusin

ubiquitination – targeting them for degradation and thereby likely prompting cells towards mitochondrial fission events in response to H_2O_2. Another study, using fibroblasts, observed that cells with severe deficiency in the first protein complex of the ETC (or simply C1) had higher ROS levels and more fragmented mitochondrial morphology (Koopman, Verkaart et al. 2007). Furthermore, they also reported that less severely impacted C1 function correlated with a smaller increase in ROS levels and somewhat less fragmented mitochondrial morphology (Koopman, Verkaart et al. 2007). In a drosophila model, high ROS concentrations promoted Drp1 activity and fragmentation of mitochondria, whereas low ROS concentrations resulted in more fused mitochondria (Muliyil and Narasimha 2014). These relationships between ROS and mitochondrial morphology were further corroborated by Picard et al in 2013, using genetic techniques to promote either fission or fusion events (Picard, Shirihai et al. 2013). Once again, fission events correlated with higher ROS levels and fusion events correlated with lower ROS levels. But there are exceptions to this general trend and association, such as a 2013 paper in which Drp1 overexpression did cause mitochondria fragmentation – but did not appear to lead to elevated ROS concentrations (Distelmaier, Valsecchi et al. 2012). But when viewed as a whole, the body of evidence produced shows there is a clear, cellular context dependent, relationship between ROS and mitochondria morphology and function that continues to be explored and verified today (Ashraf and Kumar 2022, Chang, Niu et al. 2023). These changes in mitochondria morphology are thought to be connected to modulation of function, in a structure-function relationship that exists throughout several areas of biology (e.g. protein structure and function relationships) (Picard, Shirihai et al. 2013). Although, the full detail of how mitochondrial structure informs function requires more study, some clues already indicate the profound cellular significance of these fusion/fission events. For example, abnormal mitochondrial dynamics are known to disturb biogenetics and are implicated in promoting various diseases, effectively summarised by Chan et al in 2020 (Chen, Chomyn et al. 2005, Waterham, Koster et al. 2007, Yu-Wai-Man, Griffiths et al. 2010, Stuppia, Rizzo et al. 2015, Chan 2020).

But the picture of cellular redox homeostasis is broader than just mitochondrial superoxide and involves various other pathways, proteins and enzymes (He, He et al. 2017). For example, nitric oxide may be formed enzymatically by nitric oxide synthases, which catalyse the release of nitric oxide from Arginine (Ghafourifar and Cadenas 2005). The fact that this is an enzymatic process drives home the biological importance of these reactive compounds as signalling molecules, despite the fact that they may be damaging to cells. Indeed, nitric oxide has proven itself as being a significant molecular signal in the regulation of mitochondrial membrane potential and oxygen consumption (Ghafourifar and Cadenas

2005). It is worth noting that there are also several non-mitochondrial sources of both ROS/RNS. Examples include the plasma membrane-bound NADPH oxidase, which generates superoxide, or rare by-products resulting from the imperfect breakdown of toxicants and many other compounds in the liver by the Cytochrome-P450 (CYP) superfamily of enzymes (Fleming, Michaelis et al. 2001, Newsholme, Haber et al. 2007, Veith and Moorthy 2018).

As described earlier, redox homeostasis is the process of balancing generation of these various reactive chemicals with their clearance in order to prevent excessive molecular damage and oxidative stress from occurring. This is achieved by antioxidant systems that function to eliminate reactive species through a variety of pathways. Some of these are enzymatic antioxidants, with prominent examples being superoxide dismutases (SODs), catalases (CATs) and glutathione peroxidases (GPXs) (Ighodaro and Akinloye 2018). But there are non-enzymatic antioxidant defence mechanisms also, with some known examples being metal binding proteins (MBPs), glutathione (GSH), uric acid (UA), melatonin (MEL), bilirubin (BIL) and polyamines (PAs) (Mirończuk-Chodakowska, Witkowska et al. 2018). Enzymatic antioxidants typically convert their substrates into less toxic compounds, a process which may iteratively bring reactive compounds progressively closer to being biologically benign. A good example of this is in the activity of SOD and CAT enzymes, which first convert superoxide into oxygen and hydrogen peroxide then convert hydrogen peroxide into oxygen and water, respectively (Ighodaro and Akinloye 2018). Alternatively, GPX enzymes are a family of “selenoproteins” (i.e. those containing a Selenocysteine animo acid residue) that are widely known to provide protection against both hydrogen peroxide and hydroperoxides (e.g. -OOH anion) by catalysing their conversion to water or appropriate alcohols, respectively, using reduced glutathione (GSH) (Margis, Dunand et al. 2008).

In terms of non-enzymatic antioxidant responses, GSH is one of the most important, most well-studied components of this area of cellular biology, although, many other non-enzymatic antioxidants are known to exist (Mirończuk-Chodakowska, Witkowska et al. 2018). GSH is a 3-residue peptide comprised of cysteine, glycine, and glutamic acid and it is found at significant concentrations in all mammalian cells (Averill-Bates 2023). It exists in two forms – a reduced form, glutathione (GSH) and an oxidised form, glutathione disulfide (GSSG) (Averill-Bates 2023). It can function directly as an antioxidant itself, by acting as a reducing agent while in its reduced form to react with ROS such as peroxides and free radicals. But it is also involved in many other cellular processes, including acting as a cofactor for enzymes (as seen with GPX activity), protein folding and degradation, cell cycle regulation and more (Franco and Cidlowski 2009, Averill-Bates 2023). It is so critical to redox homeostasis, that

the ratio of GSSG to GSH is itself one of the key cellular indicators of redox state – and if this ratio rises too high in favour of GSSG, cells enter into a state of oxidative stress and a variety of responses and signalling cascades are initiated as a result (Franco and Cidlowski 2009, Zitka, Skalickova et al. 2012, Averill-Bates 2023). But it is worth pointing out that the redox signalling system is complex, involving many entities, and cannot comfortably be compressed down to a single compound ratio (Jones 2006). A clear example of the relevance of GSH and redox signalling is observed in regulation of apoptotic responses. Depletion of GSH and consequent increased ROS concentrations is known to induce apoptosis, with activation of mediators such as nuclear factor kappa B and caspase release being key downstream targets in the cell-death signalling cascade, of which GSH/GSSG is a key component (Armstrong, Steinauer et al. 2002, Friesen, Kiess et al. 2004).

Other key players in redox signalling include SOD enzymes and their oxidative counterparts, superoxide and hydrogen peroxide (Holmström and Finkel 2014, Wang, Branicky et al. 2018). While thought to contribute to redox signalling to some extent, superoxide is far less stable when compared to hydrogen peroxide – and perhaps most significantly, far less able to move between cellular compartments than hydrogen peroxide (Wang, Branicky et al. 2018). For these reasons, superoxide likely acts primarily in the vicinity of formation sites (e.g. C1 and C3 of the ETC), whereas hydrogen peroxide may move throughout the cell and exert influence in different compartments, arguably making it better suited as a signalling molecule candidate (Cardoso, Chausse et al. 2012, Wang, Branicky et al. 2018). Signalling pathways that involve hydrogen peroxide include; platelet-derived growth factor (PDGF) signal transduction, c-fos signalling and downstream AP-1 activity and epidermal growth factor (EGF) signalling, with several others also being considered in literature (Lo and Cruz 1995, Sundaresan, Yu et al. 1995, Bae, Kang et al. 1997, Wang, Branicky et al. 2018). Redox signalling is also known to be of particular importance in the context of regulating programmed cell death, as described earlier (Hampton, Fadeel et al. 1998, Armstrong, Steinauer et al. 2002, Circu and Aw 2010, Sevrioukova 2011, Chang, Niu et al. 2023). Control of many of these redox signal transduction pathways involves reversible oxidation and reduction of essential cystine residues found on tyrosine kinase enzymes – which controls the activity of said enzymes (Bae, Kang et al. 1997, Holmström and Finkel 2014). A common H_2O_2 redox signal response begins with oxidation of these residues and inactivation of tyrosine kinase activity – modulating the activity of various targets downstream of these enzymes (Holmström and Finkel 2014).

The entirety of RNS/ROS generation, clearance by antioxidant systems and signalling pathways associated with cellular redox state is very complicated, involving many different

molecules, only some of which have been described here (Sevrioukova 2011, Holmström and Finkel 2014, Ursini, Maiorino et al. 2016, He, He et al. 2017, Wang, Branicky et al. 2018, Winterbourn 2020, Le Gal, Schmidt et al. 2021). But it is clear that the interplay between oxidation and reduction is critical to cells and disruptions to redox homeostasis systems are strongly associated with disease outcomes (Spector 2000, Kang 2002, Barzilai and Yamamoto 2004, Kryston, Georgiev et al. 2011, Forman and Zhang 2021). Given that many papers have reported a link between RF-EMF exposure and disturbances to redox homeostasis, it might reasonably be expected that long-term use of telecoms devices that harness these radio waves could, and probably should, be associated with increased risk of disease (Lantow, Lupke et al. 2006, Zeni, Di Pietro et al. 2007, Yao, Wu et al. 2008, Agarwal, Desai et al. 2009, Luukkonen, Hakulinen et al. 2009, Kang, Lee et al. 2014, Usselman, Hill et al. 2014, Choi, Min et al. 2020). But the overall stance of regulatory bodies, such as the ICNIRP, is such that provided cellular networks stay within prescribed power limits for signal emissions, then there is no meaningful increase in disease risk and people are essentially safe (Protection 1998, ICNIRP 2020). As previously discussed, there is a back-and-forth on the truthfulness or accuracy of this viewpoint, with some basic researchers feeling that they are poorly represented within relevant regulatory bodies (Hardell, Nilsson et al. 2021, ICBE-EMF 2022, Nordhagen and Flydal 2023).

But it is certainly true that some fairly robust epidemiology evidence exists suggesting no link between mobile phone use and disease burden, with many studies showing minimal risk associated with mobile phone use (Ahlbom, Feychting et al. 2009). A good example of this is the large INTERPHONE study, which reported no increase in cancer risk for all but the heaviest mobile phone users, essentially concluding that their use appears to largely be safe for most people (Group 2010, Group 2011, Swerdlow, Feychting et al. 2011). But there are flaws within the INTERPHONE study design, which the authors acknowledge themselves, mostly relating to participant bias (Group 2010, Swerdlow, Feychting et al. 2011). It is also important to note that several other studies have reported an increase in disease risk associated with RF-EMF exposure (Szmigielski 1996, Hardell, Hallquist et al. 2002, Hardell, Mild et al. 2006, Hepworth, Schoemaker et al. 2006, Lahkola, Auvinen et al. 2007, Lahkola, Salminen et al. 2008, Cancer 2011, Falcioni, Bua et al. 2018, TR 2018).

Given this background of conflicting evidence regarding disease risk in the context of RF-EMF and that oxidative stress is overwhelmingly associated with disease, it begs the question; if telecoms signals are capable of disturbing redox homeostasis, should chronic exposure cause cells to enter into a state of oxidative stress? And if this does happen, should we expect a strong, undeniable link between mobile phone use and disease burden?

Another possibility, of course, is that any exogenous pressure exerted on redox homeostasis, if sufficiently small in intensity, may be resisted by cellular compensatory mechanisms, even with prolonged exposure – effectively masking the effects of these exposures. Regardless of the underlying biological truth, it is clear from these observations that, from the perspective of regulatory bodies, there is a lack of definitive proof of the promotion of oxidative stress in response to exposure to telecoms signals (Protection 1998, ICNIRP 2020). Moreover, epidemiology evidence on the matter is somewhat conflicted – casting doubt on the seriousness of the disease risk posed by telecoms technology. We need to know if these signals promote oxidative stress and disease, conclusively, and more work is required to reach this point. Particularly in light of ever more advanced communications technology and increasingly EMF saturated environments for most people.

With these considerations in mind, the objectives of this chapter are as follows;

1. Explore the capacity of telecoms signals to influence metabolic viability in the following contexts;
    a. Unmodulated sine waves within the Faraday shield setup
    b. QAM modulated waveforms in Faraday shield
    c. Mixed signals (cellular data and WiFi) using the 5G phone
2. Investigate the ability of RF-EMF exposure to promote ROS formation, as reported in literature
3. Probe mitochondrial function for any signs of perturbation in response to RF-EMF exposure
4. Analyse homeostatic responses following RF-EMF exposure, using metrics such as SOD1 and GSH activity

4.2 – Methods

4.2.1 – CellTiter-Blue metabolic viability assay

Initially, SH-SY5Y cells were differentiated in T75 flasks (Thermo Scientific™ Nunc™ Cell Culture Treated EasYFlasks™, catalogue number 156499) using all-trans retinoic acid (Thermo Scientific Chemicals Retinoic Acid 97%, catalogue number 044540.02) and neurotrophic growth factor (Gibco™ Human/Mouse/Rat BDNF Recombinant Protein, PeproTech®, catalogue number 450-02-10UG) according to the differentiation protocol previously described.

Once this process was complete, cells were detached using X1 Trypsin (Gibco™ Trypsin-EDTA, no phenol red, product code 10779413), counted and then plated out into 96-well plates (Corning® 96-well Clear Flat Bottom TC-treated Microplate, 20 per Bag, with Lid, Sterile, product number 3628) at a seeding density of 20,000 cells per well and left to settle overnight in supplemented Neurobasal media (Gibco™ Neurobasal™ Medium, catalogue number 21103049) in a standard cell culture incubator at 37ºC.

The following day, media in wells was changed to pre-warmed CO_2 Independent Media (CIM, Gibco™ CO_2 Independent Medium, product code 11580536) and plates were transferred to either the 5G phone in mini-incubator setup or the Faraday shield setup for experimentation. For control and background signal removal purposes, each plate contained cell-free wells which were otherwise treated the same. Additionally, positive control wells were included using a known oxidative stressor, Menadione (Sigma-Aldrich, Crystalline Menadione, 2-Methyl-1,4-naphthoquinone, Vitamin K3, product code M5625-25G) (Thor, Smith et al. 1982, Hollensworth, Shen et al. 2000). For these Menadione control wells, Menadione was added to the CellTiter-Blue (CTB) reagent incubation step give a final concentration of 2 μM.

For RF exposure, plates were either irradiated or not in both experimental setups. For the Faraday shield only, there were two different types of radiation exposures – with and without QAM modulation applied. This gave a total of 5 exposure groups across both setups; the 5G phone on and emitting mixed signals or with the phone switched off, the Faraday shield with either no signal, unmodulated sine wave signal (4.9 GHz, SAR = 8.9898E-04 W/kg) or a QAM modulated signal (4.9 GHz, 256-QAM, SAR = 4.016E-05 W/kg). In each case, RF exposure was applied to plates for 24, 48 or 72 hours before being processed through the CTB protocol.

When ready for processing at the appropriate time point, media in wells was gently removed and replaced with 100µl of pre-warmed Neurobasal media. To this, 20µl CTB reagent was added to each well and plates were incubated for 2 hours at 37ºC in an incubator. Following incubation, plates were read on a fluorescent plate reader (TECAN SPARK 10M, software SPARKCONTROL V2.2) with the following settings; $560_{EX}/590_{EM}$. At all times care was taken to cover plates and protect them from light exposure – which can otherwise lead to degradation of detected fluorescent signal.

4.2.2 – Flow cytometry using MitoSOX superoxide indicator and Tetramethylrhodamine Methyl Ester Perchlorate (TMRM)

SH-SY5Y cells were first differentiated as described above (Thermo Scientific Chemicals Retinoic Acid 97%, catalogue number 044540.02, Gibco™ Human/Mouse/Rat BDNF Recombinant Protein, PeproTech®, catalogue number 450-02-10UG), then detached (Gibco™ Trypsin-EDTA, no phenol red, product code 10779413), before being counted and seeded into T25 flasks at a seeding density of ~300,000 cells per flask (Thermo Scientific™ Nunc™ EasYFlask™ Cell Culture Flasks, catalogue number 156367). They were then left to rest in a standard cell culture incubator overnight at 37ºC in supplemented Neurobasal media (Gibco™ Neurobasal™ Medium, catalogue number 21103049).

The following day, media was changed to pre-warmed CIM (Gibco™ CO_2 Independent Medium, product code 11580536) and flasks were transferred either to the 5G phone in mini-incubator setup or to the Faraday shield. Several different types of signal were used for RF-EMF exposure, in addition to non-irradiated controls. The 5 different conditions applied were;

- 5G phone in incubator setup with phone off (control)
- 5G phone in incubator setup with phone on and emitting mixed signals (WiFi and cellular data)
- Faraday shield with signal generator off (control)
- Faraday shield with unmodulated sine wave transmission (4.9 GHz, SAR = 8.9898E-04 W/kg)
- Faraday shield with QAM modulated waveform (4.9 GHz, 256-QAM, SAR = 4.016E-05 W/kg)

Flasks from each exposure group were incubated in either experimental setup for 4, 8, 24 or 48 hours before being processed further. Following RF exposure, cells were detached from flasks using Trypsin which was then quenched with FBS-containing media, before being spun down to a pellet using a desktop centrifuge spinning at 200 RCF for 5 minutes. Pellets

were then resuspended in PBS (Gibco™ PBS, pH 7.4, catalogue number 10010023) and transferred to 1.5 ml Eppendorf tubes (Eppendorf™ Safe-Lock Tubes 1.5 mL – Microtube, product code 15625367), then spun down using 200 RCF for 5 minutes. After this, the relevant experimental dye was added, either 1 µM MitoSOX for indirect visualisation of mitochondrial superoxide moieties (Invitrogen™ MitoSOX™ Mitochondrial Superoxide Indicator, catalogue number M36008) or 20 nM TMRM to analyse mitochondrial membrane potential and permeability (Thermo Scientific™ MitoProbe™ TMRM Assay Kit for Flow Cytometry, catalogue number M20036). In both MitoSOX and TMRM contexts, samples were incubated with dyes for 30 minutes in the dark, as per the reagent instructions. As a control, a 2-hour incubation with 2 µM Menadione was used (Sigma-Aldrich, Crystalline Menadione, 2-Methyl-1,4-naphthoquinone, Vitamin K3, product code M5625-25G). For TMRM samples, kit supplied CCCP ((Carbonyl cyanide 3-chlorophenylhydrazone) was used as a positive control at 20 mM concentration – which required only 5 minutes incubation in accordance with the kit protocol. Each experiment also included blanks, samples which were not given any dye or control compound – instead being incubated in PBS alone. After incubation, cells were pelleted down using 200 RCF for 5 minutes in a centrifuge, then washed in PBS a final time before being resuspended in 300 µl PBS and put through a flow cytometer (BD Accuri™ C6 Plus Flow Cytometer). Settings used in the cytometer were; FL2 detector (585 +/- 20 nm) and the PE Fluorochrome, which was appropriate for both mitochondrial dyes according to their respective product specification sheets, with a slow flow rate and 10,000 event limit.

4.2.3 – GSH-Glo™ Glutathione Assay

This assay attempts to quantify the availability of the reduced form of GSH by generation of a luminescent signal. It is based on the following underlying reaction, in which a luciferin derivative is converted to luciferin in the presence of reduced GSH and an enzyme called glutathione S-transferase. This initial reaction is coupled to photon release by the activity of firefly luciferase enzyme in the presence of luciferin. In this way, light generated is taken to be proportional to the amount of GSH present in the initial reaction step.

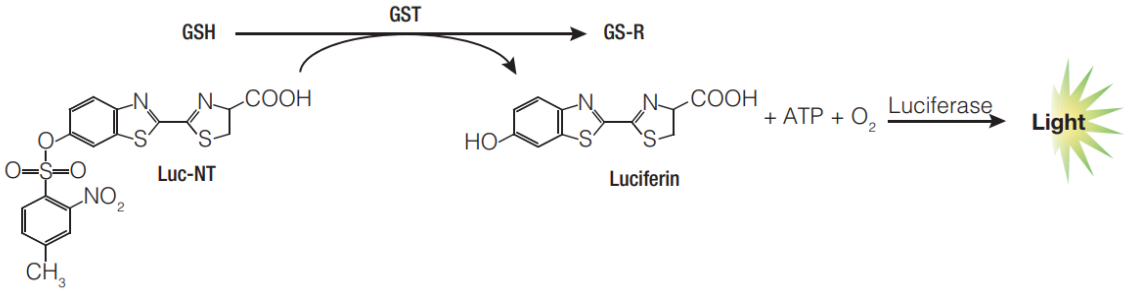

Figure 17 – an overview of the GSH-Glo™ Glutathione Assay, taken from the Promega GSH-Glo™ Glutathione Assay technical manual.

Initially, SH-SY5Y cells were differentiated as previously described. After this process was complete, cells were detached and transferred to white plastic 96-well plates specifically designed for luminescent assays (Thermo Scientific™ Nunc™ 96-Well Optical-Bottom Microplate, white, TC Surface, product code 10158721) at a seeding density of 20,000 cells per well. Plates were left to settle overnight in supplemented Neurobasal media (Gibco™ Neurobasal™ Medium, catalogue number 21103049) within a standard cell incubator at 37ºC.

The following day, media in wells was changed to pre-warmed supplemented CIM (Gibco™ CO_2 Independent Medium, product code 11580536) and plates were transferred to either the 5G phone mini-incubator or Faraday shield experimental setups. Once transferred, cells were exposed to either mixed signals from the 5G phone (WiFi and cellular data) or a QAM modulated waveform in the Faraday shield (4.9 GHz, 256-QAM) for 4 or 18 hours. Alternatively, plates were left in their respective experimental setups with the 5G phone or signal generator switched off (no radiation exposure). Each plate included triplicate cell-free control wells to be used for background signal removal purposes and triplicate positive control wells into which 2 µM Menadione (Sigma-Aldrich, Crystalline Menadione, 2-Methyl-1,4-naphthoquinone, Vitamin K3, product code M5625-25G) was added in addition to standard assay reagents. Additionally, each plate contained cell-free wells in which known concentrations of supplied GSH were added in order to generate a standard curve for analysis and confirmation of expected signal linearity. These known concentrations included 5 µM, 2.5 µM, 1.25 µM and 0.625 µM GSH.

After appropriate RF exposure had been applied, media in wells was replaced with 100 µl X1 GSH-Glo™ Reagent, which is a mixture that contains Luciferin-NT substrate and Glutathione

S-Transferase diluted 1:100 in GSH-Glo™ Reaction Buffer. Plates were incubated with this GSH-Glo™ Reagent for 30 minutes at room temperature under dark conditions, as directed by the kit protocol. This step is where 2 µM Menadione was added to appropriate wells to be included in the 30-minute incubation. Following this initial incubation step, a further 100 µl of reconstituted Luciferin Detection Reagent was added to each well, for a total volume of 200 µl. Plates were then incubated again at room temperature under dark conditions for a further 15 minutes. Finally, plates were taken to a plate reader and luminescence was detected (TECAN SPARK 10M, software SPARKCONTROL V2.2).

4.2.4 – Agilent Seahorse XF Cell Mito Stress Test

Initially, SH-SY5Y cells were differentiated as previously described, then detached and plated out into 24-well XF24 cell culture microplates (Seahorse XFe24 FluxPak, part number 102340-100) at a seeding density of 30,000 cells per well in supplemented Neurobasal media (Gibco™ Neurobasal™ Medium, catalogue number 21103049). Cells were left to attach in class 2 biological safety cabinets for ~1 hour before being gently placed in a standard cell incubator and left to settle overnight at 37ºC. The following day, media in wells was replaced with pre-warmed CIM (Gibco™ CO_2 Independent Medium, product code 11580536) and plates were transferred to the appropriate experimental setup for RF exposure (either the 5G phone inside a mini-incubator or the Faraday shield). Each XF24 cell culture microplate included 4 cell-free wells that were otherwise treated the same to serve as blanks and provide background removal as directed by the kit protocol.

Exposure conditions applied to plates were as follows;

- 5G phone in mini-incubator with phone switched off (no radiation)
- 5G phone in mini-incubator with mixed signal emission (WiFi and cellular data)
- Faraday shield with signal generator off (no radiation)
- Faraday shield with QAM modulated signal radiation (4.9 GHz, 256-QAM, SAR = 4.016E-05 W/kg)

RF exposure was applied for 18 hours overnight before progressing to the Oxygen Consumption Rate (OCR) assay the following day. The day before performing the assay, Seahorse XFe24 sensor cartridges were hydrated overnight using ~800 µl Seahorse XF Calibrant solution per well, which is supplied with the assay kit (Seahorse XFe24 FluxPak, part number 102340-100). This was done in the desktop mini-incubator at 37ºC, in a non-CO_2 enriched environment in accordance with the kit protocol. Additionally, specialised Seahorse medium was prepared for carrying out the assay, using Seahorse XF RPMI media

at pH 7.4 as a base (Seahorse XF RPMI medium, pH 7.4, 500 mL, part number 103576-100) and adding the following additives to it;

- 10 mM Glucose (Gibco™ Glucose powder, catalogue number 15023021)
- 1 mM Pyruvate (Gibco™ Sodium Pyruvate (100 mM), catalogue number 11360070)
- 2 mM Glutamine (Gibco™ L-Glutamine (200 mM), catalogue number 25030081)

On the day of the assay, this supplemented Seahorse media was warmed to ~37ºC then used to wash cell culture microplate wells twice, by gently replacing media with ~500 µl Seahorse medium, being very careful to remove as much fluid as possible without disturbing cells. Cell culture microplates were then left to rest in the CO_2 free mini-incubator at 37ºC for ~1 hour. During this time the Seahorse XFe24 Analyzer was switched on an allowed to complete its warming cycle. Additionally, several Mito Stress Test drugs were prepared and carefully loaded into the appropriate wells in the hydrated Seahorse XFe24 sensor cartridge. Those compounds are;

- Oligomycin, final concentration 1 µM (Sigma-Aldrich Oligomycin, product code 495455-10MG)
- FCCP, final concentration 3 µM (Sigma-Aldrich, Carbonyl cyanide 4-(trifluoromethoxy)phenylhydrazone, product code C2920-10MG)
- Antimycin A + Rotenone, final concentration 0.5 µM each (Sigma-Aldrich Antimycin A, product code A8674-25MG and Sigma-Aldrich Rotenone, product code R8875-1G)

After loading was completed, the hydrated Seahorse XFe24 sensor cartridge was loaded into the Seahorse XFe24 Analyzer for calibration. Once calibration was complete and the cell culture microplate had incubated for ~1 hour, the sensor cartridge was removed and replaced with the cell culture microplate and the OCR assay was performed using the standard Mito Stress Test protocol.

4.2.5 – Superoxide Dismutase (SOD) Activity Assay

The kit used for this assay determines SOD1 activity based on the extent of colorimetric signal reduction due to the conversion of superoxide into H_2O_2 by SOD1 (Sigma-Aldrich Superoxide Dismutase Activity Assay Kit, product code CS0009-1KT). The kit includes Xanthine Oxidase, which is an enzyme that catalyses several reactions and can produce superoxide. WST dye is also included – a dye which superoxide can react with to form formazan dye, yielding a colorimetric signal at 450 nm that can be read by an appropriate plate reader. Thus, SOD1 activity in sample lysates will reduce the availability of superoxide

produced by Xanthine Oxidase activity, which will mean there is a proportional reduction in the formazan dye signal. This may be expressed as both a percentage inhibition or in terms of enzymatic activity units using a known SOD standard. Prior to experimentation, a sample serial dilution was performed using the provided dilution buffer (CS0009B) to ensure values fell within the dynamic range of the assay kit.

To begin the experiment, differentiated SH-SY5Y cells were seeded into 6-well plates (Corning™ Costar™ 6-well Clear TC-treated Multiple Well Plates, product code 10578911) at a seeding density of 1,000,000 cells per well and left to settle overnight in supplemented Neurobasal media (Gibco™ Neurobasal™ Medium, catalogue number 21103049) in a standard cell incubator at 37ºC. The following day, media in wells was replaced with pre-warmed CIM (Gibco™ CO_2 Independent Medium, product code 11580536) and plates were transferred to the mini-incubator with a 5G phone inside or the Faraday shield for RF exposure. Plates were either given no radiation exposure, with the signal generator/5G phone switched off, or exposed to the following signals for 18 hours overnight;

- 5G phone with mixed signals (WiFi and cellular data)
- Signal generator emitting QAM modulated signal (4.9 GHz, 256-QAM, SAR = 4.016E-05 W/kg)

After RF exposure, cells were lysed on ice in preparation for the SOD1 assay. This was done by first removing media from wells and briefly washing in ~300 µl of cold PBS (Gibco™ PBS, pH 7.4, catalogue number 10010023). Ice-cold cell lysis buffer with pH 7.4 was prepared according to the SOD1 activity assay kit protocol (Sigma-Aldrich Superoxide Dismutase Activity Assay Kit, product code CS0009-1KT), using a Trizma-based buffer with the following ingredients;

- 0.1 M Trizma-HCl (Sigma-Aldrich Trizma® hydrochloride, product code T3253-1KG)
- 0.5 % Triton X-100 (Sigma-Aldrich Triton™ X-100, product code X100-100ML)
- 5 mM beta-mercaptoethanol (Sigma-Aldrich 2-Mercaptoethanol, product code M6250-100ML)
- Protease inhibitors (Thermo Scientific™ Halt™ Protease Inhibitor Cocktail, EDTA-Free (100X), catalogue number 87785)

The SOD standard curve was prepared on each plate according to the kit protocol, giving 0, 0.3, 0.6, 0.9, 1.5, 3 and 6 unit/ml standards. This was done by first preparing a SOD working solution by diluting 3 µl SOD enzyme stock (CS0009C) in 147 µl dilution buffer (CS0009B). This 6 unit/ml SOD working solution then had different amounts of dilution buffer added to it

to give lower concentrations used in the standard curve, ranging from 0 µl dilution buffer added to using 20 µl dilution buffer in place of SOD working solution. 0 units (no SOD added, only dilution buffer) gives maximal absorbance, due to no loss of signal via SOD activity. This becomes progressively lower as SOD units increase. WST working solution was prepared, again according to the kit protocol, by diluting 2 µl of 80X WST dye (CS0009D) in 158 µl of assay buffer (CS0009A), for a total volume of 160 µl per well. Xanthine oxidase working solution was prepared by diluting 0.2 µl of X100 stock (CS0009E) in 19.8 µl dilution buffer (CS0009B), for a total volume of 20 µl per well. Note, blanks were also included for background removal purposes (only 40 µl dilution buffer and 160 µl WST working solution added).

To analyse lysate samples, 20 µl sample was added to wells first, followed by 160 µl of WST working solution and finally 20 µl Xanthine oxidase working solution to start the reaction. Plates were then incubated under dark conditions at room temperature (~21C) for 30 minutes. Plates were then transferred to a microplate reader (TECAN SPARK 10M, software SPARKCONTROL V2.2) and absorbance at 450 nm was measured.

4.3 – Results

4.3.1 – RF-EMF exposure changes metabolic viability responses

To investigate the potential of RF-EMFs used in telecoms to modulate cellular metabolism, CellTiter-Blue (CTB) assay was performed with and without these signals present in both experimental setups. Furthermore, Menadione was selected as a good compound to use for control purposes – because it is known to promote superoxide formation, which is thought to be an important feature of RF-EMF biological effects and is likely to disturb cell metabolism (Thor, Smith et al. 1982, Hollensworth, Shen et al. 2000, Consales, Merla et al. 2012, Panagopoulos, Karabarbounis et al. 2021). The signal generator in the Faraday shield also allowed us to explore the relevance of signal modulation in this context – by including experiments with unmodulated sine waves and 256-QAM applied. The results of these experiments are shown below in figure 18.

The 5G phone emitting mixed signals (figure 18a) showed no significant difference in metabolic viability between non-irradiated controls and RF irradiation alone (blue and green bars, respectively). But there was a small, non-significant trend of lowered viability due to radiation, with a magnitude ranging from 3-9% reduction compared to controls. In the absence of Menadione, viability values steadily increased with time, rising from 24-hour baseline values to ~140% of the initial value by the 48-hour time point and ~160% by the 72-hour time point. Menadione had a strong impact on metabolic viability, with or without the presence of additional radiation exposure (black and red bars). For example, at the 24-hour time point Menadione exposure alone pushed viability down to ~12% of 24-hour non-irradiated controls, which climbed slightly to ~20% at 48 hours and ~30% at 72 hours. Interestingly, viability values were noticeably higher if cells had been irradiated prior to Menadione insult (red bars). In this exposure group, values were ~41%, ~50% and ~69% at 24, 48 and 72 hours respectively. These increases all proved to be statistically significant when a student's T-test was performed comparing MEN- vs MEN+ at each time point (p-values ~0.004 to ~0.005). There was an overall similar pattern of results seen in the Faraday shield setup when using an unmodulated sine wave (figure 18b). Again, there was a small, non-significant lowering of viability by radiation exposure alone (blue and green bars), with values in the region of just 1-2% lower relative to non-irradiated 24-hour controls. It is also true that viability steadily rose over the course of the experiment, climbing to ~148% of starting values at the 48-hour time point and ~167% at the 72-hour time point. Menadione alone produced a marked reduction in metabolic viability, falling to just ~5% of non-irradiated controls at 24-hour time point, which rose to ~27% by 72 hours (black bars).

18a

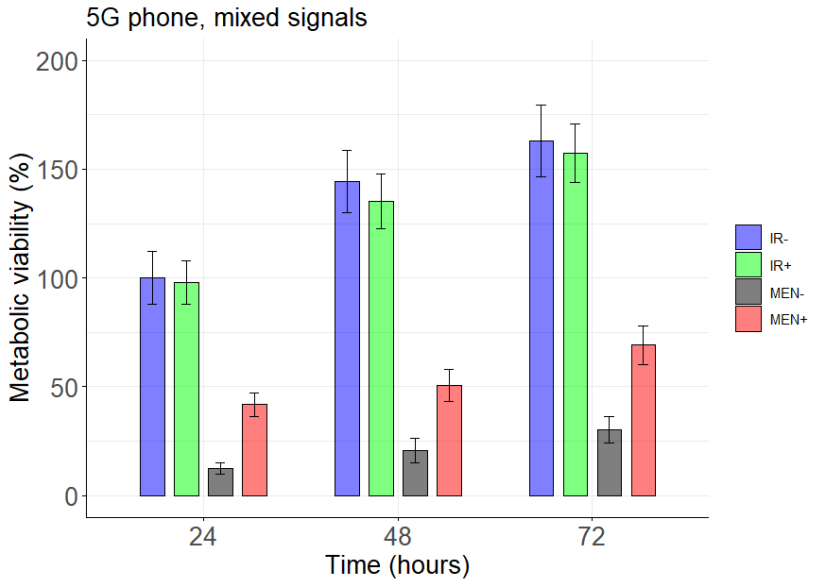

18b

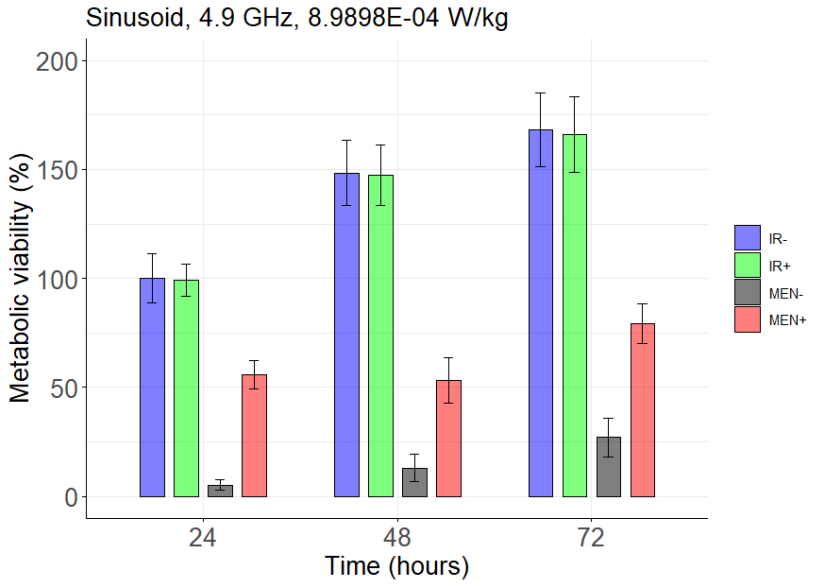

18c

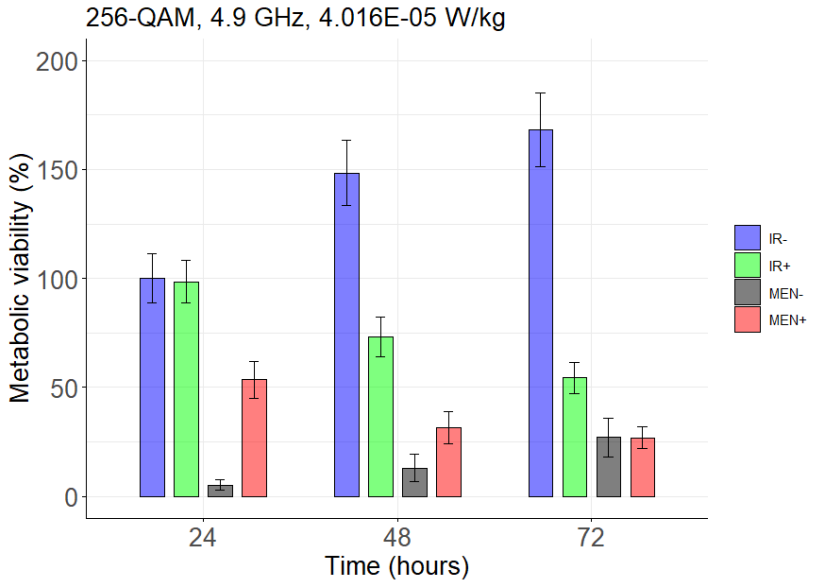

Figure 18 – metabolic viability of differentiated SH-SY5Y cells with 4 different condition groups; non-irradiated controls (IR- with no irradiation, no Menadione, BLUE bars), irradiation alone (IR+, GREEN bars), no irradiation but with 2 µm Menadione insult (MEN-, GREY bars) and irradiation prior to Menadione insult (MEN+, RED bars). Three different types of radiation were applied, 5G phone with WiFi and cellular data switched on (**18a**), inside the Faraday shield with a signal generator emitting a sinusoid (**18b**) or a 256-QAM modulated waveform (**18c**). EMFs were applied for 24, 48 or 72-hours before CellTiter-Blue viability assays were performed. Error bars show sample standard deviation. Data is representative of 3 independent experiments.

The apparent effect of RF radiation being protective against Menadione insult was also present in the case of sine wave signals in the Faraday shield (figure 18b, red bars). Viability values relative to controls were ~55%, ~53% and ~79% after 24, 48 and 72 hours respectively, which is more than double those of samples given Menadione alone (black bars). All of these differences comparing MEN- to MEN+ exposure groups proved to be statistically significant, with Student's t-test p-values ranging from 0.002 to 0.008.

Exposure to a modulated signal in the Faraday shield setup (256-QAM, figure 18c) produced results quite unlike the other two approaches. More specifically, radiation exposure alone appeared to lower metabolic viability over time (green bars). Although, at the 24-hour time point viability was comparable to non-irradiated controls (blue bars), by 48 hours it had dropped to ~73% of baseline, before dropping further to ~54% at the 72-hour time point. In both cases, these viability reductions were statistically significant using a Student's t-test, resulting in p-values of 0.0006 and 0.002 for the 48 and 72-hour time point comparisons (CON vs IR+).

A similar protective effect of radiation exposure was observed at the 24-hour time point, with a ~48% difference between MEN- and MEN+ groups at this time point (figure 18c, black and red bars). But this effect diminished with time, dropping to ~18% difference at the 48-hour time point and disappearing entirely by 72 hours. This was reflected in the p-values of a t-test comparing these two groups at each time point, going from p=0.006 at the 24-hour time point, to 0.03 at 48-hours and 0.9 at 72-hours, becoming expectedly non-significant by the end of the time course.

4.3.2 – GSH availability is influenced by RF exposure in a signal-dependent manner

To further explore the influence of telecoms signals on cellular metabolism and how reduced form GSH availability might contribute to understanding results obtained using the CTB assay, particularly the Menadione responses observed, a GSH assay was performed on differentiated SH-SY5Y cells. The results of this experiment can be seen below in figure 19.

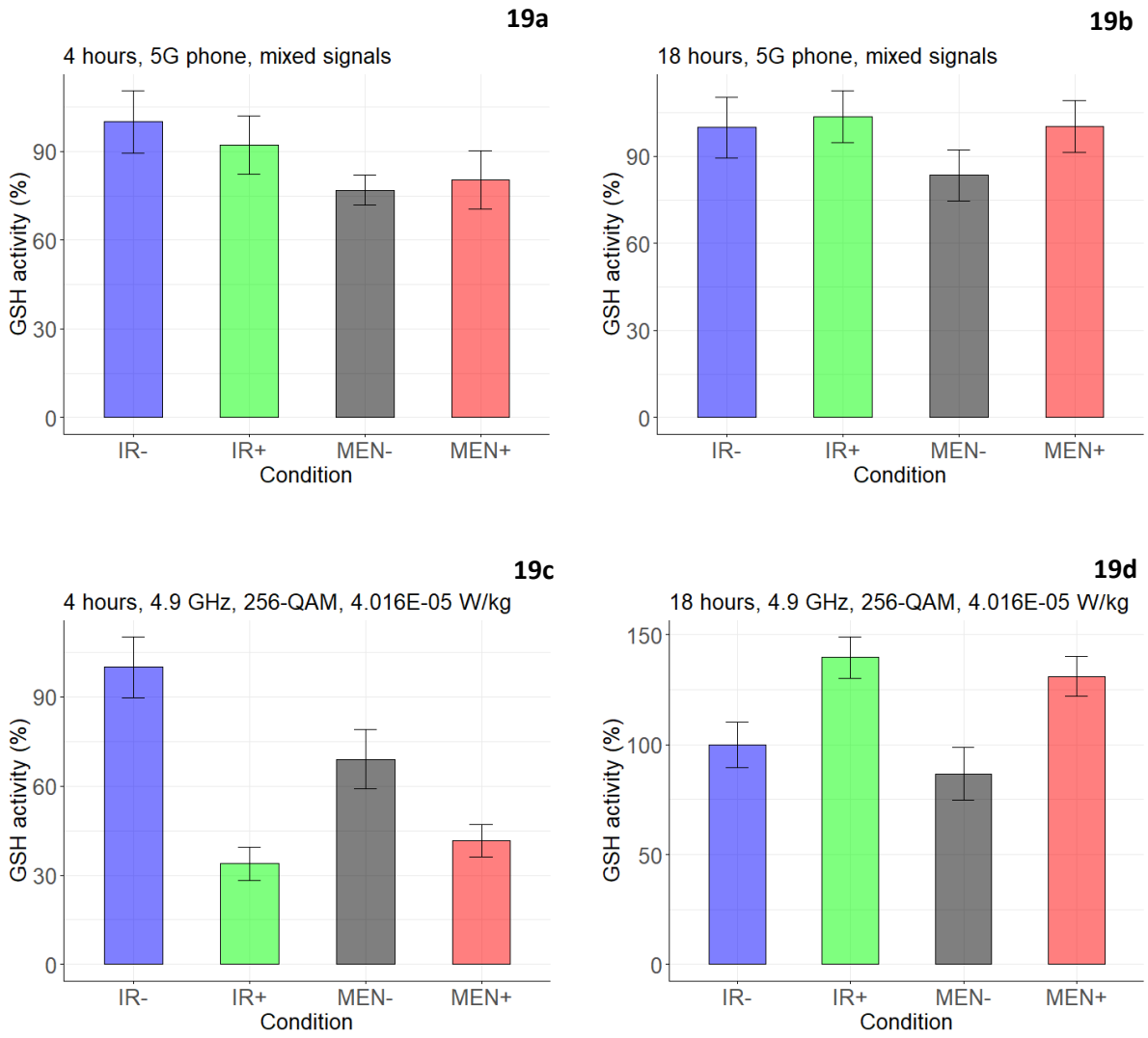

Figure 19 – Results obtained from a GSH assay using differentiated SH-SY5Y cells. Four different exposure groups were used; non-irradiated controls (IR-, no irradiation, no Menadione, BLUE bars), RF irradiation alone (IR+, GREEN bars), no irradiation but with 2 µm Menadione insult (MEN-, GREY bars) and RF irradiation prior to Menadione insult (MEN+, RED bars). Experimental conditions were applied for either 4 or 18 hours. Two different signal exposures were used, either a 5G phone emitting WiFi and cellular data signals (**19a & 19b**), or a 256-QAM modulated waveform generated using a signal generator (**19c & 19d**). Error bars on graphs show sample standard deviation. Data is representative of 3 independent experiments.

When considering the 4-hour exposure using the 5G phone (figure 19a), RF radiation appeared to a have small, non-significant effect on GSH availability – which dropped ~8% relative to non-irradiated controls. A t-test comparing those two groups gave a p-value of ~0.4. Interestingly, Menadione insult did not appear to have an overly strong effect in this context, but it did cause a reduction in GSH availability between ~20-24% relative to

controls. Comparing Menadione alone to Menadione plus RF irradiation using a t-test showed no significance, with a p-value of ~0.6.

There was an overall similar story of small, statistically insignificant changes at the later 18-hour time point using the 5G phone setup (figure 19b). Irradiation alone actually resulted in slightly increased GSH activity relative to controls, rising ~4% higher, but this difference was not significant (t-test, p-value ~0.7). Menadione alone reduced GSH activity by ~17%, but interestingly, RF irradiation prior to Menadione insult resulted in there being no reduction relative to controls. However, the difference between MEN- and MEN+ groups did not prove to be statistically significant using a t-test (p-value ~0.08).

The Faraday shield setup using 256-QAM modulated signals produced very different results (figures 19c and 19d). Looking at the 4-hour time point (figure 19c), irradiation alone resulted in a large reduction in GSH activity relative to non-irradiated controls, falling down to ~34% activity. This difference was statistically significant (t-test, p-value ~0.002). Menadione insult alone lowered activity to ~69%, whereas RF irradiation prior to Menadione insult lowered GSH activity even further, down to ~41%. A t-test comparing these two groups at this time point (MEN- vs MEN+) gave a p-value of ~0.02, indicating this difference is statistically significant.

The later time point using the Faraday shield setup (figure 19d) produced contrasting results. When comparing non-irradiated controls to 256-QAM radiation exposure, there was a substantial increase in GSH activity, rising ~40% higher than controls. This difference also proved to be statistically significant (t-test, p-value of 0.008). Menadione alone caused a slight drop in GSH activity relative to non-irradiated controls, down to ~87%, but RF irradiation prior to Menadione insult resulted in a sizeable increase in GSH activity, rising ~31% higher than control values. When comparing the MEN- group to the MEN+ group using a t-test, the difference was also significant (p-value ~0.008 again).

4.3.3 – SOD1 activity is modulated by 18-hour RF-EMF exposure

To investigate how SOD1 activity might also be influenced by exposure to these signals as part of a redox homeostasis response, a SOD1 activity assay was performed using the Sigma-Aldrich Superoxide Dismutase Activity Assay Kit (CS0009). The results of this 18-hour exposure experiment can be seen below in figure 20.

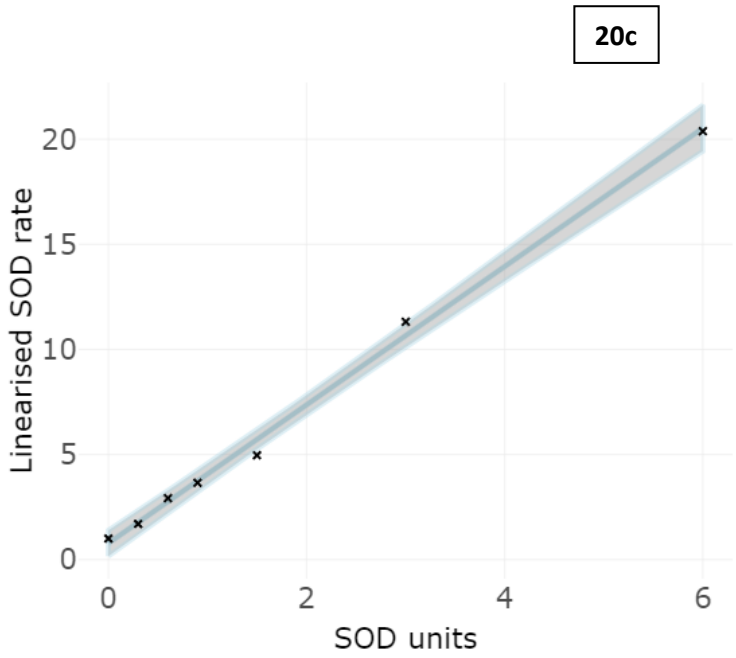

Figure 20 – results from a SOD activity assay following an 18-hour exposure in either the mini-incubator setup (**20a**) or the Faraday shield setup (**20b**). Samples were either given no radiation exposure (IR-, white bars), or exposed to one of two types of radiation (IR+, black bars); phone signals (WiFi & cellular data) or a 256-QAM, 4.9 GHz, 4.016E-05 W/kg modulated waveform. Error bars show sample standard deviation. Data is representative of 3 independent experiments. **20c** shows a representative example of a linearised standard curve used to calculate SOD units as per kit instructions.

In both experimental setups, 18-hour RF irradiation appeared to induce an increase in detected SOD1 activity (20a and 20b). In the 5G phone mini-desktop incubator setup, the average SOD units/ml recorded increased from ~7.4 to ~10.6 when comparing non-irradiated controls to irradiated samples (20a, black bar vs white bar). This increase proved to be statistically significant when applying a Student's t-test, with a p-value of ~0.02.

The Faraday shield setup produced a similar overall pattern, with slightly elevated SOD1 activity being recorded in irradiated samples (figure 20b). In this context, SOD units/ml activity of non-irradiated controls was an average of ~12 (white bar), which rose to ~14 following irradiation with 256-QAM RF-EMR (black bar). Unlike the mini-incubator setup increase, this was not statistically significant when subjected to a t-test comparing the two groups (p-value of ~0.06).

For each plate, a set of standards containing known amounts of SOD units were used to produce a linearised SOD rate with which to compare to values obtained when analysing lysate samples (an example of which can be seen in figure 20c). Prior to experimentation, a serial dilution experiment was performed to ensure obtained sample values fell within the dynamic range of the assay kit – which could later be factored into calculations using dilution factor multiplication.

4.3.4 – Mitochondrial superoxide formation in the presence of RF-EMR

Superoxide has long been suggested as a significant factor in redox signalling, particularly as a pre-cursor to the more stable hydrogen peroxide (Auchère and Rusnak 2002, Wang, Branicky et al. 2018, Winterbourn 2020). For this reason, we wanted to investigate its potential role in regulating observed cellular responses when exposed to RF-EMR. To do this, MitoSOX indicator was used in a flow cytometer to attempt to quantify any effect RF-EMR exposure might have on mitochondrial-based superoxide formation. The results of this assay can be seen in the figures below.

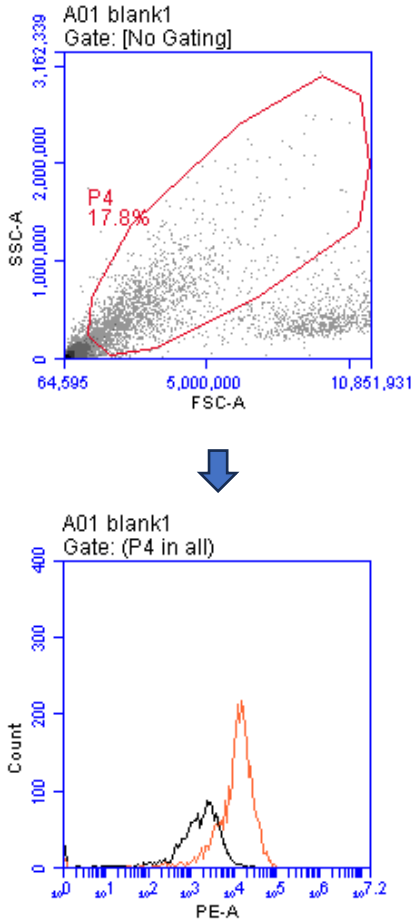

Figure 21 – a representative example of gating applied to blank samples (no MitoSOX added) for cell selection purposes. This ultimately allowed generation of overlaid histograms using the appropriate PE fluorescent probe, comparing results obtained in blanks to various conditions (e.g. blanks vs 2 µM Menadione treated samples, overlaid in orange here). From these gated plots, MFI values were obtained then used to apply statistical analysis and compare conditions.

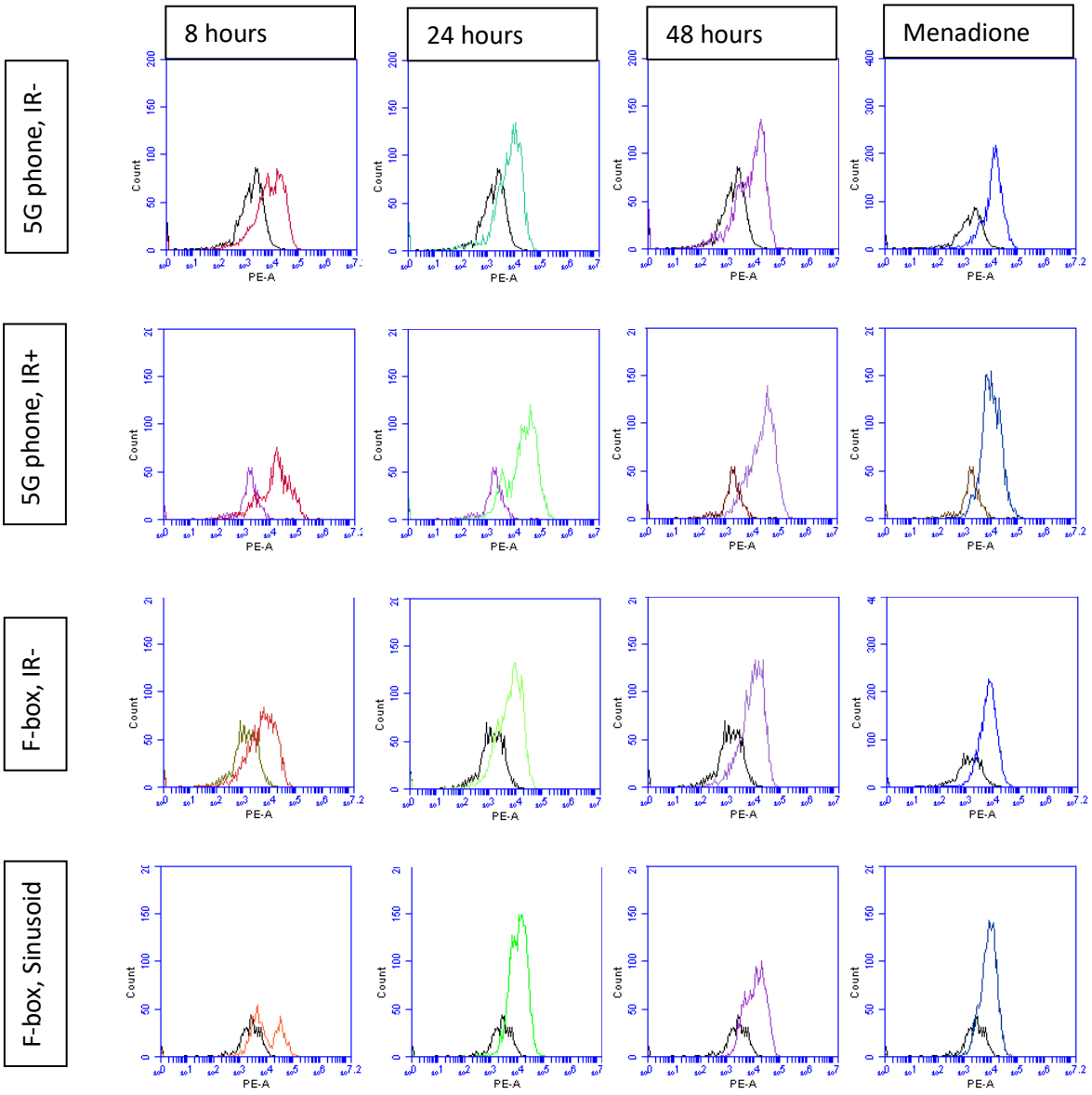

Figure 22 – overlaid histograms showing MitoSOX signal after gating under various conditions. The 5G phone setup used WiFi & cellular data for RF signal exposure, the Faraday box used an unmodulated sine wave. Plots are representative of results obtained. Data is representative of 3 independent experiments. Menadione controls were left non-irradiated in all cases, instead being incubated for 2 hours with 2 µM Menadione to show MitoSOX signal generation.

Incubation with MitoSOX produced the expected right shift of peaks using the appropriate probe under all test conditions, but to varying degrees, as seen above in figure 22. In terms of MFI values and comparisons between RF irradiation and no radiation, these are illustrated below in figure 23. Note that in this instance, Menadione insult was given independently of irradiation and was the same 2-hour incubation in all cases.

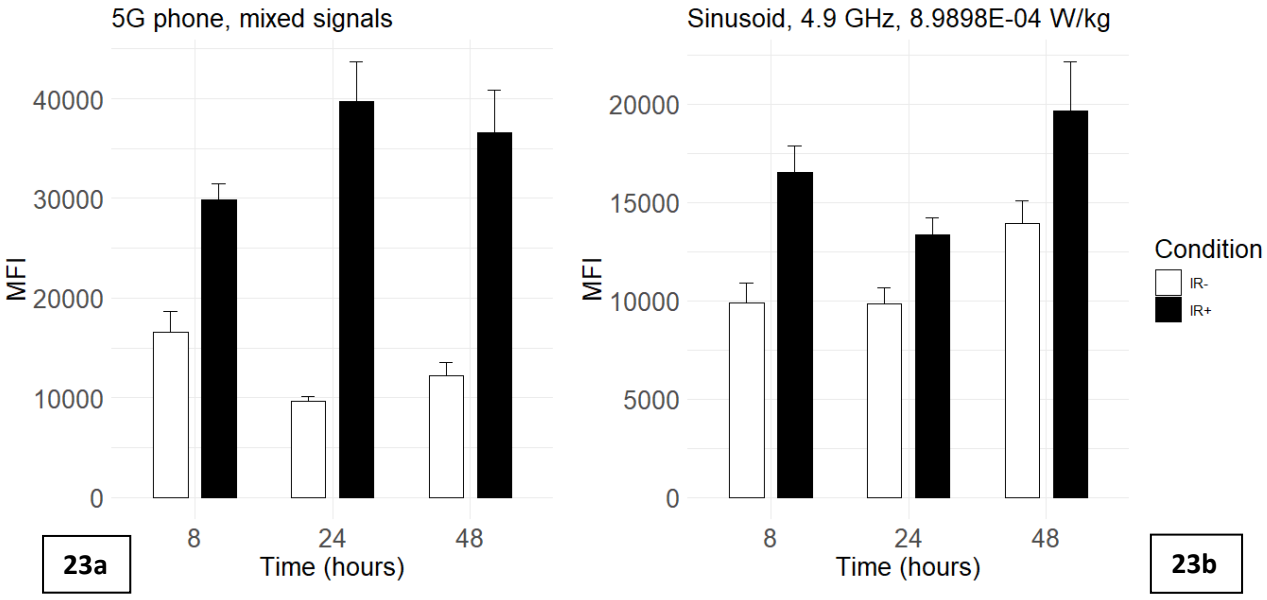

Figure 23 – average MFI values obtained using mitoSOX indicator in two experimental setups, with (**BLACK** bars) and without (WHITE bars) RF radiation exposure for different lengths of time. Error bars show sample standard deviation. Data is representative of 3 independent experiments.

In all instances, RF irradiation resulted in an increase in the MFI values recorded (23a and 23b). In the context of the 5G phone emitting mixed signals (23a), the increases at each time point were as follows; 16,546 to 29,835 at 8 hours, 9,592 to 39,738 at 24 hours and 12,158 to 36,614 at 48 hours. These increases represent approximately a 2x-fold, 4x-fold and 3x-fold increase at 8, 24 and 48 hours respectively. A t-test comparing the two groups proved significant for all 3 time points, with p-values ~0.0014, ~0.0052 and 0.0056 for 8, 24 and 48 hours respectively. By comparison, increases in MFI values were lower in the Faraday shield emitting a sine wave (23b). Average values increased from 9,898 to 16,520 at 8 hours, 9,850 to 13,369 at 24 hours and 13,934 to 19,657 at 48 hours. Again, all three of these increases proved significant when subjected to a t-test, giving p-values of ~0.003, ~0.006 and ~0.04 respectively.

In order to explore potential demodulation effects and examine how RF radiation might modulate cellular responses to Menadione insult as seen in other assays, an additional flow cytometry experiment was conducted using the Faraday shield. This time a 256-QAM modulated waveform was used and samples were irradiated for different lengths of time prior to incubation with Menadione. The results of this are illustrated below in figure 24.

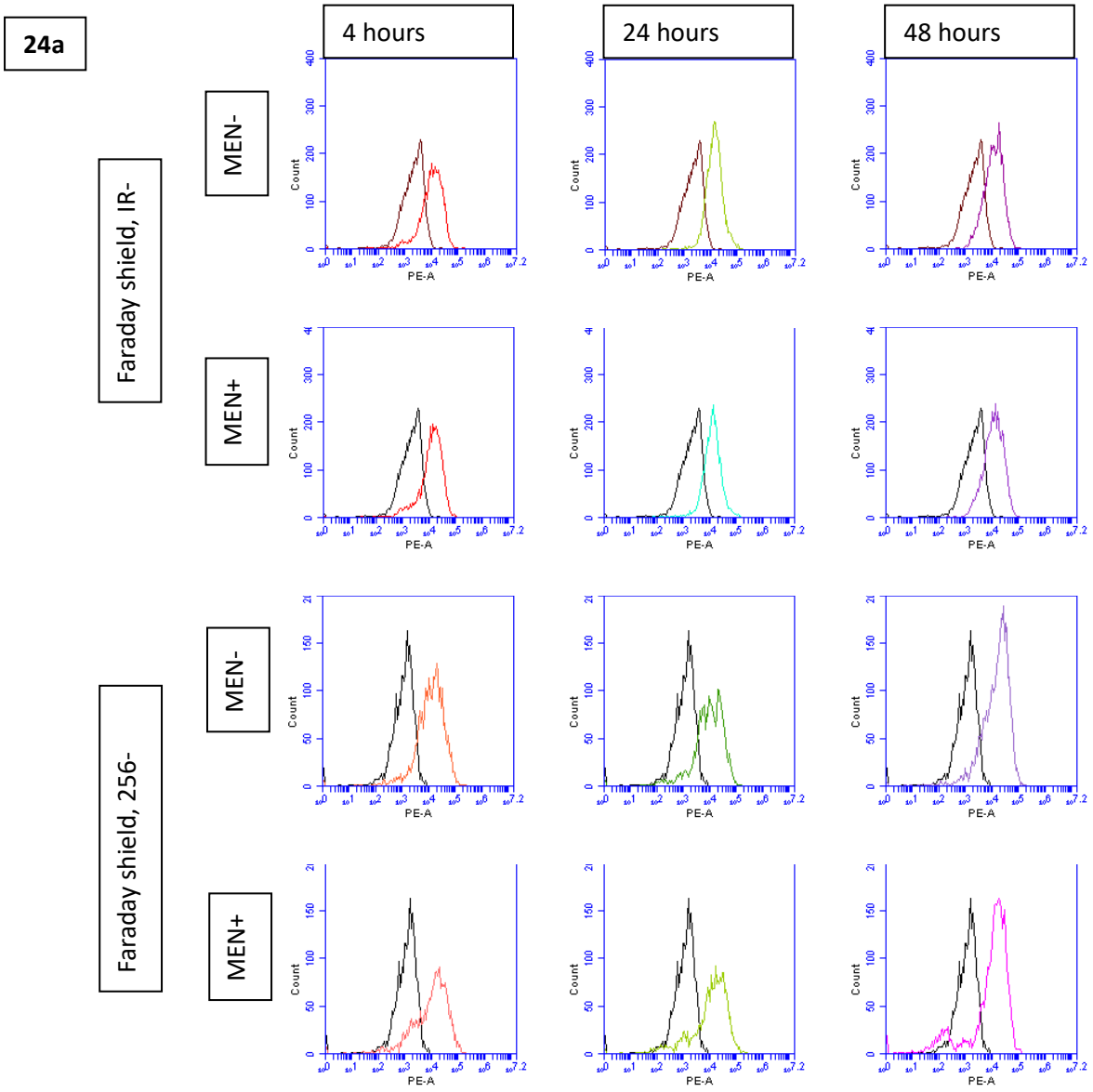

Figure 24 – mitoSOX signal generated under various conditions, comparing blanks to experimental samples (**24a**). This experiment included a 256-QAM modulated waveform for EMF exposure (4.9 GHz, SAR = 4.016E-05 W/kg, IR+), or no irradiation (IR-), or irradiation and an additional Menadione insult (2 µM, 2 hours, MEN+) or no radiation and no Menadione insult (MEN-). Histograms depicted are representative of dataset. **24b** below shows average MFI values obtained under each condition, error bars show sample standard deviation. Data is representative of 3 independent experiments.

24b

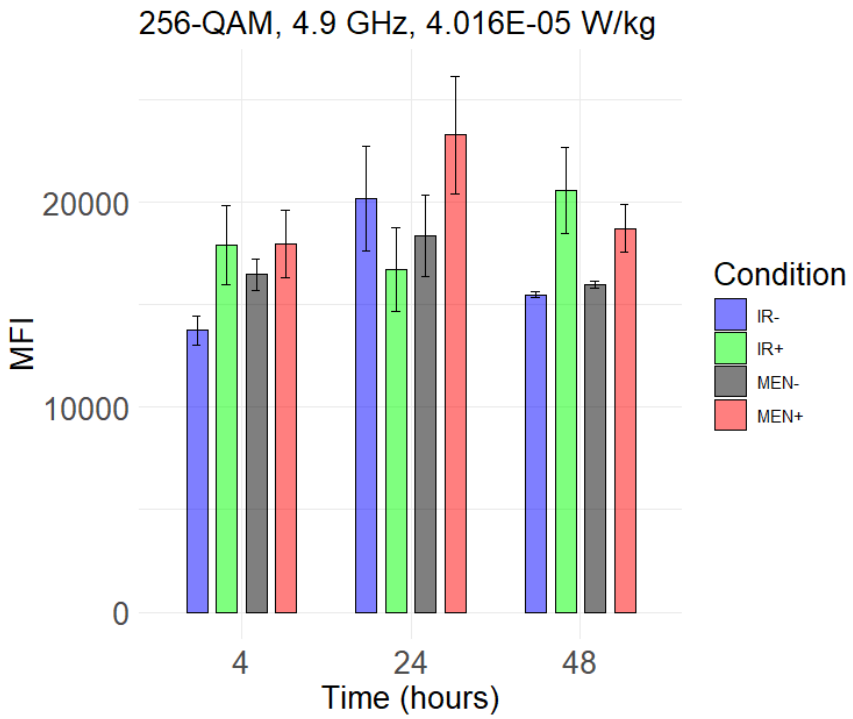

In this context, there was no clear overall trend, as observed with the previous two flow experiments (figure 23). Looking at RF irradiation alone (IR- blue bars vs IR+ green bars), radiation resulted in an increase from 13,749 to 17,896 average MFI at the 4-hour time point, a decrease from 20,190 to 16,715 at 24 hours and an increase from 15,495 to 20,597 at 48 hours. None of these changes proved statistically significant (Student's t-test), with p-values ~0.051, ~0.14 and ~0.051, respectively. When considering Menadione responses (MEN- black bars vs MEN+ red bars), prior radiation exposure consistently led to a small elevation in recorded average MFI values, with increases ranging from ~1000 to ~5000. But none of these changes were statistically significant, with p-values ~0.26, ~0.078 and ~0.054 at the 4, 24 and 48-hour time points respectively.

4.3.5 – Mitochondrial membrane potential in the presence of RF-EMR

TMRM (Tetramethylrhodamine Methyl Ester Perchlorate) was used in another flow cytometry experiment to explore the capacity of RF-EMR exposure to modulate mitochondrial membrane potential. The results of this experiment can be seen below in figure 25.

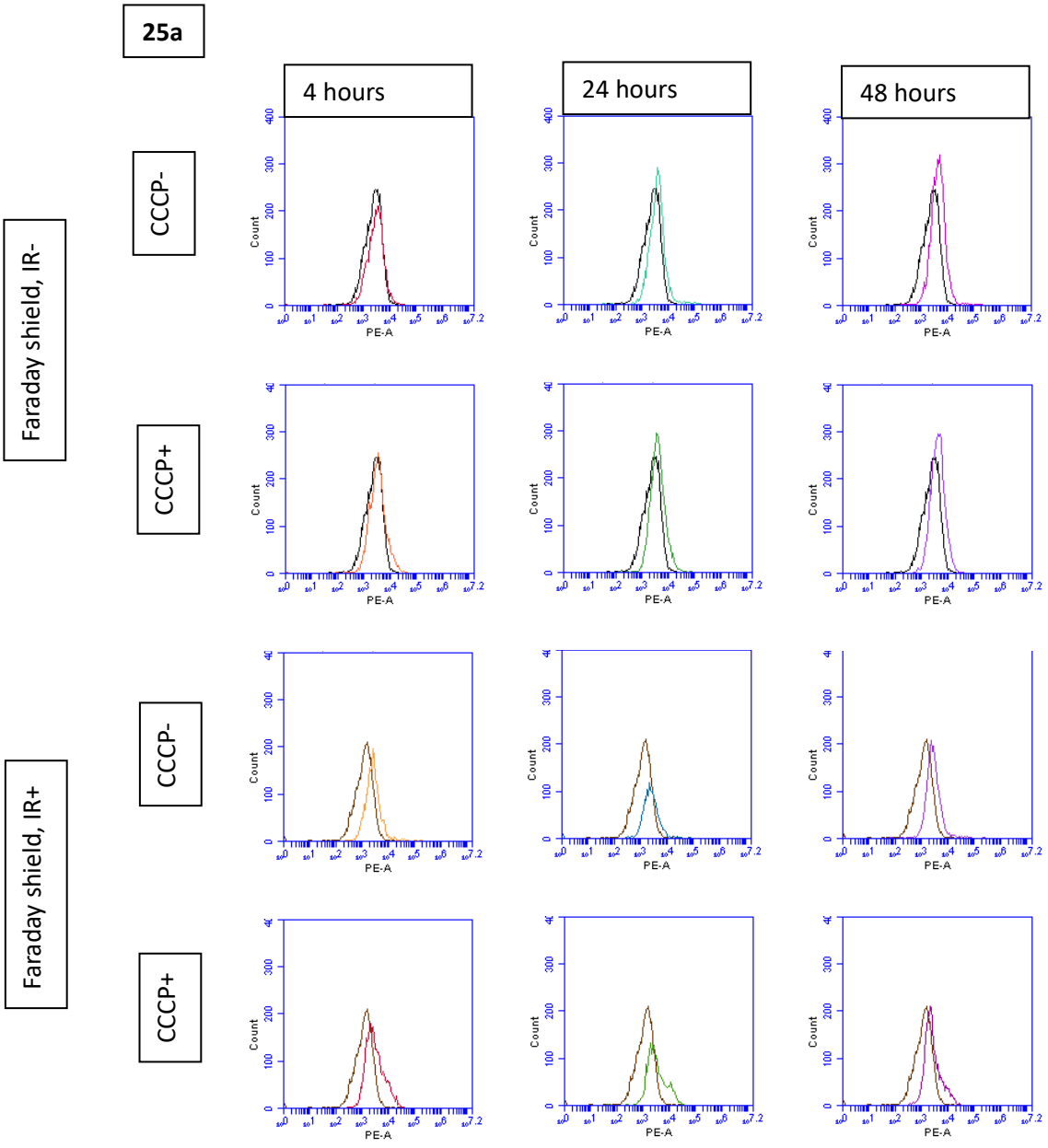

Figure 25 – TMRM signal generated under various conditions, comparing blanks to experimental samples (**25a**). This experiment used a 256-QAM modulated waveform for EMF exposure (4.9 GHz, SAR = 4.016E-05 W/kg , IR+), or no radiation exposure (IR-), or irradiation and an additional CCCP incubation (20 mM, 5 minutes, CCCP+) or no radiation and no CCCP (CCCP-). Histograms depicted are representative of dataset. **25b** below shows average MFI values obtained under each condition, error bars show sample standard deviation. Data is representative of 3 independent experiments.

25b

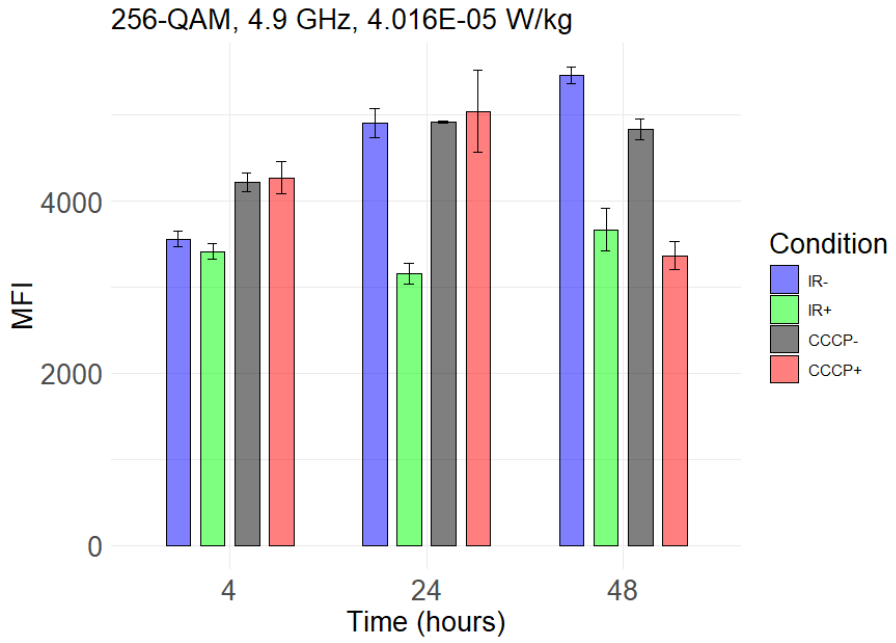

When comparing non-irradiated controls (IR- blue bars) to samples given 256-QAM irradiation alone (IR+ green bars), average MFI values recorded were lower following radiation, particularly at the 24 and 48-hour time points (figure 25b). Although, they were comparable at the 4-hour time point, 3,560 vs 3,414, they had dropped from 4,905 to 3,159 at 24 hours and from 5,461 to 3,667 at 48 hours. This was reflected in t-tests comparing the two contexts, which gave p-values of ~0.12, ~0.00022 and ~0.0025 for the 4, 24 and 48-hour time points respectively. MFI results obtained for both CCCP- (black bars) and CCCP+ (red bars) conditions were very similar for the 4 and 24-hour time points – but not for the 48-hour time point. Recorded values were lower for previously irradiated samples at this time point. At this late time point, non-irradiated samples given CCCP had an average MFI of 4,838, but irradiated samples given CCCP had an average MFI of 3,365. T-tests used to compare these two groups proved insignificant at the 4 and 24-hour time points (p-values ~0.71, ~0.69, respectively), but statistically significant at the 48-hour time point (p-value ~0.00033).

It is worth noting that non-irradiated control samples tended to give high MFI values in this dataset. This is expected, given robust signal generation is a sign of good mitochondrial health and proper electrochemical gradient maintenance. Strangely, CCCP incubation failed to lower recorded MFI in most instances – suggesting it did not cause membrane uncoupling as intended.

4.3.6 – Mitochondrial drug responses are altered by short-term RF-EMR exposure

A Seahorse Mito Stress Test was performed to interrogate mitochondrial function in the presence and absence of RF radiation. The primary metric derived from this assay is the Oxygen Consumption Rate (OCR), in which aerobic respiration is quantified in real-time using a mono layer of live cells. Two different types of radiation were applied for 18 hours and the results of this assay are visualised below in figure 26.

26a

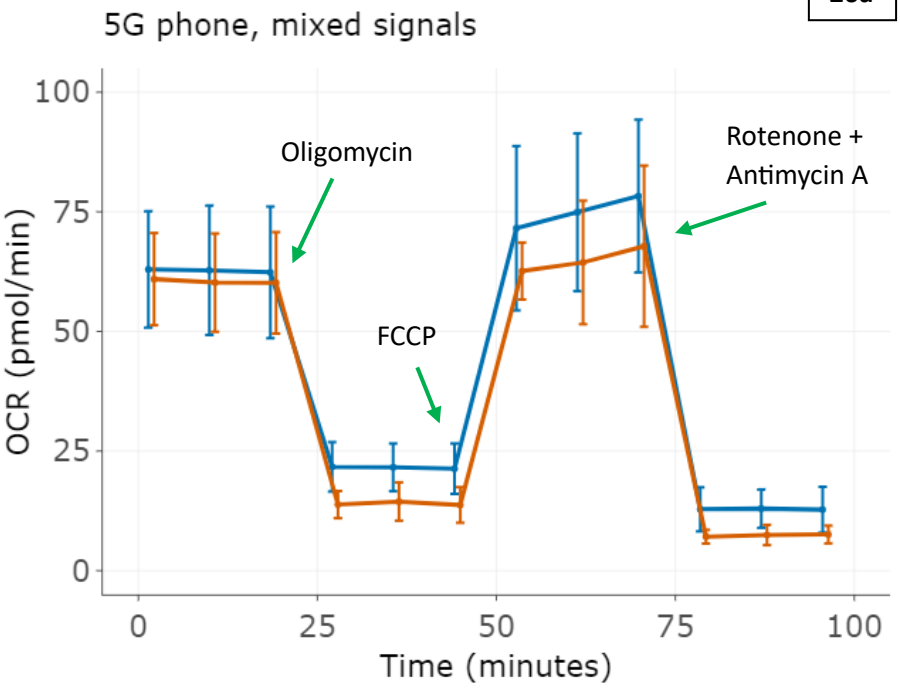

26b

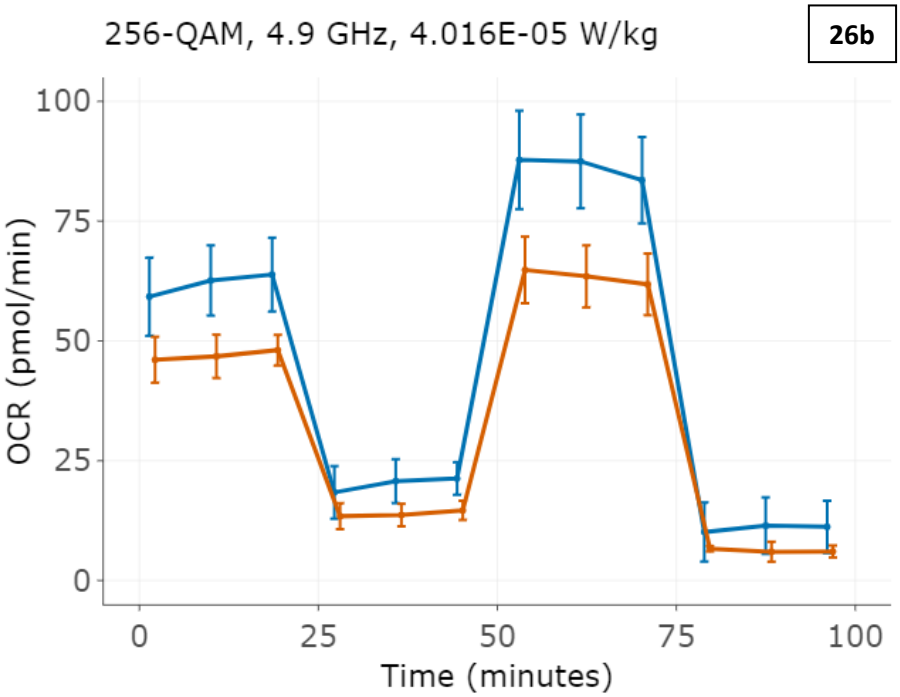

Figure 26 – Oxygen Consumption Rate (OCR) of differentiated SH-SY5Y cells under several conditions. BLURE LINES show results of non-irradiated controls, ORANGE LINES show results following 18 hours irradiation – either WiFi and cellular signals from a mobile phone (**26a**) or a modulated waveform using a signal generator in the Faraday shield (**26b**). The step-wise pattern is characteristic of Seahorse Mito Stress Test drug compounds, Oligomycin, FCCP, Rotenone and Antimycin A. Error bars show sample standard deviation. Data is representative of 3 independent experiments.

Results from both experimental setups successfully produced the expected step-wise pattern typical to Mito Stress Tests (figure 26a and 26b). In the initial portion of the assay, baseline OCR readings are taken before injection of the first drug, Oligomycin (~25-minute mark). Oligomycin inhibits ATP synthase (protein complex 5 in the ETC), blocking the final step of oxidative phosphorylation and thereby reducing mitochondrial respiration associated with ATP generation. This is clearly shown in both graphs, for example, in figure 26a baseline OCR of the IR- condition is ~62 pmol/min average, which then dropped to ~21 pmol/min upon addition of Oligomycin. FCCP is injected next (~50-minute mark), which uncouples the mitochondrial membrane, allowing free flow of protons across the membrane and pushing ETC complex 4 oxygen consumption to its maximal rate. This pushed the OCR up significantly higher than baseline OCR, e.g. up to ~75 pmol/min in the case of no irradiation in the 5G phone setup (26a, IR-). The third and final injection is a combination of Rotenone and Antimycin A, which inhibit complexes 1 and 3 respectively and completely shut down mitochondrial-based respiration – revealing all other cellular sources of respiration. This pushed OCR below Oligomycin-treated levels in all instances, pushing oxygen consumption very low (e.g. phone signal irradiation in the mini-incubator, 26a orange lines, OCR dropped as low as ~7 pmol/min during this final phase).

In terms of irradiation, exposure to mobile phone signals in a desktop mini-incubator resulted in a small lowering of detected OCR values across the entire duration of the assay (figure 26a). The average OCR values for each stage were as follows;

- Baseline OCR (s1); ~62 pmol/min for non-irradiated controls (IR-) and ~60 pmol/min for irradiated samples (IR+).
- Oligomycin stage (s2); ~21 pmol/min for IR- and ~14 pmol/min for IR+
- FCCP stage (s3); ~75 pmol/min for IR- and ~65 pmol/min for IR+
- Rotenone + Antimycin A stage (s4); ~13 pmol/min for IR- and ~7 pmol/min for IR+

In the 5G phone experiment setup, t-tests comparing irradiated and non-irradiated results at each experimental stage showed that this apparent OCR lowering effect by radiation exposure was not statistically significant for s1 or s3 (p-values ~0.64 and ~0.13 respectively), but did prove significant for stages 2 and 4 (p-values ~0.00092 and ~0.0026 respectively). So, mitochondrial responses to both Oligomycin and a combination of Rotenone and Antimycin A were significantly different following radiation exposure in this context.

There was a similar overall pattern observed in the Faraday shield setup using a 256-QAM modulated waveform, where irradiation appeared to lower recorded OCR values (figure 26b). Average OCR recorded for each experimental stage was as follows;

- Baseline OCR (s1); ~62 pmol/min for non-irradiated controls (IR-) and ~47 pmol/min for irradiated samples (IR+).
- Oligomycin stage (s2); ~20 pmol/min for IR- and ~14 pmol/min for IR+
- FCCP stage (s3); ~86 pmol/min for IR- and ~63 pmol/min for IR+
- Rotenone + Antimycin A stage (s4); ~11 pmol/min for IR- and ~6 pmol/min for IR+

In terms of statistical testing comparing each stage of IR+ and IR- in the Faraday shield, t-tests showed that this lowering effect proved statistically significant for some stages (stages 2 and 3, with p-values of ~0.0204 and ~0.027 respectively), but non-significant for others (s1 and s4, p-values ~0.54 and ~0.069 respectively). Once again, baseline OCR was not significantly affected by RF irradiation, but responses to Oligomycin and FCCP were altered by radiation exposure.

4.4 – Discussion

There is a sizeable portion of scientific evidence to suggest that some telecoms signals and RF-EMR in general may be able to promote formation of reactive oxygen species and nudge cells towards an imbalance between clearance and generation of these species, i.e. that some signals may promote oxidative stress (Repacholi 1998, Ahlbom and Feychting 2003, Oktem, Ozguner et al. 2005, Zamanian and Hardiman 2005, Consales, Merla et al. 2012, Kang, Lee et al. 2014, Razavinasab, Moazzami et al. 2016, Yakymenko, Tsybulin et al. 2016, Bortkiewicz 2019, Choi, Min et al. 2020, Panagopoulos, Karabarbounis et al. 2021, Sofri, Rahim et al. 2021). But this depends largely on the nature of the signals and context being considered – for example, the power level of the emission source or exact frequency used can and will greatly change the way radiant energy propagates and interacts with tissue (Feynman, Leighton et al. 1965, Protection 1998, Rappaport, Xing et al. 2017, ICNIRP 2020). It is also true that the picture of RF-EMR safety is far from clear, with some papers finding no such association between exposure and adverse biological effects, additionally, there is a lack of strong epidemiology evidence showing disease burden as a result of increased human RF-EMR exposure – which might reasonably be expected due to the undeniable link between oxidative stress and disease (Spector 2000, Kang 2002, Barzilai and Yamamoto 2004, Kryston, Georgiev et al. 2011, Swerdlow, Feychting et al. 2011, Distelmaier, Valsecchi et al. 2012, Di Meo, Reed et al. 2016, Forman and Zhang 2021).

So, further clarity is needed in order to pin down an undeniable causal relationship between exposure to RF-EMFs, like those employed in telecoms, and biological effects and how such a relationship might impose an as yet unknown and unquantified disease risk on human populations.

The first assay employed here to further this scientific effort was a metabolic viability assay, the CellTiter-Blue assay. Several RF signals were included;

- Mixed WiFi and cellular data signals from an actual 5G mobile phone (~5.1-5.3 GHz for WiFi and ~840 MHz for the cellular data signals)
- A simple sinusoid at 4.9 GHz, SAR = 8.9898E-04 W/kg
- A modulated waveform using a 256-QAM scheme, at 4.9 GHz, SAR = 4.016E-05 W/kg

Choi et al had previously reported increased ROS generation and reduced proliferation of the same cell line used here (SH-SY5Y) in response to exposure to mobile phone signals, over similar time scales (Choi, Min et al. 2020). Because of this work and others, it was

expected that there may be differences in metabolic viability due to RF-EMFs employed here – but this did not prove to be the case for two out of three types of RF signals used. Both the mobile phone signals and sinusoid did not directly lower metabolic viability (figures 18a and 18b). In both cases, viability values steadily increased over the duration of the experiment, regardless of radiation exposure, likely a result of the steady growth of cell populations over the course of the experiment. It is difficult to theorise why RF radiation exposure did not directly lower viability here, given the work presented by Choi et al. If cells proliferate less over these time scales when irradiated, then there ought to be fewer of them available to metabolise the CTB dye – which should result in lowered metabolic viability. But there are several differences between our experimental setups used here and those employed in Choi 2020 paper and others, they include; the cell model used (most papers utilise undifferentiated cells), the types of signals used and the general culture conditions (media type and CO_2 enrichment etc). It is especially relevant to consider signal characteristics, which are highly likely to inform what biological effects, if any, manifest. Relevant parameters include; frequency, power level and modulation scheme – all of which are may influence any potential biological effects.

Interestingly, for the third and final RF signal type, a 256-QAM modulated waveform, a sharp reduction in metabolic viability was observed (figure 18c). This suggests demodulation effects may play a critical role in influencing the ability of telecoms signals to produce biological effects – a point which runs contrary to most scientific opinion on the matter, but aligns with evidence suggesting the potential significance of specific types of modulation (Protection 1998, Foster and Repacholi 2004, Silny 2007, Juutilainen, Höytö et al. 2011, ICNIRP 2020). Although, it is difficult to account for the intensity of the viability-lowering effect seen in this particular experimental context – an effect which is entirely absent in the 5G phone setup, which also utilises complex modulation schemes common among all modern telecoms signals (Banelli, Buzzi et al. 2014, Barnela and Kumar 2014, Hong, Sagong et al. 2014, Wu, Wang et al. 2016, Cai, Qin et al. 2017, Faruque 2017). Still, there are differences between the two signal types (frequencies, power etc), which could explain differences in results obtained, at least to some degree.

Moving on from this potential direct influence on metabolic viability, one trend that was clear among all scenarios tested was the alteration of cellular responses to Menadione insult (figure 18). Paradoxically, irradiation with telecoms signals prior to Menadione insult appeared to be protective against the deleterious effects of Menadione at these concentrations. This was true of every type of radiation applied at every time point with only one exception – the 256-QAM signal at the 48-hour time point, by which time viability

appeared to have dropped so low as to be comparable to Menadione insult (figure 18c). Nonetheless, it was a highly reproduceable and statistically significant pattern, which raises interesting questions. Why would short-term RF-EMR exposure be protective against oxidative stressor insult? A working theory suggested here is that RF irradiation causes cells to activate homeostatic mechanisms to combat subtle effects and disturbances associated with RF-EMR exposure – and that activation of these pathways means cells are, in essence, "primed" to deal with subsequent oxidative insults a little better. This would explain what is observed here and there are already several biological precedents for this type of adaptive cellular response occurring in other contexts. Examples of this include;

- The well-established *ada* operon in microbes such as *E.coli*, which can provide resistance to Alkylating agents via activation of DNA repair pathways, such as "suicide enzymes" that repair the highly disruptive O6 Methyl Guanine DNA adducts (Teo, Sedgwick et al. 1984, Lemotte and Walker 1985)
- Heat Shock Protein 70 (HSP70) mediated radioresistance – evidence exists in both cell lines and animal cells indicating the importance of this protein in providing cellular resistance to ionizing radiation insult (Park, Lee et al. 2000, Kang, Park et al. 2002)
- Acquired resistance to ionizing radiation by cancer stem cells. Several mechanisms have been suggested in this context and, interestingly, some evidence points to the importance of ROS levels in this process of radioresistance acquisition (Diehn, Cho et al. 2009, Rycaj and Tang 2014, Li, Zhou et al. 2016)

But perhaps the most studied example of this "priming" effect comes in the context of cancer therapy – both radio and chemo. Tumours in patients becoming resistant to treatments and recurring is a continuous and on-going battle in the world of cancer therapy and an excellent example of cells adapting to environmental stimuli and pressures (Barker, Paget et al. 2015, Liu, Zheng et al. 2021, Wu, Song et al. 2023). This is why great care is taken when formulating treatment plans for cancer patients – attacking tumours with multiple sources simultaneously to try and overwhelm adaptive responses and prevent them from manifesting.

This type of response behaviour could possibly be considered a part of the "hormesis effect" – where cells mount adaptive responses to moderately intense stressor stimuli leading to an increase in function (Mattson 2008). Prominent and common examples of this can be seen in microtears of muscle tissue during exercise or calorie restriction diets (Mattson 2008). But as to how cells may be generating adaptive responses to Menadione here in our

experimental context, it is very difficult to suggest a specific mechanism without further study. Subsequent experiments carried out here, following the discovery of this apparent protective effect of RF-EMR exposure, were designed to explore and verify this response using a variety of approaches. Because Menadione is a known oxidative stressor, promoting the generation of superoxide – antioxidant responses dealing with superoxide were thought to be potentially relevant here (Thor, Smith et al. 1982, Hollensworth, Shen et al. 2000). GSH and SOD1 especially are at the forefront of antioxidant responses to superoxide and other ROS species derived from superoxide, such as hydrogen peroxide (He, He et al. 2017, Ighodaro and Akinloye 2018, Le Gal, Schmidt et al. 2021, Averill-Bates 2023). It was suspected changes in the activities of these antioxidant mechanisms might contribute to explaining the results obtained in the initial CTB assay comparing different types of RF radiation exposures.

However, when considering results obtained from the GSH activity assay, the 5G phone signals appeared to exert little influence on GSH activity (figures 19a and 19b). 256-QAM radiation, again, produced significantly different results – indicating a much stronger effect on GSH activity (figures 19c and 19d). Interestingly, this is reflective of the discrepancy between metabolic viability changes witnessed in the CTB assay – where phone signals had no direct effect (an overall weaker ability to influence biology), but 256-QAM radiation directly impacted viability (i.e. produced a stronger effect). In terms of the GSH responses in the presence of 256-QAM radiation, the early time point (figure 19c) showed a marked reduction in GSH activity. This was later reversed by the 18-hour time point, where irradiation appeared to result in increased GSH activity relative to non-irradiated controls (figure 19d). These time points were chosen specifically to catch early effects and contrast them with later effects, when cells had been given time to initiate transcriptional and signalling pathway responses. It could be argued that this reduction in GSH activity early could indicate an increased ROS burden that has been suggested elsewhere in literature relating to RF-EMR (Oktem, Ozguner et al. 2005, Lantow, Lupke et al. 2006, Zeni, Di Pietro et al. 2007, Luukkonen, Hakulinen et al. 2009, Kang, Lee et al. 2014, Bortkiewicz 2019, Choi, Min et al. 2020). The results obtained at the later time point could be a consequence of cells engaging homeostatic and compensatory mechanisms in response to irradiation – which had been given sufficient time to take effect by this later time point. This pattern of GSH activity (reduced early, elevated later) could also neatly contribute to explaining why cells appeared to tolerate Menadione insult better when irradiated for 24 hours in the earlier CTB experiment. In order for cells to mount an adaptive response to some harmful stimuli, it must be sufficiently intense to provoke a response – i.e. we would expect to see a meaningfully increased ROS/oxidative burden early for there to be an adaptive response

later. Indeed, by the 18-hour time point, cells appeared to have fully recovered GSH activity, which was shown to be higher than basal levels in non-irradiated controls (figure 19d).

SOD1 activity assay results largely corroborated these findings (figure 20). An 18-hour irradiation was performed in both experimental setups and in both instances increased SOD1 activity was recorded relative to non-irradiated controls. But it is important to note that this increase was only statistically significant in the 5G phone setup (figure 20a). Still, the pattern was consistent, but strangely, in contrast to previous assays, the 5G phone setup produced a stronger effect here than was observed using the Faraday shield with a 256-QAM signal (figure 20b). It is not clear why this discrepancy exists, as previous results implicated the 256-QAM signal as being more biologically provocative. Unfortunately, in large part due to the financial cost of assay kits, it was not possible to conduct early and late phase investigations here. It would have been interesting to similarly probe early responses and contrast them with late responses, as seen with the GSH assay. It remains unclear if there is a reduction in SOD1 activity as an early-phase response to RF-EMR exposure and would be one experiment that might significantly add to this project in the future.

Moving on to the flow cytometry results using MitoSOX superoxide indicator, there was a clear trend of elevated superoxide formation in the presence of RF-EMR exposure (figures 23a and 23b). Or at the very least, MFI values generated by the MitoSOX dye were elevated at every time point and in both experimental setups in irradiated samples, with all increases proving to be statistically significant also. However, there were some limitations to this experiment which require mention. Firstly, the inclusion of Menadione in this early experiment was done separately to RF irradiation – i.e. we did not probe Menadione responses in the presence and absence of radiation exposure (figure 22). This is an unfortunate omission and largely a result of the chronological order in which experiments were performed. This initial flow assay was actually one of the first major assays performed and was carried out before the CTB assay, which is what revealed differing cellular responses to Menadione insult – i.e. we were not yet aware of this area of interest when designing this flow cytometry experiment. It could have potentially been interesting to examine Menadione responses here in a similar fashion to what was done in the CTB assay. Thankfully this was remedied with a later experiment which included this aspect in its design, which will be discussed later. A second concern with this dataset was the distribution of events when viewed in a simple FSC vs SSC format. There was an expected clustering of cells towards the bottom left corner of the distribution – because simple microscopy of detached, differentiated SH-SY5Y cells shows that they form a suspension filled mostly with small, circular cells (so a large FSC value would not be expected here). But our flow

cytometry data also produced a thin smear of events along much of the length of the FSC axis – which is exponential in scale and therefore makes it unclear what this actually represents (i.e. the start and end of this smear, from left to right, have vastly different FSC values which in-turn suggests vastly different object sizes). Attempts to remove doublets and clumped cells were not able to remedy this problematic cluster of events. Gating performed here focused on the main lower-left quadrant clustering of cells, which is believed to be representative of small detached SH-SY5Y cells as observed under a light microscope. This had the natural consequence of lowering the proportion of overall events that were subsequently analysed, which turned out to be ~18% in the example shown (figure 21). Additionally, numerical and statistical analysis of the smear of events spread out along the FSC axis towards the bottom-right quadrant gave nonsensical results – where even addition of Menadione had little or no effect on MFI values recorded when using the appropriate MitoSOX filter. Regrettably, some type of nuclear staining was not included here – which may have made appropriate gating of viable cells easier to perform and more clearly identifiable.

Given the phenotype that develops as a result of the SH-SY5Y differentiation process, it was suspected that detachment (which results in small spherical cells in suspension) in order to perform flow analysis may prove significantly disruptive to this cell model – which otherwise has long, branching protrusions while comfortably attached. To test this idea, a placement student conducted a similar flow cytometry experiment with two populations of SH-SY5Y cells – one differentiated and one undifferentiated. It became clear from observing results obtained using undifferentiated cells that the cluster in the bottom-left quadrant is indeed the main live cell population, with a much more intense and obvious clustering pattern. In this way, undifferentiated cells were confirmed to be much more amenable to flow cytometry. This is an unfortunate downside of using differentiated cells, which were chosen as a cell model because of their more neuron-like phenotype and increased sensitivity (see 1st results chapter) – which is especially relevant when investigating potentially subtle disruptions to metabolism and redox state. Still, despite these issues, there was a clear overall trend showing RF irradiation provoking superoxide formation – as was anticipated based on existing literature (Oktem, Ozguner et al. 2005, Usselman, Hill et al. 2014, Bortkiewicz 2019, Choi, Min et al. 2020, Panagopoulos, Karabarbounis et al. 2021, Sofri, Rahim et al. 2021).

Surprisingly, this same pattern of radiation causing consistently increased MitoSOX signal did not manifest in a later experiment, which also included an investigation into how RF irradiation might alter Menadione responses in the context of superoxide formation (figure 24b). Unlike the previously described flow experiment, which utilised a simple sinusoid for

irradiation, this attempt also made use of a 256-QAM waveform. Results discussed earlier from other assays led us to anticipate a potentially stronger biological effect using this modulated signal type, possibly due to demodulation effects, but this was not the case. In this instance, irradiation appeared to cause increases in superoxide formation at some time points, while lowering detected MFI at other times – with none of those changes proving statistically significant (figure 24b). RF irradiation prior to Menadione insult did cause a trend of slightly increased superoxide formation – but again, these increases did not prove to be statistically significant. It is unclear why this second batch of MitoSOX flow cytometry data does not align with earlier results. It may, at least partially, be attributed to differences in radiation source (sinusoid vs 256-QAM signal) and general difficulty in applying flow cytometry techniques using this particular cell model, effectively muddying results. But even with these factors in mind, it is difficult to explain why such different results were obtained here – particularly in light of other assays which showed the 256-QAM signal to be biologically active.

The final flow cytometry experiment used TMRM to interrogate mitochondrial membrane permeability under different conditions (figure 25). In this experiment, signal generation using the appropriate filter is high in healthy cells and lowered by disruption to the mitochondrial membrane potential (e.g. as a result of uncoupling events associated with entering an apoptotic state). With the exception of the early 4-hour time point, radiation alone (IR+) appeared to result in lower MFI values relative to non-irradiated controls – which is suggestive of a loss of signal due to a reduced ability to maintain the mitochondrial membrane potential compared to non-irradiated controls. This MFI-lowering effect of RF irradiation at the 24 and 48-hour time points was statistically significant and resulted in MFI values that remained stagnant over the course of the experiment. Cells that were not irradiated instead saw a steady increase in MFI values over time (figure 25b).

In terms of comparisons between samples irradiated then given CCCP vs those not irradiated then given CCCP (CCCP+ vs CCCP-), MFI recorded was comparable for two out of three time points, with a significantly lower CCCP+ value at the final 48-hour time point (figure 25b). But it is hard to make any inferences or suggestions based on this component of the dataset, because of a general issue with the assay – an apparent failure of CCCP treatment to lower signal generated. It is not clear why, but in most cases CCCP did not have the intended effect of signal reduction – which should be happening because the role of CCCP here is to act as an uncoupling agent and force TMRM entry into the mitochondria and cause a resultant signal loss. The assay called for a mere 5-minute incubation with a moderate concentration of CCCP. It is possible a longer incubation was needed here in this

experimental context, which would have allowed more time for CCCP to act upon mitochondrial membranes and, potentially, could have had the desired effect of lowering signal generation. Sadly, both time and financial constraints did not allow for much optimisation of the assay, which is why the protocol was followed as written. In hindsight, this experiment could have benefitted from an additional optimisation step, with both a time and concentration gradient for CCCP treatment to find the optimal conditions – something which should definitely be considered for future work.

The last experiment to consider here was the Seahorse Mito Stress Test, or OCR assay. Both experimental setups were used, exposing cells to two different types of signal - WiFi (~5.3 GHz) mixed with cellular data (~840 MHz) in a desktop mini-incubator and a 256-QAM waveform in the Faraday shield (4.9 GHz, SAR = 4.016E-05 W/kg). RF-EMFs were applied for 18 hours prior to carrying out the assay. There was a very consistent trend across both experimental setups and at every assay stage, where radiation appeared to slightly lower mitochondrial performance and oxygen consumption (figure 26). However, these differences were generally small in magnitude and not always statistically significant. For example, baseline readings were not significantly affected by radiation, even if they were non-significantly reduced in both experimental setups. This is reassuring for two reasons. Firstly, such direct impact on mitochondrial function would raise very ominous implications for the general population, who are widely and chronically exposed to broadly similar telecoms signals (Obile 2016, Ericsson 2021, Ericsson 2024). Secondly, if these types of RF signals were capable of directly modulating mitochondrial function with significant intensity it could reasonably be expected that there would be a large, overwhelming body of evidence linking use of telecoms signals to disease – which is not necessarily the case, even if there is some evidence of biological effects (Protection 1998, Group 2010, Swerdlow, Feychting et al. 2011, ICNIRP 2020, ICBE-EMF 2022). It seems very likely that chronically disturbed mitochondrial respiration would precipitate substantial disease burden in such exposed general populations and pose significant risk to human health (Schon and Manfredi 2003, Schapira 2006, Chaturvedi and Beal 2013).

However, some of the responses to injection with different mitochondrial-modulating compounds were significantly different in irradiated samples (figure 26a and 26b). In the context of 5G phone signals (figure 26a), there was a statistically significant lowering of Oligomycin and Rotenone + Antimycin A responses – i.e. of the respiration taking place, a higher proportion of it may be attributed to mitochondrial respiration in irradiated samples. That is to say, there appeared to be slightly increased respiration taking place not directly associated with the mitochondria in samples that had not been irradiated. This observation,

combined with the trend of slightly non-significantly lowered baseline OCR, is indicative of a generalised small and subtle suppression of cellular respiration by RF-EMR exposure here in this experimental context.

The Faraday shield setup revealed a similar pattern of results – non-significant lowering of baseline OCR, and reduced OCR in response to drug insults, this time being significantly lowered in the context of Oligomycin and FCCP injection (figure 26b). The reduced OCR of irradiated samples during the FCCP injection phase is potentially significant, as it suggests this population of cells have reduced “spare respiratory capacity” – i.e. that they have reduced ability to respond to increased energy demands or stressful conditions, as outlined in the assay protocol describing FCCP responses.

Overall, it is interesting to see further indirect evidence of RF-EMR associated biological effects being revealed by insults with different drug compounds – as seen earlier in the context of the CTB assay and Menadione. Although there are reservations and concerns with some of the datasets considered here, the emerging picture is one of subtle, small intensity effects correlating with RF-EMR exposure. This subtle effect conclusion meshes up quite well with the background literature of the field – which is, at least to some extent, conflicted and ambiguous or debateable. There are numerous papers reporting different types of biological effects in different contexts, but there are also papers, some of them very robust such as the Interphone study, reporting no clear link between disease or biological effects and different types of EMR exposures (Barron and Baraff 1958, Cohen, Lilienfeld et al. 1977, Robinette, SILVERMAN et al. 1980, Protection 1998, Group 2010, Group 2011, Swerdlow, Feychting et al. 2011, Kang, Lee et al. 2014, ICNIRP 2020). Again, if there were a biological effect of strong intensity, then we might expect to see a significantly stronger body of evidence linking telecoms signal exposure and disease. But it is similarly undeniable that there is a meaningful body of evidence showing the capacity of low frequency radiant energy to cause changes to biology in many and varied contexts (Szmigielski 1996, Hardell, Hallquist et al. 2002, Hossmann and Hermann 2003, Challis 2005, Zamanian and Hardiman 2005, Lantow, Lupke et al. 2006, Akdag, Bilgin et al. 2007, Simkó 2007, Kovacic and Somanathan 2010, Cancer 2011, Consales, Merla et al. 2012, Schneider and Stangassinger 2014, Tang, Zhang et al. 2015, Falcioni, Bua et al. 2018, Bortkiewicz 2019, Choi, Min et al. 2020). Based on the results presented here, it is theorised that, depending on the signal and biological context, RF radiation like that used in telecoms systems might possess the ability to exert small, subtle effects on living material, as also suggested by some background literature within the field.

Chapter 5 – Results

Transcriptome changes in response to RF-EMF exposure

Preface

If RF-EMF exposure is able to provoke physiological changes in exposed cells and tissue, such as promotion of ROS generation and disturbance of redox state, signalling pathway changes that could occur as a result of this external pressure are likely to manifest changes in the transcriptome of exposed cells. The objective of this chapter was to perform transcriptomics analysis in order to investigate the capacity of RF-EMF exposure to cause transcriptome changes in neuron-like SH-SY5Y cells. This should offer new insights into the biological mechanisms underpinning cellular responses to RF-EMFs, in a field of study that, to date, is lacking in published transcriptomics research.

5.1 – Introduction

Transcriptomics is an investigation of the transcriptome, which is the entire transcriptional output that is produced when cells “express” genes by using molecular machines to transcribe DNA into RNA. The earliest forms of transcriptomics began to emerge in the 1990’s, which could only capture and analyse part of the transcriptome initially (Adams, Kelley et al. 1991). But in the decades since that time there has been much improvement, with several new types of transcriptomics approaches emerging, including RNA microarrays and serial analysis of gene expression (Lowe, Shirley et al. 2017). This technological advancement has massively improved the analytical power of transcriptomics approaches, enabling scientists to routinely sequence entire transcriptomes of samples at relatively low-cost when compared to the earliest technologies. The most recent and popular form of this technology employed today is RNA sequencing, or simply RNA-seq (Lowe, Shirley et al. 2017). RNA-seq affords users several advantages over previous technologies, for example, RNA microarrays requires the use of predefined probes, which is not needed with RNA-seq (Barbulovic-Nad, Lucente et al. 2006). Crucially, the sensitivity and scalability of RNA-seq is unmatched among transcriptomics approaches and it also boasts a broad dynamic range and low RNA quantity requirement, culminating in a tool that is widely regarded as a revolution in the field (Wang, Gerstein et al. 2009, Lowe, Shirley et al. 2017).

One of the main research outputs of RNA-seq is identification and quantification of Differentially Expressed Genes (DEGs). When cells are exposed to external or endogenous pressures or influences, they can respond by initiating signalling cascades that often lead to genetic expression changes in an attempt to adapt to their environment (Huelsken and Behrens 2002, Lizcano and Alessi 2002, Pires-daSilva and Sommer 2003). This process of genetic expression modulation is what can be captured in great detail by using RNA-seq to analyse DEGs, giving good insight into which specific pathways and genes are being turned on or off in response to experimental conditions. These changes in genetic expression involve complex regulation of genetic material, where the availability of genes to molecular machinery is modulated by histone modification and tightly coordinated recruitment of protein complexes to facilitate the process of transcription – the means by which DNA code is used as a template to build RNA molecules (McAdams and Arkin 1997, Hampsey 1998, Thomas and Chiang 2006, Gibney and Nolan 2010). Although there are several forms RNA can take, messenger RNA, or mRNA, is the key molecule at the heart of transcriptomics analysis (Lowe, Shirley et al. 2017). mRNA acts as a template for the expression of genetic material, functioning as a middle-man between genes and proteins. mRNA transcripts can be read by molecular machines called ribosomes to ultimately produce protein products

whose amino acid sequences are based on the original DNA sequence that was used to encode the mRNA transcript, in a process called translation (Ramakrishnan 2002). The process of translation is a sensitive one, where the abundance, stability and processing of mRNA transcripts can greatly influence the downstream protein expression of cells (Koritzinsky, Seigneuric et al. 2005). Disruption and dysregulation of transcription can lead to downstream consequences for protein expression and, ultimately, cause cellular dysfunction and promote disease (Lee and Young 2013). That is partly why there has been such an interest in transcriptomics in recent years as an investigative tool – RNAseq is a powerful technique that allows basic researchers to rapidly process vast quantities of transcriptional information in a cost-effective manner, often comparing entire transcriptomes of diseased cells versus healthy cells and highlighting genes of interest (Costa, Aprile et al. 2013, Potter 2018). Indeed, even when transcriptional control is maintained, subtle deviations from typical physiological transcriptome profiles is itself often informative about cellular state and stress levels (Desikan, A.-H.-Mackerness et al. 2001, Kreps, Wu et al. 2002).

Because of this, it is hoped that by employing RNAseq here and comparing irradiated cells to non-irradiated cells, we will be able to use analysis of DEGs to elucidate detail on how cells are changing in response to radiation exposure – specifically which genes and pathways are changing. As such, the objective of this chapter is to produce two sets of whole-cell RNA preparations from two populations of neuron-like differentiated SH-SY5Y cells; one population exposed to RF-EMFs and a non-irradiated control population. It is theorised, based on existing literature and previous results presented here, that the two cell populations should produce distinct transcriptome profiles – moreover, that the differences between these profiles could shed light on cellular responses to RF-EMR exposure.

5.2 – Methods

5.2.1 – RNA extraction

Initially, SH-SY5Y cells were differentiated into a more neuron-like phenotype using all-trans Retinoic acid as previously described. Once this process was completed, cells were plated out into 6-well plates, with a seeding density of ~800,000 cells per well (Corning™ Costar™ 6-well Clear TC-treated Multiple Well Plates, product code 10578911). These plates were then left to settle overnight in a standard CO_2 enriched cell culture incubator using supplemented Neurobasal media (Gibco™ Neurobasal™ Medium, catalogue number 21103049). The following day, media was replaced with pre-warmed CO_2 Independent Media (Gibco™ CO_2 Independent Medium, product code 11580536) and plates were transferred into the Faraday shield or mini-incubator and irradiated overnight for 18 hours or given no RF radiation exposure for the same period. The signals used for radiation were a 256-QAM modulated waveform at 4.9 GHz frequency and SAR = 4.016E-05 W/kg in the Faraday shield or mixed WiFi and cellular data signals using a 5G phone in the mini-incubator. RNA extraction was carried out the following day on a benchtop using ice to keep samples and reagents cool.

To perform the extraction, an appropriate RNA extraction kit was purchased from Qiagen (RNeasy Mini Kit (50), product ID 74104). Extraction was carried out in accordance with the protocol supplied with the kit. Firstly, media was removed and wells were briefly washed with chilled PBS to remove traces of media (Gibco™ PBS, pH 7.4, catalogue number 10010023). Then, 350 µl RLT buffer was added to wells to lyse cells. To encourage complete lysis, RLT buffer was pipetted over the surface of wells several times and gentle scratching using a pipette tip was applied. This process was repeated on two other wells, transferring the same 350 µl RLT buffer between wells, to give a final lysate sample pooled from 3 wells. This pooled lysate was mixed with 350 µl of 70% ethanol and transferred to a RNeasy Mini spin column placed in a 2 ml collection tube. This tube was placed into a refrigerated centrifuge and spun for 15 seconds at 10,000 RCF, after which flow through was discarded. Several washing steps occurred after this, each step using different buffers and/or centrifuge parameters – as outlined in the assay protocol. After each wash, flow through was discarded. Washes were carried out in the following order;

1. 700 µl of RW1 buffer, 15 seconds spin at 10,000 RCF
2. 500 µl of RPE buffer, 15 seconds spin at 10,000 RCF
3. 500 µl of RPE buffer, 2 minutes spin at 10,000 RCF

After these washes were completed, existing 2 ml collection tubes were replaced with fresh ones and 30 µl of RNase-free water was added directly to spin column membranes. Columns were then spun for 1 minute at 10,000 RCF to elute RNA. Note, final RNA elution step was repeated an additional time, re-using the same 30 µl of RNase-free water to further concentrate samples. These sample tubes were frozen and stored at -80C until all samples had been processed and were ready for transcriptional analysis.

5.2.2 – Transcriptomics

To assess the mRNA expression profiles in neuron-like SH-SY5Y cells, differential expression analysis was undertaken with a company that specialises in transcriptomics analysis called Novogene (Cambridge UK, www.novogene.com). RNA sequencing was carried out on Illumina platforms, based on the mechanism of SBS (sequencing by synthesis), which offers high throughput and high accuracy output, with low sample requirements. Samples from four condition groups were submitted for analysis as follows;

1. BN1-3; **B**ox (Faraday shield) **N**egative (no radiation) samples 1 to 3
2. BP1-3; **B**ox (Faraday shield) **P**ositive (256-QAM irradiation) samples 1 to 3
3. MN1-3; **M**ini-Incubator **N**egative (no radiation) samples 1 to 3
4. MP1-3; **M**ini-Incubator **P**ositive (mixed phone signals irradiation) samples 1 to 3

5.2.3 – RNA-seq datasets

Twelve paired-end mRNA-Seq libraries (BN1–3, BP1–3, MN1–3, MP1–3; 2 × 150 bp) were supplied as raw FASTQ files (≈ 2 GB each) generated on an Illumina NovaSeq 6000 by Novogene (Cambridge UK, www.novogene.com).

5.2.4 – Computational environment

All analyses were performed under Ubuntu 22.04 LTS running inside Windows 10 WSL 2 on a workstation with 12 physical CPU cores (Intel Xeon E5-1607, 64 GB RAM) and a 1 TB NVMe SSD. Tools and versions are listed in Table 5. All figures, unless otherwise stated, were generated using python (v3.9.230) and associated publicly available libraries.

TOOL	VERSION	KEY PARAMETERS
FASTP[1]	0.22.0	-p -w 8 (paired-end, 8 threads)
STAR[2]	2.7.11b	genomeGenerate: --sjdbOverhang 99; align: --runThreadN 12, --readFilesCommand zcat, --outSAMtype BAM SortedByCoordinate
FEATURECOUNTS[3]	2.0.6	-T 12 -p -B -C
DESEQ2[4]	1.42.0	Default settings
BIOMART[5]	2.58.0	Ensembl 110 (GRCh38.p14)
MULTIQC[6]	1.18	Default settings

Table 5 – Software versions and principal run-time options.

5.2.5 – RNA-Seq Data Quality Control

Raw sequencing reads were subjected to quality control and adapter trimming using fastp (v0.23.4). Fastp 5.2.45.2.4 was run with default parameters, and both HTML and JSON reports were generated for all samples. Quality metrics including per-base sequence quality, duplication rates and adapter content were summarised using MultiQC (v1.18). After trimming, read quality and yield were inspected for all samples.

For alignment, reads were mapped to the reference genome using STAR (v2.7.11b) with default settings. The homo sapiens reference (GRCh38, release 110) FASTA and GTF files were downloaded from Ensembl (January 2025). Alignment statistics (e.g., percent uniquely mapped reads) were aggregated with MultiQC. Gene-level counts were generated using featureCounts (v2.0.3). Assignment statistics and mapping rates for all samples were included in the MultiQC report to assess overall dataset quality.

The quality and consistency of RNA-Seq data across all samples was visualised by the distribution of gene expression values following normalisation. Raw gene counts were obtained from featureCounts and normalised using the DESeq2 variance-stabilising transformation (VST). The VST method reduces the dependence of the variance on the mean, facilitating visualisation and clustering. The distribution of VST-transformed gene expression values was visualised for each sample using both kernel density plots and boxplots.

5.2.6 – Principal-Component Analysis

Each gene vector was centred and scaled to unit variance (z-score). PCA was performed with scikit-learn v1.3.0 yielding two principal components (PC) that together explain 76.8 % of the total variance (PC1 = 57.9 %, PC2 = 19.0 %). Sample scores were visualised with matplotlib v3.8.0.

5.2.7 – Differential-expression analysis

Raw gene counts were imported into DESeq2. For each pairwise comparison (BP vs BN, MP vs MN, BN vs MN and BP vs MP), a negative binomial generalised linear model was fitted. Genes with an adjusted p-value (FDR) < 0.05 were considered significantly differentially expressed. The results of each differential expression analysis were visualised as an MA plot, where each gene is plotted according to its mean normalised expression (baseMean) and log2 fold change between conditions. Significant genes (FDR < 0.05) were highlighted in red.

Filtered counts were imported into DESeq2 using default settings. Sample groups were encoded as a four-level factor (BN, BP, MN, MP). Size factors and dispersion estimates were calculated by the median-ratio and parametric methods, respectively. Wald tests were performed for four contrasts:

1. BP vs BN; effect of RF irradiation on cells in box (256-QAM signal)

2. MP vs MN; effect of RF irradiation on cells in incubator (WiFi & cellular data signals)

3. BN vs MN; baseline difference between control cells (no IR)

4. BP vs MP; difference between RF irradiated cells

P-values were adjusted using the Benjamini–Hochberg FDR procedure (FDR = 0.05). Significance thresholds were $|\log_2 FC| \geq 1$ and FDR < 0.05 unless stated otherwise.

For heatmaps, variance-stabilised (VST) normalised expression values for the selected genes were extracted for all samples. For each gene, expression values were standardised (z-score transformation) across samples. Hierarchical clustering of both genes (rows) and samples (columns) was performed using Euclidean distance and average linkage.

5.2.8 – Gene annotation

DESeq2 result tables were annotated with HGNC symbols, gene biotype, descriptions, Entrez IDs and Gene Ontology (GO) terms via the biomaRt (v2.58.0) interface to Ensembl 110.

5.2.9 – Gene Ontology (GO) and KEGG Enrichment Analysis

To investigate the biological processes associated with differential gene expression, GO and KEGG enrichment analyses were performed on significant DEGs from each pairwise group comparison. For each contrast, genes with adjusted p-value (padj) < 0.05 and $|\log_2$ fold change| > 1 were selected from DESeq2 results. Enrichment analysis was conducted using the enrichGO and enrichKEGG functions from the clusterProfiler package in R with the org.Hs.eg.db annotation database.

The top enriched GO Biological Process (BP) terms and KEGG pathways were visualised using both horizontal bar plots and dot plots. In bar plots, bar length indicates the number of DEGs, and colour corresponds to the adjusted p-value (FDR). In dot plots, dot size represents the number of DEGs per term and colour reflects the adjusted p-value (FDR).

5.3 – Results

5.3.1 – RNA-Seq Quality Control (QC)

RNA-Seq data demonstrated high sequencing and mapping quality across all samples (Figure 27). Before fastp processing, duplication rates ranged from ~15–28%, but after their removal the majority of reads passed quality filtering with consistently high GC content (~50–51%) and minimal residual adapter content (<3%). The total number of assigned reads per sample after filtering ranged from ~32 to ~48 million, ensuring robust transcriptome coverage. Alignment to the reference genome with STAR yielded uniquely mapped read rates between 81–91%, and FeatureCounts assigned 73–79% of reads to annotated genes. The absolute numbers of uniquely mapped and assigned reads were consistently high for all samples (~19–27 million). No samples showed outlier quality or mapping rates, confirming the suitability of the dataset for downstream differential expression and functional analyses.

27a

Sample Name	% Duplication	M Reads After Filtering	GC content	% PF	% Adapter
MP3_1	16.8%	59.2	51.2%	99.2%	1.0%
MP2_1	27.6%	46.0	50.1%	99.2%	0.8%
MP1_1	15.0%	48.5	50.5%	99.2%	0.7%
MN3_1	18.7%	45.3	50.0%	99.1%	0.9%
MN2_1	15.1%	45.4	51.5%	99.2%	0.9%
MN1_1	16.3%	49.1	51.1%	99.3%	2.0%
BP3_1	15.0%	45.7	50.5%	99.2%	0.9%
BP2_1	23.0%	50.2	49.8%	99.1%	0.6%
BP1_1	16.2%	52.3	50.5%	99.2%	0.9%
BN3_1	15.3%	52.3	51.6%	99.1%	2.9%
BN2_1	16.0%	53.3	50.5%	99.3%	2.2%
BN1_1	15.4%	60.7	50.4%	99.2%	1.7%

27b

Sample Name	% Assigned	M Assigned	% Aligned	M Aligned
BN1	76.7%	47.5	90.4%	27.4
BN2	76.3%	41.1	89.1%	23.7
BN3	74.4%	40.8	91.0%	23.8
BP1	76.6%	38.2	83.8%	21.9
BP2	77.2%	36.5	83.5%	21.0
BP3	77.4%	33.3	84.7%	19.4
MN1	76.7%	37.5	90.2%	22.1
MN2	77.7%	34.5	87.7%	19.9
MN3	78.9%	32.1	81.8%	18.5
MP1	77.5%	36.7	86.9%	21.1
MP2	73.0%	31.6	81.3%	18.7
MP3	73.5%	45.5	88.3%	26.1

Figure 27 – RNA-Seq data quality overview. (**27a**) MultiQC summary of fastp QC statistics for all samples. Shown are duplication rate before filtering (% Duplication), total reads after filtering (M Reads After Filtering), GC content after filtering (%), percent reads passing filter (% PF), and percentage of adapter-trimmed reads (% Adapter). (**27b**) MultiQC summary of STAR alignment and featureCounts quantification. Shown are the percentage of reads assigned to genes by featureCounts (% Assigned), number of assigned reads (M Assigned), percentage of uniquely mapped reads by STAR (% Aligned), and number of uniquely mapped reads (M Aligned). These metrics confirm high mapping rates and sequencing consistency across all samples.

To evaluate the uniformity and quality of gene expression measurements across samples, we examined the distribution of VST-transformed expression values using density and boxplots (Figure 28). All samples displayed nearly identical unimodal distributions, with a primary peak at VST ≈ 5, characteristic of lowly expressed genes, and a long right-skewed tail corresponding to moderately and highly expressed genes. The medians and interquartile ranges were highly consistent across all samples, with no evidence of global shifts, batch effects, or technical artifacts. These results indicate successful normalisation and high technical consistency, supporting the suitability of the dataset for downstream analyses.

28a

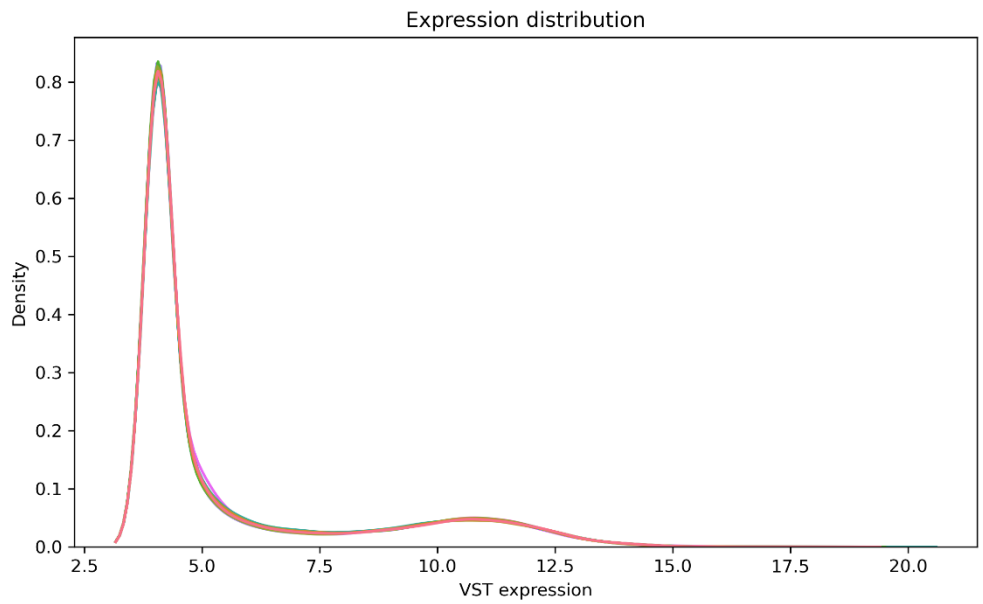

28b

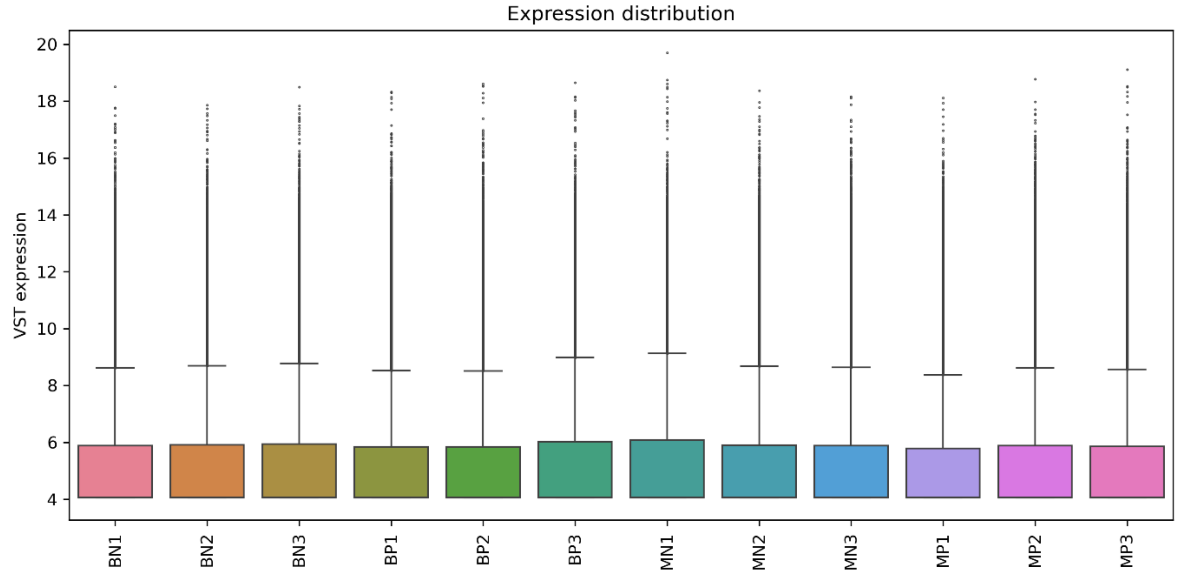

Figure 28 – Expression distribution of normalised RNA-seq data across all samples. (**28a**) Density plot and (**28b**) boxplot of variance-stabilised (VST) gene expression values for each RNA-seq sample. The nearly identical distributions across samples indicate effective normalisation and high technical consistency, with no evidence of batch effects or sample-specific expression biases.

5.3.2 – Principal Component Analysis (PCA)

Principal component analysis (PCA) of the log_2-CPM expression matrix (top 5,000 variable genes) revealed that RF-EMF exposure is a major source of transcriptomic variance (Figure 29). PC1 (57.9% variance explained) separated irradiated (BP, MP) from control (BN, MN) samples, with incubator IR exposed (MP) cells showing the most pronounced response. PC2 (19.0% variance explained) distinguished samples by growth environment, separating Faraday box non-irradiated controls from mini-incubator non-irradiated controls. Most replicates clustered tightly by condition, confirming high technical reproducibility. Two samples (MP2, BP3) appeared as moderate outliers but remained more similar to their respective groups than to other conditions, suggesting either heightened biological response or minor technical variation. Overall, PCA confirms that irradiation, and to a much lesser extent environmental factors, substantially shape differentiated SH-SY5Y gene expression, validating the experimental model.

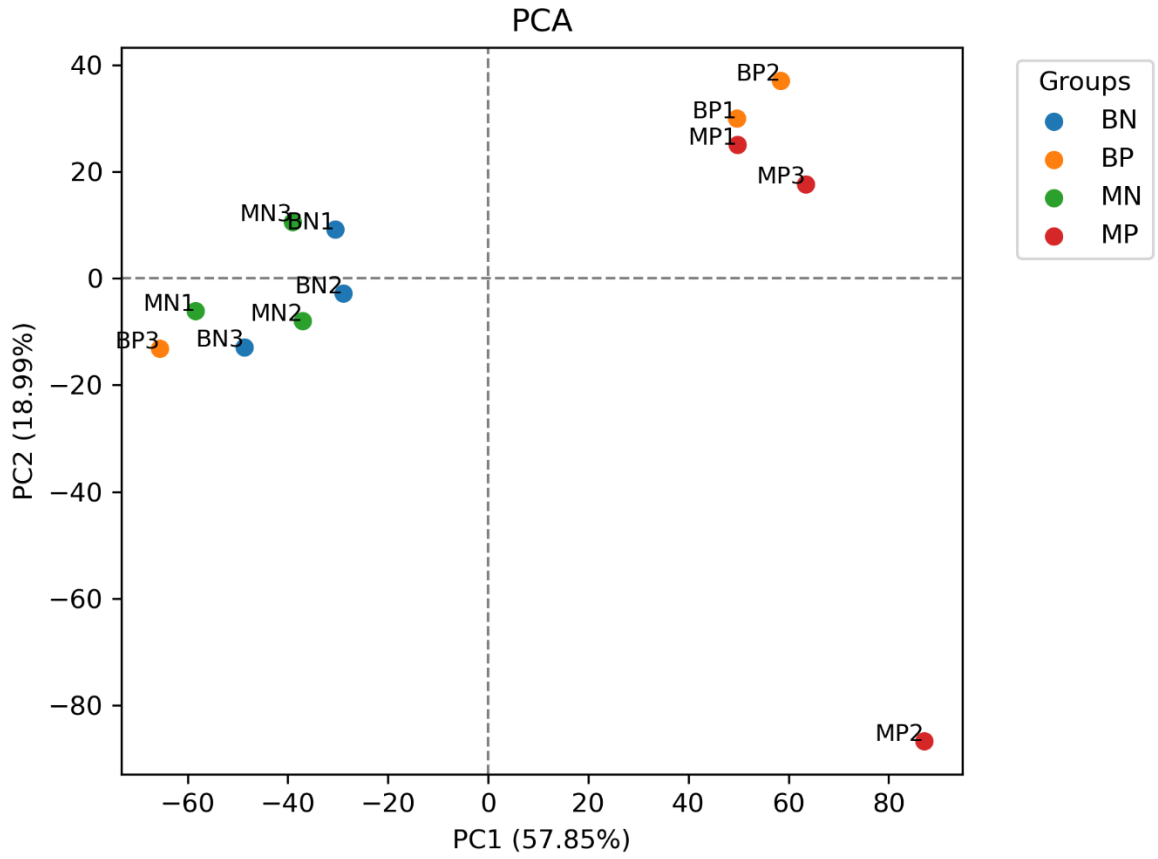

Figure 29 – PCA of global gene expression in SH-SY5Y cells following RF irradiation. PCA of log_2-CPM values from the 5,000 most variable genes shows separation of samples by irradiation status (PC1, 57.9% variance) and culture environment (PC2, 19.0% variance). Each point represents one biological replicate (3 samples per experimental group), coloured by group. Notable outliers BP3 and MP2 are indicated. Together, PC1 and PC2 explain 76.9% of total variance.

5.3.3 – Differential Gene Expression

Differential expression analysis was performed for both BP vs BN and MP vs MN comparisons, corresponding to the effects of IR exposure on cells in the box (B) or incubator (M). In the BP vs BN comparison, the majority of genes exhibited log2 fold changes close to zero, and only a modest subset reached statistical significance (Figure 30a). This indicates a limited transcriptional response to irradiation under experimental conditions within the Faraday shield (256-QAM, 4.9 GHz, SAR = 4.016E-05 W/kg). In contrast, the MP vs MN comparison revealed a pronounced shift, with a large number of genes significantly up or down-regulated and a wide range of log2 fold changes, some exceeding ±10 (Figure 30b). This suggests that the mixed 5G phone signals inside the incubator environment are capable of provoking a stronger transcriptional response, resulting in robust and widespread gene expression changes. As a control, we also compared BN vs MN (Figure 30c) and BP vs MP (Figure 30d) corresponding to the effect of growing in a box or incubator without (N) or with exposure (P) to IR. Very few genes were differentially expressed, suggesting that the culture environment had minimal effect on gene expression.

30a

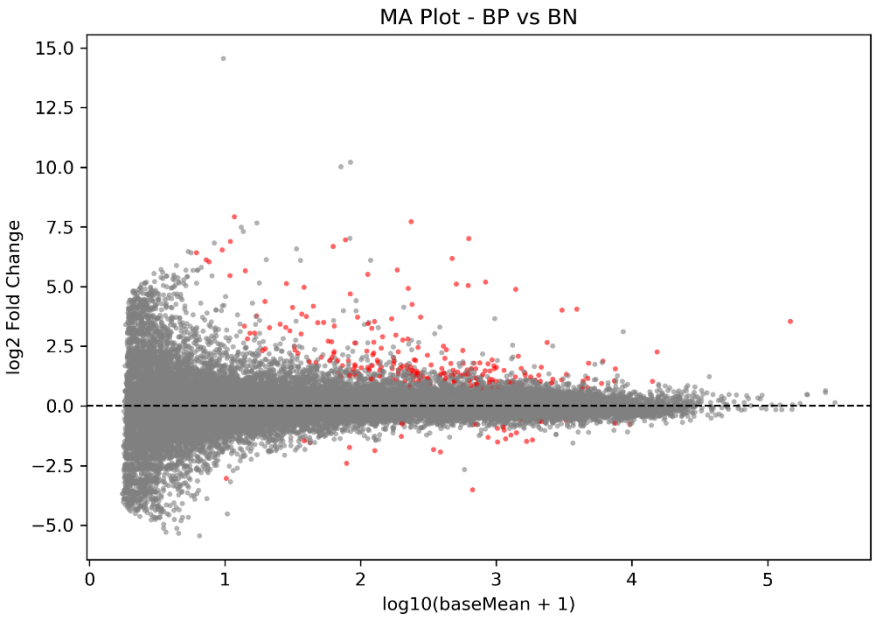

30b

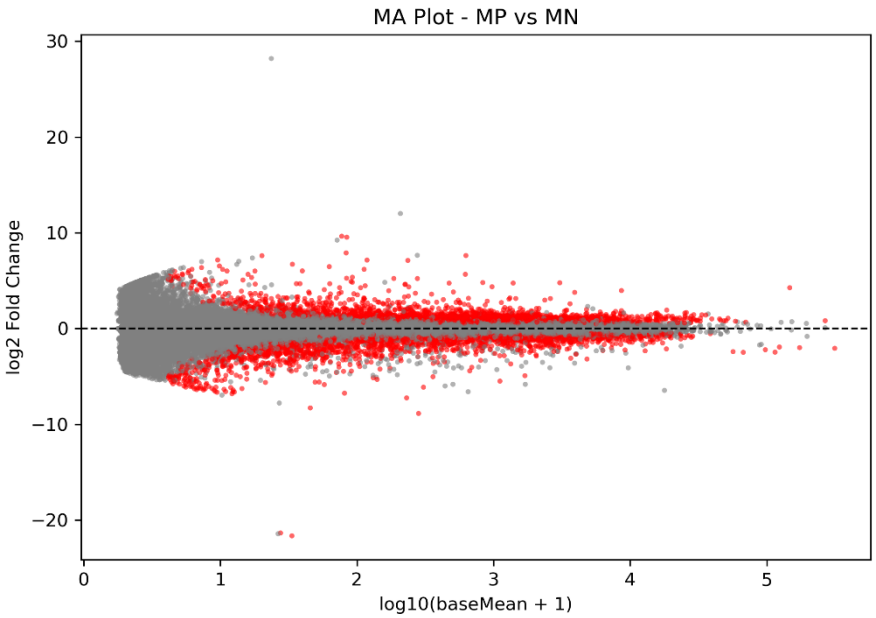
MA Plot - MP vs MN
log2 Fold Change
log10(baseMean + 1)
30
20
10
0
−10
−20
0
1
2
3
4
5

30c


MA Plot - BN vs MN
log2 Fold Change
log10(baseMean + 1)
5
0
−5
−10
−15
0
1
2
3
4
5

30d

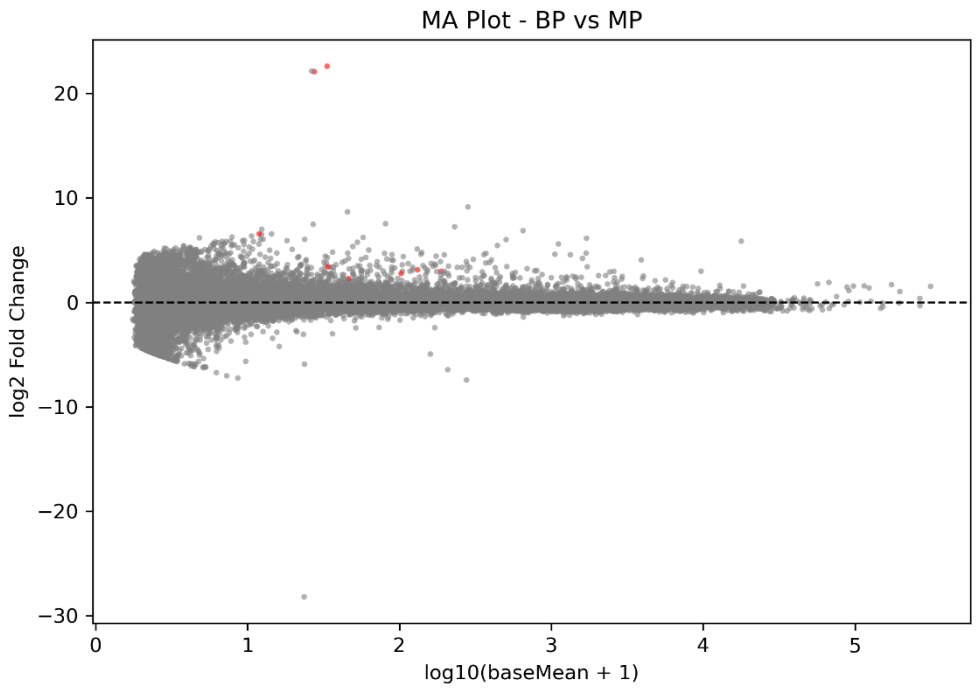

Figure 30 – MA plots showing differential gene expression between irradiated and control samples in the Faraday box and mini-incubator setups. (**30a**) BP vs BN and (**30b**) MP vs MN comparisons. A much broader and more pronounced transcriptional response is observed in the MP vs MN comparison. (**30c**) BN vs MN and (**30d**) BP vs MP comparisons. Very few genes are significantly differentially regulated when comparing growth in the box or the incubator, without or with IR. Each gene is plotted by mean normalised expression (log10 scale, x-axis) and log2 fold change (y-axis). Red points are genes with FDR < 0.05.

Global patterns of differential expression between experimental groups were visualised using volcano plots, which depict the statistical significance (–log10 FDR) against the magnitude of change (log2 fold change) for each gene (Figures 31-34). Significant genes (FDR < 0.05 and |log2FC| > 1) are highlighted in red and annotated with gene symbols. Detailed information, such as the fold-change, FDR, gene type and function, of the top 20 significantly differentially upregulated and downregulated genes for each comparison is shown in Tables 6-9.

The comparison of BP (box IR exposure) vs BN (box control) revealed a moderate set of differentially expressed genes, with both upregulated and downregulated transcripts identified (Figure 31). Notably, several genes including *ZBTB7C*, *CARTPT*, *RSPO1* and *POU4F2* showed meaningful changes in expression combined with high statistical significance. The volcano plot demonstrates a classic distribution, with most genes clustered around log2FC = 0 and significant hits distributed to both sides. In contrast, the MP (incubator IR exposure) vs MN (control) comparison exhibited a substantially greater number

of significantly differentially expressed genes, with a wide range of log2 fold changes (Figure 32). Strikingly, a subset of genes such as *IFI16* and *TMEM156* were among the most strongly downregulated, while many others showed pronounced and significant upregulation, such as *CARTPT* and *TNNT3*. This indicates a robust and extensive transcriptional response to mixed signal irradiation in the incubator environment. When comparing BN and MN (non-irradiated samples grown in box or incubator), only a handful of genes reached statistical significance, suggesting minimal baseline transcriptional differences attributable to the culture environment alone (Figure 33). Comparing irradiated samples between box and incubator (BP vs MP) identified very few significant genes (Figure 34). The most notable were *IFI16* and *TMEM156*, again highly downregulated in the MP group. This suggests that the signal exposure environment modulates the magnitude of the irradiation-induced response, but the core transcriptional changes are largely shared. Collectively, these results indicate that irradiation induces a broad shift in gene expression, particularly in the 5G phone incubator environment (MP vs MN, Figure 32), while baseline differences between culture environments (BN vs MN, Figure 33) or between irradiated samples (BP vs MP, Figure 34) are much more limited.

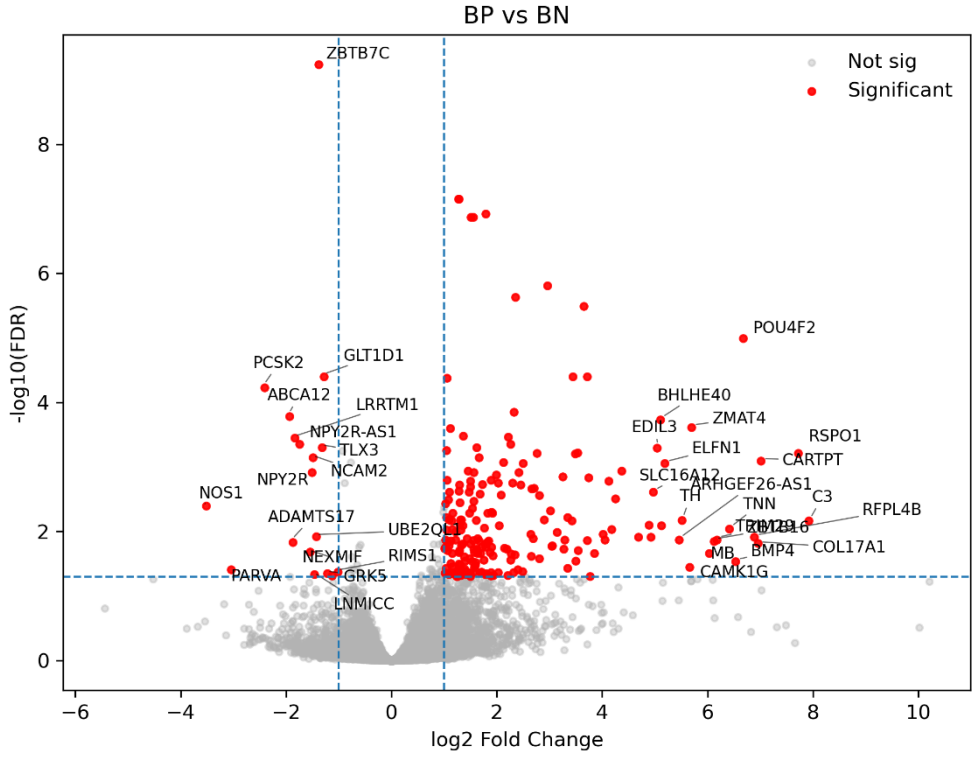

Figure 31 – Volcano plot of differential gene expression in box-cultured samples exposed to IR versus controls. Significantly (FDR<0.05, $|\log_2 FC| \geq 1$) altered genes are show in red. The top 20 differentially expressed genes are labelled. The x-axis represents $\log_2$ fold change (FC) and the y-axis shows statistical significance as $-\log_{10}$(FDR).

Table 6 – DEGs when comparing irradiated and non-irradiated Faraday box samples.

	Top 20 most upregulated and downregulated genes in BPvsBN (FDR<0.05)			
Gene symbol	**log2 Fold Change**	**padj (FDR)**	**Gene_biotype**	**Description**
C3	7.92	6.76E-03	protein_coding	complement C3
RSPO1	7.72	6.11E-04	protein_coding	R-spondin 1
CARTPT	7.01	8.07E-04	protein_coding	CART prepropeptide
COL17A1	6.96	1.53E-02	protein_coding	collagen type XVII alpha 1 chain
RFPL4B	6.89	1.22E-02	protein_coding	ret finger protein like 4B
POU4F2	6.68	1.02E-05	protein_coding	POU class 4 homeobox 2
BMP4	6.53	2.92E-02	protein_coding	bone morphogenetic protein 4
TNN	6.42	9.11E-03	protein_coding	tenascin N
TRIM29	6.18	1.34E-02	protein_coding	tripartite motif containing 29
ZBTB16	6.12	1.42E-02	protein_coding	zinc finger and BTB domain containing 16
MB	6.03	2.18E-02	protein_coding	myoglobin
ZMAT4	5.69	2.45E-04	protein_coding	zinc finger matrin-type 4
CAMK1G	5.66	3.60E-02	protein_coding	calcium/calmodulin dependent protein kinase IG
TH	5.51	6.74E-03	protein_coding	tyrosine hydroxylase
ARHGEF26-AS1	5.46	1.35E-02	lncRNA	ARHGEF26 antisense RNA 1
ELFN1	5.19	8.79E-04	protein_coding	extracellular leucine rich repeat and fibronectin type III domain containing 1
ENSG00000280135	5.12	8.10E-03	predicted	novel transcript
BHLHE40	5.11	1.84E-04	protein_coding	basic helix-loop-helix family member e40
EDIL3	5.04	5.09E-04	protein_coding	EGF like repeats and discoidin domains 3
SLC16A12	4.97	2.46E-03	protein_coding	solute carrier family 16 member 12
NOS1	-3.52	4.04E-03	protein_coding	nitric oxide synthase 1
PARVA	-3.04	3.89E-02	protein_coding	parvin alpha
PCSK2	-2.40	5.87E-05	protein_coding	proprotein convertase subtilisin/kexin type 2
ABCA12	-1.93	1.65E-04	protein_coding	ATP binding cassette subfamily A member 12
ADAMTS17	-1.87	1.47E-02	protein_coding	ADAM metallopeptidase with thrombospondin type 1 motif 17
LRRTM1	-1.83	3.54E-04	protein_coding	leucine rich repeat transmembrane neuronal 1
NPY2R-AS1	-1.74	4.40E-04	lncRNA	NPY2R antisense RNA 1
NEXMIF	-1.54	2.05E-02	protein_coding	neurite extension and migration factor
NPY2R	-1.51	1.21E-03	protein_coding	neuropeptide Y receptor Y2
NCAM2	-1.49	7.09E-04	protein_coding	neural cell adhesion molecule 2
LNMICC	-1.46	4.63E-02	lncRNA	lncRNA associated with lymph node metastasis in cervical cancer
UBE2QL1	-1.43	1.20E-02	protein_coding	ubiquitin conjugating enzyme E2 QL1
ZBTB7C	-1.38	5.80E-10	protein_coding	zinc finger and BTB domain containing 7C
TLX3	-1.32	4.95E-04	protein_coding	T cell leukemia homeobox 3
GLT1D1	-1.28	3.99E-05	protein_coding	glycosyltransferase 1 domain containing 1
GRK5	-1.22	4.44E-02	protein_coding	G protein-coupled receptor kinase 5
ENSG00000278928	-1.13	4.87E-02	predicted	novel transcript
RIMS1	-1.02	4.21E-02	protein_coding	regulating synaptic membrane exocytosis 1
FGF14	-0.94	5.65E-04	protein_coding	fibroblast growth factor 14
JAKMIP1-DT	-0.89	1.78E-03	transcribed_unp	JAKMIP1 divergent transcript

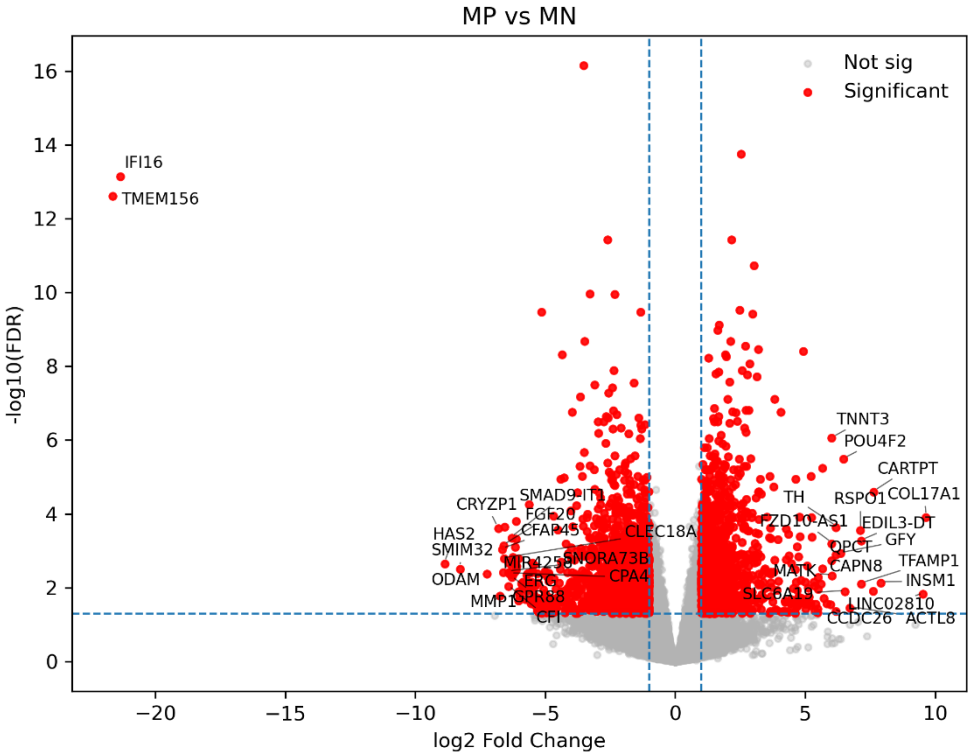

Figure 32 – Volcano plot of differential gene expression in incubator-cultured samples exposed to IR versus controls. Significantly (FDR<0.05, $|\log_2 FC| \geq 1$) altered genes are show in red. The top 20 differentially expressed genes are labelled. The x-axis represents $\log_2$ fold change (FC) and the y-axis shows statistical significance as $-\log_{10}$(FDR).

Table 7 – DEGs when comparing irradiated and non-irradiated mini-incubator samples.

	Top 20 most upregulated and downregulated genes in MPvsMN (FDR<0.05)			
Gene symbol	**log2 Fold Change**	**padj (FDR)**	**Gene_biotype**	**Description**
COL17A1	9.64	1.24E-04	protein_coding	collagen type XVII alpha 1 chain
LINC02810	9.54	1.48E-02	lncRNA	long intergenic non-protein coding RNA 2810
INSM1	7.90	7.43E-03	protein_coding	INSM transcriptional repressor 1
CARTPT	7.62	2.56E-05	protein_coding	CART prepropeptide
ENSG00000258717	7.61	1.25E-02	lncRNA	novel transcript
EDIL3-DT	7.16	5.45E-04	lncRNA	EDIL3 divergent transcript
TFAMP1	7.15	8.05E-03	processed_pseudogene	transcription factor A, mitochondrial pseudogene 1
RSPO1	7.11	2.83E-04	protein_coding	R-spondin 1
ACTL8	6.71	3.58E-02	protein_coding	actin like 8
SLC6A19	6.53	1.29E-02	protein_coding	solute carrier family 6 member 19
POU4F2	6.46	3.28E-06	protein_coding	POU class 4 homeobox 2
GFY	6.36	1.17E-03	protein_coding	golgi associated olfactory signaling regulator
TH	6.18	2.32E-04	protein_coding	tyrosine hydroxylase
CCDC26	6.18	4.34E-02	lncRNA	CCDC26 long non-coding RNA
QPCT	6.17	1.28E-03	protein_coding	glutaminyl-peptide cyclotransferase
MATK	6.03	4.84E-03	protein_coding	megakaryocyte-associated tyrosine kinase
TNNT3	6.02	8.86E-07	protein_coding	troponin T3, fast skeletal type
FZD10-AS1	6.01	6.39E-04	lncRNA	FZD10 antisense divergent transcript
CAPN8	6.00	1.81E-03	protein_coding	calpain 8
ENSG00000253362	5.97	2.89E-02	unprocessed_pseudogene	tropomyosin 3 (TPM3) pseudogene
TMEM156	-21.64	2.46E-13	protein_coding	transmembrane protein 156
IFI16	-21.34	7.18E-14	protein_coding	interferon gamma inducible protein 16
HAS2	-8.86	2.24E-03	protein_coding	hyaluronan synthase 2
SMIM32	-8.28	3.10E-03	protein_coding	small integral membrane protein 32
ODAM	-7.24	4.20E-03	protein_coding	odontogenic, ameloblast associated
CRYZP1	-6.80	2.45E-04	processed_pseudogene	crystallin zeta pseudogene 1
MMP1	-6.75	1.67E-02	protein_coding	matrix metallopeptidase 1
CFAP45	-6.65	9.09E-04	protein_coding	cilia and flagella associated protein 45
ENSG00000248458	-6.62	3.91E-03	lncRNA	novel transcript, antisense to SGIP1
FGF20	-6.60	7.34E-04	protein_coding	fibroblast growth factor 20
CLEC18A	-6.58	1.65E-03	protein_coding	C-type lectin domain family 18 member A
ENSG00000270926	-6.56	2.29E-04	unprocessed_pseudogene	WAS protein family homolog 4 pseudogene
SNORA73B	-6.42	3.87E-03	snoRNA	small nucleolar RNA, H/ACA box 73B
MIR4258	-6.41	2.15E-03	miRNA	microRNA 4258
CFI	-6.41	9.17E-03	protein_coding	complement factor I
ERG	-6.37	4.30E-03	protein_coding	ETS transcription factor ERG
CPA4	-6.34	4.21E-03	protein_coding	carboxypeptidase A4
SMAD9-IT1	-6.29	4.52E-04	lncRNA	SMAD9 intronic transcript 1
GPR88	-6.29	5.22E-03	protein_coding	G protein-coupled receptor 88
ENSG00000255050	-6.27	2.75E-03	lncRNA	novel transcript

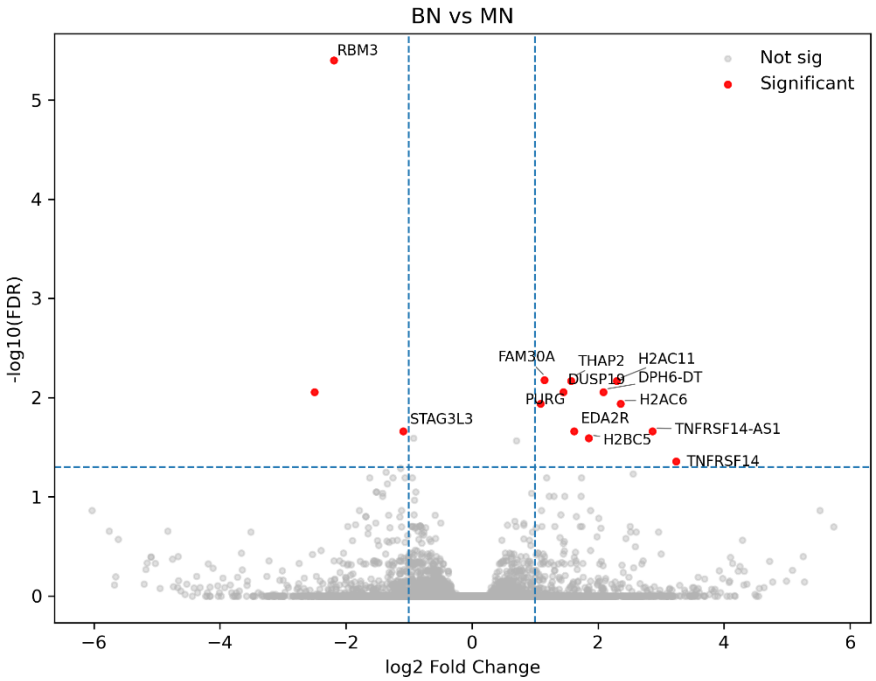

Figure 33 – Volcano plot of differential gene expression in cells cultured in the box vs the incubator without exposure to IR. Significantly (FDR<0.05, $|\log_2 FC| \geq 1$) altered genes are show in red. The x-axis represents $\log_2$ fold change (FC) and the y-axis shows statistical significance as $-\log_{10}(FDR)$.

	Upregulated and downregulated genes in BNvsMN (FDR<0.05)			
Gene symbol	**log2 Fold Change**	**padj (FDR)**	**Gene_biotype**	**Description**
TNFRSF14	3.24	4.38E-02	protein_coding	TNF receptor superfamily member 14
TNFRSF14-AS1	2.86	2.17E-02	lncRNA	TNFRSF14 antisense RNA 1
H2AC6	2.35	1.16E-02	protein_coding	H2A clustered histone 6
H2AC11	2.30	6.81E-03	protein_coding	H2A clustered histone 11
DPH6-DT	2.08	8.75E-03	lncRNA	DPH6 divergent transcript
H2BC5	1.86	2.57E-02	protein_coding	H2B clustered histone 5
EDA2R	1.62	2.17E-02	protein_coding	ectodysplasin A2 receptor
THAP2	1.57	6.81E-03	protein_coding	THAP domain containing 2
DUSP19	1.45	8.75E-03	protein_coding	dual specificity phosphatase 19
FAM30A	1.15	6.68E-03	lncRNA	family with sequence similarity 30 member A
PURG	1.08	1.16E-02	protein_coding	purine rich element binding protein G
ISL1-DT	0.71	2.71E-02	lncRNA	ISL1 divergent transcript
ZNF76	-0.93	2.57E-02	protein_coding	zinc finger protein 76
STAG3L3	-1.09	2.17E-02	transcribed_unprocessed_pseudogene	STAG3 cohesin complex component like 3
RBM3	-2.19	3.99E-06	protein_coding	RNA binding motif protein 3
ENSG00000267244	-2.50	8.75E-03	lncRNA	novel transcript, antisense to REXO1
RBM3	-2.19	3.99E-06	protein_coding	RNA binding motif protein 3
STAG3L3	-1.09	2.17E-02	transcribed_unprocessed_pseudogene	STAG3 cohesin complex component like 3
ZNF76	-0.93	2.57E-02	protein_coding	zinc finger protein 76

Table 8 – DEGs when comparing non-irradiated Faraday box and mini-incubator samples.

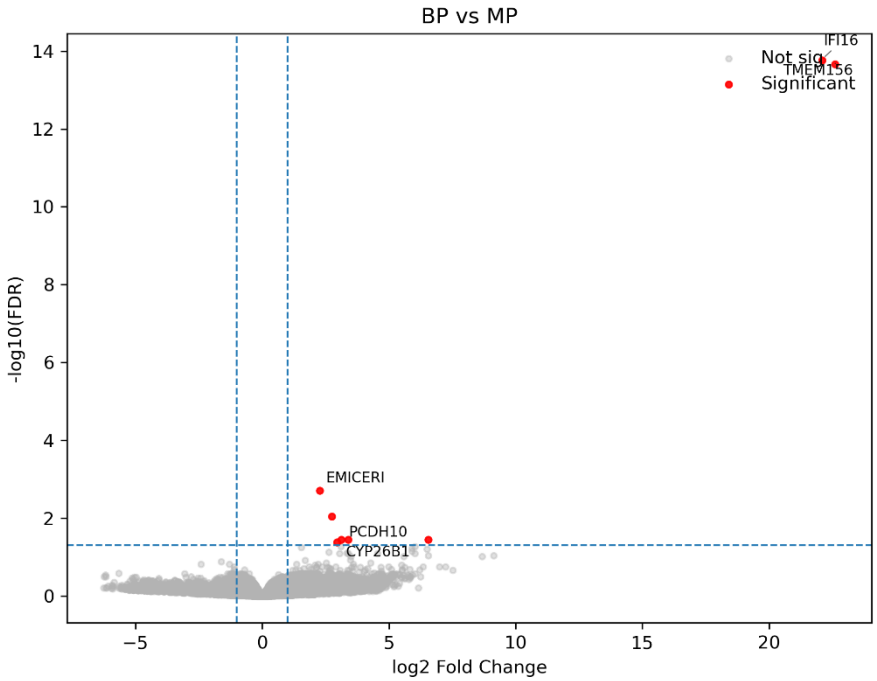

Figure 34 – Volcano plot of differential gene expression in cells cultured in the box vs the incubator with exposure to IR. Significantly (FDR<0.05, $|\log_2 FC| \geq 1$) altered genes are show in red. The x-axis represents $\log_2$ fold change (FC) and the y-axis shows statistical significance as $-\log_{10}$(FDR).

	Upregulated genes in BPvsMP (FDR<0.05)			
Gene symbol	**log2 Fold Change**	**padj (FDR)**	**Gene_biotype**	**Description**
TMEM156	22.60	2.19E-14	protein_coding	transmembrane protein 156
IFI16	22.09	1.73E-14	protein_coding	interferon gamma inducible protein 16
ENSG00000224950	6.55	3.57E-02	lncRNA	novel transcript
ENSG00000261136	3.39	3.57E-02	lncRNA	novel transcript, antisense to FSIP1
PCDH10	3.12	3.57E-02	protein_coding	protocadherin 10
CYP26B1	2.96	4.19E-02	protein_coding	cytochrome P450 family 26 subfamily B member 1
ENSG00000279382	2.75	8.91E-03	predicted	novel transcript
EMICERI	2.27	1.98E-03	lncRNA	EQTN MOB3B IFNK C9orf72 enhancer RNA I

Table 9 – DEGs when comparing irradiated Faraday box and mini-incubator samples.

Clustered heatmaps of the top 20 differentially expressed genes from each comparison revealed clear separation between experimental groups and highlighted sets of co-regulated genes (Figures 35-38). In the BP vs BN comparison, the heatmap demonstrated partial clustering of irradiated (BP) and control (BN) samples, with BP1 and BP2 clustering tightly and BP3 being an outlier (Figure 35). Several genes that were upregulated in the BP1/2

cluster were also upregulated in the MP3 sample, including *CARTPT*, *RSPO1* and *COL17A1*. In the MP vs MN comparison, a robust pattern was observed, with strong segregation of irradiated (MP) and control (MN) samples, and genes such as *IFI16*, *TMEM156*, and *FGF20* markedly downregulated in the MP group (Figure 36). The BN vs MN comparison showed more modest changes, consistent with the limited number of DEGs, while the overall sample structure reflected minor differences between these conditions (Figure 37). The BP vs MP heatmap reveals minimal clustering by sample environment, consistent with limited differential expression between irradiated groups (Figure 38). These results confirm that the primary axis of variation among samples is defined by irradiation status—particularly in the 5G phone min-incubator environment (MP vs MN)—and that the top differentially expressed genes are effective markers for distinguishing experimental groups.

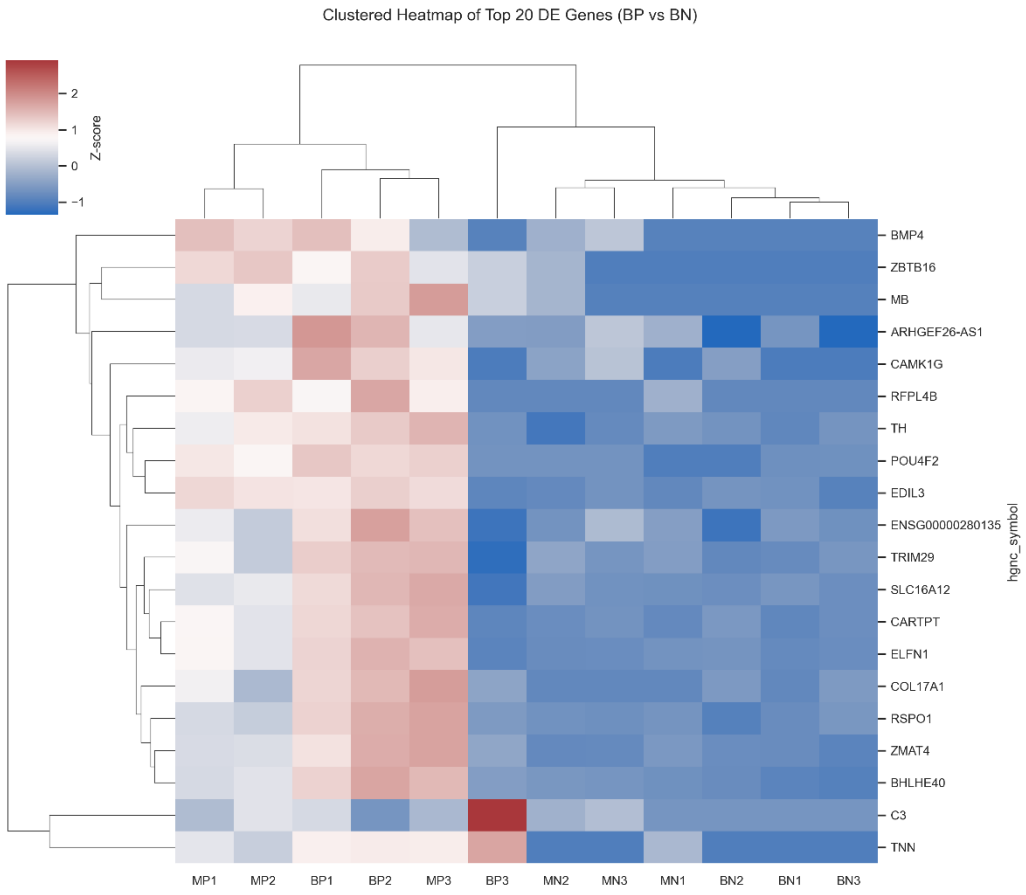

Figure 35 – Clustered heatmap of the top 20 differentially expressed genes for BP vs BN. The heatmap shows the z-scored VST expression levels of the top 20 most strongly regulated, statistically significant genes (FDR < 0.05), between BP and BN samples. Genes and samples were hierarchically clustered using Euclidean distance and average linkage. Red indicates high expression; blue indicates low expression relative to the mean for each gene.

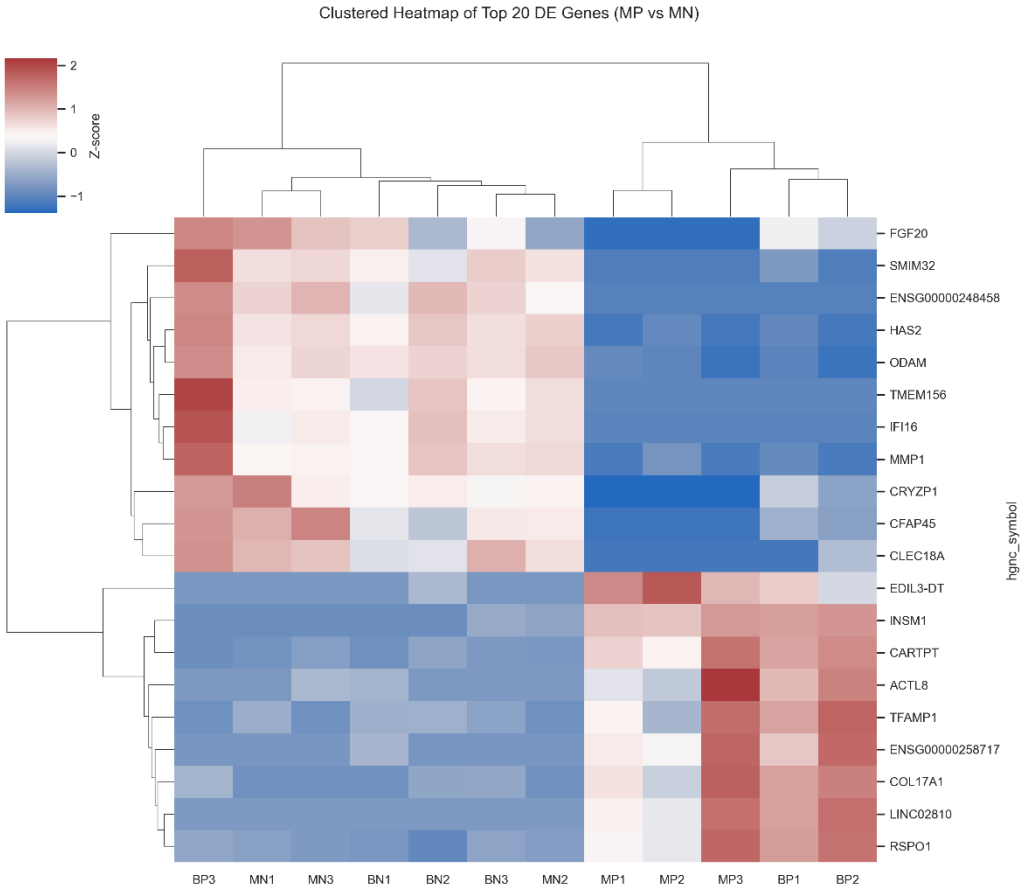

Figure 36 – Clustered heatmap of the top 20 differentially expressed genes for MP vs MN. The heatmap shows the z-scored VST expression levels of the top 20 most strongly regulated, statistically significant genes (FDR < 0.05), between MP and MN samples. Genes and samples were hierarchically clustered using Euclidean distance and average linkage. Red indicates high expression; blue indicates low expression relative to the mean for each gene.

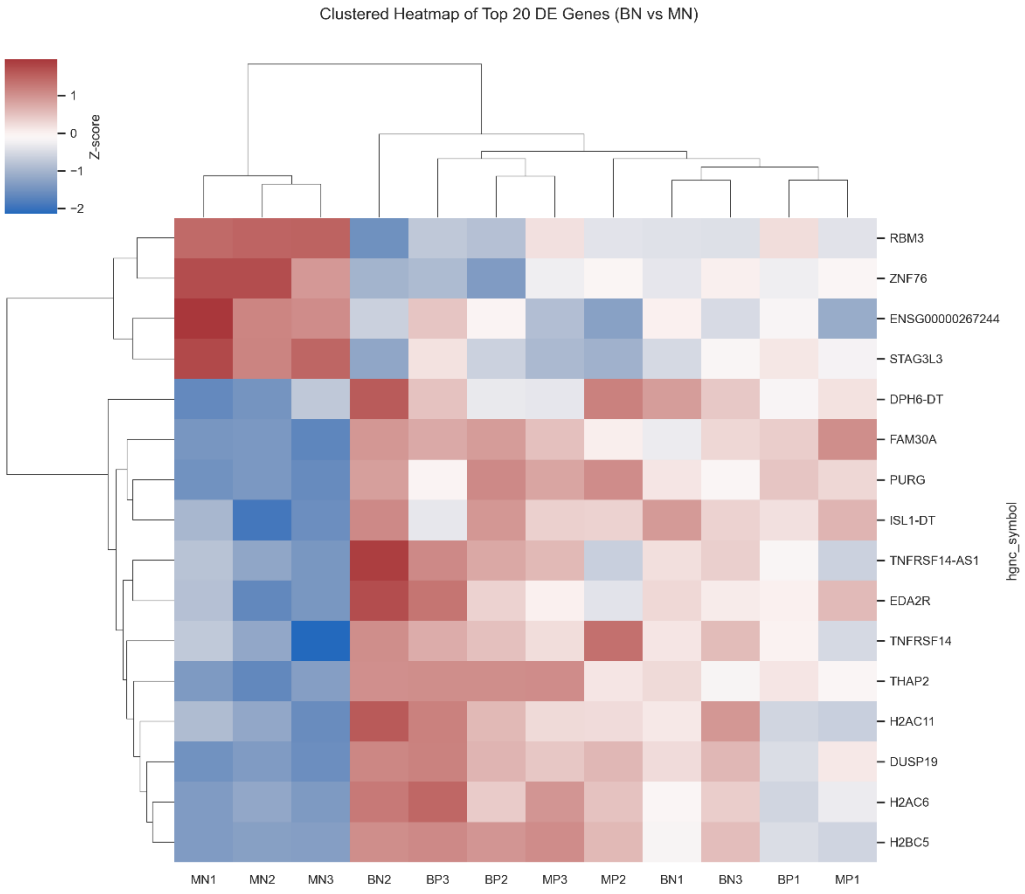

Figure 37 – Clustered heatmap of the top 20 differentially expressed genes for BN vs MN. The heatmap shows the z-scored VST expression levels of the top 20 most strongly regulated, statistically significant genes (FDR < 0.05), between BN and MN samples. Genes and samples were hierarchically clustered using Euclidean distance and average linkage. Red indicates high expression; blue indicates low expression relative to the mean for each gene.

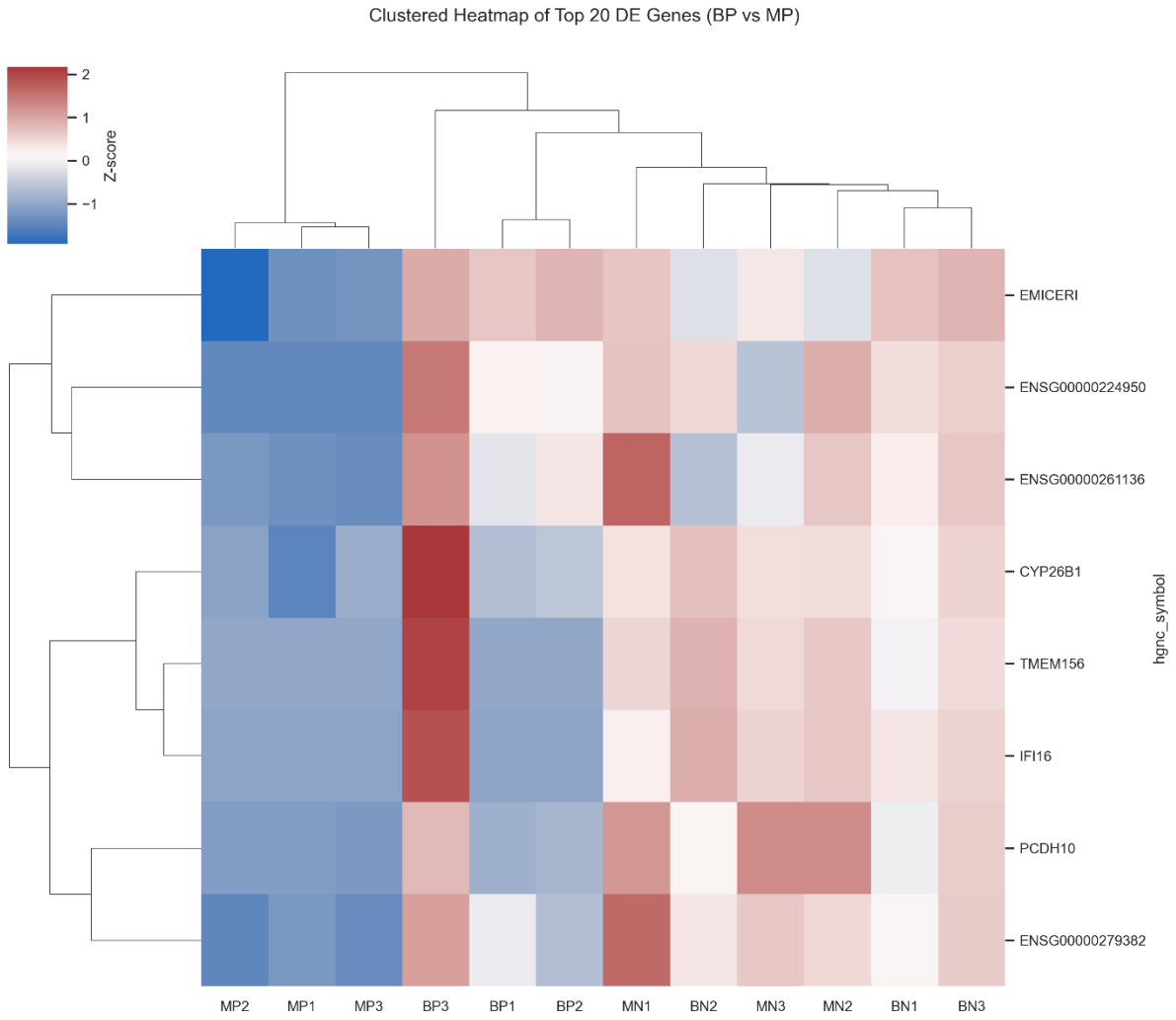

Figure 38 – Clustered heatmap of the top 20 differentially expressed genes for BP vs MP. The heatmap shows the z-scored VST expression levels of the top 20 most strongly regulated, statistically significant genes (FDR < 0.05), between BP and MP samples. Genes and samples were hierarchically clustered using Euclidean distance and average linkage. Red indicates high expression; blue indicates low expression relative to the mean for each gene.

5.3.4 – Gene Ontology (GO) Enrichment Analysis

Differential gene expression analysis revealed distinct biological responses to irradiation in both box-exposed and incubator-exposed SH-SY5Y cells. For BP vs BN (irradiated vs non-irradiated in the Faraday Box), differentially expressed genes were significantly enriched for developmental processes related to neuronal differentiation, including axon guidance, neuron projection guidance, axonogenesis, neuron projection extension, and developmental

cell growth (Figures 39a and 39b). These findings indicate that irradiation in the box environment primarily affected neural development and differentiation pathways. No significantly enriched KEGG pathways were identified for this comparison.

In contrast, MP vs MN (irradiated vs non-irradiated in the mini-incubator) showed a marked enrichment for processes such as cytoplasmic translation, heart development and contraction, oxidative phosphorylation, and kidney epithelium development (Figures 40a and 40b). The most significant term, cytoplasmic translation, suggests a robust activation of protein synthesis in response to irradiation under mini-incubator conditions.

KEGG pathway analysis for MP vs MN (Figure 40c) revealed significant enrichment for neurodegeneration-related and metabolic pathways, including Alzheimer's, Parkinson's, and Huntington's disease pathways, as well as oxidative phosphorylation, reflecting widespread transcriptional remodelling in response to mixed phone signal irradiation. GO and KEGG enrichment analysis for BN vs MN and BP vs MP was not performed due to insufficient numbers of differentially expressed genes for meaningful pathway analysis.

39a

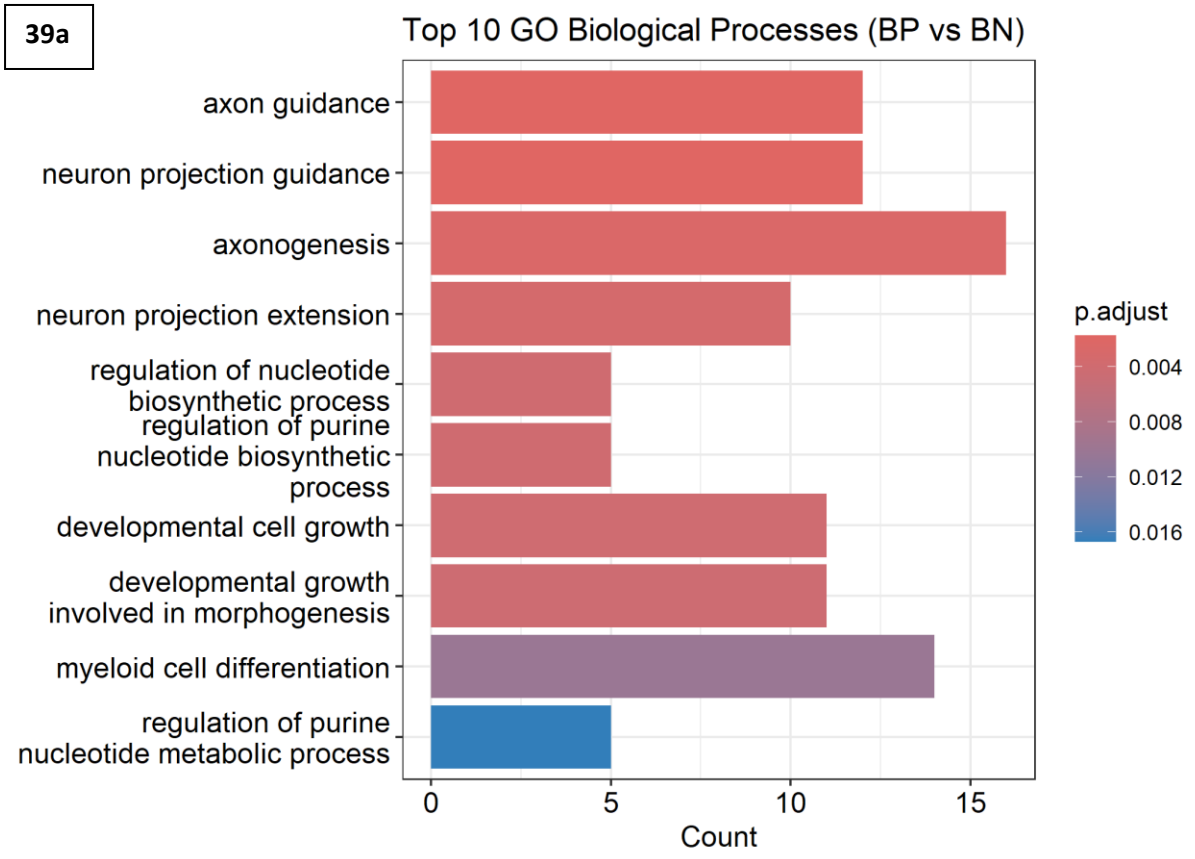

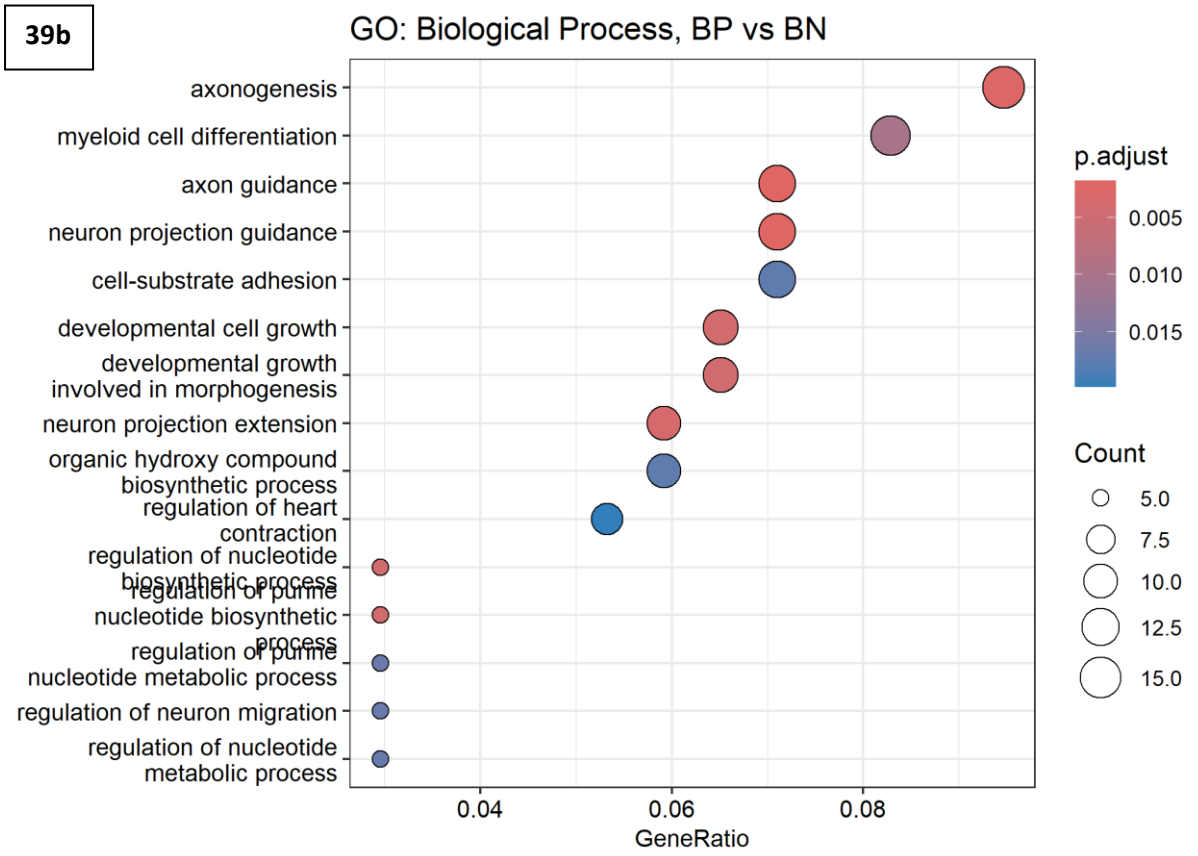

Figure 39 – GO Biological Process enrichment for DEGs in BP vs BN comparison. Horizontal bar plot (**39a**) and dot plot (**39b**) of the most significantly enriched GO Biological Process (BP) terms (padj < 0.05, $|\log_2 FC| > 1$). Bar length and dot size represent the number of DE genes annotated to each term; colour reflects adjusted p-value. The results highlight neuronal development and differentiation pathways. No KEGG pathways were significantly enriched for this comparison.

40a

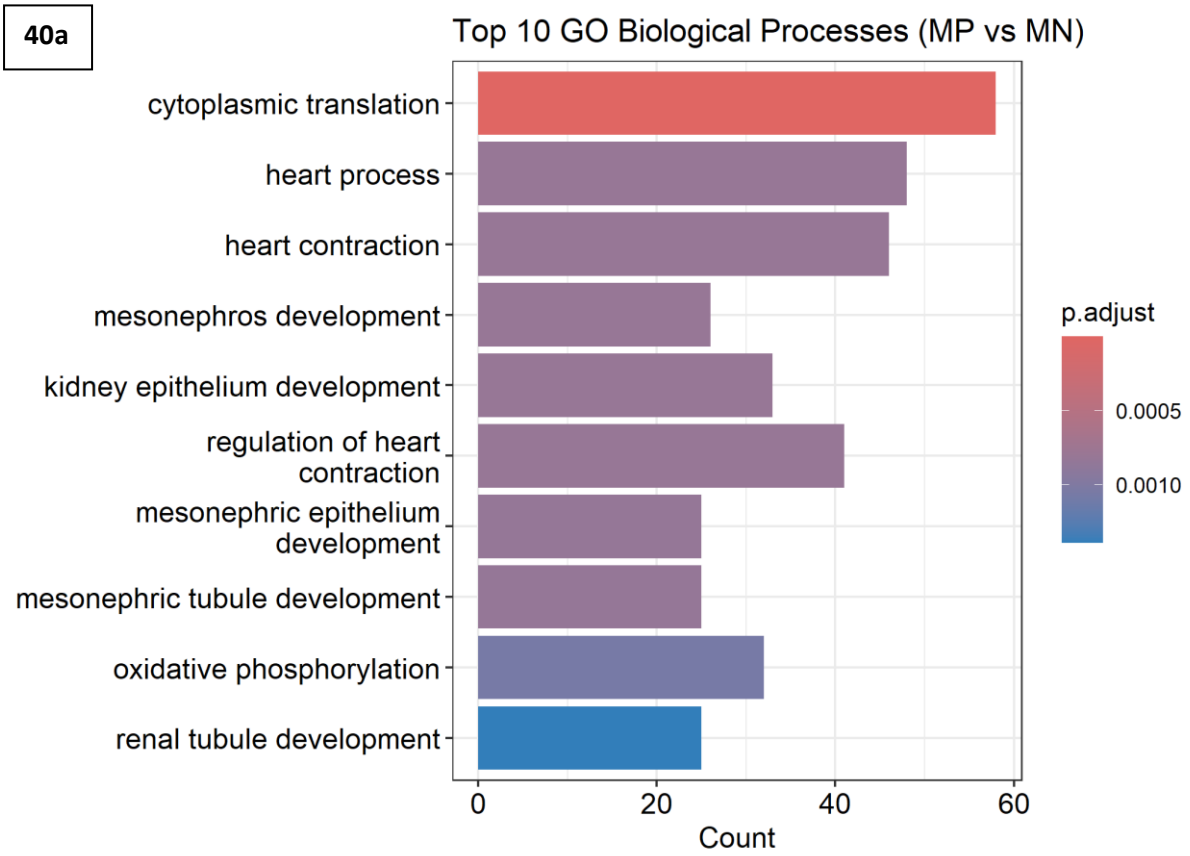
Top 10 GO Biological Processes (MP vs MN)
cytoplasmic translation
heart process
heart contraction
mesonephros development
kidney epithelium development
regulation of heart contraction
mesonephric epithelium development
mesonephric tubule development
oxidative phosphorylation
renal tubule development
0
20
40
60
Count
p.adjust
0.0005
0.0010

40b

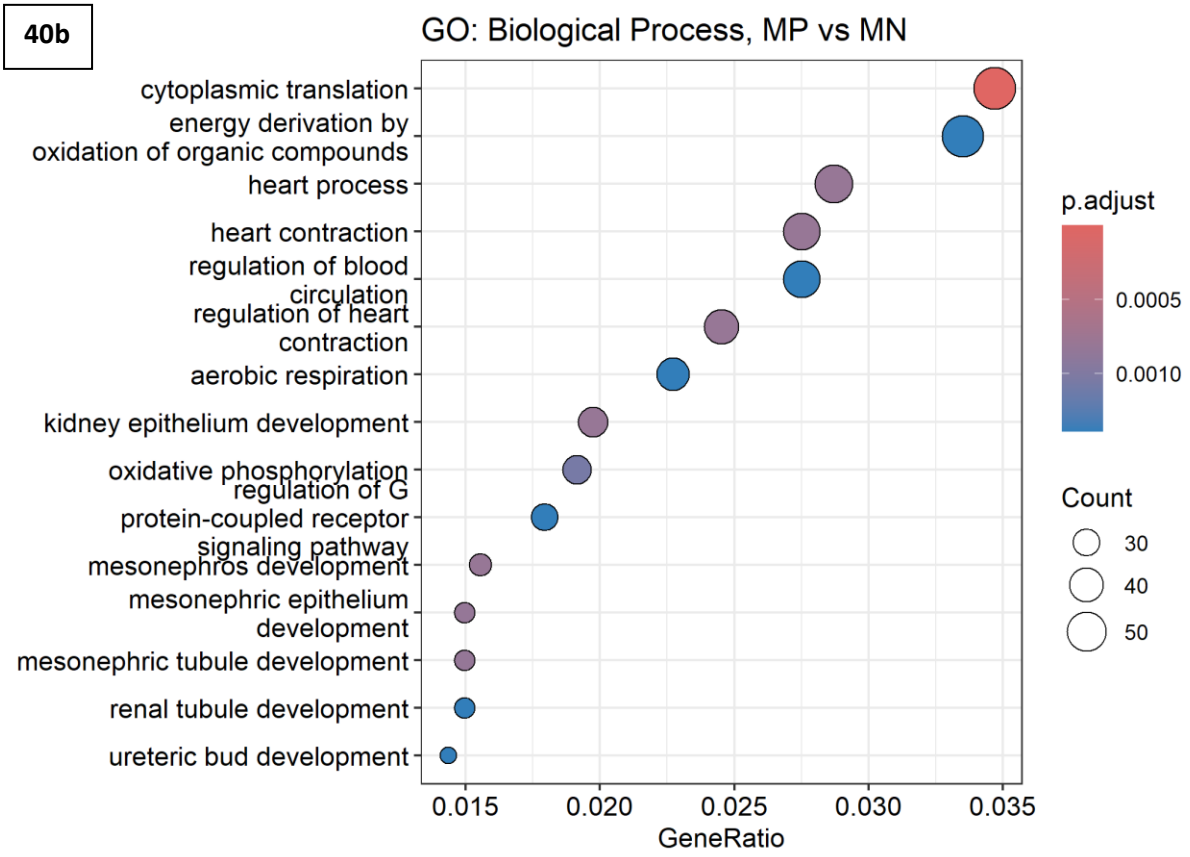
GO: Biological Process, MP vs MN
cytoplasmic translation
energy derivation by oxidation of organic compounds
heart process
heart contraction
regulation of blood circulation
regulation of heart contraction
aerobic respiration
kidney epithelium development
oxidative phosphorylation
regulation of G protein-coupled receptor signaling pathway
mesonephros development
mesonephric epithelium development
mesonephric tubule development
renal tubule development
ureteric bud development
0.015
0.020
0.025
0.030
0.035
GeneRatio
p.adjust
0.0005
0.0010
Count
30
40
50

40c

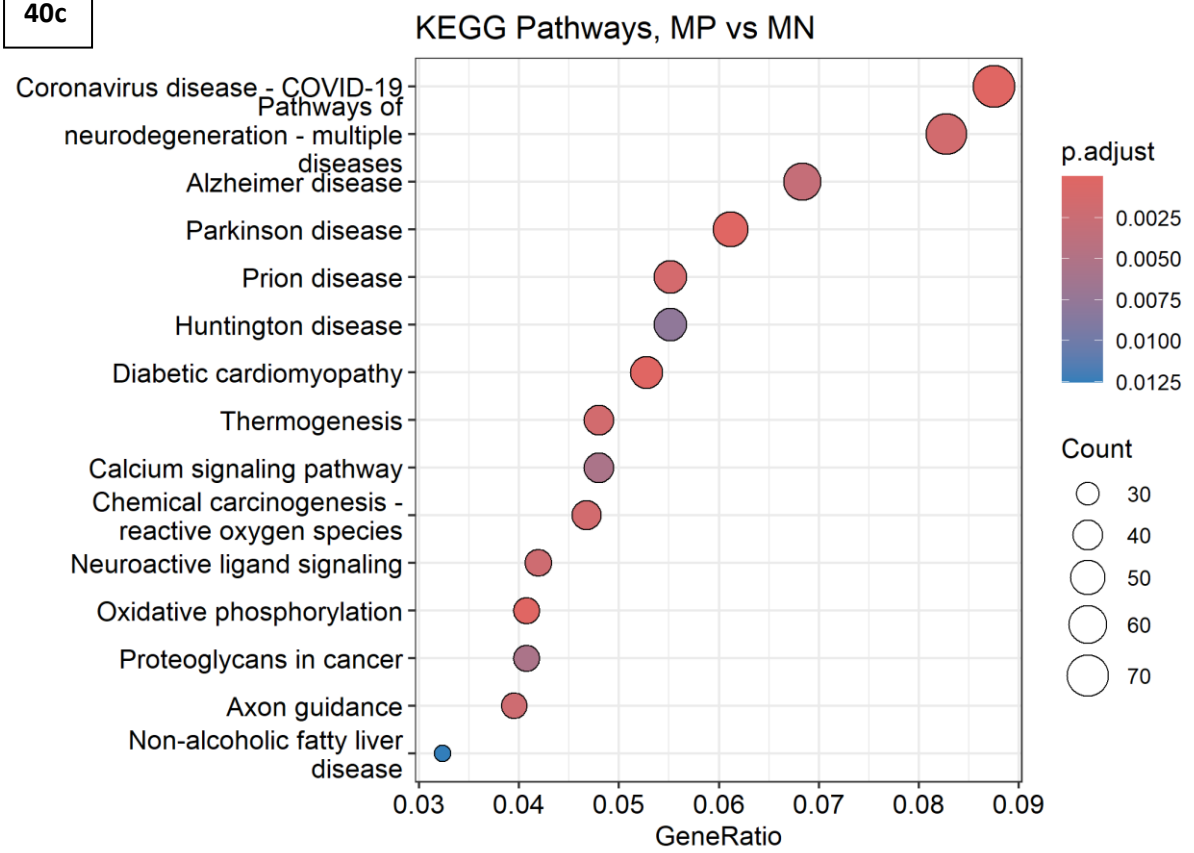

Figure 40 – GO and KEGG pathway enrichment for DEGs in MP vs MN comparison. Horizontal bar plot (**40a**) and dot plot (**40b**) of the top enriched GO Biological Process (BP) terms (padj < 0.05, $|\log_2 FC| > 1$). Dot plot of the top 15 enriched KEGG pathways (**40c**), with dot size reflecting gene count and colour indicating adjusted p-value. Neurodegeneration and metabolic pathways are among the most significantly enriched categories.

5.4 – Discussion

The RNA-seq dataset generated in this study provided a high-quality foundation for downstream transcriptional analyses. This was evidenced in the results of quality control testing, which showed that, after removal of duplicates, there was high GC content, low adapter residuals, good genome coverage and high consistency across samples (figures 27 and 28). Furthermore, Principal Component Analysis (PCA) using PC1 and PC2 accounted for a large proportion of variation among samples and showed a good clustering pattern of irradiated and non-irradiated groups – with the notable exceptions of outliers MP2 and BP3 (figure 29). This provided us a good degree of confidence in the ability of this dataset to inform us about the potential transcriptional impact of RF-EMR exposure in neuron-like SH-SY5Y cells.

The transcriptional responses documented here potentially shed light on how RF-EMFs are able to influence not only neuronal function, but, crucially, cellular stress responses. Interestingly, the intensity and nature of these biological effects appear to be strongly associated with the specific type of radiation used, highlighting the importance of signal parameters when considering the health risks posed by RF-EMFs. The relevance of these findings is indicated by the modulation of genes and pathways linked to neurodevelopment, stress signalling, inflammation, and neurodegenerative disease, outlining a mechanistic framework for understanding how RF-EMFs may affect neuronal cells.

One of the most noteworthy features within the dataset was the downregulation of stress response and innate immune signalling genes – which was observed in the subset of samples which had been exposed to mixed signals from the 5G phone. There was strong reduction in the expression of *IFI16*, a cytoplasmic DNA sensor and regulator of type I interferon signalling, suggesting a suppression of inflammatory pathways typically associated with viral defence or genotoxic stress (Unterholzner, Keating et al. 2010). The capacity of low frequency EMR to modulate immune system activity has been studied and considered for some time, particularly in the context of pulsed EMFs and wound healing (Walleczek 1991, Grant, Cadossi et al. 1994, Di Lazzaro, Capone et al. 2013, Fini, Pagani et al. 2013, Varani, Vincenzi et al. 2017). But this immune-modulatory effect is not restricted to pulsed EMFs, with some studies reporting similar effects on NK cells using microwaves instead (Nakamura, Seto et al. 1998). But it is important to note that this is an ongoing area of research in which signal context matters and a clear consensus has yet to be reached, with some conflicting evidence showing opposite, pro-inflammatory and stress promotion

effects (Simkó and Mattsson 2004, Tokalov and Gutzeit 2004, Blank and Goodman 2009, Kim, Yu et al. 2018, Rosado, Simkó et al. 2018).

The downregulation of *TMEM156* was also very pronounced in the phone signal irradiated group. It belongs to a large family of Transmembrane proteins (TMEMs) and its biological role is poorly characterised, similar to several other members of the TMEM family (Koteluk, Bielicka et al. 2021). It has been suspected to play a role in cancer metastasis, but interestingly, has also been queried in immunology contexts – being identified in extracellular vesicles within the milk of cows infected with a virus (Cheishvili, Stefanska et al. 2015, Rahman, Ishikawa et al. 2023). This further supports the idea that cells belonging to this experimental group could be exhibiting a suppressed immune activity phenotype, which raises questions about potential disease risk burden – particularly in the context of cancer, a disease cluster which is known to involve immune suppression (Whiteside 2006).

In the Faraday box samples irradiated with a 256-QAM signal (BP vs BN), where the transcriptional response was more moderate, the differentially expressed genes were enriched for axon guidance, neuron projection extension, and developmental cell growth. Genes such as *ZBTB7C* and *POU4F2*, which are key regulators of neuronal differentiation and synaptic function, were significantly altered, suggesting that even modest irradiation insults can influence neurodevelopmental programs (Kiefer, Tung et al. 2013, Wu, Kaczynski et al. 2015). This observation is consistent with literature linking RF-EMF exposure to altered neuronal morphology and synaptic plasticity during development (Odaci, Bas et al. 2008, Maskey, Pradhan et al. 2010). These transcriptional changes may therefore be particularly relevant during periods of heightened plasticity, such as foetal or early postnatal stages, which are known to be more susceptible to environmental insults (Applegate, Findlay et al. 2021, Gómez-Roig, Pascal et al. 2021).

The fact that these developmental pathways were differentially impacted depending on exposure type (256-QAM vs WiFi and cellular data) again highlights the crucial role of specific signal parameters in modulating EMF sensitivity. Variables such as frequency, power and modulation scheme all exert strong influence on how radiant energy interacts with and deposits energy into matter and living tissue (Protection 1998, Ishimaru 2017, Rappaport, Xing et al. 2017).

It is also worth highlighting the upregulation of *CARTPT* being consistent among both Faraday box and mini-incubator irradiation groups. It encodes something called Cocaine- and amphetamine-regulated transcript (CARTPT, alternatively CART), a postulated neurotransmitter that has neuro-regulatory and neuroprotective roles (Vicentic and Jones

2007, Zhang, Han et al. 2012). This further enhances the argument that, at least under the experimental conditions and time scales used here, among the biological effects of RF irradiation is a kind of neuroprotective response.

Perhaps the most striking biological finding was the enrichment of oxidative phosphorylation, cytoplasmic translation, and neurodegenerative disease pathways in the mini-incubator 5G phone irradiated samples (MP vs MN). These changes point to a widespread metabolic and functional remodelling in neuronal cells following EMF exposure.

The upregulation of oxidative phosphorylation genes could reflect a compensatory increase in mitochondrial activity in response to bioenergetic stress or increased ATP demand. Previous studies have demonstrated mitochondrial alterations, including swelling, membrane potential disruption, and ROS production in EMF-exposed neuronal models (Yao, Wu et al. 2008, Kim, Yu et al. 2018). Notably, the involvement of KEGG pathways linked to neurodegeneration suggests that the transcriptional response to EMF overlaps with that observed in disease states involving mitochondrial dysfunction, protein aggregation, and synaptic loss (Lin and Beal 2006). This finding is also supported by other work which has already suggested EMFs as a possible risk factor in neurodegenerative disease (Consales, Merla et al. 2012).

This raises critical concerns regarding the long-term neurological effects of chronic EMF exposure, particularly in vulnerable populations such as children or the elderly. While short-term in vitro models do not capture cumulative or systemic effects, it could be argued that the identification of disease-relevant pathways warrants further investigation in longitudinal in vivo models (Belyaev 2017).

This study also showed that the RF signal environment significantly influences the transcriptional response to EMF exposure. While irradiation induced some overlapping changes in both experimental setups, the response was more robust in the 5G phone mini-incubator setting, affecting a broader range of genes and pathways.

The exact cause of this discrepancy remains speculative but is likely attributable to electromagnetic waveform differences. Many of the same genes were differentially expressed in both irradiation groups and expression profiles were broadly similar in both control groups (figures 30c and 33). This suggests a difference in intensity of biological effect being associated with signal parameters, rather than a consequence of culture environment.

But it is possible other confounding factors relating to cell culture environment also contributed to variations observed. For example, the desktop incubator maintains its own internal temperature and uses a fan to control air flow and circulate warm air throughout the internal chamber, whereas the Faraday shield stands atop a hot plate which conducts heat up through the metal of the chamber and has no air flow through the interior space. Small differences in these factors, such as heating application, air flow and humidity, could prime cells for heightened sensitivity, possibly by altering basal stress signalling or mitochondrial priming. Similar context-dependent effects have been described in radiation biology, where co-exposure to thermal or oxidative stress enhances cellular responses to EMFs (Belyaev 2010).

These results highlight the importance of experimental standardisation and environmental awareness in EMF research – particularly with respect to detailing the radiation source. Apparent inconsistencies across studies may also stem in part from unaccounted environmental variables that influence cellular reactivity. But the specific parameters of EMR employed is likely to be the primary factor in determining the nature and extent of any biological effects observed.

Collectively, these findings provide meaningful evidence that EMFs, like those used in telecoms, can modulate gene expression in human neuronal cells. The transcriptional signatures involve stress responses, neurodevelopmental programs, metabolic shifts, and pathways implicated in neurodegenerative disease. These data support the hypothesis that even low-dose RF-EMF exposure can act as a biological modulator of neuronal function, particularly under specific exposure conditions.

While these effects are not necessarily pathogenic, they raise important questions about cumulative biological impact, particularly in the context of long-term or chronic exposure. Future studies should aim to dissect the mechanisms underpinning EMF sensitivity, validate these findings in primary or in vivo neuronal models, and explore the relevance of these transcriptional shifts for functional outcomes such as synaptic activity, neuroinflammation, and behaviour.

Chapter 6 – Discussion

The overall aim of this project was to investigate biological effects of RF-EMFs in a neuronal context. Our results show that the Faraday shield used here functions as an effective EMF experimental chamber and that radiation exposure in both experimental setups was able to induce several biological effects in neuron-like SH-SY5Y cells. We have also shown that the specific type of signal used is able to heavily influence the nature and intensity of these biological effects.

In several instances, RF irradiation was able to modulate cellular responses to some other, secondary drug treatment, such as Menadione or Oligomycin. For example, in all three radiation conditions tested (5G phone mixed signals, sine wave or 256-QAM waveform) the metabolic viability of cells was less severely impacted by Menadione insult if they had been previously irradiated. Conversely, in the Seahorse Mito Stress Test mitochondrial performance was more severely impacted by drug insult if cells had been irradiated beforehand. In both cases, these patterns of drug response modulation were highly consistent across samples and statistically significant in most instances. This drug response modulatory effect possibly reveals RF-EMF sensitivity that would otherwise go undetected directly by the assays themselves, showing how biological effects of these fields can be subtle and, to some extent, masked by cells that are able to function within normal ranges under standard assay conditions.

However, based on previous studies using somewhat similar experimental setups and radiation sources, such as the 3G/4G LTE phone used by Choi et al, a stronger, more direct effect was anticipated in most cases (Choi, Min et al. 2020). For example, our exact cell line (SH-SY5Y), albeit undifferentiated, was reported to have proliferated significantly less in the presence of phone signal radiation. This trend prompted us to expect reduced metabolic viability of irradiated samples relative to non-irradiated controls – which only happened in one out of three radiation types, the 256-QAM waveform in the Faraday box and, crucially, did not appear in the 5G phone results. Although, there are some differences between the experimental conditions used here and those used in other papers (such as signal type, neuron-like differentiation, cell culture media etc), which may account for these discrepancies, it nonetheless produced results contrary to our initial theories.

This was part of a broader pattern of results wherein some RF signal types produced biological effects, whilst others produced either reduced effects or none at all. There were many such examples of these signal-specific effects throughout our project, these include;

- In the CTB assay, only the 256-QAM signal appeared to directly lower metabolic viability
- In the GSH assay, the 5G phone signals appeared to have minimal effect while QAM signal suppressed GSH activity early (4hr) and appeared to result in increased activity at a later time point (18hr)
- In the SOD1 assay, 5G phone signals appeared to have a stronger impact on enzymatic activity
- In the flow cytometry MitoSOX assay, 5G phone signals appeared to provoke a stronger increase in superoxide formation when compared to 256-QAM irradiation

The most obvious example of this signal-specific sensitivity came in the RNAseq analysis. Mixed 5G phone signals produced a markedly more pronounced response than the 256-QAM waveform in this dataset – with many more differentially expressed genes, some of which were highly statistically significant (e.g. downregulation of *IFI16* and *TMEM156*). In this manner, the most biologically active RF signal type changed between different assays – sometimes the 256-QAM waveform being the most potent, sometimes the mixed signals from the 5G phone proving more provocative. This was a surprising finding and speaks to how critically important signal parameters can be in these types of studies – where relatively small changes in frequency or modulation pattern may result in a large shift in observed results. It serves to highlight the need for absolute clarity when defining signal parameters of applied EMFs and points to the potential value of standardisation within these types of investigations into RF-EMF safety. This is a point which has been persistently raised as a primary concern among regulatory bodies, such as the ICNIRP, and is part of the reasoning and justification for study selection and weighting when considering scientific merit of articles and how relevant they are to safety standards (Protection 1998, ICNIRP 2020). The observation that different signal types still tended to produce the same type of response, but at a different intensity (e.g. increased SOD1 activity or superoxide formation), supports the idea that these biological effects are a genuine consequence of RF-EMR exposure – which might otherwise be in doubt if such similar signals as those tested here were provoking different or opposite effects. This was further evidenced in the RNAseq analysis, which showed little overall variation in expression profiles when comparing BP vs MP and BN vs MN groups – with several of the same DEGs appearing in both BP and MP groups (e.g. *CARTPT* upregulation).

When trying to account for these discrepancies in the intensity of biological effect based on signal applied, it is worth considering the fundamental differences that exist between the

output of the signal generator and the 5G phone. When a signal is generated by the signal generator inside the Faraday shield, it is emitted constantly, without interruption at the exact parameters specified by the researcher for the entirety of the exposure period. This is not the case with the 5G phone, which generates a much more fluid and dynamic exposure profile. Signals being sent and received by the phone, even with constant video streaming, are highly intermittent – rapidly pinging on and off as data packets are sporadically exchanged between the phone and the nearest router and/or cell tower. Because both cellular data and WiFi were switched on, while streaming the phone would dynamically switch between cellular data and WiFi – each with their own set of frequency bands, over which the data stream may shift between freely at any given time. For example, the most common cellular data frequency band used was the 840 MHz band, which produced a sharp, narrow peak centred on this frequency. But at other times activity was detected over the 3.1 GHz and 3.4 GHz bands. Similarly, the most commonly detected WiFi band utilised was a broad, flat peak centred on 5.1 GHz. But WiFi activity was also recorded taking place at 5.3 and 5.5 GHz. There are many other frequency bands besides these (both cellular data and WiFi), which may have been used to an unknown extent during EMF exposures (e.g. the older 2.5 GHz WiFi band). The use of these different frequency bands and technologies was determined entirely by the device and was inaccessible to the researcher – a deliberate choice to better emulate real-world conditions in which people typically have both enabled, freely making use of both. But the natural consequence of this is that there was a degree of randomness to the radiation being emitted and received by the 5G phone inside the incubator. This manifested in fluctuations in frequency and other signal parameters (broad, flat peaks vs narrow peaks etc) and sporadic dosing of samples – which could go some way to explaining the apparent fluctuations in the intensity of the effect associated with mobile phone radiation exposure. It could simply be that some frequency bands and signal types are more potent than others, with the phone arbitrarily switching between them – resulting in, effectively, a stronger overall dose in some assays when compared to others. These signal differences could also explain discrepancies in results when comparing Faraday box irradiation to those obtained using the 5G phone.

Another important aspect of this project was timing of biological effects. The vast majority of experiments took place following an 18-hour exposure – in which cells had been given time to mount compensatory responses to RF irradiation. A period of 18 hours was thought to be sufficient for cells to complete an expression profile shift in response to radiation stimuli, entering into a new steady-state profile, as can been seen in other contexts such as hypoxia environments on comparable time scales (Lal, Peters et al. 2001). But it is widely-known that cellular responses to environmental stimuli and consequent expression profile changes can

have both an early, rapid response followed by a slower, steady-state shift (Chechik and Koller 2009). Unfortunately, only in the GSH assay were we able to explore this chronological aspect by using a significantly earlier time point (4 hours) – which indeed revealed a temporally shifting response pattern in the Faraday box setup, where GSH activity was lowered early but appeared to have increased by the 18-hour time point. Time and financial restraints greatly restricted our ability to probe a wider range of early phase cell responses, which may have yielded additional insight into rapid responses (e.g. <2-hour time points). The nature and intensity of early phase responses can differ greatly to those of later responses, as seen here in the GSH assay and as seen in other contexts and articles (Zeisel, Köstler et al. 2011). Longer irradiation periods were favoured because it was felt that this was likely to ensure detectible adaptive steady-state changes could be captured, whereas shorter duration irradiation may or may not have given cells sufficient time to produce detectible changes. Still, it leaves room for further discovery in future work to explore rapid responses and potentially contrast them with those manifesting at later time points, as seen with GSH activity. In terms of understanding GSH activity being reduced early but elevated later, this is consistent with the theory that RF-EMFs do promote oxidative stress – but also that cells strive to adapt to this pressure and initiate pathways to ultimately improve ROS clearance rates and restore redox homeostasis. There is a substantial amount of evidence indicating that similar types of RF signals can place increased ROS burden on cells, which would explain why GSH activity was lowered early here (Yao, Wu et al. 2008, Luukkonen, Hakulinen et al. 2009, Kang, Lee et al. 2014, Choi, Min et al. 2020). It could also explain why both GSH activity and SOD1 activity was higher at the 18-hour time point – because if cells are to mount compensatory changes in response to some external stimuli, the stimuli must first be sufficiently intense to disturb cellular homeostasis, as seen at the 4-hour time point. Adaptive responses like these, leading to the acquisition of resistance against the initial insult, are documented elsewhere in several contexts, including ionizing radiation and methylating agents (Teo, Sedgwick et al. 1984, Park, Lee et al. 2000, Diehn, Cho et al. 2009, Rycaj and Tang 2014, Barker, Paget et al. 2015, Li, Zhou et al. 2016, Liu, Zheng et al. 2021, Wu, Song et al. 2023). This line of thinking was further supported by the observation of increased superoxide formation in both experimental setups from the 8-hour time point onwards, in accordance with background literature linking RF-EMFs to oxidative stress – which would explain why cells would need to increase efforts to increase ROS clearance and SOD1/GSH activity. The final piece of evidence supporting this idea of oxidative stress compensatory mechanism engagement was seen in the RNAseq analysis of samples irradiated using the 5G phone – in which pathways associated with oxidative phosphorylation and neurodegeneration were modulated. ROS signalling is known to be closely involved with mitochondrial activity and energy metabolism and the co-modulation of

neurodegenerative pathways further suggests bioenergetic disturbance – which is a classic hallmark of neurodegenerative disorders (Duchen 1999, Lin and Beal 2006, Newsholme, Haber et al. 2007, Consales, Merla et al. 2012, Mailloux, McBride et al. 2013, Holmström and Finkel 2014, Di Meo, Reed et al. 2016, Wang, Branicky et al. 2018). That is to say, cells irradiated with 5G phone signals appeared to have engaged pathways relating to energy metabolism likely in an attempt to restore redox homeostasis and, importantly, the activation of these pathways is indicative of ROS burden which, over time, predisposes the human brain to degenerative disease.

This chronological aspect also relates to another interesting facet of our findings presented here – the apparent neuro-protective effect of some RF radiation exposure. Whether in terms of dealing with Menadione insult as seen in the CTB assay, increased ability to deal with ROS as seen in elevated GSH and SOD1 activity at the 18-hour time point or the upregulation of neuroprotective genes such as *CARTPT* – it was clear that radiation can, paradoxically, improve cellular resilience in some contexts. At least, this is the case for the relatively short time scales studied here. This phenomenon of adapting to stressor stimuli leading to improvement of function could be considered an example of the hormesis effect occurring here in the context of RF irradiation.

But the hormesis effect is typically thought of as a response to transient stressor stimuli, which raises serious concerns given the chronic nature of RF-EMR exposure for most people (Mattson 2008, Ericsson 2025). Engagement of homeostatic mechanisms to improve cell and tissue health outcomes often comes at a cost in terms of resources or chemical energy to mediate phosphorylation events underpinning signalling cascades – that is to say, while activation of signalling pathways associated with these protective effects may be beneficial in the short-term, these pathways are at risk of exhaustion, error accumulation or aberrant signalling if chronically stimulated. This is seen in other contexts, where chronic engagement of homeostatic mechanisms often correlates with disease burden (Boucher, Kleinridders et al. 2014). A classic, well-characterised example of this is the insulin signalling system, particularly in the context of obesity. Chronic overstimulation of insulin signalling is associated with increased activation of Serine and Threonine kinases which leads to inhibitory phosphorylation of the insulin receptor and Insulin Receptor Substrate (IRS) proteins – ultimately leading to a phosphorylation state that results in reduced insulin sensitivity in relevant tissues (Dunaif, Xia et al. 1995, Aguirre, Uchida et al. 2000, Shao, Catalano et al. 2000, Li, Soos et al. 2004, Boucher, Kleinridders et al. 2014). Indeed, even insulin itself can promote insulin resistance when elevated in the bloodstream (hyperinsulinemia), via hyperactivation of inhibitory regulators such as PHLPP1 and Grb14

(Boucher, Kleinridders et al. 2014). Another example can be seen in energy metabolism and neurodegeneration, where disruption of bioenergetic homeostasis is strongly correlated with disease outcomes and considered a possible causative factor (Beal, Hyman et al. 1993, Dupuis, Oudart et al. 2004, Mochel, Durant et al. 2012).

These concerns regarding consequences associated with chronic exposure were further cemented upon discovery of modulation of pathways associated with neurodegeneration in the phone-irradiated subset of RNAseq results. This reinforces the idea that short-term benefit might, paradoxically, foretell long-term neurological harm. But it is important to note that EMFs can have beneficial effects, seen here and elsewhere, and that these positive effects do not necessarily go hand-in-hand with disease predisposition in all instances. A good example of this is seen in UV radiation; which on one hand can damage DNA and promote cancer, but also plays an important role in the natural synthesis of vitamin D and endorphins in the skin, ultimately causing both positive and negative effects in the context of human health (McKenzie, Liley et al. 2009). It has also been shown that specific types of low frequency EMFs may improve joint health and aid wound and bone fracture healing, a practice that is now incorporated as an adjuvant therapy in orthopaedic medicine (Darendeliler, Darendeliler et al. 1997, Boopalan, Chittaranjan et al. 2009, Cadossi, Massari et al. 2020). While it may be true that some of the apparent neuroprotective effects documented here could occur independently of other, negative biological effects, the overall impact of exposure to these EMFs is likely to result in a net negative impact on neuronal health – particularly in light of chronic exposure, as opposed to short exposures. This would be in accordance with the abundance of evidence linking RF-EMFs to oxidative stress promotion in cells and other articles linking oxidative stress burden with various major disease clusters (Spector 2000, Kang 2002, Oktem, Ozguner et al. 2005, Lin and Beal 2006, Akdag, Bilgin et al. 2007, Zeni, Di Pietro et al. 2007, Yao, Wu et al. 2008, Luukkonen, Hakulinen et al. 2009, Circu and Aw 2010, Kryston, Georgiev et al. 2011, Ziech, Franco et al. 2011, Brieger, Schiavone et al. 2012, Consales, Merla et al. 2012, Kang, Lee et al. 2014, Usselman, Hill et al. 2014, Yakymenko, Tsybulin et al. 2016, Choi, Min et al. 2020, Panagopoulos, Karabarbounis et al. 2021).

It was suspected that manipulation of mitochondrial membrane potential might play a role in the mechanism underlying biological effects of EMFs observed here and elsewhere. Evidence already exists linking man-made EMFs to disturbances in membrane permeability and Calcium signalling via voltage-gated ion channels (Adey 1993, Pall 2013). Given that electrochemical gradients across the mitochondrial membrane and voltage-gated ion channels play a pivotal role in oxidative phosphorylation, the TMRM assay was designed to

probe this aspect of bioenergetics in the presence of RF-EMFs. In accordance with our initial theory, RF-EMF exposure appeared to destabilise maintenance of mitochondrial membrane potential in all but the earliest time point (4 hours). This result corroborates previous work investigating membrane potential maintenance in the presence of EMFs and could contribute to mechanistic understanding and explanation of some of the other results presented here. If these fields are able to disrupt the mitochondrial membrane potential and thereby interfere with the Electron Transport Chain (ETC) and mitochondrial function, it could explain, at least in part, the increase in superoxide formation and consequent disturbances to redox homeostasis in the form of modulated SOD1 and GSH activity. The mitochondria is widely established as a critically important site in redox homeostasis and is one of the major sources of superoxide generation in cells – particularly through reactions taking place at the protein complexes embedded in the mitochondrial membrane as part of the ETC, which relies on the mitochondrial membrane potential to function properly (Lambert and Brand 2009, Murphy 2009). At a basic level, it makes a fundamental kind of sense that these fields could interact with voltage-gated channels. They are sensitive to changes in voltage or electrical fields by their very nature – and oscillations in the electric field is a component of all electromagnetic waves. As is common when considering the interactions of EMFs and biology, it can become a question of intensity – whether or not the specific waveform in question carries sufficient energy for its oscillations to provoke an effect on these electrically-sensitive receptors. Our data suggests that, under the conditions tested here, the signal generated inside the Faraday shield can, with an emission power of just 3 dBm, which is equivalent to 4.016E-05 W/kg SAR.

The implications of findings presented here is that these fields can have biological effects on neuron-like cells. This influence is manifested primarily in redox homeostasis, energy metabolism and mitochondrial function. But perhaps more importantly, these effects occur at emission power levels far below the energy threshold required to reasonably expect heating effects to occur, i.e. they are sub thermal effects. This is especially relevant because regulatory bodies that produce safety recommendations and essentially control safe exposure limits in most developed nations place heavy emphasis on keeping power levels below tissue heating thresholds (Protection 1998, ICNIRP 2020). It is believed, to a large degree, that if the telecoms industry keeps within these low-power limits, that people are safe and there is little or no consequence to living within these fields. But it is becoming increasingly clear that this may not necessarily be the truth. Why were the signals used here able to change responses to drug insults? To provoke genetic expression shifts? Or alter antioxidant activity? If they are biologically safe, they should not be able to do this. Furthermore, the telecoms industry is continuously seeking to develop new technology and

techniques to improve networks – focusing on performance metrics that require higher base station density, use more frequency bands and increase overall EMF exposure (Wang, You et al. 2023).

But it is important retain a clear, measured view when considering the impact of any research output and to acknowledge the limitations of any given study. There are several such limitations that must be acknowledged here, too. Arguably, the most relevant to this project is the element of time. Due to the strict deadlines associated with pursuing a PhD and the need to generate sufficient data to compile an original thesis, many of the experiments carried out here were performed over relatively short timeframes – ranging from 4 hours to 72 hours at most. This means that the scope of this investigation is restricted to short-term biological responses to EMFs and that effects associated with chronic exposure to EMFs cannot be captured here. An obvious question arising from the biological effects reported here is; what are the long-term consequences of exposure to these fields? If cells are activating pathways in response to EMF exposure in an attempt to deal with the biological effects they cause, what happens if these pathways are stimulated for longer periods of time?

In a similar vein, time constraints did not permit us to explore what effect, if any, different frequencies and other signal parameters might have upon biological effects of EMFs. The upper frequency limit of our equipment (4.9 GHz) was used, in order to have the highest photon energy available to us. It was not possible to explore the 20 to 70 GHz frequency bands that will come into use with 5G technology. The signal generator we used was also not able to emulate full OFDM schemes, which is widely used in modern telecoms industries. Because of this it was not possible to fully explore demodulation effects which may be associated with OFDM or other, more complex modulation schemes.

Another important consideration when weighing the impact of this project relates to the cell model used. SH-SY5Y cells are a thrice sub-cloned neuroblastoma cell line and therefore have characteristics common to cell lines; unstable genomes, aberrant signalling and the ability to proliferate indefinitely (Korecka, van Kesteren et al. 2013, Kovalevich and Langford 2013, Xicoy, Wieringa et al. 2017, de Medeiros, De Bastiani et al. 2019). This makes them very convenient as an investigative tool, but means there is a level of abstraction between our experimental observations and clinical relevance. As always when using a human cancer derived cell line, it must be stressed that there are major differences between healthy cells of the body and cancer cells. It is unknown how these differences may be informing biological

responses to EMF exposure reported here. Somatic cells may exhibit distinct EMF sensitivity, similar EMF sensitivity or none at all.

Finally, another limitation of our project relates to the cell culture environment within each experimental setup. In both cases, an unusual media type was used to deal with the fact that experiments were taking place outside the typical CO_2 enriched incubator microenvironment. While CO_2 independent media did a good job of regulating pH levels without the need for carbonic acid formation, it may have placed unintended stress on cells – potentially priming them to exhibit different or more intense responses to EMF exposure. Humidity within our experimental setups may also differ from that of typical cell culture incubators, particularly in the case of the Faraday box, which is almost airtight. Most standard incubators allow some level of gas exchange with the outside environment and can regulate humidity using sensors. Water baths were included in both experimental setups, but this did not necessarily closely replicate humidity conditions within a normal incubator and humidity was not quantified or analysed here. Small discrepancies in this parameter may also have modulated cell responses to EMFs unintentionally.

In terms of future recommendations, it is highly advised that longitudinal work be carried out to investigate potential long-term biological effects associated with EMF exposure that were not explored here. It seems plausible that chronic activation of homeostatic mechanisms, as is suggested happening here, will have deleterious effects on cells and could promote disease. Parallels to this may be seen in other contexts, like chronic insulin or pro-inflammatory signalling and consequent disease predisposition (Furman, Campisi et al. 2019). A failure to return to some basal, resting cellular state for a prolonged period of time is strongly correlated with numerous disease outcomes. This is particularly worrying when applied to EMF contexts because of the abundant and chronic exposure to telecoms signals for most human populations on earth – where there is little or no respite from these signals and whatever biological effects they may be causing.

A second suggestion for future work would be to expand investigative models to include either primary cells, induced pluripotent stem cells (IPSCs) or even whole organisms, such as *Drosophila* flies. Use of primary cells or IPSCs would yield results that are better able to reflect the biology of healthy human tissue – arguably making the findings more directly translatable to human health (Robinton and Daley 2012, Katzenell, Cabrera et al. 2017, Goshi, Morgan et al. 2020, Ghiasvand, Amirfazli et al. 2024). Whereas use of *Drosophila* would incorporate the complexity of a whole organism into research efforts, allowing for the presentation of potential disease states correlated with EMF exposure (Lu and Vogel 2009,

Yamaguchi and Yoshida 2018). As a model organism, they have the advantage of being relatively easy to care for and work with, combined with a fast generational turnover rate. This could allow for the growth of many generations of flies within these fields, potentially capturing any cumulative DNA effects, which have been suggested in literature, and revealing downstream functional consequences to chronic homeostatic disturbances (Yao, Wu et al. 2008, Yao, Wu et al. 2008, Luukkonen, Hakulinen et al. 2009, Panagopoulos, Karabarbounis et al. 2021).

It may also be fruitful to direct future research efforts towards exploration of alternative signal parameters than those used here. This could involve testing different frequencies, modulation schemes or power levels to find specific effects and energy thresholds for causation of biological effects. Of particular interest are the higher frequency bands proposed for 5G, ranging from 20 to 70 GHz, which are unlike any previous generation. 1G through to 4G all operated using frequencies below 6 GHz, meaning this will be the first time in history >20 GHz bands are widely deployed in urban environments (Parkvall, Dahlman et al. 2018, Simkó and Mattsson 2019). These new frequencies will possess higher photon energies than previous generations and deposit much more of their energy into the surface layer of skin (Protection 1998, Parkvall, Dahlman et al. 2018, ICNIRP 2020). Because of the newness of 5G technology, research into the safety of these new high frequency bands is minimal when compared to older technologies and lower (<6 GHz) frequency bands (Protection 1998, Repacholi 1998, Ahlbom and Feychting 2003, Zamanian and Hardiman 2005, Bortkiewicz 2019, Simkó and Mattsson 2019, ICNIRP 2020). This creates a pressing need to properly analyse the capacity of these new types of signals to interact with and influence cellular biology, preferably before the world is saturated in them.

In conclusion, through this project we have demonstrated the capacity of radiofrequency electromagnetic radiation to produce biological effects in neuron-like cells. The low emission power used means it is practically impossible to attribute those effects to heating. Whilst the intensity of these effects is thankfully relatively moderate, they raise serious concerns about the chronic exposure of people to similar signals used in wireless technologies such as WiFi and mobile phones. We should therefore like to add our voice to others calling for further investigation into the safety of telecoms technologies. This is particularly important for recent advances being deployed to improve network performance, whose signals may have distinct and unintended biological effects yet to be discovered.

List of references

Abid, F. A., et al. (2023). 5G and 6G WiFi transceiver comparison in multi modulation schemes performance with MATLAB Simulink. 2023 Third International Conference on Advances in Electrical, Computing, Communication and Sustainable Technologies (ICAECT), IEEE.

Adams, J. A., et al. (2014). "Effect of mobile telephones on sperm quality: a systematic review and meta-analysis." Environment international **70**: 106-112.

Adams, M. D., et al. (1991). "Complementary DNA sequencing: expressed sequence tags and human genome project." Science **252**(5013): 1651-1656.

Adey, W. R. (1993). "Biological effects of electromagnetic fields." Journal of cellular biochemistry **51**(4): 410-416.

Afolabi, O. O. and M. Sohail (2017). "Microwaving human faecal sludge as a viable sanitation technology option for treatment and value recovery–A critical review." Journal of Environmental Management **187**: 401-415.

Agarwal, A., et al. (2009). "Effects of radiofrequency electromagnetic waves (RF-EMW) from cellular phones on human ejaculated semen: an in vitro pilot study." Fertility and sterility **92**(4): 1318-1325.

Aguirre, V., et al. (2000). "The c-Jun NH2-terminal kinase promotes insulin resistance during association with insulin receptor substrate-1 and phosphorylation of Ser307." Journal of Biological Chemistry **275**(12): 9047-9054.

Ahlbom, A. and M. Feychting (2003). "Electromagnetic radiation: environmental pollution and health." British medical bulletin **68**(1): 157-165.

Ahlbom, A., et al. (2009). "Epidemiologic evidence on mobile phones and tumor risk: a review." Epidemiology **20**(5): 639-652.

Ainsworth, M., et al. (2012). "Rates and rhythms: a synergistic view of frequency and temporal coding in neuronal networks." Neuron **75**(4): 572-583.

Akdag, M. Z., et al. (2007). "Alteration of nitric oxide production in rats exposed to a prolonged, extremely low-frequency magnetic field." Electromagnetic biology and medicine **26**(2): 99-106.

Alex, S. P. and L. M. Jalloul (2008). "Performance evaluation of MIMO in IEEE802. 16e/WiMAX." IEEE Journal of Selected Topics in Signal Processing **2**(2): 181-190.

Andersen, M. L. and L. M. Winter (2017). "Animal models in biological and biomedical research-experimental and ethical concerns." Anais da Academia Brasileira de Ciências **91**(suppl 1): e20170238.

Applegate, K. E., et al. (2021). "Radiation exposures in pregnancy, health effects and risks to the embryo/foetus—information to inform the medical management of the pregnant patient." Journal of Radiological Protection **41**(4): S522.

Arendash, G. W., et al. (2012). "Electromagnetic treatment to old Alzheimer's mice reverses β-amyloid deposition, modifies cerebral blood flow, and provides selected cognitive benefit." PloS one **7**(4): e35751.

Arendash, G. W., et al. (2010). "Electromagnetic field treatment protects against and reverses cognitive impairment in Alzheimer's disease mice." Journal of Alzheimer's disease **19**(1): 191-210.

Armstrong, J. (2009). "OFDM for optical communications." Journal of lightwave technology **27**(3): 189-204.

Armstrong, J., et al. (2002). "Role of glutathione depletion and reactive oxygen species generation in apoptotic signaling in a human B lymphoma cell line." Cell Death & Differentiation **9**(3): 252-263.

Artaud, A. (1905). "1. Quantum Phenomena." Ann. Phys **17**: 132.

Ashraf, R. and S. Kumar (2022). "Mfn2-mediated mitochondrial fusion promotes autophagy and suppresses ovarian cancer progression by reducing ROS through AMPK/mTOR/ERK signaling." Cellular and Molecular Life Sciences **79**(11): 573.

Attwell, D. and S. B. Laughlin (2001). "An energy budget for signaling in the grey matter of the brain." Journal of Cerebral Blood Flow & Metabolism **21**(10): 1133-1145.

Auchère, F. and F. Rusnak (2002). "What is the ultimate fate of superoxide anion in vivo?" JBIC Journal of Biological Inorganic Chemistry **7**(6): 664-667.

Averill-Bates, D. A. (2023). The antioxidant glutathione. Vitamins and hormones, Elsevier. **121:** 109-141.

Aydin, D., et al. (2011). "Mobile phone use and brain tumors in children and adolescents: a multicenter case–control study." Journal of the National Cancer Institute **103**(16): 1264-1276.

Bae, Y. S., et al. (1997). "Epidermal growth factor (EGF)-induced generation of hydrogen peroxide: role in EGF receptor-mediated tyrosine phosphorylation." Journal of Biological Chemistry **272**(1): 217-221.

Balanis, C. A. (2016). Antenna theory: analysis and design, John wiley & sons.

Banelli, P., et al. (2014). "Modulation formats and waveforms for 5G networks: Who will be the heir of OFDM?: An overview of alternative modulation schemes for improved spectral efficiency." IEEE Signal Processing Magazine **31**(6): 80-93.

Banker, G. A. and W. M. Cowan (1977). "Rat hippocampal neurons in dispersed cell culture." Brain research **126**(3): 397-425.

An in vitro system has been developed for the study of isolated hippocampal neurons from 18- or 19-day rat featuses. Following trypsinization the cells are plated out at low density on polylysine-treated coverslips in an enriched medium. The isolated neurons rapidly attach to the substrate and initiate process extension. Little reaggregation occurs and the number of non-neuronal cells present is minimal. Unless co-cultured with tissue explants the neurons survive for only a few days; in the presence of hippocampal explants the initial growth of the isolated cells is improved and their survival in culture is extended to about two weeks. Some of the cells in such cultures develop a characteristic branching pattern closely resembling that of maturing hippocampal pyramidal cells in vivo. There is a clear relationship between the stage of the cells' development and their growth in culture. Cells which had completed DNA synthesis about 48 h before dissociation, and which were in the process of migration to the cortical plate, survived best in our cultures. Early post-mitotic cells which were still within the ventricular zone and cells which had already reached the cortical plate grew poorly. This system should permit the study not only of process formation by these cells, but also of their capacity to form specific synapses in vitro and of the biochemical constituents of their surfaces.

Banu, M. S., et al. (2013). UWB microwave detection of breast cancer using SAR. 2013 International Conference on Energy Efficient Technologies for Sustainability, IEEE.

Barash, S., et al. (1999). "Saccadic dysmetria and adaptation after lesions of the cerebellar cortex." Journal of Neuroscience **19**(24): 10931-10939.

Barbulovic-Nad, I., et al. (2006). "Bio-microarray fabrication techniques—a review." Critical reviews in biotechnology **26**(4): 237-259.

Barker, H. E., et al. (2015). "The tumour microenvironment after radiotherapy: mechanisms of resistance and recurrence." Nature Reviews Cancer **15**(7): 409-425.

Barnela, M. and D. S. Kumar (2014). "Digital modulation schemes employed in wireless communication: A literature review." International Journal of Wired and Wireless Communications **2**(2): 15-21.

Barnett, M. W. and P. M. Larkman (2007). "The action potential." Practical neurology **7**(3): 192-197.

Barron, C. I. and A. A. Baraff (1958). "Medical considerations of exposure to microwaves (radar)." Journal of the American Medical Association **168**(9): 1194-1199.

Barzilai, A. and K.-I. Yamamoto (2004). "DNA damage responses to oxidative stress." DNA repair **3**(8-9): 1109-1115.

Bauréus Koch, C., et al. (2003). "Interaction between weak low frequency magnetic fields and cell membranes." Bioelectromagnetics: Journal of the Bioelectromagnetics Society, The Society for Physical Regulation in Biology and Medicine, The European Bioelectromagnetics Association **24**(6): 395-402.

Beal, M. F., et al. (1993). "Do defecs in mitochondrial energy metabolism underlie the pathology of neurodegenerative diseases?" Trends in neurosciences **16**(4): 125-131.

Beall, C., et al. (1996). "Brain tumors among electronics industry workers." Epidemiology: 125-130.

Belyaev, I. (2010). "Dependence of non-thermal biological effects of microwaves on physical and biological variables: implications for reproducibility and safety standards." Non-thermal effects and mechanisms of interaction between electromagnetic fields and living matter. Bologna (IT): Ramazzini institute: 187-218.

Belyaev, I. (2017). Duration of exposure and dose in assessing nonthermal biological effects of microwaves. Dosimetry in Bioelectromagnetics, CRC Press**:** 171-184.

Belyaev, I. Y., et al. (1994). "Cooperative response of Escherichia coli cells to the resonance effect of millimeter waves at super low intensity." Electro-and Magnetobiology **13**(1): 53-66.

Bertagna, F., et al. (2021). "Effects of electromagnetic fields on neuronal ion channels: a systematic review." Annals of the New York Academy of Sciences **1499**(1): 82-103.

Bezzi, P. and A. Volterra (2001). "A neuron–glia signalling network in the active brain." Current opinion in neurobiology **11**(3): 387-394.

Biedler, J. L., et al. (1973). "Morphology and growth, tumorigenicity, and cytogenetics of human neuroblastoma cells in continuous culture." Cancer research **33**(11): 2643-2652.

Biedler, J. L., et al. (1978). "Multiple neurotransmitter synthesis by human neuroblastoma cell lines and clones." Cancer research **38**(11_Part_1): 3751-3757.

Blackman, C. (2009). "Cell phone radiation: evidence from ELF and RF studies supporting more inclusive risk identification and assessment." Pathophysiology **16**(2-3): 205-216.

Blanchet, L., et al. (2011). "Isolated mitochondrial complex I deficiency: explorative data analysis of patient cell parameters." Current pharmaceutical design **17**(36): 4023-4033.

Blank, M. and R. Goodman (2009). "Electromagnetic fields stress living cells." Pathophysiology **16**(2-3): 71-78.

Bolcskei, H. (2006). "MIMO-OFDM wireless systems: basics, perspectives, and challenges." IEEE wireless communications **13**(4): 31-37.

Boopalan, P., et al. (2009). "Pulsed electromagnetic field (PEMF) treatment for fracture healing." Current Orthopaedic Practice **20**(4): 423-428.

Bortkiewicz, A. (2019). "Health effects of radiofrequency electromagnetic fields (RF EMF)." Industrial health **57**(4): 403-405.

Bota, M. and L. W. Swanson (2007). "The neuron classification problem." Brain research reviews **56**(1): 79-88.

Boucher, J., et al. (2014). "Insulin receptor signaling in normal and insulin-resistant states." Cold Spring Harbor perspectives in biology **6**(1): a009191.

Braeuer, A. (2015). Interaction of matter and electromagnetic radiation. Supercritical Fluid Science and Technology, Elsevier. **7:** 41-192.

Brewer, G. J. (1997). "Isolation and culture of adult rat hippocampal neurons." Journal of neuroscience methods **71**(2): 143-155.

Brewer, G. J. and J. R. Torricelli (2007). "Isolation and culture of adult neurons and neurospheres." Nature protocols **2**(6): 1490-1498.

Brieger, K., et al. (2012). "Reactive oxygen species: from health to disease." Swiss medical weekly **142**(3334): w13659-w13659.

Bulman, A. (1994). "Electromagnetic Fields (300 Hz to 300 GHz) Environmental Health Criteria, No: 137." Occupational and Environmental Medicine **51**(10): 720.

Cadossi, R., et al. (2020). "Pulsed electromagnetic field stimulation of bone healing and joint preservation: cellular mechanisms of skeletal response." JAAOS Global Research & Reviews **4**(5): e19.

Cai, Y., et al. (2017). "Modulation and multiple access for 5G networks." IEEE Communications Surveys & Tutorials **20**(1): 629-646.

Camoes, F., et al. (2009). "Organelle dynamics and dysfunction: a closer link between peroxisomes and mitochondria." Journal of inherited metabolic disease **32**(2): 163-180.

Cancer, I. A. f. R. o. (2011). "IARC classifies radiofrequency electromagnetic fields as possibly carcinogenic to humans." Press release **208**.

Cardoso, A. R., et al. (2012). "Mitochondrial compartmentalization of redox processes." Free Radical Biology and Medicine **52**(11-12): 2201-2208.

Carrì, M. T., et al. (1997). "Expression of a Cu, Zn superoxide dismutase typical of familial amyotrophic lateral sclerosis induces mitochondrial alteration and increase of cytosolic Ca2+ concentration in transfected neuroblastoma SH-SY5Y cells." FEBS letters **414**(2): 365-368.

Challis, L. (2005). "Mechanisms for interaction between RF fields and biological tissue." Bioelectromagnetics **26**(S7): S98-S106.

Chan, D. C. (2012). "Fusion and fission: interlinked processes critical for mitochondrial health." Annual review of genetics **46**(1): 265-287.

Chan, D. C. (2020). "Mitochondrial dynamics and its involvement in disease." Annual review of pathology: mechanisms of disease **15**(1): 235-259.

Chang, X., et al. (2023). "ROS-Drp1-mediated mitochondria fission contributes to hippocampal HT22 cell apoptosis induced by silver nanoparticles." Redox biology **63**: 102739.

Chapman, S. J., et al. (2015). "Mathematics of the Faraday cage." Siam Review **57**(3): 398-417.

Chaturvedi, R. K. and M. F. Beal (2013). "Mitochondrial diseases of the brain." Free Radical Biology and Medicine **63**: 1-29.

Chaudhury, P., et al. (1999). "The 3GPP proposal for IMT-2000." IEEE communications magazine **37**(12): 72-81.

Chechik, G. and D. Koller (2009). "Timing of gene expression responses to environmental changes." Journal of Computational Biology **16**(2): 279-290.

Cheishvili, D., et al. (2015). "A common promoter hypomethylation signature in invasive breast, liver and prostate cancer cell lines reveals novel targets involved in cancer invasiveness." Oncotarget **6**(32): 33253.

Chen, C.-C., et al. (1998). "A sensory neuron-specific, proton-gated ion channel." Proceedings of the National Academy of Sciences **95**(17): 10240-10245.

Chen, C., et al. (2022). "Overview and performance evaluation of Wi-Fi 7." IEEE Communications Standards Magazine **6**(2): 12-18.

Chen, H., et al. (2005). "Disruption of fusion results in mitochondrial heterogeneity and dysfunction." Journal of Biological Chemistry **280**(28): 26185-26192.

Chesselet, M.-F. and S. T. Carmichael (2012). "Animal models of neurological disorders." Neurotherapeutics **9**(2): 241-244.

Chiaraviglio, L., et al. (2021). "Massive measurements of 5G exposure in a town: Methodology and results." IEEE Open Journal of the Communications Society **2**: 2029-2048.

Chicco, D., et al. (2025). "A simple guide to the use of Student's t-test, Mann-Whitney U test, Chi-squared test, and Kruskal-Wallis test in biostatistics." BioData mining **18**(1): 56.

Choi, J., et al. (2020). "Continuous exposure to 1.7 GHz LTE electromagnetic fields increases intracellular reactive oxygen species to decrease human cell proliferation and induce senescence." Scientific reports **10**(1): 9238.

Choi, S., et al. (2023). Efficient hardware implementation of soft demapper for WiFi7 4096-QAM. 2023 IEEE 98th Vehicular Technology Conference (VTC2023-Fall), IEEE.

Circu, M. L. and T. Y. Aw (2010). "Reactive oxygen species, cellular redox systems, and apoptosis." Free Radical Biology and Medicine **48**(6): 749-762.

Cohen, B. H., et al. (1977). "Parental factors in Down's syndrome-results of the second Baltimore case-control study." Population cytogenetics-studies in humans. Academic Press, New York: 301-352.

Committee, I. L. M. S. (2009). "IEEE Standard for Information technology-Telecommunication and information exchange between systems-Local and metropolitan area networks-Specific requirements Part11: Wireless LAN Medium Access Control (MAC) and Physical Layer (PHY) Specifications Amendment1: Radio Resource Measurement of Wireless LANs." http://standards. ieee. org/getieee802/download/802.11 n-2009. pdf.

Consales, C., et al. (2012). "Electromagnetic fields, oxidative stress, and neurodegeneration." International journal of cell biology **2012**(1): 683897.

Costa, V., et al. (2013). "RNA-Seq and human complex diseases: recent accomplishments and future perspectives." European Journal of Human Genetics **21**(2): 134-142.

Council, N. R., et al. (1997). Possible health effects of exposure to residential electric and magnetic fields, National Academies Press.

D'Andrea, J. A., et al. (1986). "Intermittent exposure of rats to 2450 MHz microwaves at 2.5 mW cm2: Behavioral and physiological effects." Bioelectromagnetics: Journal of the Bioelectromagnetics Society, The Society for Physical Regulation in Biology and Medicine, The European Bioelectromagnetics Association **7**(3): 315-328.

D'Andrea, J., et al. (1979). "Physiological and Behavioral Effects of Chronic Exposure te 2450-MHz Microwaves." Journal of microwave power **14**(4): 351-362.

Daels, J. (1973). "Microwave heating of the uterine wall during parturition." Obstetrics & Gynecology **42**(1): 76-79.

Darendeliler, M. A., et al. (1997). "Effects of static magnetic and pulsed electromagnetic fields on bone healing." The International journal of adult orthodontics and orthognathic surgery **12**(1): 43-53.

de Lorge, J. O. (1984). "Operant behavior and colonic temperature of Macaca mulatta exposed to radio frequency fields at and above resonant frequencies." Bioelectromagnetics: Journal of the Bioelectromagnetics Society, The Society for Physical Regulation in Biology and Medicine, The European Bioelectromagnetics Association **5**(2): 233-246.

de Lorge, J. O. and C. S. Ezell (1980). "Observing-responses of rats exposed to 1.28-and 5.62-GHz microwaves." Bioelectromagnetics: Journal of the Bioelectromagnetics Society, The Society for Physical Regulation in Biology and Medicine, The European Bioelectromagnetics Association **1**(2): 183-198.

de Medeiros, L. M., et al. (2019). "Cholinergic differentiation of human neuroblastoma SH-SY5Y cell line and its potential use as an in vitro model for Alzheimer's disease studies." Molecular neurobiology **56**(11): 7355-7367.

de Vries, H. E., et al. (2008). "Nrf2-induced antioxidant protection: a promising target to counteract ROS-mediated damage in neurodegenerative disease?" Free Radical Biology and Medicine **45**(10): 1375-1383.

De Winter, J. C. (2013). "Using the Student's" t"-Test with Extremely Small Sample Sizes." Practical assessment, research & evaluation **18**(10): n10.

DeFelipe, J. and E. G. Jones (1992). "Santiago Ramón y Cajal and methods in neurohistology." Trends in neurosciences **15**(7): 237-246.

Deng, C., et al. (2020). "IEEE 802.11 be Wi-Fi 7: New challenges and opportunities." IEEE Communications Surveys & Tutorials **22**(4): 2136-2166.

Desikan, R., et al. (2001). "Regulation of the Arabidopsis transcriptome by oxidative stress." Plant physiology **127**(1): 159-172.

Di Lazzaro, V., et al. (2013). "A consensus panel review of central nervous system effects of the exposure to low-intensity extremely low-frequency magnetic fields." Brain stimulation **6**(4): 469-476.

Di Meo, S., et al. (2016). "Role of ROS and RNS sources in physiological and pathological conditions." Oxidative medicine and cellular longevity **2016**(1): 1245049.

Diehn, M., et al. (2009). "Association of reactive oxygen species levels and radioresistance in cancer stem cells." Nature **458**(7239): 780-783.

Distelmaier, F., et al. (2012). "Trolox-sensitive reactive oxygen species regulate mitochondrial morphology, oxidative phosphorylation and cytosolic calcium handling in healthy cells." Antioxidants & redox signaling **17**(12): 1657-1669.

Dolińska, I., et al. (2017). Interference comparison in wi-fi 2.4 ghz and 5 ghz bands. 2017 International Conference on Information and Digital Technologies (IDT), IEEE.

Duchen, M. R. (1999). "Contributions of mitochondria to animal physiology: from homeostatic sensor to calcium signalling and cell death." The Journal of physiology **516**(1): 1-17.

Dunaif, A., et al. (1995). "Excessive insulin receptor serine phosphorylation in cultured fibroblasts and in skeletal muscle. A potential mechanism for insulin resistance in the polycystic ovary syndrome." The Journal of clinical investigation **96**(2): 801-810.

Dupuis, L., et al. (2004). "Evidence for defective energy homeostasis in amyotrophic lateral sclerosis: benefit of a high-energy diet in a transgenic mouse model." Proceedings of the National Academy of Sciences **101**(30): 11159-11164.

Durney, C. H., et al. (1986). Radiofrequency radiation dosimetry handbook, The Division.

Eccles, J. C. (1973). The understanding of the brain, McGraw-Hill.

Ekspong, G. (1999). "The dual nature of light, as reflected in the Nobel Archive." Proceedings of the American Philosophical Society **143**(1): 42-49.

Encinas, M., et al. (2000). "Sequential treatment of SH-SY5Y cells with retinoic acid and brain-derived neurotrophic factor gives rise to fully differentiated, neurotrophic factor-dependent, human neuron-like cells." Journal of neurochemistry **75**(3): 991-1003.

Engel, A. K., et al. (1992). "Temporal coding in the visual cortex: new vistas on integration in the nervous system." Trends in neurosciences **15**(6): 218-226.

Ericsson, T. L. (2021). Ericsson mobility report november 2021. Ericsson Mobility Report, Ericsson.

Ericsson, T. L. (2024). "Ericsson Mobility Report November 2024."

Ericsson, T. L. (2025). Ericsson mobility report June 2025. https://www.ericsson.com/49e9b6/assets/local/reports-papers/mobility-report/documents/2025/ericsson-mobility-report-june-2025.pdf.

Falcioni, L., et al. (2018). "Report of final results regarding brain and heart tumors in Sprague-Dawley rats exposed from prenatal life until natural death to mobile phone radiofrequency field representative of a 1.8 GHz GSM base station environmental emission." Environmental research **165**: 496-503.

Farley, T. (2005). "Mobile telephone history." Privateline. com, http://www. privateline. com/wp-content/uploads/2016/01/TelenorPage_022-034. pdf.

Faruque, S. (2017). Radio frequency modulation made easy, Springer.

Ferreri, F., et al. (2006). "Mobile phone emissions and human brain excitability." Annals of Neurology: Official Journal of the American Neurological Association and the Child Neurology Society **60**(2): 188-196.

Feynman, R. P., et al. (1965). "The feynman lectures on physics; vol. i." American Journal of Physics **33**(9): 750-752.

Fini, M., et al. (2013). "Functional tissue engineering in articular cartilage repair: is there a role for electromagnetic biophysical stimulation?" Tissue Engineering Part B: Reviews **19**(4): 353-367.

Fleming, I., et al. (2001). "Endothelium-derived hyperpolarizing factor synthase (Cytochrome P450 2C9) is a functionally significant source of reactive oxygen species in coronary arteries." Circulation research **88**(1): 44-51.

Forman, H. J. and H. Zhang (2021). "Targeting oxidative stress in disease: promise and limitations of antioxidant therapy." Nature Reviews Drug Discovery **20**(9): 689-709.

Foster, K. R. and M. H. Repacholi (2004). "Biological effects of radiofrequency fields: does modulation matter?" Radiation research **162**(2): 219-225.

Franco, R. and J. Cidlowski (2009). "Apoptosis and glutathione: beyond an antioxidant." Cell Death & Differentiation **16**(10): 1303-1314.

Frezza, C., et al. (2006). "OPA1 controls apoptotic cristae remodeling independently from mitochondrial fusion." Cell **126**(1): 177-189.

Friesen, C., et al. (2004). "A critical role of glutathione in determining apoptosis sensitivity and resistance in leukemia cells." Cell Death & Differentiation **11**(1): S73-S85.

Furman, D., et al. (2019). "Chronic inflammation in the etiology of disease across the life span." Nature medicine **25**(12): 1822-1832.

Gabriel, C., et al. (1996). "The dielectric properties of biological tissues: I. Literature survey." Physics in medicine & biology **41**(11): 2231.

Garcia-Roger, D., et al. (2020). "V2X support in 3GPP specifications: From 4G to 5G and beyond." IEEE Access **8**: 190946-190963.

Garratt, G. R. M. (1994). The early history of radio: from Faraday to Marconi, Iet.

Gawas, A. U. (2015). "An overview on evolution of mobile wireless communication networks: 1G-6G." International journal on recent and innovation trends in computing and communication **3**(5): 3130-3133.

Gerstner, W., et al. (1996). "A neuronal learning rule for sub-millisecond temporal coding." Nature **383**(6595): 76-78.

Gerstner, W., et al. (1997). "Neural codes: firing rates and beyond." Proceedings of the National Academy of Sciences **94**(24): 12740-12741.

Ghafourifar, P. and E. Cadenas (2005). "Mitochondrial nitric oxide synthase." Trends in pharmacological sciences **26**(4): 190-195.

Ghiasvand, K., et al. (2024). "The role of neuron-like cell lines and primary neuron cell models in unraveling the complexity of neurodegenerative diseases: A comprehensive review." Molecular biology reports **51**(1): 1024.

Gibney, E. and C. Nolan (2010). "Epigenetics and gene expression." Heredity **105**(1): 4-13.

Gilbert, P. and W. Thach (1977). "Purkinje cell activity during motor learning." Brain research **128**(2): 309-328.

Gillet, J.-P., et al. (2013). "The clinical relevance of cancer cell lines." Journal of the National Cancer Institute **105**(7): 452-458.

Gómez-Roig, M. D., et al. (2021). "Environmental exposure during pregnancy: influence on prenatal development and early life: a comprehensive review." Fetal diagnosis and therapy **48**(4): 245-257.

Gordon, J. and S. Amini (2021). General Overview of Neuronal Cell Culture. Neuronal Cell Culture: Methods and Protocols. S. Amini and M. K. White. New York, NY, Springer US**:** 1-8.

> In this introductory chapter, we provide a general overview of neuronal cell culture. This is a rapidly evolving area of research and we provide an outline and contextual framework for the different chapters of this book. These chapters have all been contributed by scientists actively working in the field who are currently using state-of-the-art techniques to advance our understanding of the molecular and cellular biology of the central nervous system. Each chapter provides detailed descriptions and experimental protocols for a variety of techniques ranging in scope from basic neuronal cell line culturing to advanced and specialized methods.

Goshi, N., et al. (2020). "A primary neural cell culture model to study neuron, astrocyte, and microglia interactions in neuroinflammation." Journal of Neuroinflammation **17**(1): 155.

Goshi, N., et al. (2022). "Correction to: A primary neural cell culture model to study neuron, astrocyte, and microglia interactions in neuroinflammation." Journal of Neuroinflammation **19**(1): 49.

Grace, A. A. and B. S. Bunney (1984). "The control of firing pattern in nigral dopamine neurons: burst firing." Journal of Neuroscience **4**(11): 2877-2890.

Grant, G., et al. (1994). "Protection against focal cerebral ischemia following exposure to a pulsed electromagnetic field." Bioelectromagnetics: Journal of the Bioelectromagnetics Society, The Society for Physical Regulation in Biology and Medicine, The European Bioelectromagnetics Association **15**(3): 205-216.

Grayson, J. K. (1996). "Radiation exposure, socioeconomic status, and brain tumor risk in the US Air Force: a nested case-control study." American Journal of Epidemiology **143**(5): 480-486.

Greenland, S., et al. (2004). "The value of risk-factor ("black-box") epidemiology." Epidemiology **15**(5): 529-535.

Greiling, R. O. and H. Obermeyer (2010). "Natural electromagnetic radiation (EMR) and its application in structural geology and neotectonics." Journal of the Geological Society of India **75**: 278-288.

Grider, M. H., et al. (2019). "Physiology, action potential."

Group, I. S. (2010). "Brain tumour risk in relation to mobile telephone use: results of the INTERPHONE international case–control study." International journal of epidemiology **39**(3): 675-694.

Group, I. S. (2011). "Acoustic neuroma risk in relation to mobile telephone use: results of the INTERPHONE international case–control study." Cancer epidemiology **35**(5): 453-464.

Grover, W. H., et al. (2011). "Measuring single-cell density." Proceedings of the National Academy of Sciences **108**(27): 10992-10996.

Gummadi, R., et al. (2007). "Understanding and mitigating the impact of RF interference on 802.11 networks." ACM SIGCOMM Computer Communication Review **37**(4): 385-396.

Guo, R., et al. (2018). "Structure and mechanism of mitochondrial electron transport chain." Biomedical journal **41**(1): 9-20.

Hamid, R., et al. (2004). "Comparison of alamar blue and MTT assays for high through-put screening." Toxicology in vitro **18**(5): 703-710.

Hampsey, M. (1998). "Molecular genetics of the RNA polymerase II general transcriptional machinery." Microbiology and Molecular Biology Reviews **62**(2): 465-503.

Hampton, M. B., et al. (1998). "Redox regulation of the caspases during apoptosis a." Annals of the New York Academy of Sciences **854**(1): 328-335.

Hanzo, L., et al. (2004). "Quadrature amplitude modulation: From basics to adaptive trellis-coded, turbo-equalised and space-time coded OFDM, CDMA and MC-CDMA systems."

Hardell, L., et al. (2002). "Cellular and cordless telephones and the risk for brain tumours." European Journal of Cancer Prevention **11**(4): 377-386.

Hardell, L., et al. (2006). "Tumour risk associated with use of cellular telephones or cordless desktop telephones." World Journal of Surgical Oncology **4**(1): 74.

Hardell, L., et al. (2021). "Aspects on the international commission on non-ionizing radiation protection (ICNIRP) 2020 guidelines on radiofrequency radiation." Journal of Cancer Science and Clinical Therapeutics **5**(2): 250-285.

He, L., et al. (2017). "Antioxidants maintain cellular redox homeostasis by elimination of reactive oxygen species." Cellular Physiology and Biochemistry **44**(2): 532-553.

Hegyi, H. and M. Gerstein (1999). "The relationship between protein structure and function: a comprehensive survey with application to the yeast genome." Journal of molecular biology **288**(1): 147-164.

Hepworth, S. J., et al. (2006). "Mobile phone use and risk of glioma in adults: case-control study." Bmj **332**(7546): 883-887.

Herzfeld, D. J., et al. (2015). "Encoding of action by the Purkinje cells of the cerebellum." Nature **526**(7573): 439-442.

Hocking, B., et al. (1996). "Cancer incidence and mortality and proximity to TV towers." Medical Journal of Australia **165**(11-12): 601-605.

Hodgkin, A. L. and A. F. Huxley (1939). "Action potentials recorded from inside a nerve fibre." Nature **144**(3651): 710-711.

Hollensworth, S. B., et al. (2000). "Glial cell type-specific responses to menadione-induced oxidative stress." Free Radical Biology and Medicine **28**(8): 1161-1174.

Holmström, K. M. and T. Finkel (2014). "Cellular mechanisms and physiological consequences of redox-dependent signalling." Nature reviews Molecular cell biology **15**(6): 411-421.

Hong, S., et al. (2014). "Frequency and quadrature-amplitude modulation for downlink cellular OFDMA networks." IEEE Journal on selected areas in communications **32**(6): 1256-1267.

Hossmann, K. A. and D. Hermann (2003). "Effects of electromagnetic radiation of mobile phones on the central nervous system." Bioelectromagnetics: Journal of the Bioelectromagnetics Society, The Society for Physical Regulation in Biology and Medicine, The European Bioelectromagnetics Association **24**(1): 49-62.

Howard, J. and R. Clark (2002). "Mechanics of motor proteins and the cytoskeleton." Appl. Mech. Rev. **55**(2): B39-B39.

Huelsken, J. and J. Behrens (2002). "The Wnt signalling pathway." Journal of cell science **115**(21): 3977-3978.

Huurdeman, A. A. (2003). The worldwide history of telecommunications, John Wiley & Sons.

Hwang, T., et al. (2008). "OFDM and its wireless applications: A survey." IEEE Transactions on Vehicular Technology **58**(4): 1673-1694.

Hyman, S. E. (2005). "Neurotransmitters." Current Biology **15**(5): R154-R158.

ICBE-EMF (2022). "Scientific evidence invalidates health assumptions underlying the FCC and ICNIRP exposure limit determinations for radiofrequency radiation: implications for 5G." Environmental Health **21**(1): 92.

ICNIRP (2020). "Guidelines for limiting exposure to electromagnetic fields (100 kHz to 300 GHz)." Health physics **118**(5): 483-524.

IEEE (1999). "IEEE Standard for Telecommunications and Information Exchange Between Systems - LAN/MAN Specific Requirements - Part 11: Wireless Medium Access Control (MAC) and physical layer (PHY) specifications: High Speed Physical Layer in the 5 GHz band." IEEE Std 802.11a-1999: 1-102.

IEEE (2013). "IEEE Standard for Information technology-- Telecommunications and information exchange between systemsLocal and metropolitan area networks-- Specific requirements--Part 11: Wireless LAN Medium Access Control (MAC) and Physical Layer (PHY) Specifications--Amendment 4: Enhancements for Very High Throughput for Operation in Bands below 6 GHz." IEEE Std 802.11ac-2013 (Amendment to IEEE Std 802.11-2012, as amended by IEEE Std 802.11ae-2012, IEEE Std 802.11aa-2012, and IEEE Std 802.11ad-2012): 1-425.

Ighodaro, O. and O. Akinloye (2018). "First line defence antioxidants-superoxide dismutase (SOD), catalase (CAT) and glutathione peroxidase (GPX): Their fundamental role in the entire antioxidant defence grid." Alexandria journal of medicine **54**(4): 287-293.

Iqbal-Faruque, M., et al. (2014). "Effects of mobile phone radiation onto human head with variation of holding cheek and tilt positions." Journal of applied research and technology **12**(5): 871-876.

Ishimaru, A. (2017). Electromagnetic wave propagation, radiation, and scattering: from fundamentals to applications, John Wiley & Sons.

Jajte, J., et al. (2002). "Effect of 7 mT static magnetic field and iron ions on rat lymphocytes: apoptosis, necrosis and free radical processes." Bioelectrochemistry **57**(2): 107-111.

Jämsä, A., et al. (2004). "The retinoic acid and brain-derived neurotrophic factor differentiated SH-SY5Y cell line as a model for Alzheimer's disease-like tau phosphorylation." Biochemical and biophysical research communications **319**(3): 993-1000.

Jolley, D. and J. L. Paterson (2020). "Pylons ablaze: Examining the role of 5G COVID-19 conspiracy beliefs and support for violence." British journal of social psychology **59**(3): 628-640.

Jones, D. P. (2006). "Redefining oxidative stress." Antioxidants & redox signaling **8**(9-10): 1865-1879.

Juutilainen, J., et al. (2011). "Review of possible modulation-dependent biological effects of radiofrequency fields." Bioelectromagnetics **32**(7): 511-534.

Kang, C.-M., et al. (2002). "Hspa4 (HSP70) is involved in the radioadaptive response: results from mouse splenocytes." Radiation research **157**(6): 650-655.

Kang, D.-H. (2002). "Oxidative stress, DNA damage, and breast cancer." AACN Advanced Critical Care **13**(4): 540-549.

Kang, K. A., et al. (2014). "Effects of combined radiofrequency radiation exposure on levels of reactive oxygen species in neuronal cells." Journal of Radiation Research **55**(2): 265-276.

Katzenell, S., et al. (2017). Isolation, purification, and culture of primary murine sensory neurons. Innate Antiviral Immunity: Methods and Protocols, Springer**:** 229-251.

Kaushik, S. (2012). "An overview of technical aspect for WiFi networks technology." International Journal of Electronics and Computer Science Engineering (IJECSE, ISSN: 2277-1956) **1**(01): 28-34.

Kesari, K. K., et al. (2018). "Radiations and male fertility." Reproductive Biology and Endocrinology **16**(1): 118.

Khadrawy, Y., et al. (2009). "Effect of electromagnetic radiation from mobile phone on the levels of cortical amino acid neurotransmitters in adult and young rats." Romanian J Biophys **19**(4): 295-305.

Kiefer, A. K., et al. (2013). "Genome-wide analysis points to roles for extracellular matrix remodeling, the visual cycle, and neuronal development in myopia." PLoS genetics **9**(2): e1003299.

Kim, J. H., et al. (2018). "Exposure to 835 MHz radiofrequency electromagnetic field induces autophagy in hippocampus but not in brain stem of mice." Toxicology and Industrial Health **34**(1): 23-35.

Kim, S., et al. (2021). "Effects of mobile phone usage on sperm quality–No time-dependent relationship on usage: A systematic review and updated meta-analysis." Environmental research **202**: 111784.

Koivisto, M., et al. (2000). "Effects of 902 MHz electromagnetic field emitted by cellular telephones on response times in humans." Neuroreport **11**(2): 413-415.

Kola, I. and J. Landis (2004). "Can the pharmaceutical industry reduce attrition rates?" Nature Reviews Drug Discovery **3**(8): 711-716.

Koopman, W. J., et al. (2010). "Mammalian mitochondrial complex I: biogenesis, regulation, and reactive oxygen species generation." Antioxidants & redox signaling **12**(12): 1431-1470.

Koopman, W. J., et al. (2007). "Human NADH: ubiquinone oxidoreductase deficiency: radical changes in mitochondrial morphology?" American Journal of Physiology-Cell Physiology **293**(1): C22-C29.

Korecka, J. A., et al. (2013). "Phenotypic characterization of retinoic acid differentiated SH-SY5Y cells by transcriptional profiling." PloS one **8**(5): e63862.

Koritzinsky, M., et al. (2005). "The hypoxic proteome is influenced by gene-specific changes in mRNA translation." Radiotherapy and oncology **76**(2): 177-186.

Koteluk, O., et al. (2021). "The landscape of transmembrane protein family members in head and neck cancers: their biological role and diagnostic utility." Cancers **13**(19): 4737.

Kottou, S., et al. (2014). "How safe is the environmental electromagnetic radiation." Journal of Physical Chemistry & Biophysics **4**(3): 1-10.

Kovacic, P. and R. Somanathan (2010). "Electromagnetic fields: mechanism, cell signaling, other bioprocesses, toxicity, radicals, antioxidants and beneficial effects." Journal of Receptors and Signal Transduction **30**(4): 214-226.

Kovalevich, J. and D. Langford (2013). Considerations for the use of SH-SY5Y neuroblastoma cells in neurobiology. Neuronal cell culture: methods and protocols, Springer**:** 9-21.

Kowalczuk, C., et al. (2010). "Absence of nonlinear responses in cells and tissues exposed to RF energy at mobile phone frequencies using a doubly resonant cavity." Bioelectromagnetics **31**(7): 556-565.

Krahe, R. and F. Gabbiani (2004). "Burst firing in sensory systems." Nature Reviews Neuroscience **5**(1): 13-23.

Kreps, J. A., et al. (2002). "Transcriptome changes for Arabidopsis in response to salt, osmotic, and cold stress." Plant physiology **130**(4): 2129-2141.

Kryston, T. B., et al. (2011). "Role of oxidative stress and DNA damage in human carcinogenesis." Mutation Research/Fundamental and Molecular Mechanisms of Mutagenesis **711**(1-2): 193-201.

Kumar, A., et al. (2025). "Analysis of throughput and error rate of 16-QAM, 64-QAM, and 256-QAM O-NOMA waveforms." Journal of Optical Communications **45**(s1): s2093-s2099.

Kumbhar, A. (2017). "Overview of ISM bands and Software-defined Radio Experimentation." Wireless Personal Communications **97**(3): 3743-3756.

Lackner, L. L. and J. Nunnari (2010). "Small molecule inhibitors of mitochondrial division: tools that translate basic biological research into medicine." Chemistry & biology **17**(6): 578-583.

Lahkola, A., et al. (2007). "Mobile phone use and risk of glioma in 5 North European countries." International journal of cancer **120**(8): 1769-1775.

Lahkola, A., et al. (2008). "Meningioma and mobile phone use—a collaborative case-control study in five North European countries." International journal of epidemiology **37**(6): 1304-1313.

Lai, H. (2021). "Genetic effects of non-ionizing electromagnetic fields." Electromagnetic biology and medicine **40**(2): 264-273.

Lal, A., et al. (2001). "Transcriptional response to hypoxia in human tumors." Journal of the National Cancer Institute **93**(17): 1337-1343.

Lambert, A. J. and M. D. Brand (2009). "Reactive oxygen species production by mitochondria." Mitochondrial DNA: methods and protocols: 165-181.

Lantow, M., et al. (2006). "ROS release and Hsp70 expression after exposure to 1,800 MHz radiofrequency electromagnetic fields in primary human monocytes and lymphocytes." Radiation and environmental biophysics **45**(1): 55-62.

Larsen, A. I. (1991). "Congenital malformations and exposure to high-frequency electromagnetic radiation among Danish physiotherapists." Scandinavian journal of work, environment & health: 318-323.

Larsson, E. G., et al. (2014). "Massive MIMO for next generation wireless systems." IEEE communications magazine **52**(2): 186-195.

Le Gal, K., et al. (2021). "Cellular redox homeostasis." Antioxidants **10**(9): 1377.

Lee, K., et al. (2012). "Mobile data offloading: How much can WiFi deliver?" IEEE/ACM Transactions on networking **21**(2): 536-550.

Lee, T. I. and R. A. Young (2013). "Transcriptional regulation and its misregulation in disease." Cell **152**(6): 1237-1251.

Lemotte, P. K. and G. C. Walker (1985). "Induction and autoregulation of ada, a positively acting element regulating the response of Escherichia coli K-12 to methylating agents." Journal of bacteriology **161**(3): 888-895.

Levitan, I. B. and L. K. Kaczmarek (2002). The neuron: cell and molecular biology, Oxford University Press, USA.

Levy, W. B. and R. A. Baxter (1996). "Energy efficient neural codes." Neural computation **8**(3): 531-543.

Li, F., et al. (2016). "Radiation induces the generation of cancer stem cells: A novel mechanism for cancer radioresistance." Oncology letters **12**(5): 3059-3065.

Li, Y., et al. (2004). "Protein kinase C θ inhibits insulin signaling by phosphorylating IRS1 at Ser1101." Journal of Biological Chemistry **279**(44): 45304-45307.

Liao, R., et al. (2014). "MU-MIMO MAC protocols for wireless local area networks: A survey." IEEE Communications Surveys & Tutorials **18**(1): 162-183.

Lin, M. T. and M. F. Beal (2006). "Mitochondrial dysfunction and oxidative stress in neurodegenerative diseases." Nature **443**(7113): 787-795.

Linet, M. S., et al. (1997). "Residential exposure to magnetic fields and acute lymphoblastic leukemia in children." New England journal of medicine **337**(1): 1-8.

Litwin, L. and M. Pugel (2001). "The principles of OFDM." RF signal processing **2**: 30-48.

Liu, X., et al. (2022). "The uniformity and stability of cellular mass density in mammalian cell culture." Frontiers in cell and developmental biology **10**: 1017499.

Liu, Y. P., et al. (2021). "Molecular mechanisms of chemo-and radiotherapy resistance and the potential implications for cancer treatment." MedComm **2**(3): 315-340.

Lizcano, J. M. and D. R. Alessi (2002). "The insulin signalling pathway." Current Biology **12**(7): R236-R238.

Lo, Y. Y. and T. F. Cruz (1995). "Involvement of reactive oxygen species in cytokine and growth factor induction of c-fos expression in chondrocytes." Journal of Biological Chemistry **270**(20): 11727-11730.

Lönn, S., et al. (2004). "Output power levels from mobile phones in different geographical areas; implications for exposure assessment." Occupational and Environmental Medicine **61**(9): 769-772.

Lopes, F. M., et al. (2010). "Comparison between proliferative and neuron-like SH-SY5Y cells as an in vitro model for Parkinson disease studies." Brain research **1337**: 85-94.

Losón, O. C., et al. (2013). "Fis1, Mff, MiD49, and MiD51 mediate Drp1 recruitment in mitochondrial fission." Molecular biology of the cell **24**(5): 659-667.

Lotz, W. G. (1985). "Hyperthermia in radiofrequency-exposed rhesus monkeys: a comparison of frequency and orientation effects." Radiation research **102**(1): 59-70.

Lowe, R., et al. (2017). "Transcriptomics technologies." PLoS computational biology **13**(5): e1005457.

Lu, B. and H. Vogel (2009). "Drosophila models of neurodegenerative diseases." Annual review of pathology: mechanisms of disease **4**(1): 315-342.

Luukkonen, J., et al. (2009). "Enhancement of chemically induced reactive oxygen species production and DNA damage in human SH-SY5Y neuroblastoma cells by 872 MHz radiofrequency radiation." Mutation Research/Fundamental and Molecular Mechanisms of Mutagenesis **662**(1-2): 54-58.

Ma, Y., et al. (2019). "Modulation format identification based on constellation diagrams in adaptive optical OFDM systems." Optics Communications **452**: 203-210.

Magistretti, P. J., et al. (1999). "Energy on demand." Science **283**(5401): 496-497.

Mailloux, R. J., et al. (2013). "Unearthing the secrets of mitochondrial ROS and glutathione in bioenergetics." Trends in biochemical sciences **38**(12): 592-602.

Mains , R. E. and P. H. Patterson (1973). "PRIMARY CULTURES OF DISSOCIATED SYMPATHETIC NEURONS : I. Establishment of Long-Term Growth in Culture and Studies of Differentiated Properties." Journal of Cell Biology **59**(2): 329-345.

Rat sympathetic ganglia were disrupted by mechanical agitation to yield dissociated primary neurons, and the conditions for long-term growth in culture of the isolated neurons were examined. The neurons were grown with or without non-neural cells, simply by the addition or deletion of bicarbonate during growth in culture. Fluorescence histochemistry indicated that the isolated neurons contained catecholamines; incubations with radioactive precursors were used to verify the synthesis and accumulation of both dopamine and norepinephrine. The neurons also produced octopamine using tyramine as precursor, but not with tyrosine as the precursor. In the presence of eserine, older cultures synthesized and stored small amounts of acetylcholine. The cultures did not synthesize and accumulate detectable levels of radioactive γ-aminobutyric acid, 5-hydroxytryptamine, or histamine.

Mandl, A. M. (1964). "The radiosensitivity of germ cells." Biological Reviews **39**(3): 288-367.

Mann, S., et al. (2000). "Exposure to radio waves near mobile phone base stations." Radiological Protection Bulletin **4**(7): 13-16.

Margis, R., et al. (2008). "Glutathione peroxidase family–an evolutionary overview." The FEBS journal **275**(15): 3959-3970.

Markussen, P. and G. T. Svendsen (2005). "Industry lobbying and the political economy of GHG trade in the European Union." Energy Policy **33**(2): 245-255.

Maskey, D., et al. (2010). "Chronic 835-MHz radiofrequency exposure to mice hippocampus alters the distribution of calbindin and GFAP immunoreactivity." Brain research **1346**: 237-246.

Masland, R. H. (2004). "Neuronal cell types." Current Biology **14**(13): R497-R500.

Mattson, M. P. (2008). "Hormesis defined." Ageing research reviews **7**(1): 1-7.

McAdams, H. H. and A. Arkin (1997). "Stochastic mechanisms in gene expression." Proceedings of the National Academy of Sciences **94**(3): 814-819.

McBride, W. H. and D. Schaue (2020). "Radiation-induced tissue damage and response." The Journal of pathology **250**(5): 647-655.

McKay, B. E. and R. W. Turner (2005). "Physiological and morphological development of the rat cerebellar Purkinje cell." The Journal of physiology **567**(3): 829-850.

McKenzie, R. L., et al. (2009). "UV radiation: balancing risks and benefits." Photochemistry and photobiology **85**(1): 88-98.

Meeusen, S., et al. (2004). "Mitochondrial fusion intermediates revealed in vitro." Science **305**(5691): 1747-1752.

Michaelis, J., et al. (1997). "Childhood leukemia and electromagnetic fields: results of a population-based case-control study in Germany." Cancer Causes & Control **8**: 167-174.

Michaloliakos, A., et al. (2016). "Performance modeling of next-generation WiFi networks." Computer Networks **105**: 150-165.

Mirabelli, P., et al. (2019). "Cancer cell lines are useful model systems for medical research." Cancers **11**(8): 1098.

Mirończuk-Chodakowska, I., et al. (2018). "Endogenous non-enzymatic antioxidants in the human body." Advances in medical sciences **63**(1): 68-78.

Mitchell, P. (1961). "Coupling of phosphorylation to electron and hydrogen transfer by a chemi-osmotic type of mechanism." Nature **191**(4784): 144-148.

Mochel, F., et al. (2012). "Early alterations of brain cellular energy homeostasis in Huntington disease models." Journal of Biological Chemistry **287**(2): 1361-1370.

Muliyil, S. and M. Narasimha (2014). "Mitochondrial ROS regulates cytoskeletal and mitochondrial remodeling to tune cell and tissue dynamics in a model for wound healing." Developmental cell **28**(3): 239-252.

Murphy, M. P. (2009). "How mitochondria produce reactive oxygen species." Biochemical journal **417**(1): 1-13.

Naik, G., et al. (2020). "Next generation Wi-Fi and 5G NR-U in the 6 GHz bands: Opportunities and challenges." IEEE Access **8**: 153027-153056.

Nakamura, H., et al. (1998). "Natural killer cell activity reduced by microwave exposure during pregnancy is mediated by opioid systems." Environmental research **79**(2): 106-113.

Negrini, S., et al. (2010). "Genomic instability—an evolving hallmark of cancer." Nature reviews Molecular cell biology **11**(3): 220-228.

Newsholme, P., et al. (2007). "Diabetes associated cell stress and dysfunction: role of mitochondrial and non-mitochondrial ROS production and activity." The Journal of physiology **583**(1): 9-24.

Niven, J. E. (2016). "Neuronal energy consumption: biophysics, efficiency and evolution." Current opinion in neurobiology **41**: 129-135.

Nonaka, T., et al. (2009). "Phosphorylated and ubiquitinated TDP-43 pathological inclusions in ALS and FTLD-U are recapitulated in SH-SY5Y cells." FEBS letters **583**(2): 394-400.

Noor, N., et al. (2011). "Variations in amino acid neurotransmitters in some brain areas of adult and young male albino rats due to exposure to mobile phone radiation." European Review for Medical & Pharmacological Sciences **15**(7).

Nordhagen, E. K. and E. Flydal (2023). "Self-referencing authorships behind the ICNIRP 2020 radiation protection guidelines." Reviews on environmental health **38**(3): 531-546.

O'brien, J., et al. (2000). "Investigation of the Alamar Blue (resazurin) fluorescent dye for the assessment of mammalian cell cytotoxicity." European journal of biochemistry **267**(17): 5421-5426.

O'Collins, V. E., et al. (2006). "1,026 experimental treatments in acute stroke." Annals of neurology **59**(3): 467-477.

Obile, W. (2016). "Ericsson mobility report." Nov.

Odaci, E., et al. (2008). "Effects of prenatal exposure to a 900 MHz electromagnetic field on the dentate gyrus of rats: a stereological and histopathological study." Brain research **1238**: 224-229.

Ojakangas, C. L. and T. J. Ebner (1992). "Purkinje cell complex and simple spike changes during a voluntary arm movement learning task in the monkey." Journal of neurophysiology **68**(6): 2222-2236.

Oktem, F., et al. (2005). "Oxidative damage in the kidney induced by 900-MHz-emitted mobile phone: protection by melatonin." Archives of Medical Research **36**(4): 350-355.

Orengo, C. A., et al. (1999). "From protein structure to function." Current opinion in structural biology **9**(3): 374-382.

Oscar, K. J. and T. D. Hawkins (1977). "Microwave alteration of the blood-brain barrier system of rats." Brain research **126**(2): 281-293.

Ouellet-Hellstrom, R. and W. F. Stewart (1993). "Miscarriages among female physical therapists who report using radio-and microwave-frequency electromagnetic radiation." American Journal of Epidemiology **138**(10): 775-786.

Pahlavan, K. and P. Krishnamurthy (2021). "Evolution and impact of Wi-Fi technology and applications: A historical perspective." International Journal of Wireless Information Networks **28**: 3-19.

Pakhomov, A. G. and M. R. Murphy (2000). "A comprehensive review of the research on biological effects of pulsed radiofrequency radiation in Russia and the former Soviet Union." Advances in electromagnetic fields in living systems: 265-290.

Pall, M. L. (2013). "Electromagnetic fields act via activation of voltage-gated calcium channels to produce beneficial or adverse effects." Journal of cellular and molecular medicine **17**(8): 958-965.

Panagopoulos, D. J., et al. (2002). "Mechanism for action of electromagnetic fields on cells." Biochemical and biophysical research communications **298**(1): 95-102.

Panagopoulos, D. J., et al. (2021). "Human-made electromagnetic fields: Ion forced-oscillation and voltage-gated ion channel dysfunction, oxidative stress and DNA damage." International Journal of Oncology **59**(5): 1-16.

Park, S.-H., et al. (2000). "Inducible heat-shock protein 70 is involved in the radioadaptive response." Radiation research **153**(3): 318-326.

Park, T. I., et al. (2020). "Isolation and culture of functional adult human neurons from neurosurgical brain specimens." Brain Communications **2**(2): fcaa171.

Parkvall, S., et al. (2018). "NR: The new 5G radio access technology." IEEE Communications Standards Magazine **1**(4): 24-30.

Pettersson, D., et al. (2014). "Long-term mobile phone use and acoustic neuroma risk." Epidemiology **25**(2): 233-241.

Picard, M., et al. (2013). "Mitochondrial morphology transitions and functions: implications for retrograde signaling?" American Journal of Physiology-Regulatory, Integrative and Comparative Physiology **304**(6): R393-R406.

Pires-daSilva, A. and R. J. Sommer (2003). "The evolution of signalling pathways in animal development." Nature reviews genetics **4**(1): 39-49.

Poole, I. (2006). Cellular communications explained: from basics to 3G, Newnes.

Postow, E. and M. L. Swicord (1986). Modulated fields and" window" effects," Boca Raton, FL: CRC Press.

Potter, S. S. (2018). "Single-cell RNA sequencing for the study of development, physiology and disease." Nature Reviews Nephrology **14**(8): 479-492.

Prasad, M., et al. (2017). "Mobile phone use and risk of brain tumours: a systematic review of association between study quality, source of funding, and research outcomes." Neurological Sciences **38**(5): 797-810.

Protection, I. C. o. N.-I. R. (1998). "Guidelines for limiting exposure to time-varying electric, magnetic, and electromagnetic fields (up to 300 GHz)." Health physics **74**(4): 494-522.

Purcell, E. M. and D. J. Morin (2013). Electricity and magnetism, Cambridge university press.

Purkinje, J. E. (1837). "Neueste Untersuchungen aus der Nerven und Hirn Anatomie." Bericht über die Versammlung deutscher Naturforscher und Aerzte in Prag im September **1883**: 177-180.

Rahman, M. M., et al. (2023). "Characterization of mRNA Signature in Milk Small Extracellular Vesicles from Cattle Infected with Bovine Leukemia Virus." Pathogens **12**(10): 1239.

Rakovic, A., et al. (2011). "Mutations in PINK1 and Parkin impair ubiquitination of Mitofusins in human fibroblasts." PloS one **6**(3): e16746.

Ramakrishnan, V. (2002). "Ribosome structure and the mechanism of translation." Cell **108**(4): 557-572.

Rappaport, T. S., et al. (2017). "Overview of millimeter wave communications for fifth-generation (5G) wireless networks—With a focus on propagation models." IEEE Transactions on antennas and propagation **65**(12): 6213-6230.

Ray, J., et al. (1993). "Proliferation, differentiation, and long-term culture of primary hippocampal neurons." Proceedings of the National Academy of Sciences **90**(8): 3602-3606.

> Primary embryonic hippocampal neurons can develop morphologically and functionally in culture but do not survive more than a few weeks. It has been reported that basic fibroblast growth factor (bFGF) promotes the survival of and neurite elongation from fetal hippocampal neurons. We report that bFGF, in a dose-dependent manner, can induce the survival (50 pg to 1 ng/ml) and proliferation (10-20 ng/ml) of embryonic hippocampal progenitor neurons in vitro. In serum-free medium containing high concentrations of bFGF, neurons not only proliferated (4-day doubling time) and differentiated morphologically but also could be passaged and grown as continuous cell lines. The neuronal nature of the proliferating cells was positively established by immunostaining with several different neuron-specific markers and by detailed ultrastructural analyses. The proliferative effect of bFGF was used to generate nearly pure neuronal cell cultures that can be passaged, frozen, thawed, and cultured again. Neurons have been maintained > 5 months in culture. The ability to establish long-term primary neuronal cultures offers the possibility that clonal lines of distinct neuronal cell types may be isolated from specific areas of the central nervous system. Such long-term neuronal cultures should prove valuable in studying neurons at the individual cell level and also in exploring interactions between neurons in vitro. The observed dose dependence raises the possibility that cell survival and proliferation in vivo may be influenced by different levels of bFGF.

Razavinasab, M., et al. (2016). "Maternal mobile phone exposure alters intrinsic electrophysiological properties of CA1 pyramidal neurons in rat offspring." Toxicology and Industrial Health **32**(6): 968-979.

Repacholi, M. (2017). "A history of the international commission on non-ionizing radiation protection." Health physics **113**(4): 282-300.

Repacholi, M. H. (1998). "Low-level exposure to radiofrequency electromagnetic fields: Health effects and research needs." Bioelectromagnetics: Journal of the Bioelectromagnetics Society, The Society for Physical Regulation in Biology and Medicine, The European Bioelectromagnetics Association **19**(1): 1-19.

Repacholi, M. H. and B. Greenebaum (1999). "Interaction of static and extremely low frequency electric and magnetic fields with living systems: health effects and research needs." Bioelectromagnetics: Journal of the Bioelectromagnetics Society, The Society for Physical Regulation in Biology and Medicine, The European Bioelectromagnetics Association **20**(3): 133-160.

Reshef, E. and C. Cordeiro (2022). "Future directions for Wi-Fi 8 and beyond." IEEE communications magazine **60**(10): 50-55.

Robinette, C. D., et al. (1980). "Effects upon health of occupational exposure to microwave radiation (radar)." American Journal of Epidemiology **112**(1): 39-53.

Robinton, D. A. and G. Q. Daley (2012). "The promise of induced pluripotent stem cells in research and therapy." Nature **481**(7381): 295-305.

Rochman, M. I., et al. (2023). "A comprehensive analysis of the coverage and performance of 4G and 5G deployments." Computer Networks **237**: 110060.

Rolfe, D. and G. C. Brown (1997). "Cellular energy utilization and molecular origin of standard metabolic rate in mammals." Physiological reviews **77**(3): 731-758.

Rosado, M. M., et al. (2018). "Immune-modulating perspectives for low frequency electromagnetic fields in innate immunity." Frontiers in public health **6**: 323464.

Rothman, K. J., et al. (1996). "Overall mortality of cellular telephone customers." Epidemiology: 303-305.

Ruxton, G. D. (2006). "The unequal variance t-test is an underused alternative to Student's t-test and the Mann–Whitney U test." Behavioral Ecology **17**(4): 688-690.

Rycaj, K. and D. G. Tang (2014). "Cancer stem cells and radioresistance." International journal of radiation biology **90**(8): 615-621.

Saleh, A. A. and R. Valenzuela (1987). "A statistical model for indoor multipath propagation." IEEE Journal on selected areas in communications **5**(2): 128-137.

Salford, L. G., et al. (1994). "Permeability of the blood-brain barrier induced by 915 MHz electromagnetic radiation, continuous wave and modulated at 8, 16, 50, and 200 Hz." Microscopy research and technique **27**(6): 535-542.

Salford, L. G., et al. (2003). "Nerve cell damage in mammalian brain after exposure to microwaves from GSM mobile phones." Environmental health perspectives **111**(7): 881-883.

Saloojee, Y. and E. Dagli (2000). "Tobacco industry tactics for resisting public policy on health." Bulletin of the World Health Organization **78**: 902-910.

Samsung (2025). "Samsung handset SAR database." from https://www.samsung.com/sar/sarMain/.

Sankaran, S. G. and S. R. Gulasekaran (2021). Wi-Fi 6: Protocol and Network, Artech House.

Schapira, A. H. (2006). "Mitochondrial disease." The Lancet **368**(9529): 70-82.

Schneider, J. and M. Stangassinger (2014). "Nonthermal effects of lifelong high-frequency electromagnetic field exposure on social memory performance in rats." Behavioral Neuroscience **128**(5): 633.

Schon, E. A. and G. Manfredi (2003). "Neuronal degeneration and mitochondrial dysfunction." The Journal of clinical investigation **111**(3): 303-312.

Schulz, D., et al. (2008). "Mechanisms of voltage-gated ion channel regulation: from gene expression to localization." Cellular and Molecular Life Sciences **65**(14): 2215-2231.

Selvin, S., et al. (1992). "Distance and risk measures for the analysis of spatial data: a study of childhood cancers." Social Science & Medicine **34**(7): 769-777.

Sen, S. and A. Nehorai (2010). "Adaptive OFDM radar for target detection in multipath scenarios." IEEE Transactions on Signal Processing **59**(1): 78-90.

Sengupta, B. and M. B. Stemmler (2014). "Power consumption during neuronal computation." Proceedings of the IEEE **102**(5): 738-750.

Serway, R. A., et al. (2000). Physics for scientists and engineers, Saunders college publishing Philadelphia.

Sevrioukova, I. F. (2011). "Apoptosis-inducing factor: structure, function, and redox regulation." Antioxidants & redox signaling **14**(12): 2545-2579.

Shafi, M., et al. (2017). "5G: A tutorial overview of standards, trials, challenges, deployment, and practice." IEEE Journal on selected areas in communications **35**(6): 1201-1221.

Shao, J., et al. (2000). "Decreased insulin receptor tyrosine kinase activity and plasma cell membrane glycoprotein-1 overexpression in skeletal muscle from obese women with gestational diabetes

mellitus (GDM): evidence for increased serine/threonine phosphorylation in pregnancy and GDM." Diabetes **49**(4): 603-610.

Sharma, D. K., et al. (2010). "Analog & digital modulation techniques: an overview." International Journal of Computing Science and Communication Technologies **3**(1): 2007.

Siller Jr, C. A. (1984). "Multipath propagation." IEEE communications magazine **22**: 6-15.

Silny, J. (2007). "Demodulation in tissue, the relevant parameters and the implications for limiting exposure." Health physics **92**(6): 604-608.

Simkó, M. (2007). "Cell type specific redox status is responsible for diverse electromagnetic field effects." Current medicinal chemistry **14**(10): 1141-1152.

Simkó, M. and M.-O. Mattsson (2019). "5G wireless communication and health effects—A pragmatic review based on available studies regarding 6 to 100 GHz." International journal of environmental research and public health **16**(18): 3406.

Simkó, M. and M. O. Mattsson (2004). "Extremely low frequency electromagnetic fields as effectors of cellular responses in vitro: possible immune cell activation." Journal of cellular biochemistry **93**(1): 83-92.

Sizun, H. and P. de Fornel (2005). Radio wave propagation for telecommunication applications, Springer.

Sluijter, M. and G. Racz (2002). "Technical aspects of radiofrequency." Pain practice **2**(3): 195-200.

Sofri, T., et al. (2021). "Health effects of 5G base station exposure: a systematic review." IEEE Access **10**: 41639-41656.

Sowa, P., et al. (2012). "Ionizing and non-ionizing electromagnetic radiation in modern medicine." Polish Annals of Medicine **19**(2): 134-138.

Spector, A. (2000). "Oxidative stress and disease." Journal of Ocular Pharmacology and Therapeutics **16**(2): 193-201.

Squatrito, R. C., et al. (1995). "Comparison of a novel redox dye cell growth assay to the ATP bioluminescence assay." Gynecologic oncology **58**(1): 101-105.

Squire, L., et al. (2012). Fundamental neuroscience, Academic press.

Starkey, S. J. (2016). "Inaccurate official assessment of radiofrequency safety by the Advisory Group on Non-ionising Radiation." Reviews on environmental health **31**(4): 493-503.

Statista (2024). "Revenue of the smartphones market worldwide from 2019 to 2029 (in billion US dollars)." Statista.

Stevens, C. F. (1998). "Neuronal diversity: too many cell types for comfort?" Current Biology **8**(20): R708-R710.

Stuppia, G., et al. (2015). "MFN2-related neuropathies: Clinical features, molecular pathogenesis and therapeutic perspectives." Journal of the neurological sciences **356**(1-2): 7-18.

Sturley, K. R. (1945). "Frequency modulation." Journal of the Institution of Electrical Engineers-Part III: Radio and Communication Engineering **92**(19): 197-213.

Subramanian, S., et al. (2018). "Investigation on simulation-based specific absorption rate in ultra-wideband antenna for breast cancer detection." IEEE sensors journal **18**(24): 10002-10009.

Sundaresan, M., et al. (1995). "Requirement for generation of H2O2 for platelet-derived growth factor signal transduction." Science **270**(5234): 296-299.

Swerdlow, A. J., et al. (2011). "Mobile phones, brain tumors, and the interphone study: where are we now?" Environmental health perspectives **119**(11): 1534-1538.

Szmigielski, S. (1996). "Cancer morbidity in subjects occupationally exposed to high frequency (radiofrequency and microwave) electromagnetic radiation." Science of the total environment **180**(1): 9-17.

Tan, H., et al. (2015). "The analysis on the candidate frequency bands of future mobile communication systems." China Communications **12**(Supplement): 140-149.

Tang, J., et al. (2015). "Exposure to 900 MHz electromagnetic fields activates the mkp-1/ERK pathway and causes blood-brain barrier damage and cognitive impairment in rats." Brain research **1601**: 92-101.

Tang, P., et al. (2025). Preliminary perspectives on 3GPP standardization of the propagation channel model for FR3 bands for NR, Science China Press Beijing.

Teo, I., et al. (1984). "Induction of resistance to alkylating agents in E. coli: the ada+ gene product serves both as a regulatory protein and as an enzyme for repair of mutagenic damage." The EMBO journal **3**(9): 2151-2157.

Thomas, M. C. and C.-M. Chiang (2006). "The general transcription machinery and general cofactors." Critical reviews in biochemistry and molecular biology **41**(3): 105-178.

Thor, H., et al. (1982). "The metabolism of menadione (2-methyl-1, 4-naphthoquinone) by isolated hepatocytes. A study of the implications of oxidative stress in intact cells." Journal of Biological Chemistry **257**(20): 12419-12425.

Tokalov, S. V. and H. O. Gutzeit (2004). "Weak electromagnetic fields (50 Hz) elicit a stress response in human cells." Environmental research **94**(2): 145-151.

TR, N. (2018). "Toxicology and carcinogenesis studies in B6C3F1/N mice exposed to whole-body radio frequency radiation at a frequency (1,900 MHz) and modulations (GSM and CDMA) used by cell phones." National Toxicology Program Technical Report Series (596).

Turin, G. L., et al. (1972). "A statistical model of urban multipath propagation." IEEE Transactions on Vehicular Technology **21**(1): 1-9.

Tynes, T. and T. Haldorsen (1997). "Electromagnetic fields and cancer in children residing near Norwegian high-voltage power lines." American Journal of Epidemiology **145**(3): 219-226.

Ulaby, F., et al. (2019). Handbook of radar scattering statistics for terrain, Artech House.

Unterholzner, L., et al. (2010). "IFI16 is an innate immune sensor for intracellular DNA." Nature immunology **11**(11): 997-1004.

Ursini, F., et al. (2016). "Redox homeostasis: The Golden Mean of healthy living." Redox biology **8**: 205-215.

Usselman, R. J., et al. (2014). "Spin biochemistry modulates reactive oxygen species (ROS) production by radio frequency magnetic fields." PloS one **9**(3): e93065.

Valerio, A. and E. Nisoli (2015). "Nitric oxide, interorganelle communication, and energy flow: a novel route to slow aging." Frontiers in cell and developmental biology **3**: 6.

Varani, K., et al. (2017). "Adenosine receptors as a biological pathway for the anti-inflammatory and beneficial effects of low frequency low energy pulsed electromagnetic fields." Mediators of inflammation **2017**(1): 2740963.

Vecchia, P., et al. (2009). Exposure to High Frequency Electromagnetic Fields, Biological Effects and Health Consequences (100 KHz-300 GHz): Review of the Scientific Evidence on Dosimetry, Biological Effects, Epidemiological Obeservations, and Health Consequences Concerning Exposure to High Frequency Electromagnetic Fields (100 KHz-300 GHz), Icnirp.

Veith, A. and B. Moorthy (2018). "Role of cytochrome P450s in the generation and metabolism of reactive oxygen species." Current opinion in toxicology **7**: 44-51.

Vicentic, A. and D. C. Jones (2007). "The CART (cocaine-and amphetamine-regulated transcript) system in appetite and drug addiction." The Journal of pharmacology and experimental therapeutics **320**(2): 499-506.

Walleczek, J. (1991). "Electromagnetic field effects on cells of the immune system: the role of calcium signalling."

Wang, C.-X., et al. (2023). "On the road to 6G: Visions, requirements, key technologies, and testbeds." IEEE Communications Surveys & Tutorials **25**(2): 905-974.

Wang, S. and C. Ran (2016). "Rethinking cellular network planning and optimization." IEEE wireless communications **23**(2): 118-125.

Wang, Y., et al. (2018). "Superoxide dismutases: Dual roles in controlling ROS damage and regulating ROS signaling." Journal of Cell Biology **217**(6): 1915-1928.

Wang, Z., et al. (2009). "RNA-Seq: a revolutionary tool for transcriptomics." Nature reviews genetics **10**(1): 57-63.

Waring, M. J., et al. (2015). "An analysis of the attrition of drug candidates from four major pharmaceutical companies." Nature Reviews Drug Discovery **14**(7): 475-486.

Waterham, H. R., et al. (2007). "A lethal defect of mitochondrial and peroxisomal fission." New England journal of medicine **356**(17): 1736-1741.

Watteyne, T., et al. (2010). Mitigating multipath fading through channel hopping in wireless sensor networks. 2010 IEEE International Conference on Communications, IEEE.

Weibler, J. and L. Enclosures (1993). "Properties of Metals used for RF shielding." EMC Test and Design **100**.

White, M. (2010). "Information anywhere, any when: The role of the smartphone." Business Information Review **27**(4): 242-247.

Whiteside, T. L. (2006). Immune suppression in cancer: effects on immune cells, mechanisms and future therapeutic intervention. Seminars in cancer biology, Elsevier.

Wilding, J. L. and W. F. Bodmer (2014). "Cancer cell lines for drug discovery and development." Cancer research **74**(9): 2377-2384.

Willems, P. H., et al. (2015). "Redox homeostasis and mitochondrial dynamics." Cell metabolism **22**(2): 207-218.

Winterbourn, C. C. (2020). "Biological chemistry of superoxide radicals." ChemTexts **6**(1): 7.

> Superoxide radicals are produced by the one-electron reduction of molecular oxygen. These radicals are formed physiologically as a by-product of oxygen metabolism, and they are important in toxicology as a product of the metabolism of redox-active xenobiotics. Superoxide is also produced by dedicated enzymes, and in these situations it plays a role in combatting microbial pathogens and regulating cellular processes. This article covers the properties and biological chemistry of superoxide radicals. It considers how they are produced, what biomolecules they react with, and the reactions that contribute to their toxicity. It also considers the function of superoxide dismutases, the enzymes responsible for removal of most of the superoxide produced in living organisms.

Winzer, P. J. (2012). "High-spectral-efficiency optical modulation formats." Journal of lightwave technology **30**(24): 3824-3835.

Wouters, O. J. (2020). "Lobbying expenditures and campaign contributions by the pharmaceutical and health product industry in the United States, 1999-2018." JAMA internal medicine **180**(5): 688-697.

Wu, F., et al. (2015). "Two transcription factors, Pou4f2 and Isl1, are sufficient to specify the retinal ganglion cell fate." Proceedings of the National Academy of Sciences **112**(13): E1559-E1568.

Wu, S., et al. (2016). Frequency and quadrature amplitude modulation for 5G networks. 2016 European Conference on Networks and Communications (EuCNC), IEEE.

Wu, Y., et al. (2023). "Molecular mechanisms of tumor resistance to radiotherapy." Molecular Cancer **22**(1): 96.

Xicoy, H., et al. (2017). "The SH-SY5Y cell line in Parkinson's disease research: a systematic review." Molecular neurodegeneration **12**(1): 10.

Xu-Wilson, M., et al. (2009). "Cerebellar contributions to adaptive control of saccades in humans." Journal of Neuroscience **29**(41): 12930-12939.

Xu, Y., et al. (2021). "A survey on resource allocation for 5G heterogeneous networks: Current research, future trends, and challenges." IEEE Communications Surveys & Tutorials **23**(2): 668-695.

y Cajal, S. R. (1902). Textura del sistema nervioso del hombre y de los vertebrados, Imprenta y libreria de Nicolas Moya.

Yakymenko, I., et al. (2016). "Oxidative mechanisms of biological activity of low-intensity radiofrequency radiation." Electromagnetic biology and medicine **35**(2): 186-202.

Yamaguchi, M. and H. Yoshida (2018). "Drosophila as a model organism." Drosophila models for human diseases: 1-10.

Yang, M., et al. (2017). "Mobile phone use and glioma risk: A systematic review and meta-analysis." PloS one **12**(5): e0175136.

Yao, K., et al. (2008). "Electromagnetic noise inhibits radiofrequency radiation-induced DNA damage and reactive oxygen species increase in human lens epithelial cells." Molecular Vision **14**: 964.

Yao, K., et al. (2008). "Effect of superposed electromagnetic noise on DNA damage of lens epithelial cells induced by microwave radiation." Investigative ophthalmology & visual science **49**(5): 2009-2015.

Yao, Y. and W. Dai (2014). "Genomic instability and cancer." Journal of carcinogenesis & mutagenesis **5**: 1000165.

Yin, H. and S. Alamouti (2006). OFDMA: A broadband wireless access technology. 2006 IEEE sarnoff symposium, IEEE.

Yu-Hong, Z., et al. (2007). Mechanism of permeation in calcium channels activation by applied magnetic fields. 2007 29th Annual International Conference of the IEEE Engineering in Medicine and Biology Society, IEEE.

Yu-Wai-Man, P., et al. (2010). "Multi-system neurological disease is common in patients with OPA1 mutations." Brain **133**(3): 771-786.

Yu, G., et al. (2021). "Current progress on the effect of mobile phone radiation on sperm quality: an updated systematic review and meta-analysis of human and animal studies." Environmental Pollution **282**: 116952.

Yu, L. and Y. Yu (2017). "Energy-efficient neural information processing in individual neurons and neuronal networks." Journal of Neuroscience Research **95**(11): 2253-2266.

Yuan, J.-T. and K.-D. Tsai (2005). "Analysis of the multimodulus blind equalization algorithm in QAM communication systems." IEEE Transactions on Communications **53**(9): 1427-1431.

Zamanian, A. and C. Hardiman (2005). "Electromagnetic radiation and human health: A review of sources and effects." High Frequency Electronics **4**(3): 16-26.

Zeisel, A., et al. (2011). "Coupled pre-mRNA and mRNA dynamics unveil operational strategies underlying transcriptional responses to stimuli." Molecular systems biology **7**(1): 529.

Zeng, H. and J. R. Sanes (2017). "Neuronal cell-type classification: challenges, opportunities and the path forward." Nature Reviews Neuroscience **18**(9): 530-546.

Zeni, O., et al. (2007). "Formation of reactive oxygen species in L929 cells after exposure to 900 MHz RF radiation with and without co-exposure to 3-chloro-4-(dichloromethyl)-5-hydroxy-2 (5H)-furanone." Radiation research **167**(3): 306-311.

Zhang, M., et al. (2012). "Roles of cocaine-and amphetamine-regulated transcript in the central nervous system." Clinical and experimental pharmacology and physiology **39**(6): 586-592.

Zhao, R. Z., et al. (2019). "Mitochondrial electron transport chain, ROS generation and uncoupling." International journal of molecular medicine **44**(1): 3-15.

Zhao, T.-Y., et al. (2007). "Exposure to cell phone radiation up-regulates apoptosis genes in primary cultures of neurons and astrocytes." Neuroscience letters **412**(1): 34-38.

Zhao, Y.-L., et al. (2008). Effects of magnetic fields on intracellular calcium oscillations. 2008 30th Annual International Conference of the Ieee Engineering in Medicine and Biology Society, IEEE.

Zhong, Z., et al. (2015). Issues and challenges in dense WiFi networks. 2015 International Wireless Communications and Mobile Computing Conference (IWCMC), IEEE.

Ziech, D., et al. (2011). "Reactive Oxygen Species (ROS)—Induced genetic and epigenetic alterations in human carcinogenesis." Mutation Research/Fundamental and Molecular Mechanisms of Mutagenesis **711**(1-2): 167-173.

Zimmerman, D. W. (1987). "Comparative power of Student t test and Mann-Whitney U test for unequal sample sizes and variances." The Journal of Experimental Education **55**(3): 171-174.

Zitka, O., et al. (2012). "Redox status expressed as GSH: GSSG ratio as a marker for oxidative stress in paediatric tumour patients." Oncology letters **4**(6): 1247-1253.

Appendices

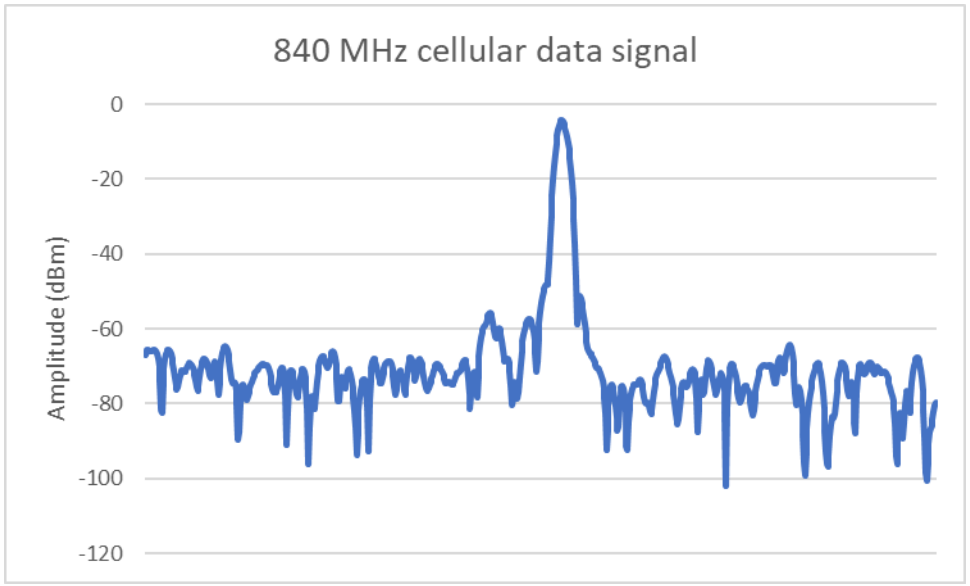
840 MHz cellular data signal
Amplitude (dBm)
0
-20
-40
-60
-80
-100
-120

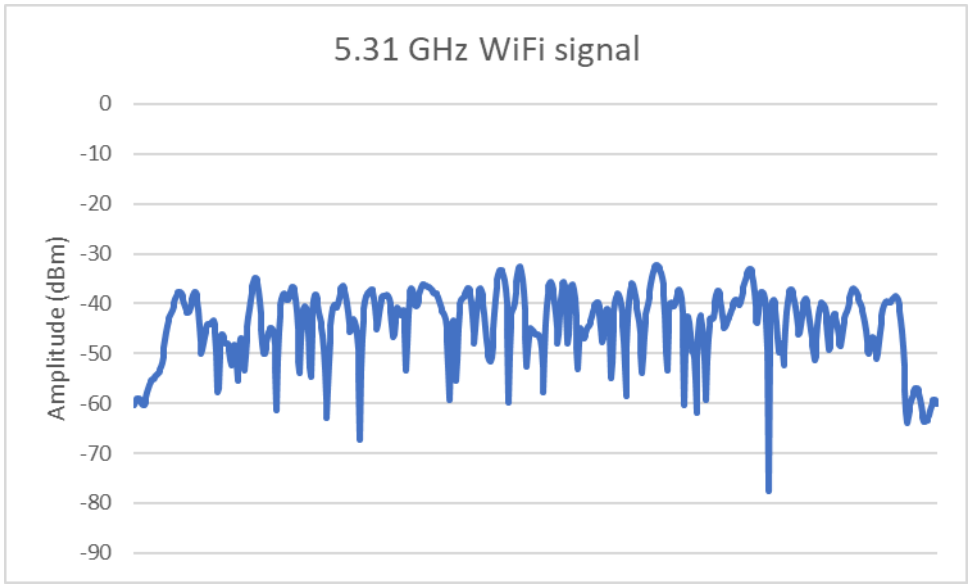
5.31 GHz WiFi signal
Amplitude (dBm)
0
-10
-20
-30
-40
-50
-60
-70
-80
-90

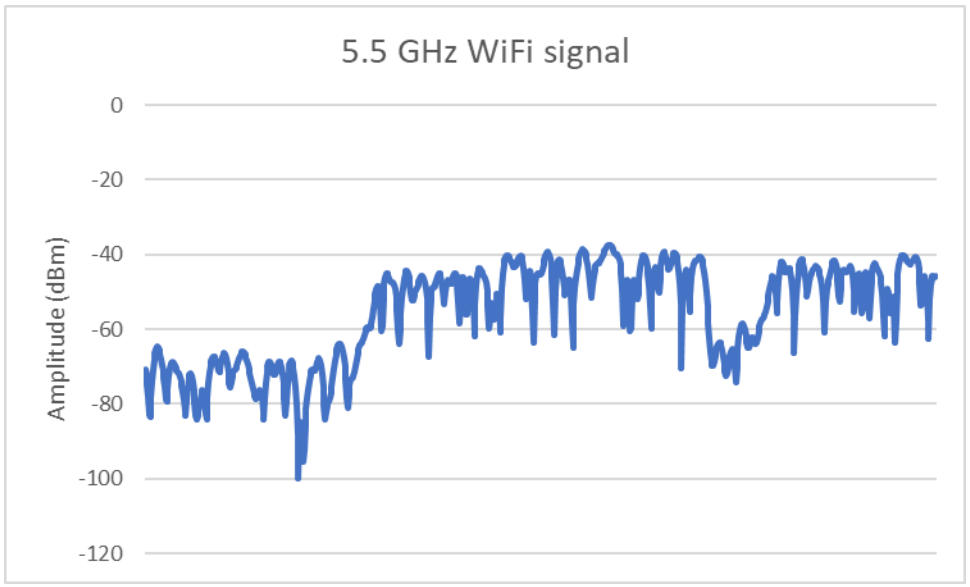
5.5 GHz WiFi signal
Amplitude (dBm)
0
-20
-40
-60
-80
-100
-120